The Activation of Small Molecules on the Surface of Nanoscopic, Highly Lewis-Acidic Aluminium Fluorides

D i s s e r t a t i o n

zur Erlangung des akademischen Grades

d o c t o r r e r u m n a t u r a l i u m

(Dr. rer. nat.)

im Fach Chemie

eingereicht an der

Mathematisch-Naturwissenschaftlichen Fakultät

der Humboldt-Universität zu Berlin

von

Dipl.-Chem. Agnieszka Kinga Siwek

Präsidentin der Humboldt-Universität zu Berlin

Prof. Dr.-Ing. Dr. Sabine Kunst

Dekan der Mathematisch-Naturwissenschaftlichen Fakultät

Prof. Dr. Elmar Kulke

Gutachter/in: 1. Prof. Dr. Thomas Braun

2. Prof. Dr. Erhard Kemnitz

Tag der mündlichen Prüfung: 15.09.2020

Kurzfassung

In der vorliegenden Arbeit wurde die Reaktivität von außergewöhnlich Lewis-sauren festen Katalysatoren: Aluminiumchlorofluorid (ACF) und *high-surface* Aluminiumfluorid (*HS*-AlF_3) unter moderaten Reaktionsbedingungen untersucht. Die Katalysatoren konnten erfolgreich für die Aktivierung von C-F- und C-Cl-Bindungen (CH_3F, CH_2F_2, CHF_3, CH_3Cl, CH_2Cl_2 und $ClCH_2$-CH_2Cl) in der Anwesenheit von Silanen eingesetzt werden.

Bei Hydrodehalogenierungsreaktionen in Batch-Reaktoren (NMR-Röhrchen) wurden höhere Umsätze mit ACF als mit *HS*-AlF_3 erreicht. Dieser Befund lässt sich mit sterischen Effekten erklären. Die kleineren Mikroporen des ACFs sind besser geeignet für die Aktivierung von kleinen Molekülen als die Mesoporen von *HS*-AlF_3. Die sterischen Aspekte wurden mit Hilfe von FTIR-Experimenten ausführlich untersucht. Unterschiedliche Beobachtungen wurden gemacht, wenn ein zusätzliches Substrat anwesend war, z.B. C_6D_6 zur Synthese des Friedel-Crafts-Produktes. *HS*-AlF_3 führte zu höheren Umsätzen bei fluorierten Substraten, während bei chlorierten Substraten ACF sich als der bessere Katalysator erwies.

Die Herausforderung bestand darin, die Katalysatoren unter sehr anspruchsvollen Bedingungen wie kurze Kontaktzeiten im Flow-Reaktor zu testen. Die Aktivierung von fluorierten und chlorierten Substraten war möglich. Der Unterschied in der Reaktivität der Katalysatoren war nicht so ausgeprägt wie bei Reaktionen in Batch-Reaktor. Aufgrund der kurzen Kontaktzeiten können nur kurze Diffusionswege ausgenutzt werden, was zu ähnlichen Reaktivitäten führt.

Mit Hilfe von Experimenten im Flow-Reaktor als auch MAS NMR-, EA-, NH_3-TPD-, XRD-, FTIR-, PulseTA®-Experimenten konnte der Mechanismus aufgeklärt werden. Der Katalysator muss zunächst mit Silan gesättigt werden, welcher eine Schutzfunktion hat und die Fluorierung des Katalysators unterdrückt.

Ausserdem konnten die Katalysatoren erfolgreich für die Hydrosilylierungsreaktionen und weiterhin zu Deoxygenierung von Ketonen eingesetzt werden.

.

Abstract

This thesis investigated the reactivity of extraordinarily lewis-acidic solid catalysts under moderate reaction conditions: aluminium chorofluoride (ACF) und *high-surface* aluminium fluoride (*HS*-AlF_3).The catalysts could be successfully applied in the activation of C-F and C-Cl bonds (CH_3F, CH_2F_2, CHF_3, CH_3Cl, CH_2Cl_2 und $ClCH_2$-CH_2Cl) in the presence of silanes.

Higher conversions were reached for hydrodehalogenation batch-reactions (NMR tubes) with ACF than for *HS*-AlF_3. This finding can be explained by steric effects. The smaller micropores of ACF are better suited for the activation of small molecules than mesopores of *HS*-AlF_3. Steric aspects were examined extensively by FTIR experiments. Different observations were made in cases where an additional substrate was present, for example C_6D_6 led to the formation of the Friedel-Crafts product. In this case *HS*-AlF_3 showed higher conversions of fluorinated substrates, while for chlorinated substrates ACF was found to be more efficient.

The challenge of this work was to optimize conditions under which the catalysts are not only efficient in batch reactors with long contact times but also under short contact times in flow reactors. Experiments demonstrated that fluorinated and chlorinated substrates can be activated under such conditions. The difference in reactivity of both catalysts was not as extensive as for reactions in a batch reactor. Short contact times require short diffusion pathways, thus more similar reactivities.

Experiments in a flow reactor, supported by further analyses by MAS NMR, EA, NH_3-TPD, XRD, FTIR and PulseTA® led to the elucidation of the catalytic mechanism. The catalyst must first be saturated by silane, which inhibits and protects the catalyst from fluorination.

The catalysts were also successfully applied for hydrosilylation reactions and deoxygenation of ketones.

“Remember to look up at the stars and not down at your feet. Try to make sense of what you see and wonder about what makes the universe exist. Be curious. And however difficult life may seem, there is always something you can do and succeed at. It matters that you don't just give up.”

Prof. S. Hawking

For my daughter Julia and my parents

Table of Content

Abbreviations

ACF	Aluminium chlorofluoride
BET	Brunauer–Emmett–Teller
CFC	Chlorofluorocarbons
CP	Cross Polarization
DTA	Differential Thermal Analyses
EA	Elemental Analysis
ESR	Electron Spin Resonance
FID	Free Induction Decay
FTIR	Fourier-Transform Infrared Spectroscopy
GC	Gas Chromatography
HOMO	Highest Occupied Molecular Orbital
HSAB	Hard and Soft Acid and Bases
HS-AlF_3	*High-Surface* Aluminium Fluoride
I effect	Inductive effect
LUMO	Lowest Unoccupied Molecular Orbital
MAS	Magic-Angle-Spinning
M effect	Mesomeric effect
MS	Mass Spectrometry
NMR	Nuclear magnetic resonance
PFTE NMR tube	Polytetrafluoroethylene NMR tube

TA	Thermal Analysis
TG	Thermogravimetric Analysis
TOF	Turnover Frequency
TON	Turnover Number
TPD	Temperature Programmed Desorption
UV	Ultraviolet
XANES	X-ray Absorption Near Edge Structure
XRD	X-ray diffraction
ZCF	Zirconium chlorofluoride

1 Introduction

1.1 General concepts in catalysis

1.1.1 Historical aspects

The roots of catalysis date back to ancient times, when alcohol was first produced by fermentation. However, the term 'catalysis' was coined by Berzelius in the early 19th century, when he realized on the basis of Mitscherlich´s work that chemical reactions can be initiated in the presence of additional substances like sulfuric acid without affecting them.[1–3] The definition of catalysis was later properly formulated by Ostwald in 1895.[4–6] He postulated "catalysis is the acceleration of a slowly proceeding chemical reaction through the presence of a foreign substance" without changing the equilibrium of the reaction. Furthermore, Faraday added that the reaction must occur on the surface of the catalyst.[3,4] Subsequently, Sabatier complemented the definition, stating that the catalytic reaction rate depended on the adsorption energies of the intermediates formed on the reaction surface.[7] With these discoveries, a new era of industrial chemistry was about to begin. Just more than 100 years ago, BASF introduced an industrial method for the production of sulfuric acid in a contact process using Pt and V_2O_5 as catalysts.[6,8] A few years later, in 1903 Haber and Bosch developed a method for the production of ammonia from its elements.[9] Just 10 years later, the first commercial BASF plant for ammonia production began operating.

Catalysis has become indispensable in modern chemistry. Traditional stoichiometric reactions have been replaced by catalytic approaches in more than 95% of chemical processes.[10] Social awareness of environmentally safe industrial processes has resulted in improved efficiency of chemical processes and has made them more environmentally friendly. Thus, the development of heterogeneously catalysed processes and their optimization have constantly been the focus of interest of both academic research and industrial applications.

1.1.2 Catalysts – theoretical basis

Chemical reactions do not always occur spontaneously. This is due to the activation energy, which is defined as initial amount of the energy needed for a reaction to proceed. Catalysts working successfully do so by offering a different energetic path with lower activation energy. Many reactions that are thermodynamically favourable do not proceed due to kinetic inhibition. This means that the reaction does not work because the activation energy barrier is too high. Catalysts allow reactions to proceed by lowering the energy of the transition state

without altering the reaction equilibrium. This effect is illustrated by the energy diagram below (Figure **1**).

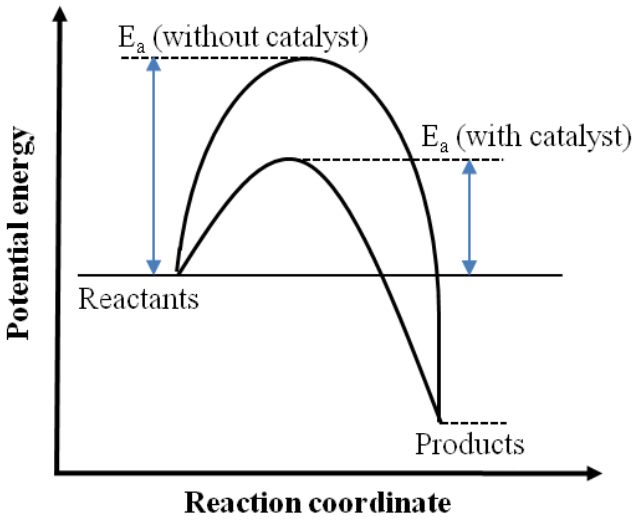

Figure 1. Comparison of reaction energy profiles with and without catalysts present.

The required activation energy for each reaction can be calculated with the Arrhenius equation,

$$k = A \cdot e^{\frac{-Ea}{RT}}$$

where k is the rate constant, A is the pre-exponential factor, E_a is the activation energy, and RT is the average kinetic energy. The Arrhenius equation correlates the rate constant and the activation energy. By lowering Ea, the rate constant k increases.

1.1.3 Heterogeneous *vs.* homogeneous catalysts

Traditionally, catalysts are divided into two categories: heterogeneous and homogeneous, depending on the phase they occupy during reaction. In heterogeneous catalysis, the catalytic material operates in a different phase than the reactants. Conversely, a homogeneous catalyst works in the same phase as the substrates. Homogeneous catalysts offer a number of advantages, such as high activity and excellent chemo- and regioselectivity. Their major drawback is the inconvenience of their recovery from the reaction mixture, which is especially problematic for toxic compounds. Also, problems due to difficult separation in batch reactions should not be disregarded.

Unlike their homogeneous counterparts, heterogeneous catalysts are characterized by high temperature stability and easy separation from the reaction mixture. High throughput under steady flow conditions is another major benefit.[11–13]

The benefits of both types of catalyst are combined when using nano-sized materials. Such solids are defined as nanoparticles, if their size is between 1 to 100 nm. Compared to conventional catalysts, smaller particles have a higher ratio of surface area to volume. Thus, the chemical and physical properties of nano-sized materials differ from those possessed by common bulk materials.[11,14] With increased surface effects they enhance reactivity, thus offering new catalytic applications.

1.1.4 Mechanisms of heterogeneous catalysis [15]

As mentioned previously, nano-sized materials are ideal candidates for catalysis. The interactions between the surface and substrates as well as diffusion processes have an inherent effect on kinetics, especially for catalysis in flow reactors. Molecules undergoing diffusion have to follow several elementary steps (Figure 2.).

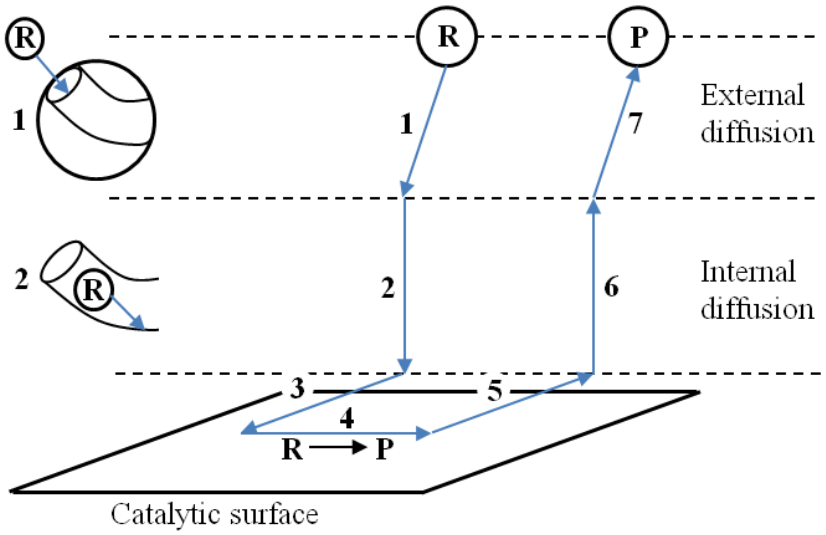

Figure 2. Basic steps in a heterogeneous mechanism.[16]

The substrates are governed by external diffusion into a pore of the catalyst **1**, followed by internal diffusion to the active surface **2**. When the substrate approaches active sites located on the surface **3**, it can be activated. Activation requires sufficiently strong adsorption of the substrate. However, if adsorption is too strong, the products cannot diffuse from the surface, which can be disadvantageous for highly active catalysts. When the reaction **4** is completed, the products will be desorbed **5** and again undergo internal **6** and external diffusion **7**. In such

processes, the catalytic activity is determined by the particle size of the catalyst, the geometry of the pores, and the type of interactions between substrates, products, and the catalyst.

Unlike homogeneously catalysed mechanisms, in which reactions depend solely on the rate constant and substrate concentrations, the diffusion effects and various interactions with the surface make heterogeneous processes more complex. In heterogeneous catalysis, three kinetic models are distinguished to describe the reaction mechanism.[15] In the Eley-Rideal mechanism only one reactant, **A**, is chemisorbed on the surface. Substrate **B** remains in the surrounding media. The reaction occurs when both collide, resulting in subsequent desorption of the product, **A-B**, as shown on Figure 3.

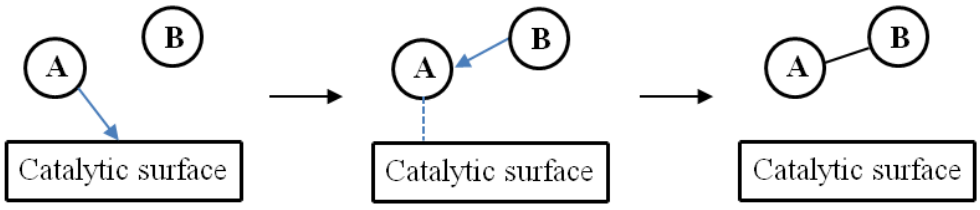

Figure 3. Eley-Rideal surface reaction.[17]

If the reaction follows the Langmuir-Hinshelwood mechanism, **A** and **B** react while both are adsorbed on the catalyst´s surface (Figure 4.).

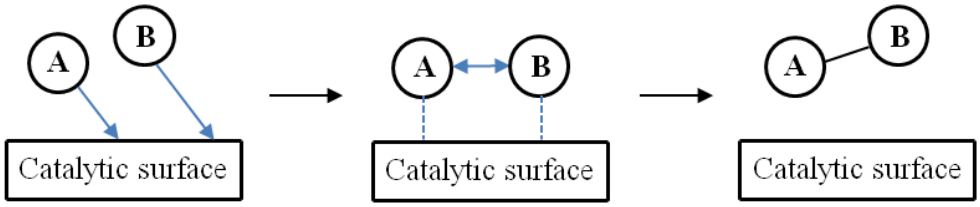

Figure 4. Langmuir-Hinshelwood surface reaction.[17]

The third option is known as the Mars Van Krevelen mechanism, where the surface itself acts not only as catalyst but also is an active part in the reaction. Either the substrate adsorbs on the catalyst surface and forms a thin metal-substrate layer, which is directly involved in the reaction. Or the catalyst surface itself acts as reactant. The second reactant diffuses in directly from the gas phase. Most examples are known for oxides, carbides or sulfides e.g. CO oxidation on platinium calatyst.[18] However, a analogue mechanism can be discussed for the dismutation or isomerisation reaction of flurochlorocarbons on fluorinated chromia surfaces, where bulk halogens as F^- or Cl^- takes part in the reaction.[19]

1.1.5 Lewis acids

Catalyst can not only be distinguished by homo- or heterogeneous nature but also by which type of reaction their catalytic activity is based on, for example transition metals, redox or acid-base reaction. This work only covers acid-base catalysts with special focus on Lewis acidic catalysts.

In 1923, G. N. Lewis developed a general concept to classify chemical substances in Lewis acids and bases.[20] According to his theory, Lewis acids are capable of accepting an electron pair from Lewis bases. The reaction involves the transfer of electron density from the basic substrate to an empty orbital of the Lewis acid, which is prone to nucleophilic attack. In 1968, Pearson refined this concept by classifying chemical substances based on the *hard and soft acid and bases* (HSAB) concept. Chemical substances are distinguished as "hard" or "soft" depending on their polarizability, electronegativity, charge density, and ionic radii.[21] Substances of high polarizing potential, high charge density and ensuing small ion radius are considered hard. In contrast, the so-called soft species are characterized by the opposite properties. Based on this classification, the stability of Lewis acid-base complexes can be estimated. A hard Lewis acid preferably interacts with a hard Lewis base, and the same is true for soft Lewis pairs. In hard-hard complexes, the large energy difference between the highest occupied (HOMO) and the lowest unoccupied orbital (LUMO) results in no electron transfer, as shown in Figure 5. Therefore, ionic forces predominate in such complexes. In soft-soft complexes HOMO and LUMO are closer in terms of energy difference and the bonding state has a more covalent character.

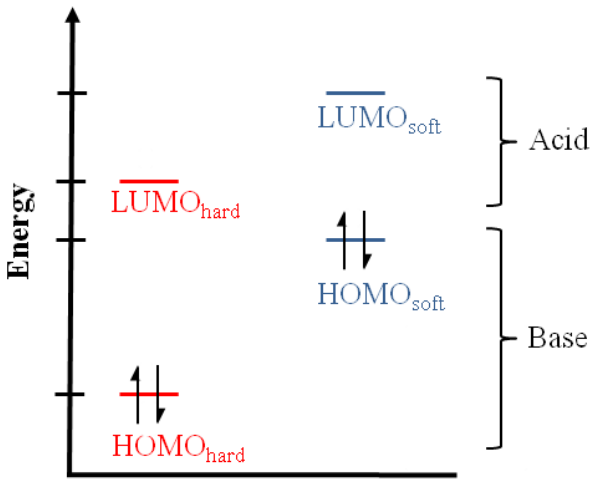

Figure 5. HOMO-LUMO interactions in soft-soft and hard-hard complexes.

The strength of the Lewis acidic metal chlorides and fluorides is quantified involving the pF scale introduced by Christe *et al*. in 1999.[22] This pF scale is calculated based on fluoride affinities for various metal fluorides in the gas phase (Scheme 1.).

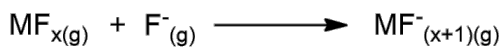

Scheme 1. Reaction of metal fluorides (Lewis acids) with fluoride anions (Lewis base) in the gas phase.

Based on this scale, two catalysts tested in catalytic reactions in this thesis, namely *high-surface* aluminium fluoride (*HS*-AlF_3) and aluminium chlorofluoride (ACF), should exhibit a similar acidity to each other. Their interactions with substrates should also be similar. Thus, HSAB concept cannot be utilized to estimate favorable interaction between substrate and catalyst. However, the acidity of these catalyst is comparable to SbF_5.[23] SbF_5 was considered to be the strongest accessible Lewis acid until AuF_5 was found to be even stronger.[24–27]

Lewis acids are particularly significant for industry as both heterogeneous and homogeneous catalysts. They cover a wide range of industrial applications from Friedel-Crafts alkylation ($AlCl_3$, $FeCl_3$, $Fe(OTf)_3$, SbF_5), and acetylation ($AlCl_3$, BF_3 or ZnO_2) to Diels-Alder or Aldol reactions ($RuCl_3$ or $AuCl_3$), just to mention a few.[28]

1.1.6 *HS*-AlF_3 *vs.* ACF

As previously mentioned, the activity of two solid and exceptionally strong Lewis acidic catalysts, *HS*-AlF_3 and ACF, was tested in different types of catalytic reactions. Their catalytic potential as well as their characteristics will be discussed in detail in this section by reviewing papers in this field.

Regarding the catalysts strength the theoretical calculations made by Christe *et al.*[22] are in full agreement with experimental data obtained by Krahl *et al.*[29] Performing IR studies, the authors estimated the Lewis acidity by determining the shift of the band of adsorbed CO. A strong blue shift for CO stretching frequencies adsorbed on *HS*-AlF_3 was detected. This indicates highly Lewis acidic properties.

In 2003, *HS*-AlF_3 was synthesized for the first time in sol gel process by Ruediger *et al.*[30,31] The starting material $Al(OiPr)_3$ was dissolved in isopropanol and fluorinated with HF solution yielding $AlF_{3-x}(OR)_x$ sol. This was subsequently postfluorinated in flow of

chlorodifluoromethane gas at high temperatures. In contrast, the first synthesis of non-*HS*-ACF is believed to be done in the 80ies by Krause.[32] However, it was DuPont which has estimated the real composition of ACF to finally patent it in 1992.[33,34] In our academic group, ACF is synthesised in a reaction of ACl_3 suspended in CCl_4 with CCl_3F. [35]

Both catalysts are amorphous materials (as established by X-ray diffractography) with a high surface area of 200-250 $m^2 \cdot g^{-1}$ for *HS*-AlF_3 and 100 $m^2 \cdot g^{-1}$ for ACF (based on Brunauer–Emmett–Teller (BET) experiment). [29,31,36–39] for HS-AlF_3, [40,41] for ACF The structure of *HS*-AlF_3 was studied by König *et al.* using ^{27}Al and ^{19}F MAS NMR spectroscopy. Based on these results, the existence of 6-fold coordinated aluminium species was postulated. The regular AlF-units are disturbed by octahedral AlF_xO_{6-x} (a relict of non-fluorinated intermediate phases), resulting in a disordered framework, which is presumably responsible for the catalyst´s extremely high reactivity. No under-coordinated Al-atoms were found. The 4- and 5-fold coordinated Al-species were observed only for less fluorinated $AlF_x(OR)_{3-x}$ phases. Interestingly enough, in the ^{19}F MAS NMR spectrum the terminal fluorine atoms were clearly detectable. The authors concluded that not only the irregular structural units, but also terminal fluorine atoms play an important role in the catalyst´s reactivity.

Similar results were obtained for ACF. From XANES, ESR and MAS NMR experiments, Krahl *et al.* demonstrated that chloride ions are incorporated in the AlF_3 units, resulting in $AlCl_xF_{(3-x)}$ phases as an amorphous solid. However, these catalysts differ in their thermal stability and interactions with Lewis bases. The structure of ACF remains stable up to 400 °C (at higher temperature it decomposes to α-AlF_3 and $AlCl_3$), whereas *HS*-AlF_3 can be applied in reactions in up to 600 °C. Above this temperature similarly to ACF, *HS*-AlF_3 turns into α-AlF_3 phase. Furthermore, ACF hydrolyses in presence of water resulting in α- and β-$AlF_3 \bullet 3H_2O$. For *HS*-AlF_3, the catalytic activity can be partially recovered by heating.

In context of catalytic ad- and desorption processes, these catalysts have another significant difference, in that they have different pore sizes. ACF is a microporous catalyst, while *HS*-AlF_3 is mesoporous. Thus, their catalytic potential was tested in a large number of reactions, which are presented below.

The isomerisation of 1,2-dibromohexafluoropropane to 2,2-dibromo-hexafluoropropane was chosen to test the catalytic activity of both catalysts, given that only very strong Lewis acids can catalyse this reaction (Scheme 2.).

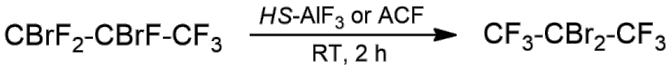

Scheme 2. Isomerisation reaction of 1,2-dibromohexafluoropropane to 2,2-dibromohexafluoropropane.

HS-AlF_3 and ACF gave excellent results reaching more than 90% conversion at room temperature after 2 h, as described by Kemnitz *et al.* and Murthy *et al.*. [36,42] In addition, an example for *HS*-AlF_3 supported on γ-Al_2O_3 (14.7 wt.%) was published by Kemnitz.[43] The conversion in this case was only 30% and significantly lower than for the unsupported catalyst. $AlCl_3$ did not show any activity in this isomerisation.

Both catalysts were also active in the isomerisation of CCl_2FCClF_2 to CCl_3CF_3, as shown in Scheme 3.[42]

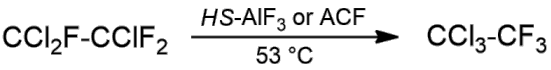

Scheme 3. Isomerisation of CCl_2FCClF_2 to CCl_3CF_3.

Up to 99% of the substrate was isomerised after 20 min using ACF as a catalyst, while only 24% conversion was achieved with *HS*-AlF_3 after 5 h. In contrast to the previous reaction, $AlCl_3$ was active resulting in 92% conversion after 3 h. It is presumed that $AlCl_3$ was transformed into ACF, because $AlCl_3$ itself is inactive. All reactions were carried out at 53 °C.

HS-AlF_3 and ACF, were remarkably active not only in the activation of C-X (X=Cl, F) bonds but also in transformation of non-halogenated compounds. Both catalysts were successfully applied in the H/D exchange reaction. Prechtl *et al.* postulated that C_6H_{12} in the presence of C_6D_6 as a deuterium source will be converted to deuterated cyclohexane and methylcyclopentane (Scheme 4).[44]

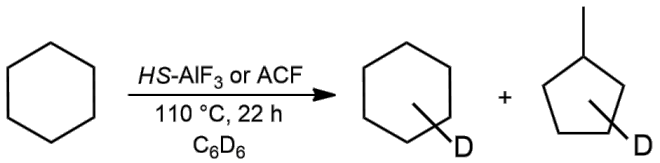

Scheme 4. H/D exchange reaction between C_6H_{12} and C_6D_6.

63% conversion was obtained using ACF as a catalyst, whereas with *HS*-AlF_3 only 34% at 110 °C after 22 h. The H/D exchange reaction occurred also in the case of aromatic substrates like C_6H_6.

The catalytic potential of ACF is known since 1996, when early reports were published by Petrov *et al.*.[45] The authors investigated the reactivity of ACF in isomerisation variants by converting *vic*-dichloroperfluoroalkanes into their *gem*-equivalents (Scheme 5).

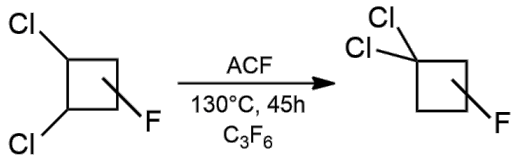

Scheme 5. Isomersiation of 1,2-dichlorohexafluorocyclobutane with ACF as catalyst.

They were able to show that the rearrangement reactions proceed for both linear and cyclic molecules. For example, the isomersiation of 1,2-dichlorohexafluorocyclobutane into 1,1-dichlorohexanflurocyclobutane proceeds at 130 °C and after 45 h to give 37% conversion.

In contrast, the linear molecules are more prone to rearrangements. 2,3-dichlorofluro-hexabutane was converted to 2,2-dichloroflurohexabutane in the presence of hexafluoro-propene with 96% conversion and 100% selectivity at 130 °C and after 5 h. (Scheme 6).

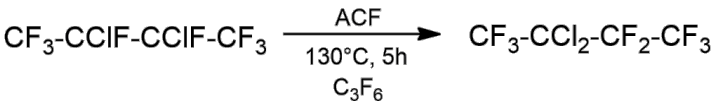

Scheme 6. Isomersiation reaction of 2,3-dichlorohexafluorobutane.

In the same year Krespan and Dixon focused on the application of ACF for condensation reactions.[46,47] The authors could show that tetrafluoroethene reacted with perfluoropentene to give 80% conversion to F-noenes (Scheme 7)

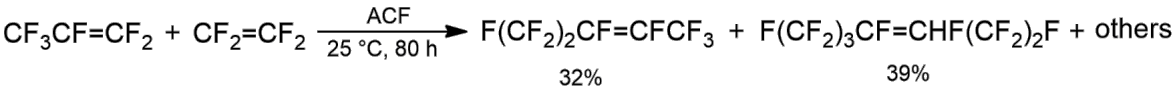

Scheme 7. Condensation of tetrafluoroethene with perfluoropentene.

A range of other hydrofluorocarbons and even chlorofluorocarbons were effectively converted in condensation reaction using ACF as a catalyst.[33]

Petrov und Krespan proved that ACF has a high catalytic potential.[47] However, its appearance in literature is rather scarce. A next break through was made by Ahrens *et al*., who applied this catalyst in hydrodefluorination reaction.[48] They translated a well known concept of homogeneous catalysis developed by Ozerov *et al*. to heterogeneous catalysis, as shown in Scheme 8.[49]

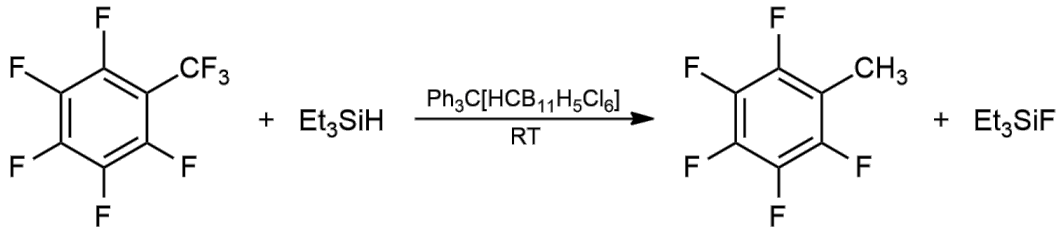

Scheme 8. Hydrodefluorination of pentafluorobenzotrifluoride using silylium-carborane catalyst.

Using Et_3SiH as a hydride source, Ahrens *et al.* were able to activate not only CH_3F but also higher fluorinated methanes in hydrodefluorination reaction. 13% of CHF_3 was converted to methane after 4 days at 70 °C. This work was the basis of this thesis.

More recently, results with ACF as a catalyst have started to appear, employing it in hydroarylation reactions. Calvo *et al.* postulated that the addition of benzene to ethene results in ethylbenzene (Scheme 9).

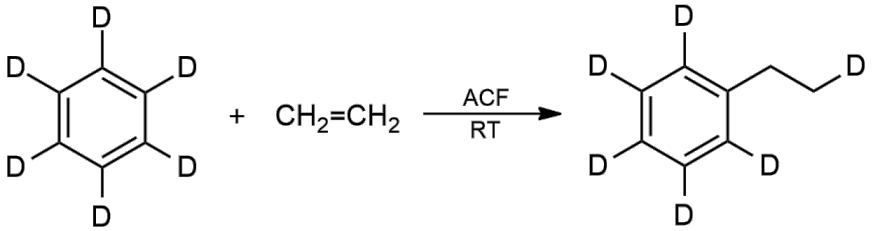

Scheme 9. Hydroarlylation of ethene with benzene.

The reaction proceeded with 100% conversion after 5 min at room temperature.[50] Also some partially fluorinated benzene with alkenes resulted in alkylated arenes. Only completely fluorinated benzene could not be activated.

Shortly thereafter, Meißner *et al.* reported a hydrodechlornation reaction involving $HGeEt_3$ as a hydride source.[51] The activation of CH_3Cl resulted in formation of 29% methane after 72 h at room temperature. ACF in the presence of $HGeEt_3$ exerted high selectivity towards activation of C-Cl bond, but in contrast to ACF◦Et_3SiH species, the C-F bonds were not activated in this case. Thus, the selective activation of $CHCl_2F$ was possible. CH_2Cl_2 and CH_2F_2 as the main products and CHF_3, $CHClF_2$, CH_2ClF, CH_2F_2 as side products were formed as a result of simultaneous dismutation and hydrodechlorination reactions. 72% conversion was achieved after 3 days at room temperature.

In recent years, *HS*-AlF_3 has also been recognized as an active heterogeneous catalyst for many challenging reactions. Rüdiger and Kemnitz reported the activation of 1,1,1,2,3,3-hexafluoropropane to 1,1,1,2,3-pentafluoropropene at 350 °C with high conversion of 95% (Scheme 10a).[52] Cis-isomer was formed in 88% selectivity. Consequently, the authors proved that a remarkably stable CF_3 group can be also activated by a simultaneous liberation of HF. 1,1,1,3,3,3-hexafluropropane underwent the dehydrofluorination to 1,1,1,3,3-pentafluoropropene at 400 °C (Scheme 10b). However, conversion decreased to 34% and selectivity to 66%. Another example of activation of a CF_3 group is the reaction of 1,1,1,2-tetrafluoroethane to trifluoroethene with only 20% conversion and 78% selectivity at 350 °C (Scheme 10c).

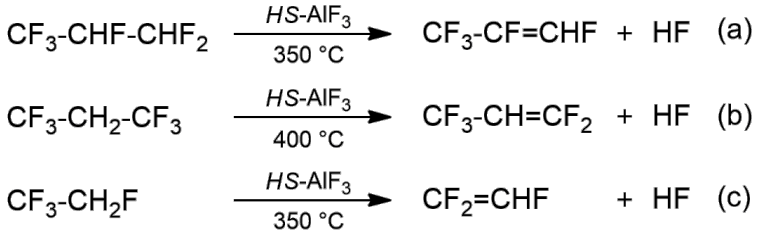

Scheme 10. Dehydrofluorination of different polyfluorinated alkanes.

A similar reactivity was observed by Teintz *et al.*.[53] The authors postulated that *HS*-AlF_3 can be applied as a selective catalyst for the dehydrofluorination by activating mixed CFCs. The catalyst demonstrated a high conversion of >99% for 3-chloro-1,1,1,3-tetrafluorobutane (Scheme 11).

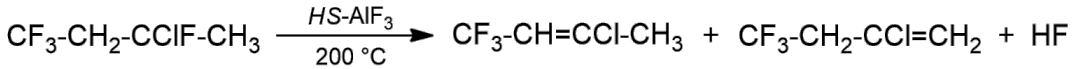

Scheme 11. Dehydrofluorination of mixed chlorofluorocarbons.

If *HS*-AlF_3 is exposed only to chlorocarbons, the C-Cl bond is activated as well. Nickkho-Amiry *et al.* reported on the catalytic dehydrochlorination of chloropropanes.[54] By FTIR, the authors observed the activation of *tert*-butyl chloride (^{t}BuCl) to trans-but-2-ene and HCl, as shown in Scheme 12.

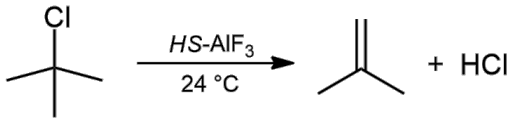

Scheme 12. Activation of *tert*-butyl chloride on the surface of *HS*-AlF_3.

The experiments were repeated with [^{36}Cl]-labelled ^{t}BuCl. In agreement with FTIR results, the formation of chemically adsorbed H^{36}Cl was measured using Geiger-Müller monitoring method.

Furthermore, Murthy *et al.* investigated the application of *HS*-AlF_3 in the isomerisation of non-halogenated substrates.[52,55] They discovered that o-xylene was transformed to m- and p-xylene at 300 °C and 1-butene to cis- and trans- butane at 200 °C (Scheme 13).

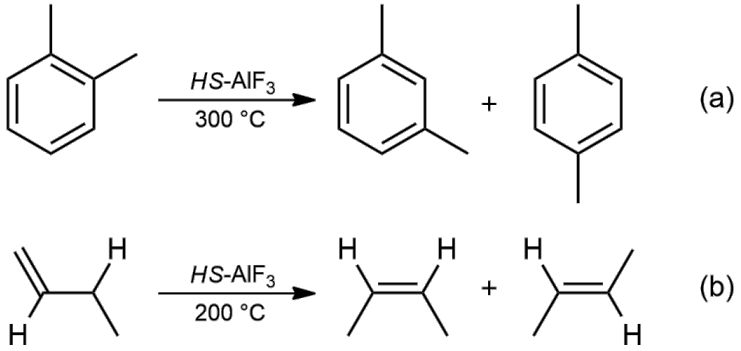

Scheme 13. Isomerisation of nonhalogenated aromatic und unsaturated hydrocarbons.

Murwani and co-workers also applied *HS*-AlF_3 in an untypical way, namely oxidation reactions.[56] Using a strong Al-based Lewis-acid as a catalyst in reactions involving heteroatoms like O and N which can act as a potential catalyst poison, was innovative. The authors reported the activation of ethylbenzene with t-butylhydroperoxide (TBHP) yielding acetophenone and benzaldehyde. A 42% conversion was achieved after 6 h at 60 °C with 36% selectivity towards benzaldehyde and only 16% towards acetophenone. Interestingly enough, Fe-doped *HS*-AlF_3 demonstrated not only a higher reactivity resulting in 70% conversion, but also 72% selectivity for the main product acetophenone and only 8% to benzaldehyde. Traces of benzoic acid were detected as well.

Another application of *HS*-AlF_3 is the cyclisation of citronellal. Coman *et al.* demonstrated that, cintronellal was transformed into isopulegol with 99% conversion after 1 h at 80 °C with *HS*-AlF_3.[57] The selectivity towards isopulegol over other isomers was 90%. Only (±)-isopulegol and (±)-neo-isopulegol were detected in the ratio of 85.5:14.5, as shown in Scheme 14.

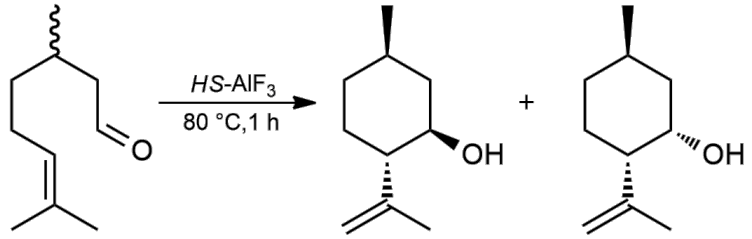

Scheme 14. Cyclisation of citronellal.

HS-AlF_3 was also successfully applied in a Friedel-Crafts alkylation (conversion 70% to product **3** at 100 °C after 1 h) in the synthesis of (all-*rac*)-a-Tocopherol **4** (Scheme 15).[58] Unfortunately, Coman discovered that the desired end-product Tocopherol **4** was only formed when using partially hydroxylated aluminium fluorides. When applying *HS*-AlF_3, the synthesis ended up in the formation of quinines and phytadienes.

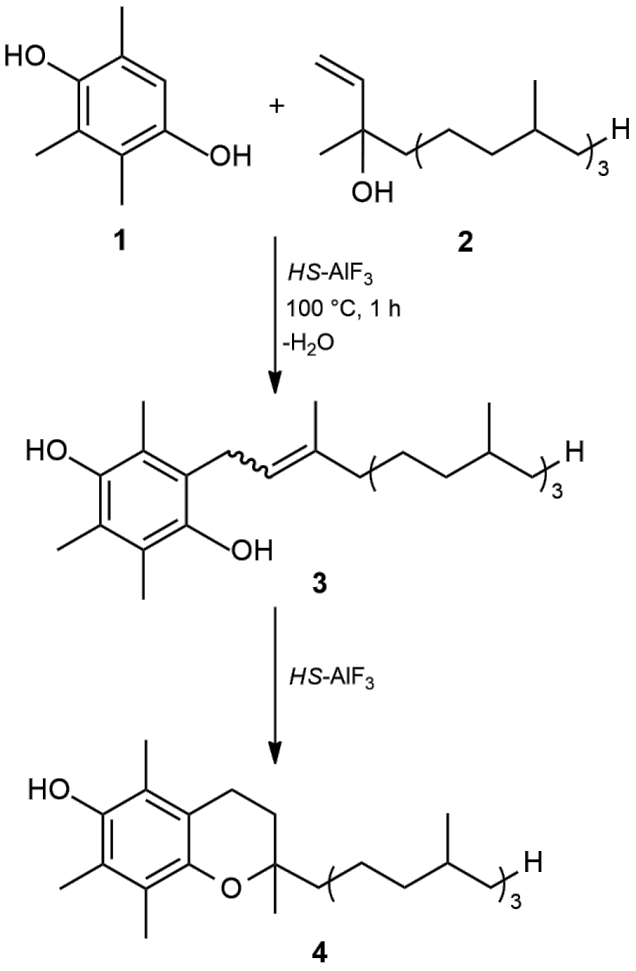

Scheme 15. Sythesis of (all-rac)-α-Tocopherol.

HS-AlF_3 can be also used in a less classical way as a support for different catalysts or even as a matrix where other catalysts can be incorporated. Patil *et al.* reported that Pd supported on *HS*-AlF_3 is active in hydrodehalogenation of $CHClF_2$ at 260 °C and a contact time of 1 s yielding ca. 86% conversion.[59] $CHClF_2$ was hydrodehaloganted to CH_4 and CH_3F. The third product CHF_3 was probably formed in a dismutation reaction, which competes with hydrodehalogenation.

A further contribution of catalyst supported on *HS*-AlF_3 was presented by Bonarowska *et al.*.[60] The authors synthesized Pd-Cu/*HS*-AlF_3 catalyst, which was tested in n-pentane hydroisomerisation. The reaction proceeded to isopentene with 90% selectivity. The reaction yielded 30-50% conversion at 350 °C.

A meaningful example of incorporated catalyst is delivered by Scheurell *et al.*.[61] The authors reported on vanadium-containing *HS*-AlF_3, which was used for the oxidative dehydrogenation of propane C_3H_8. Propylene C_3H_6 was detected as the main product (conversion 12.5%) next to

CO and CO_2. With vanadium oxide catalysts, propylene is usually detected only as a side product while CO and CO_2 are the main products in the oxidative dehydrogenation.[62]

1.2 C-X bond (X=Cl, F) activation

The overview in the previous chapter demonstrated that both ACF and *HS*-AlF_3 are excellent catalysts with a high potential for the activation of chlorofluorocarbons. The intensive research in this topic started in the 1980s.[63] The connection was made between commercial use of CFCs (as refrigerants, solvents or flame retardants [64]) and ozone depletion resulting in reduced absorption of UV radiation, which is harmful for living organisms. Thus, the activation of strong C-X (X=Cl, F) bonds became important. The first measures were inducted by the Montreal Protocol, whose provision included reduction of ozone depleting substances. As a result, the production and the use of CFCs were decreased. However, the negative effect on the stratospheric ozone layer has been already exerted. Next to health and conservation issues there is also a growing need for partially halogenated molecules. They are of special interest in agrochemicals and medicine. Such compounds behave as bioisosteres to non-fluorine containing substances.[65,66] They have been proven to have an essential advantage over non-halogenated compounds, because they are metabolically stable. Almost no natural fluoroorganic compounds exist and they can barely be composed naturally. The partially fluorinated compounds can be synthesized by cleavage and functionalization of C-F bond of readily available polyfluorinated substances.

Driven by these problematic environmental concerns and new possibilities to give access to partially fluorinated compounds, the demand on mild activation processes of C-F bond grew at a tremendous speed and it is still a subject of current research.

1.2.1 Different methods for the activation of C-F bond

1.2.1.1 Homogeneous catalyzed activation of C-F bond

The most studied systems include the homogeneous activation promoted by transition metals. The examples reported in the literature are mostly limited to the activation of $C(sp^2)$–F bonds. The activation mediated by transition metals involves an oxidative addition step utilizing electron rich metal centres. Ru, Rh, Ni, Pd and Pt have been found useful for the activation of aromatic or unsaturated fluorocarbons.[67–71] Subsequent follow-up reactions are mainly reductive defluorination and to a lesser extend cross coupling reactions. For the activation of

$C(sp^3)$–F bonds only a few examples of metal complexes based on Pd, Fe, Ir, Cu, Ni exist.[Review: 46, Ir: 50, Cu: 51, Ni: 52, 53]

Recently a strong focus in homogeneous C-F activation chemistry is on main-group Lewis acids. Using this type of approach, the activation of all aromatic, vinylic and alkyl fluorocarbons became possible. The pioneer in this field is Olah *et al.*.[77] The authors employed boron halides in stoichiometric amounts for Friedel-Crafts type reactions. Since then, other researcher groups also noticed the potential of Lewis acids exploiting the fluorophilicity of main group elements. In similar fashion, Ozerov *et al.*[49,78–80], Müller *et al.*[81], Siegel *et al.*[82–84], Roesky *et al.*[85] and very recently also Swamy *et al.*[86] used the property of silylium cations to form thermodynamically favored Si-F bonds. However, carbon[78] and aluminum electrophiles[87,88] as well as $B(C_6F_5)_3$[89] have emerged as promising tools for C-F bond activation too.[90] Rarely used lanthanide Lewis acids were also successfully established by Deacon and Werner *et al.*[91] as well as Hilmersson *et al.*[92].

Brönsted acids are only marginally explored as catalysts for C-F bond activation so far. This alternative protocol to Lewis acids was presented by Fei and Jinbo using trifluoroacetic, p-methylbenzenesulfonic acid and triflic acids in arylation reaction.[93] Recently the group of Moran reported the functionalization of C-F bond in Friedel Crafts reaction initiated by the strong Brönsted acid $B(C_6F_5)_3 \cdot H_2O$.[94]

Another interesting aspect of activation by main group elements are those with low valents, for example Al(I)-complexes. They demonstrate similar reactivity as Lewis acids towards activation of C-F bonds. Elucidation of this mechanism however showed that the pathway goes via oxidative addition and not via typical Lewis acid activation. This was postulated by Crimmin *et al.*[95] and Chu *et al.*[96] and was recently supported by theoretical calculations performed by Pitsch *et al.*[97].

In this work homogeneous catalysts were grouped in Lewis acid-bases, Brönsted acid-bases as well as transition metals. For heterogeneous catalysts this scheme cannot be applied mostly because of their amphoteric character. Also their physical properties like amount of surface has to be considered. This is why solid catalysts in the next section are arranged by the type of reaction they catalyze and not by strict separation of their chemical properties.

1.2.1.2 Heterogeneous catalyzed activation of C-F bond

The homogeneous catalysts described in the previous paragraphs can be applied to a broad range of substrates and offer high selectivity. What they lack is widespread industrial applications. In this area heterogeneous catalysts are much more useful. However, the literature in this field is limited. Such catalysts must possess sufficient level of stability for highly corrosive fluorine atoms, or otherwise they rapidly deactivate. Recently, Comas-Vives reported the activation of CH_3F on the surface of γ-Al_2O_3 at 200 °C.[98] Methyl fluoride is activated on the catalyst surface by its simultaneous fluorination. This leads to the formation of dimethyl ether and olefins like isobutene and 2-methylbutene (Scheme 16).

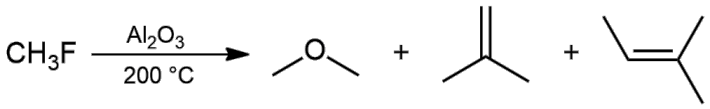

Scheme 16. Activation of fluromethane on Al_2O_3.

The highest achieved TON was only 0.6, which means that the reaction proceeded mainly stoichiometric. The catalyst was gradually fluorinated resulting in aluminium fluoride. The formation of new Al-F bonds was confirmed by ^{19}F MAS NMR spectroscopy. Besides bridged fluorine species, terminal ones were detected too. The terminal fluorine atoms are postulated to have some degree of catalytic activity. This suggests that the above reaction proceeds at least partially by activation via undercoordinated aluminium centres with terminal fluorine atoms. Nevertheless, this example demonstrates that oxides are not inert when exposed to organofluorine molecules. Similar observations were also made by e.g. Hess and Kemnitz *et al.* around 25 years ago.[99]

Similar observations were also made by other researchers.[100–102] For example Farris *et al.* detected the deactivation of the catalyst Pt/Al_2O_3 in the presence of perfluoro-propene which was attributed to fluorination of the catalyst`s support.[103]

Despite the deactivation of oxides by releasing fluoride, such catalysts are commonly applied as catalysts in two types of catalytic deconstruction reactions, namely oxidation and hydrolysis reactions. Karmakar and Greene studied the activation of dichlorodifluoromethane over titanium oxide in the presence of O_2 in a flow reactor (Scheme 17). [104] The catalyst achieved around 90% conversion at 300 °C with selectivity of 99% to CO_2.

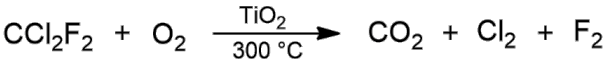

Scheme 17. Oxidation of dichlorodifluoromethane over TiO_2.

A short spike of increased conversion rate was observed before it started to drop. It was assumed that this higher conversion is related to higher surface acidity of formed aluminium fluoride, which is consistent with Comas-Vives results [98]. To avoid the deactivation of the catalyst, water was added to the system, which is a common technique to protect the catalyst from fluorination. No more loss in activity was detected after that.

An alternative approach to activate C-F bonds via oxidation is by metal pyrophosphates. Due to their weak acidic sites they have the advantage to be less reactive towards fluorination than oxides. This beneficial property was noticed by Onoda *et al.*[105] They investigated the activation of CH_3F in a stream of O_2 and H_2O. Around 70% conversion was achieved with NiP_2O_7 at 700 °C and reached 100% if magnesium was added (Mg:Ni in ratio 2:8). With this additive, the selectivity to CO_2 also increased from around 30% to 100%. The authors also investigated $AlPO_4$. This catalyst first showed better activity but it dropped after 5 h. Due to its stronger acidic sites and their larger number the catalyst´s fluorination is encouraged in contrast to pyrophosphates.

Cheap and readily available metal oxides under aqueous conditions are often applied not only in oxidation but also in hydrolysis reactions. The benefits of adding water lies in formation of hydrogen halides, which are less reactive than free halogens produced in oxidation reaction. Consequently, the catalyst´s reactivity is prolonged. Moreover, hydrolysis is thermodynamically favored compared to oxidation processes.

Hess and Kemnitz propsed a hydrolysis of dichlorodifluoromethane at 500 °C using ZrO_2/ ammonium sulfate in a flow reactor. The substrate was converted to CO_2 with 92-98% conversion. Traces of chlorotrifluoromethane were detected as well.[106]

Feaver and Rossin investigated ZrO_2-SO_4-catalyzed continuous flow hydrolysis of CHF_3 in humid air. [107] The substrate was activated to CO and CO_2 with 100% conversion at 400 °C.

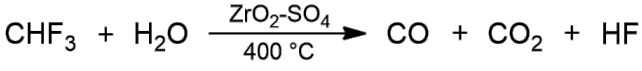

Scheme 18. Hydrolysis of CHF_3 in humid air over ZrO_2-SO_4.

More recently, Han *et al.* published results of catalytic hydrolysis of CH_3F.[108] α-Al_2O_3, γ-Al_2O_3 and AlOOH were tested as potential catalysts. 66% of the substrate was converted in the presence of γ-Al_2O_3 at 520 °C whereas with AlOOH the conversion increased to 85%. As expected, α-Al_2O_3 gave the lowest conversion of around 10% only due to its smallest surface area. The best results were achieved not with the catalyst of highest surface area (γ-Al_2O_3) but with AlOOH. Both chemical and physical properties seem to have an impact on the conversion. The positive water effect was observed here as well. A higher concentration of water retarded the catalyst`s deactivation but did not increase its activity.

Another interesting example was recently presented by Papaianina and Amsharov.[109] 2-Trifluoromethyl-biphenyl was converted in the presence of γ-Al_2O_3 via two competing mechanisms, hydrolysis and intramolecular condensation, as shown in Scheme 19. The products were 2-biphenyl carboxylic acid and 9-fluorenone with a total conversion of around 20% at room temperature. Only 5% of the substrate was transformed to 9-fluorenone. The selectivity towards ketone was shifted if the catalyst was heated and thereby releasing water. The reaction did not proceed catalytically due to strong catalyst degradation.

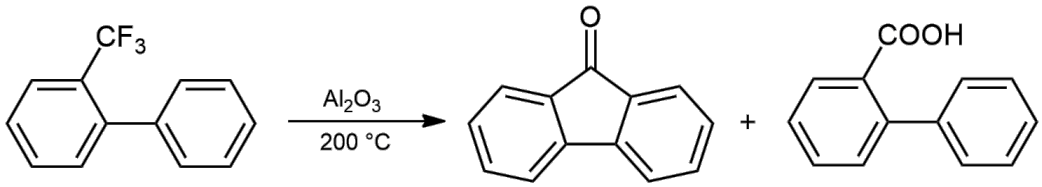

Scheme 19. Simultaneous hydrolysis and intramolecular condensation reaction by activation of 2-Trifluoromethyl-biphenyl.

Most approaches presented above were carried out at high temperatures. Under these conditions pyrolysis is also a potential pathway for decomposition of chlorofluoro-carbons, with first reports from the early '70s.[110] Since then, several examples of pyrolysis and elucidation of its mechanism have been published.[111–115] More recently, Han *et al.* proposed the pyrolysis of CHF_3 over $K_{2-x}O$/activated carbon.[116] At the space velocity of 4300 h^{-1} and at 800 °C the conversion reached 61%. The selectivity to tetrafluoroethylene was 33% and to hexafluoropropylene 24%. CF_4, C_2F_6 and C_3F_8 were formed as side products.

For hydrolysis, oxidization as well as pyrolysis processes not only C-F bonds are broken, but simultaneously the weaker C-Cl bonds are also affected. Thus, all reactions presented above can be also applied for the activation of chlorinated compounds.

Another possibility for decomposition of fluoromethanes relies on alkali hydroxides or carbonates. Vakulka *et al.* used acid-base theory as a basis for this approach.[117] For example, CHF_3 reacted with NaOH resulting in around 94% conversion at relatively low temperature of 250 °C, as shown in Scheme 20.

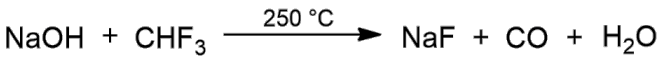

Scheme 20. Reaction of NaOH with CHF_3.

Besides activation of fluoromethanes in catalytic decomposition, they can also be transformed to reactive and useful intermediates like hydrofluoroolefines. Han *et al.* tested the reactivity of Lewis acid $CaBr_2$ at 840 °C in the reaction of CHF_3 with CH_4 in a flow reactor.[118] Under these conditions $CaBr_2$ is fluorinated to CaF_2, which is also catalytically active. Small amounts of CH_3Br and HBr were detected as a result of the fluorination of the catalyst. Around 23% of CH_4 and 36% of CHF_3 were converted to the main product $CH_2{=}CF_2$ with TOF= 1.854 mmol/h. The side products C_2H_2, C_2HF_3, C_2H_4, C_2F_4, C_3F_3 and HF were also detected.

The proposed mechanism involves initial activation of CHF_3 and formation of CF_2, which then decomposes on the catalyst´s surface, leading to its fluorination.

Many of the transformations presented in the previous examples involve an activation of C-F bonds into C-O or C-C bonds. However, the simplest mechanism for such activation is still hydrodefluorination.

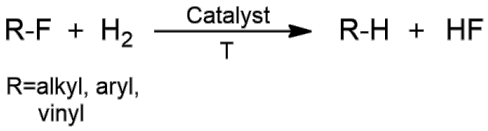

Scheme 21. Generic scheme of hydrodefluorination reactions.

Heterogeneously catalyzed hydrodefluorination found in the literature are typically applied to fluorinated aromatic compounds.[119–122] Only a few examples for hydrodefluorination of $C(sp^3)$–F bond not originating from Kemnitz group were published until now. Especially Pd-based catalysts were proven to be suitable. Coq *et al.* studied hydrodehalogenation of CF_2Cl_2 in the presence of H_2 at atmospheric pressure and 453 K using Pd black or Pd/AlF_3 as catalyst.[123] The conversions were 4.7% and 8.8%, respectively. For both catalysts the selectivity to CH_4 and CH_2F_2 was over 90%. However, the kind of catalyst´s support influenced

the distribution of the products. For Pd black the selectivity to CH_4 was 45% and to CH_2F_2 53%. Using Pd/AlF_3, the selectivity for CH_4 decreased to only 17%, but was 78% for CH_2F_2. The mechanistic investigation has demonstrated that the defluorination step occurs only after previous activation by hydrodechlorination reaction. Similar observations were made by Borokov *et al.*.[124] The authors observed that cleavage of the first C-Cl bond is the limiting step in the hydrodehalogenation of CF_3CFCl_2 on Pd/γ-Al_2O_3. Using FTIR the formation of surface species $CF_3CF=$ and $CF_3C\equiv$ was observed, which in the presence of H_2 underwent subsequent hydrogenation.

Another interesting example was published by Huang *et al.*.[125] The authors demonstrated the photoinduced hydrodefluorination of perfluorooctanoic acid in the presence of aminopropyltrimethoxysilane over SiC/Graphene catalyst at room temperature. The probable main product was $CF_3(CF_2)_4CH_3$, which formation was proven by QE-MS/MS. The highest conversion was about 58.5% (k= 0.096 h^{-1}).

1.2.2 Different methods for the activation of C-Cl bond

The amount of literature covering C-F activation is relatively small. The two main reasons are catalyst deactivation by fluorination and high activation energy of C-F bond. In contrast, literature covering C-Cl activation is much more abundant. Due to its lower activation energy it is easier to find appropriate activation conditions. The increased dissociation ability of chlorine to form radicals and thus environmental problems also made C-Cl activation a more attractive field of research. There have been many reports of activation of both aryl and alkyl chlorides. Because of the extensive volume of publications in this topic, only selected examples will be presented here.

1.2.2.1 Homogeneously catalyzed activation of C-Cl bond

Most literature about activation of C-Cl bonds by homogeneous catalysis covers transition-metals-catalyzed cross coupling reactions. The majority of reported catalysts are based on palladium, nickel and iron.[126,127] Such catalysts allow the activation of an extensive range of compounds, particularly organic iodides and bromides. During the course of research the scope of substrates was extended to their cheaper but less reactive chlorinated counterparts. Homogeneous ly catalyzed cross coupling reactions with aryl or olefinic substrates were reviewed in detail for example by Colacot and Snieckus *et al.*[127] and more recently by Wang and Guo.[126]. Using alkyl halides as substrates is less common. Panda and Jena[128] as well as Rudolph and Lautens[129] postulated that the oxidative addition is hindered due to the lack of

interaction of π electrons with the empty d orbital of the metal center. Additionally, alkyl metal intermediates are prone to undergo ß-hydride elimination. Nevertheless, Kochi and Tamura[130] demonstrated that alkyl halides are applicable in cross-coupling reactions and since their pioneering work many reactions for C(sp^3)–Cl activation were developed.[128,129,131,132]

1.2.2.2 Heterogeneously catalyzed activation of C-Cl bond

The cross coupling reactions can also be carried out successfully by heterogeneous catalysts.[133–136] The first publication dates back to 1973, when Julia *et al.* studied the Heck reaction using Pd/C as catalyst.[137] In contrast to homogeneous catalysts, where more examples of alkyl-alkyl cross coupling reactions can be found, the literature for heterogeneous activation of C(sp^3)-Cl is rare.[138–140] Kim and Chung demonstrated that copper nanoparticles performed well in the cross coupling of alkyl chlorides and various Grignard reagents.[141] For example n-octyl chloride reacted with tertbutyl magnesium chloride yielding 87% conversion at 80 °C after 12 h (Scheme 22).

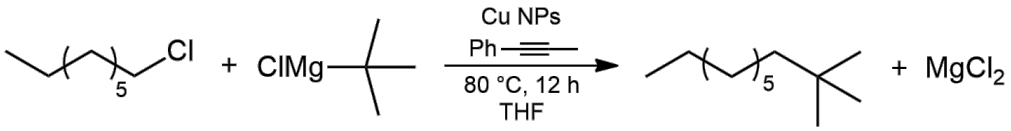

Scheme 22. Cross coupling of n-octyl chloride reacted with tertbutyl magnesium chloride.

Another way to make use of C-Cl activation are hydrodechlorination reactions. By a similar mechanism as in the hydrodefluorination reaction, chlorine atoms are replaced by hydrogen atoms, as shown in Scheme 23.

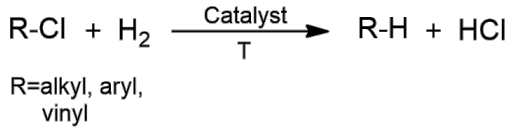

Scheme 23. Generic scheme of hydrodechlorination reactions.

While cross-coupling reactions are well established and explored as of today, research on hydrodechlorination started intensively only in the early 2000s. Numerous studies were conducted; especially Pd/C catalyzed hydrodechlorinations were in focus of research.[60,142,143] For example Álvarez-Montero *et al.* proposed the activation of $CHCl_3$ in the presence of H_2 at 125 °C.[144] The major product CH_4 was formed with conversion of 67% and selectivity of 88%. The partially hydrodechlorinated products CH_2Cl_2 and CH_3Cl were also detected.

A similar approach was introduced by Makkee *et al.*.[145] The authors tested different metals supported on carbon in the transformation of CCl_2F_2 in a micro flow reactor. The highest conversion of 80% was achieved by Pd/C after 8 h on stream at around 235 °C. CH_2F_2 was formed with selectivity of 70%, next to side products $CHClF_2$ and CH_4. More recently, similar results were reported by Martin-Martinez *et al.*.[146]

Pd/C is a broadly applicable catalyst because carbon is a very inert support. The reason to look out for other supports is to alter the activity and selectivity of the catalyst. Aytam *et al.* reported the activation of CCl_2F_2 over Pd/MgO and Pd/γ-Al_2O_3 in the presence of H_2 as hydrogen source.[147] Using Pd/MgO the reaction yielded 70% conversion at 250 °C. The distribution of the products was similar when Pd/C was applied. 64% of the substrate reacted to CH_2F_2 and 33% to CH_4. It is assumed that the basicity of MgO suppressed the formation of C_2 oligomers which were observed in increased amounts using different catalyst supports e.q. SiO_2 or ZrO_2.[148] Further, it retards coke formation and therefore prolonging the catalyst´s life. Using Pd/γ- Al_2O_3 as catalyst the conversion decreased to 27% while product distribution also changed. CH_2F_2 and CH_4 were formed with around 50% each conversion.

Oxides supports are prone to further fluorination with full loss of the catalyst´s activity. Faced with these problems described in the literature, metal fluroides were tested as a support for the activation of mixed halocarbons.[149] According to Deshmukh and d`Itri Pd/AlF_3 exhibits much lower reactivity in the activation of CCl_2F_2 with only 10% conversion.[150]

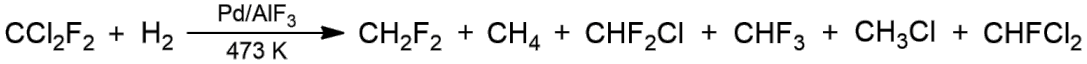

Scheme 24. Activation of CCl_2F_2 in the presence of H_2 with Pd/ γ-AlF_3.

However, the selectivity toward CH_2F_2 increased to 69%, whereas CH_4 was formed with selectivity of 18%. Partially hydrodehalogenated products CHF_2Cl and CH_3F were detected as well. An interesting issue arose when the formation of CH_3Cl and $CHFCl_2$ was observed. At first, it might suggest that hydrodefluorination dominates over hydrodechlorination. Considering the bond strengths of C-F and C-Cl bond, it is more likely for back-chlorination at the surface to occure than C-F band activation. Long-term investigations over 12 h showed only slightly reduced TOF. Fluoride supported catalysts gave constant conversions in contrast to oxide supported catalysts.

Furthermore, Pd supported on aluminum fluoride seems also to be an appropriate catalyst for a wide scope of substrates, e.q. halogenated ethanes. Berndt *et al.* have described the hydrodechlorination of CCl_2FCF_3 on Pd/β-AlF_3 and Pd/C at 473 K and a contact time of 1 s in the presence of H_2.[151] With regard to the reactivity and selectivity both catalysts were almost similar. The reaction yielded around 95% conversion and the selectivity towards CF_3CH_2F was 78% for both catalysts. Compared to Pd/AlF_3 from the previous example a higher conversion was achieved probably due to two reasons. The longer the carbon chain in the activated molecule is, the more stable cation results, which in turn leads to higher yield. Also, in contrast to AlF_3, β-AlF_3 possesses exclusively Lewis acidic sites resulting in higher reactivity for this reaction.

However, 10% yield for Pd/AlF_3 catalyst in the activation of CCl_2F_2 is a rather low conversion rate. It is assumed that the reactivity of metal could be enhanced by different interactions with the acidic support if it was high surface substance. Thus, Patil *et al.* proposed the use of Pd supported on *HS*-AlF_3, which was already described in the C-F bond activation section.[59] In this study authors activated $CHClF_2$, another abundant chlorofluorocarbon. Thus, the results cannot be compared directly with previous studies. However, next to the hydrodehalogenation products $CHClF_2$, CH_3F and CH_4, also CHF_3 was detected. This result led to the conclusion that the hydrodehalogenation competes with dismutation reaction, which occur typically for catalysts of high Lewis-acidity. The simultaneous dismutation decreases the selectivity to the desired product.

H_2 is the standard hydrogen source for hydrodehalogenation reactions besides formic acid, isopropanol and hydrazine.[152] Methanol can be employed as well, also in heterogeneous systems.[153] An efficient protocol was reported by Lu *et al.* for the activation of CCl_4 in the presence of CH_3OH by Ag/C in a batch reactor at 403 K (Scheme 25). The reaction yielded up to 90% conversion to $CHCl_3$ and CH_2Cl_2 after 9 h.

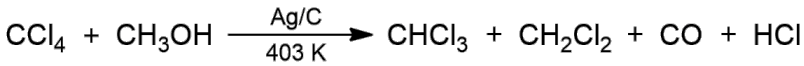

Scheme 25. Activation of CCl_4 in the presence of CH_3OH by Ag/C.

After discussion of catalytic activities of the classic metal centers on various supports and their influences on the reactivity, it was thought that supports themselves can also be used as

catalysts. Thus, in this work *high-surfaces* Lewis acids were tested as catalysts for hydrodehalogenation and hydrosilylation reactions.

1.3 Hydrosilylation

As already mentioned, a further useful application of Lewis acidic catalysts are hydrosilylation reactions.[154] This literature summary shall only cover a few examples but give no detailed literature survey, as it is not the main topic of this thesis.

The hydrosilylation involves the addition of silane to organic substances containing unsaturated bonds like carbonyls, as shown in Scheme 26 on the example of butanone and Et_3SiH. The main product of this reaction is silyl ether, which can easily be hydrolyzed to the corresponding alcohol. In some cases over reduction lead to the corresponding alkenes and alkanes.

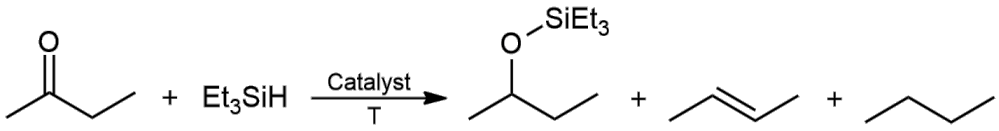

Scheme 26. Generic scheme for hydrosilylation reactions.

1.3.1 Homogeneously catalyzed hydrosilylation reactions

In contrast to hydrodehalogenation, research on homogeneously catalyzed hydrosilylation started much earlier with the first publication by Sommer *et al*. in 1947.[155] The authors described the reaction of silane with 1-octene in presence of diacetyl peroxide to n-octyltrichlorosilane at 63 °C with 46% yield. Silanes offer the advantage of mild reaction conditions when compared to other reducing agents. In addition, silanes mostly yield anti markownikow products which are more difficult to obtain by other methods. Despite these advantages only a decade later this concept was applied to carbonyl groups. Gilman and Wittenberg reacted phenylsilane with benzophenone without any additives (Scheme 27).[156] The reaction yielded 65% of bis(benzohydryloxy)phenylsilane as main product next to 20% of benzohydryloxyphenylsilane at 250 °C after 3 h.

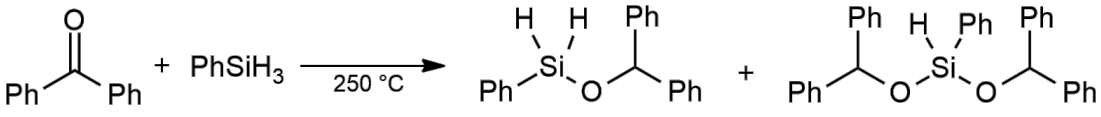

Scheme 27. Hydrosilylation of benzophenone with phenylsilane.

As an alternative for temperature sensitive conversions, hydrosilylations can also be performed by UV irradiation.[157] Photoinduced silylation is a useful method for the functionalization of silicon surfaces. [158]

Similar to C-F and C-Cl bond activation carried out by homogeneous catalysts, the transition metal mediated hydrosilylation is the most common procedure. Within this group the rhodium complexes are the most prevalent.[159] In 1972 Ojima *et al.* achieved promising results using Wilkinson's rhodium(I)complex $RhCl(PPh_3)_3$ in the hydrosilylation of terpene[160], which shortly after was also applied to catalytic asymmetric hydrosilylation of alkyl phenyl ketons.[161] The field of Rh-catalysis is still actively explored until today. For example, in 2007 Bantu *et al.* reported a high activity of $[RhCl(CH_3CONPy_2)(COD)]$ in the hydrosilylation of benzophenone.[162] The reaction led to 97% conversion (TON= 48500) at 70 °C after 1.5 h.

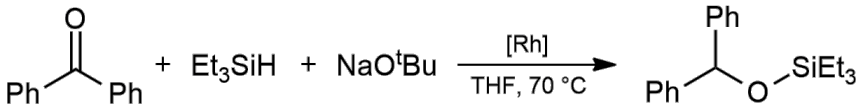

Scheme 28. Hydrosilylation of benzophenone mediated by Rh-based catalyst.

The suggested reaction mechanism is most likely based on Ojima's proposed pathway from 1972 (Scheme 29). The oxidative addition of R_3SiH (R= e.q. Ph, Et) to the metal center is followed by coordination of the carbonyl group. Silicon migrates from the metal center to the carbonyl donor. After carbonyl insertion into Rh-Si bond, the final step is the reductive elimination of silyl ether.

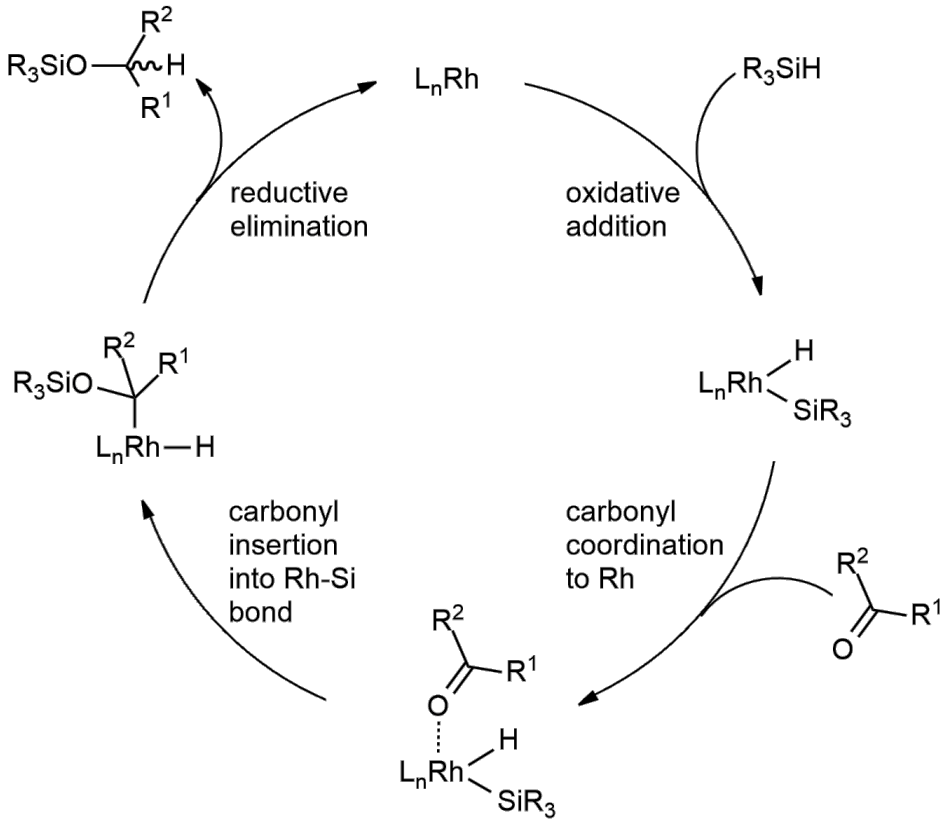

Scheme 29. Ojima's mechanism for hydrosilylation of ketone with monohydrosilane.

Further studies performed by Schneider, Hoffmann and Gade *et al.* revealed that this mechanism is applicable for R_3SiH but not for R_2SiH_2.[163] Kinetic isotope effects and increase in reaction rate using dihydrosilanes suggest that another mechanism must be involved (Scheme 30). The authors proposed, similarly to Oijama`s mechanism, that silane undergoes oxidative addition to the metal center. In contrast to the previous pathway, formation of silylene by simultaneously H-transfer occurs, the latter being the rate determining step. Additionally, carbonyl coordinates to the highly Lewis acidic Silicon and not to the metal center.

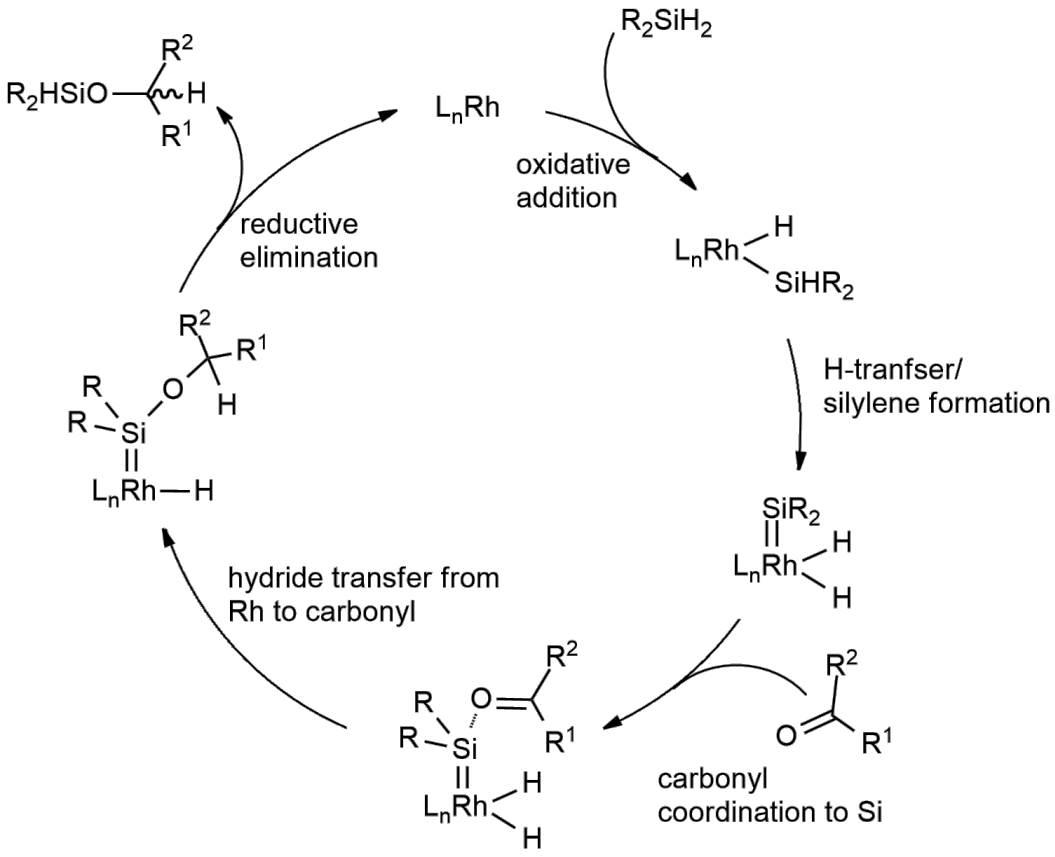

Scheme 30. Mechanism for the hydrosilylation of ketones with di- and trihydrosilane.

Although rhodium catalysts show high reactivity, the limiting factor for its use is high cost of this metal. Thus, less expensive metal complexes based on iridium[151,152], ruthenium[166], platinum or palladium[167] were explored as well. Also catalysts based on environmentally friendly metals, such as copper[168] or iron[169,170] have emerged as good catalysts. Especially the abundance and nontoxicity of iron make it very attractive. Despite these advantages the research on iron-based catalysts only started with Brunne`s and Fisch`s report in 1990 [171] and is still being pursued as of today. More recently, Addis *et al.* investigated $Fe(OAc)_2$ with different ligands in the activation of aceto-phenone (Scheme 31).[169] The reaction yielded 99% conversion at 65 °C after 16 h, but only poor enantioselectivity was achieved with (S)-binap as ligand. However, using other ligands ee values rose up to 80%.

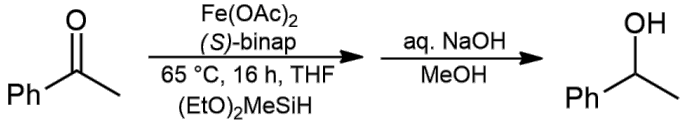

Scheme 31. Asymmetric hydrosilylation of acetophenone in the presence of $Fe(OAc)_2$.

Early transition metals and group 11 and 12 transition metals don't react according to the classic mechanism of oxidative addition but follow a σ-bond metathesis pathway to form an initial metal hydride species. Ti-based catalysts being in their highest oxidation state are typical examples for catalysts, which disfavor the oxidative addition step. Buchwald and Yun studied the hydrosilylation of ketons mediated by *(R,R)*-(EBTHI)TiF_2 in the presence of polymethylhydrosiloxane.[172] The activation of isopropyl phenyl ketone gave 17% conversion and 90% enantioselectivity to corresponding secondary alcohol at 60 °C after 39 h.

Earlier research suggested that σ-bond metathesis mechanism is only possible with early transition metals with d^0 configuration. Recent studies by Bleith and Gade revealed that it can also be applied to complexes involving late transition metals like iron, especially such with alkoxide ligands.[173]

Another mild approach to catalyze hydrosilylation reactions is by Lewis acids. In an early contribution, successful carbonyl hydrosilylation utilizing $ZnCl_2$ as catalyst was presented by Calas in 1966.[174] Since then many examples were reported where Lewis acidic catalysts were demonstrated to be good catalysts for hydrosilylation.

In 1996 Piers *et al.* reported the use of $B(C_6F_5)_3$.[175] Its advantage over classic Lewis acids is the insensitivity towards air and water (Scheme 32). The activation of acetophenone resulted in 76% conversion (TON = 45 h^{-1}) to the corresponding silyl ether at room temperature. Mechanistically, instead of activating carbonyl, silane is activated first. Closer examination showed that an excess of carbonyl inhibits the reaction. Thus, silane is activated first.

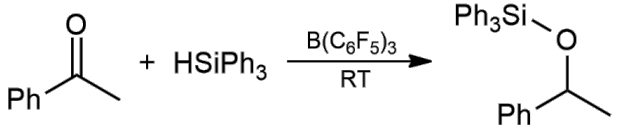

Scheme 32. $B(C_6F_5)_3$-catalzyed hydrosilylation of acetophenone.

These types of hydrosilylations do not always stop at the silylether or alkohol intermediate but can proceed further to be reduced down to the alkene and alkane. $B(C_6F_5)_3$ was discovered by Mahdi and Stephan to catalyze the deoxygenation of acetophenone (Scheme 33).[176] The reaction was carried out in the presence of H_2 and molecular sieve, the latter acting as the corresponding Lewis base. Styrene was formed with 92% yield at 70 °C after 12 h.

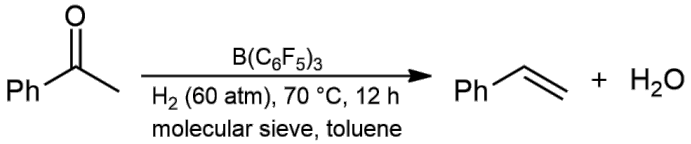

Scheme 33. Deoxygenation of acetophenone using $B(C_6F_5)_3$ as catalyst.

Analogous activation of benzophenone proceeded to ethylbenzene with 81% yield (Scheme 34).

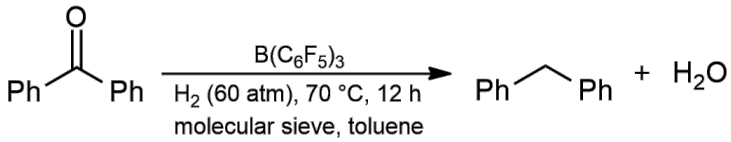

Scheme 34. Deoxygenation of benzophenone using $B(C_6F_5)_3$ as catalyst.

As hydrogen and not silane acted as hydride source in this case these three reactions can not be directly compared.

A related concept was developed using Al-based Lewis acids. However, most of the reports are limited to hydrosilylations of alkenes, especially where $AlCl_3$ was used.[177] To the best of my knowledge Koller`s and Bergman`s report is the first example of Al-based catalyst for carbonyl hydrosilylation (Scheme 35). The authors investigated [Tp*AlMe][$MeB(C_6F_5)_3$] in the hydrosilylation of acetophenone. Using 4 mol% catalyst and $HSiEt_3$ as hydride source, the reaction delivered >98% conversion at 75 °C after 19 h. Interestingly, using only 1.7 mol% catalyst was sufficient to give the same conversion after only 1.5 h when H_3SiPh was used. The main product of the reaction was the corresponding silyl ether.

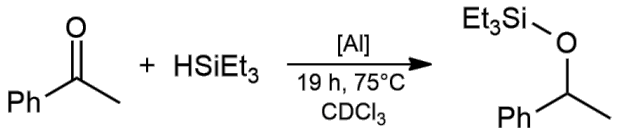

Scheme 35. Activation of actophenone using Al-based catalyst.

Similar to the previous example, also classical Lewis acids can facilitate the course of the reaction down to the alkanes. Choi und Kang employed $GaCl_3$ in the deoxygenation reaction of acetophenone (Scheme 36).[178] The reaction proceeded to give ethylbenzene with 99% conversion at 0 °C after 10 min.

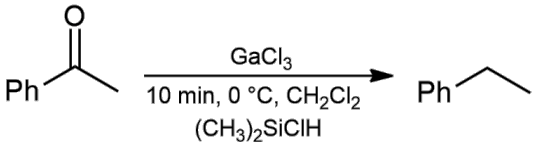

Scheme 36. $GaCl_3$-catalyzed deoxygenation of acetophenone.

1.3.2 Heterogeneously catalyzed hydrosilylation reactions

Besides those types of catalysts already mentioned, the second important class are heterogeneous catalysts, most of which are metallic nanoparticles. Corma *et al.* discovered that colloidal Au^0-nanoparticels promote full conversion of acetophenone in the presence of Ph_2SiH_2 to the corresponding silyl ether at 70 °C after 2 h (TON = 20) (Scheme 37).[179]

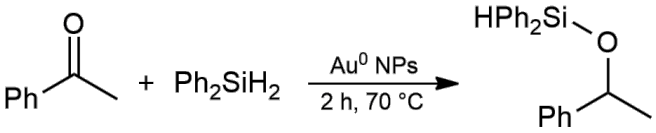

Scheme 37. Hydrosilylation of acetophenone carried out by Au-nanoparticels.

Besides metallic nanoparticles also their oxides were successfully tested. Kantam *et al.* proposed the use of nanocristalline CuO. [169] In the presence of $PhSiH_3$ and chiral compound 2,2′-bis(diphenylphosphino)-1,1′-binaphthyl ((S)-BINAP) the transformation of acetophenone to the corresponding alkohol resulted in 95% conversion and 77% ee after 30 min at room temperature. Using Ph_2SiH_2, only 30% yield, but still with 76% ee after increased reaction time to 24 h was achieved. No conversion was detected when applying Et_3SiH.

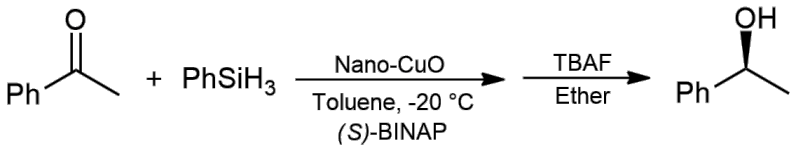

Scheme 38. Asymmertic hydrosilylation of acetophenone using nano-CuO.

Kawanami *et al.* published an interesting example where they loaded Al_2O_3 with KF to prepare an active catalyst to promote the hydrosilylation reaction (Scheme 39).[180] The reaction proceeded to methylbenzyl dimethylphenylsilyl ether giving 54% yield at 353 K in 20 h.

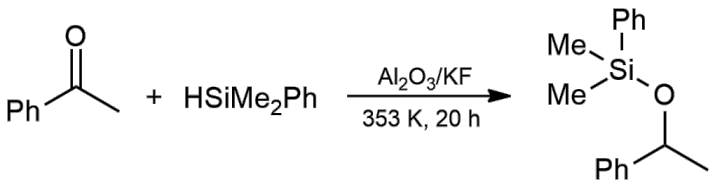

Scheme 39. Hydrosilylation of acetophenone in the presence of dimethylphenylsilane.

The successful use of palladium supported on carbon for the hydrosilylation of different carbonyl compounds was reported by Volkov *et al.* (Scheme 40).[181] The reaction proceeded well for a range of ketones. 4-Methoxyacetophenone was activated in the presence of Et_3SiH. The reaction delivered 67% conversion to the corresponding alcohol and 33% to the corresponding alkane at 65 °C after 16 h. The conversion to the corresponding alcohol increased when using $PhSiH_3$.

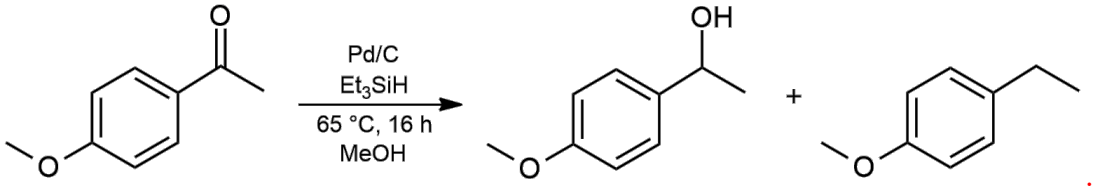

Scheme 40. Ketone deoxygenation on Pd/C in the presence of Et_3SiH.

The combination of large pores/high surface area nanoparticles with the high reactivity of metals resulted in metal–organic frameworks (MOF). MOF are also known to be chemically stable. In pioneering work, Addis *et al.* showed that MOF-catalyzed hydrosilylations are feasible.[182] Using $Cu_3(BTC)_2$ BCT= 1,3,5-benzenetricarboxylate as catalyst, acetophenone reacted with $PhSiH_3$ and base to yield full conversion to the corresponding alcohol at room

temperature after 16 h. Note that the conversions are successful in the presence of $PhSiH_3$, whereas almost no product formation is observed with Ph_2SiH_2.

A promising technology for hydrosilylation is the application of metal-free catalysts too. Poly-N-heterocyclic carbene polymer (Poly-NHC) has attracted some interest as it is recyclable and environmentally friendly.[183] The catalyst was active in the transformation of acetphenone to silyl ether at room temperature. The recycled catalyst achieved the same conversion when applied in two more consecutive reactions.

Recently the focus was shifted towards immobilized catalysts, which are regarded as crossover between classic homogeneous and heterogeneous catalysts. Hamasaka *et al.* proposed the use of $[RhCl(C_2H_4)_2]_2$ immobilized on a trialkylphosphane modified silica gel surface ([silica]-SMAP) for hydrosilylations.[184] The transformation of 2,4-dimethyl-3-pentanone in the presence of Et_3SiH to the corresponding silyl ether proceeded with 99% conversion at room temperature after 4 h. When a sterically demanding ketone was activated under the same conditions, the reaction needed 12 h to achieve a similar conversion.

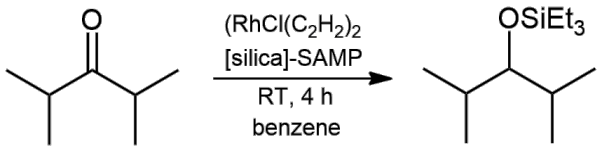

Scheme 41. Hydrosilylation carried out by the silica supported Rh-based catalyst.

Other metals like copper can be immobilized as well at the surface of a carrier material. Lipshutz *et al.* examined the activity of in situ prepared [(DTBM-segphos)CuH] supported on charcoal in hydrosilylation (Scheme 42).[185] The activation of acetophenone in the presence of an excess of poly(methylhydrosiloxane) gave 95% yield at -50 °C after 8 h. However, the authors observed leaching of the catalyst.

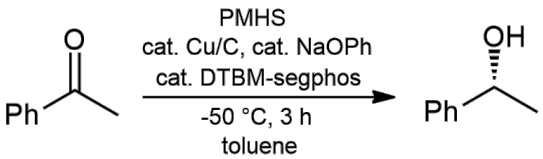

Scheme 42. [{(R)·(-)·DTBM·segphos}CuH]·in·charcoal – catalyzed asymmertic hydrosilylation.

1.4 Methods

In this section the analytical methods and devices used for the characterisation of the catalysts will be introduced.

1.4.1 Nuclear magnetic resonance (NMR)[186]

NMR is one of the most essential non-destructive, non-selective analytical tools for determining the molecular structure of chemical compounds. All nuclei possessing non-zero spins, which equal to non-zero magnetic moments **μ**, can be detected in NMR experiments. To be precise, all nuclei with an odd number of protons and/or neutrons such as ^{1}H, ^{13}C, ^{29}Si, ^{19}F are NMR-active isotopes. Standard reaction conditions require a high natural abundance of the nuclei. If this requirement is not met, measurment conditions must be adapted to run a successful experiment.

Both liquids and solids can be investigated. Advantageously, not only crystalline but also amorphous materials like heterogeneous catalysts can be examined.

During NMR experiments, a sample is immersed in the external magnetic field $\mathbf{B_0}$. After turning on $\mathbf{B_0}$, the degeneracy of energy levels will be lifted resulting in its separation, which is called nuclear Zeeman splitting, as shown in Figure 6.

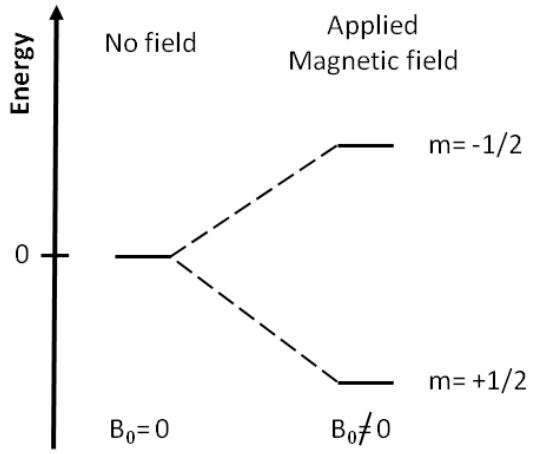

Figure 6. Energy level separation for a nucleus with spin quantum number I= ½ and corresponding magnetic quantum number **m**, with and without an applied magnetic field $\mathbf{B_0}$.

If the electromagnetic radiation matches the energy gap (resonance conditions, the so-called Larmor frequency), the spins with a low energy orientation will be excited to a higher energetic level according the Boltzmann distribution law (a small excess in lower state α

(m= +1/2) compared to β (m= -1/2)). The frequency of the radiation depends on the type of nucleus, its chemical environment and the external magnetic field $\mathbf{B_0}$. This energy absorption establishes the basis for each NMR experiment.

As mentioned before, structural information of compounds with NMR-active nuclei can be obtained in NMR experiments. The position of signals in the NMR spectrum is known as the chemical shift, which is measured relative to a reference compound, e.g. C_6D_6 for ^{13}C and ^{1}H. Such a signal shift is affected by the chemical environment of the nucleus. In other words, the arrangement of electrons in chemical bonds depends on its vicinity resulting in signals at different shifts in the spectrum.

However, distinguishing signals in solid state NMR is much more complicated than for liquid NMR. Unlike sharp transitions in high resolution liquid NMR, the lines in solid state NMR are broadened due to the occurrence of anisotropic interactions, dipolar coupling effects and possible quadrupolar effects. Nonetheless, these interactions can be averaged out by sample rotation around the axis at an angle of 54.7° oriented toward the external magnetic field, which is called Magic-Angle-Spinning (MAS).

1.4.1.1 The single-pulse experiment

The single-pulse experiment is the simplest NMR experiment. At the beginning of the experiment, the spin system is in equilibrium when the sample is exposed to magnetic field $\mathbf{B_0}$ (Figure 7, **1**). The nuclear moments **μ** will be distributed to the higher energetic state resulting in equilibrium magnetisation **2**, **M**, along the z-axis. After the 90° impulse **3**, the equilibrium will be disturbed and macroscopic magnetisation vector **M** will be deflected from the z- to y-axis, which creates transverse magnetization. The spins start to precess in the xy plane **4**. Due to field inhomogeneities, the spins precess at different speeds and lose their arrangement **5**. After a short time, the transverse magnetization decays exponentially to zero (spin-spin relaxation, $\mathbf{T_2}$) while the longitudinal magnetization is re-established (spin-lattice relaxation, $\mathbf{T_1}$). The spin system steadily returns to the z-direction **6**. The signals caused by changes in transverse magnetization are measured as free induction decay (FID), which in turn can be converted into a NMR spectrum by the Fourier transformation. This experiment is especially suitable for ^{1}H nuclei. In this study, it will be used for the measurement of catalysts preloaded with different substrates to clarify the bond situation and to investigate the interactions between substrates and active sites.

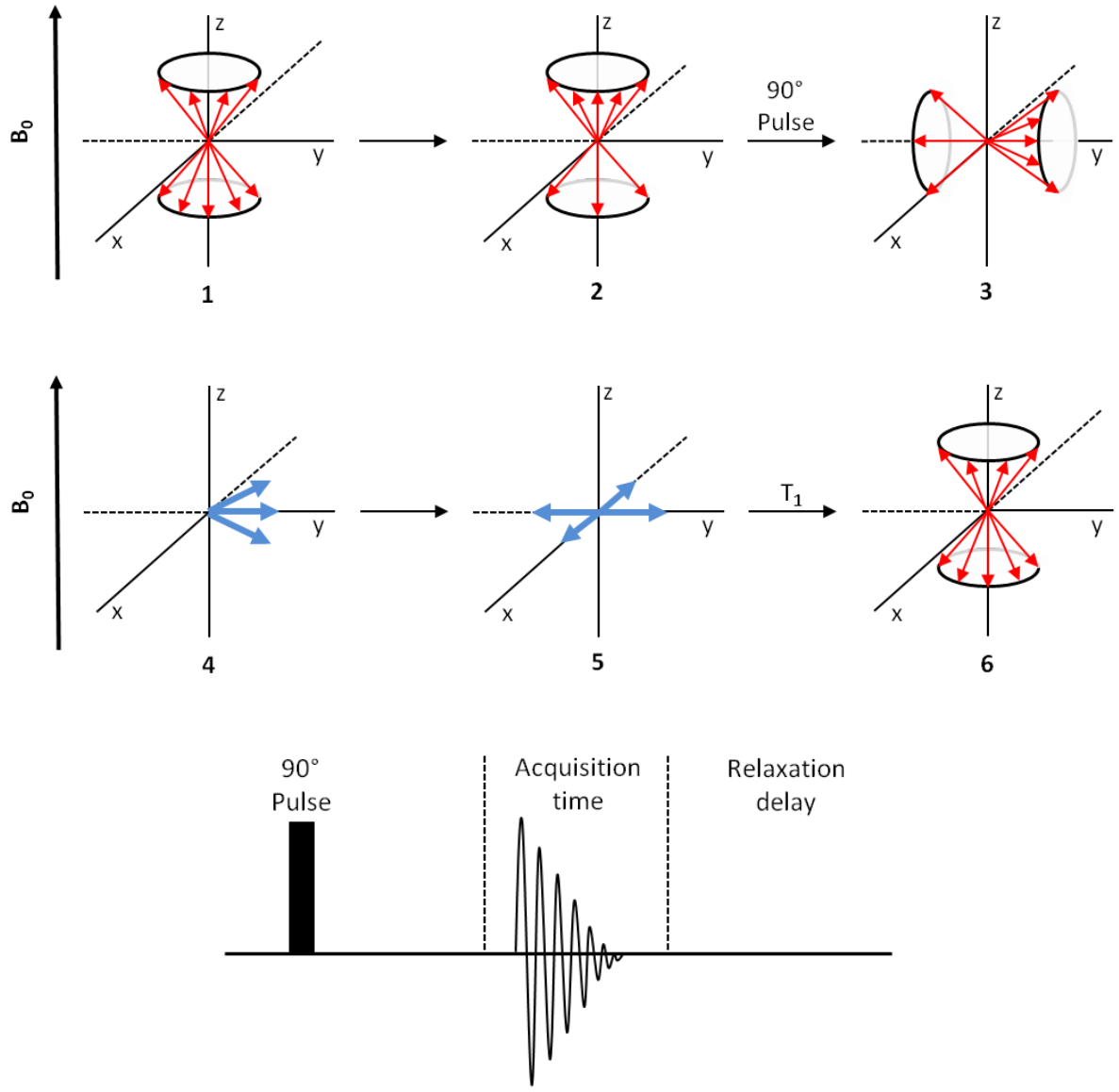

Figure 7. The single-pulse experiment**.**

1.4.1.2 Cross polarization experiments

Cross polarization (CP) experiments are used for measurements of species which suffer from low inherent sensitivity e.g. ^{13}C. Low natural abundance is often associated with species characterized by long spin-lattice relaxation time resulting in weak signals in the NMR spectrum. In order to overcome this problem, the presence of sensitive species with high natural abundance e.g. ^{1}H is exploited. To enhance the signal of ^{13}C, the magnetization is transferred from species ^{1}H to species ^{13}C via heteronuclear dipolar interactions, as shown in Figure 8. Therefore, sensitive species must be located in close proximity to those with low sensitivity so that a direct interaction between these two magnetic poles is possible. At the same time, the spins oscillate with identical frequencies, which can be achieved by adjusting the strength of

the magnetic field. Thus, the so-called Hartmann Hahn condition can be established. The maximal intensity enhancement for the insensitive species is $\gamma(^{1}H)\cdot\gamma(^{13}C)^{-1}$, where γ is a gyromagnetic ratio. The measurements are carried out by decoupling of the abundant nuclei. What is beneficial is that, the recycle time is governed by the abundant nuclei, which can significantly shorten the measurement time for species with low natural abundance.

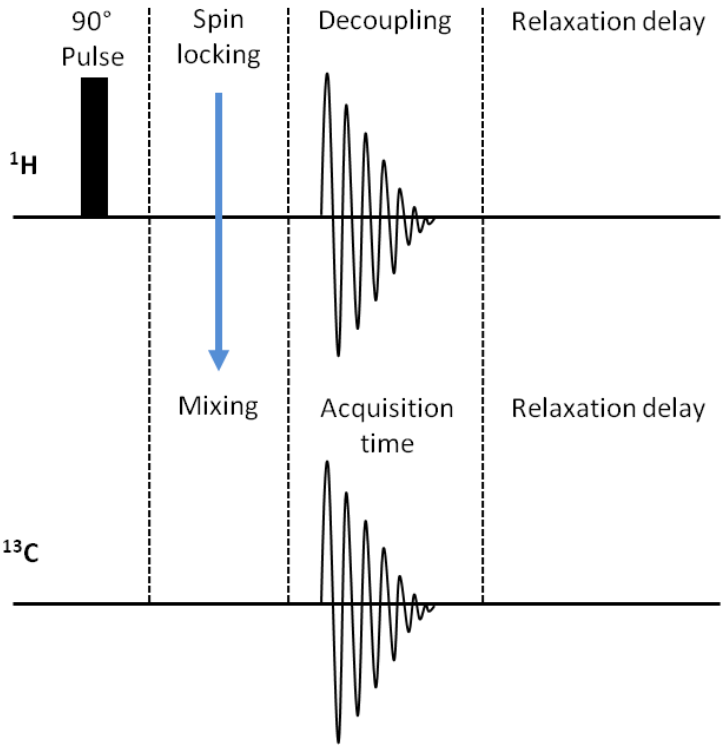

Figure 8. Cross polarization experiment ^{1}H-^{13}C.

1.4.1.3 Spin-Echo Experiment

The basic single pulse as well as cross polarization experiments are crucial tools for investigating solid materials, but they are not sufficiently sensitive to achieve satisfying signal intensity for species with long spin-spin relaxation time. Alternatively, the spin echo experiment was discovered by Hahn in 1950. This method is especially useful for chemical compounds with long spin-spin relaxation time, such as nuclear species, which interact less with each other or with other atoms. Thus, the measurement of isolated, weakly bridged atoms or, as presented in this thesis, adsorbed species on the catalyst surface is possible.

During spin echo experiments, the single pulse experiment is extended by a 180° pulse (Figure 9.). If a 90° impulse is applied, the magnetization ends up in the y-axis direction followed by a fanning out process. Hence, the spins move with different rates due to inhomogeneities of the

local field. By applying a longer wait time t (between the pulses), the faster spins drift further from the y-axis. Such spins with a fast spin-spin relaxation time cannot be acquired by a 180° reasquistion focusing impulse resulting in no signals in the spectrum. Finally, after a 180° pulse, the refocusing of spins is evident and the recording of the spectrum is completed.

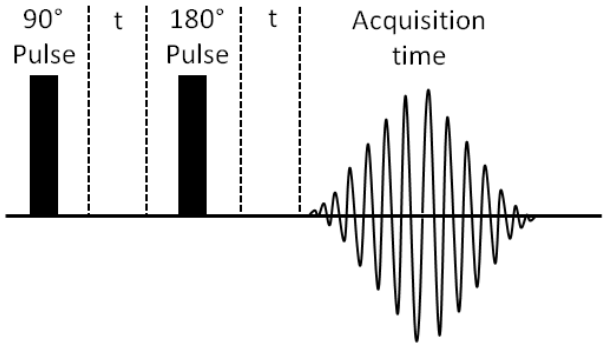

Figure 9. Spin echo NMR experiment.

1.4.2 Thermal analysis (TA)[187]

Thermal analysis is a special technique for investigating the chemical and physical properties of chemical substances as functions of time or temperature. The main adopted tools are such experiments as differential thermal analyses (DTA), thermogravimetric analysis (TG) or *Pulse*TA®.

1.4.2.1 Differential thermal analyses

The changes at a sample´s behaviour are measured, while it is subjected to a controlled temperature program. The temperature difference between the heating element of the sample and an inert reference material is recorded, resulting in a DTA curve. Statements about endothermal and exothermal processes (phase transition, decomposition, evaporation) occurring with the temperature change can be made. The measurements are carried out under conditions of constant pressure.

1.4.2.2 Thermogravimetric analysis

Using TG experiments, the thermal stability of the sample is investigated. The mass changes in the sample, which occur upon controlled heating cycles, are examined. During such heating cycles a temperature up to 1300 °C can be applied. TG experiments are especially helpful for interpreting the DTA curves. Thus, all processes can be followed e.g. phase transformations,

melting or decomposition. At such high temperatures, irreversible changes in the structure can occur, for instance amorphous solids can crystallize.

In addition, TG can be coupled with other analytical methods such as mass spectrometry (MS) or infrared spectroscopy (IR).

1.4.2.3 *Pulse*TA®

*Pulse*TA® is a special form of classical TA, where interactions between solid materials, e.g. catalysts and gaseous or liquid substrates, can be followed in situ. Therefore, a specific amount of the substrate is injected directly into the carrier gas stream. The changes resulting from the reaction occurring at the surface can be monitored quantitatively using MS and TG. If the reactant from the gas phase is adsorbed at the solid surface, the increase in the mass is detected in the TG curve. Analyzing the occurring interactions, informations about chemical (exothermal peaks) or physical adsorption (endothermal post effects) can be made.

In this thesis, this method was especially helpful for the investigation of interactions between the catalyst and reactants delivering information about the reactivity of the catalyst, which in turn allowed statements about the mechanism.

1.4.3 The temperature-programmed desorption (TPD)[188]

TPD is a quantitative method used for the characterization of the acidic properties of solid materials. This was especially helpful in this thesis for the estimation of catalyst reactivity after its contact with different substrates. The sample is loaded with a basic molecule, typically NH_3, to monitor its desorption during heating process using IR spectroscopy. For NH_3, the deformation vibrations at 930 cm^{-1} are monitored. The strength and number of the active sites can be estimated based on desorbed NH_3. The position of the peak maxima and the peak area are used for the description of acidic properties. The more strongly the molecules are bound to the solid, the higher the desorption temperature is, which results in a peak maximum shifted to a higher temperature. Additionally, upon integration of the peaks at different maxima, the amount of ammonia bonded on acidic sites with different strength can be estimated. For quantitative calculations, the absolute amount of acidic sites can be calculated by transffering the desorbed molecules into an acidic solution followed by titration. The main disadvantage of this method is the high desorption temperature, which may lead to structural changes in the catalyst. Statements about the nature (Lewis or Brönsted) of active sites are also impossible.

1.4.4 X-ray diffraction (XRD)[189]

XRD is used for the structural determination of crystalline substances. The underlying principle of this method is to irradiate regularly arranged atoms from crystalline chemical compounds with X-rays. The compound´s atoms cause the X-rays to scatter in different directions, which results in constructive or destructive interference. Such interferences are described by Bragg's Law:

$$n \cdot \lambda = 2 \cdot d \cdot \sin(\theta)$$

where **n** is a positive integer and **λ** is the wavelength of the incident wave, **d** is the distance between lattice planes, and **θ** is scattering angle.

From this equation, the interplanar distance and the lattice constancy in the unit cell can be estimated. Only constructive inferences will cause reflections detected in the diffraction pattern. However, most solid catalysts are amorphous.

In this research, XRD was applied to investigate if any structural changes occurred in the catalyst after interaction with different substrates.

1.4.5 Fourier-Transform Infrared Spectroscopy (FTIR)[190]

FTIR is commonly used for identifying organic and inorganic chemicals. It is based on the interactions between the electrical component of infrared radiation and the probe molecules. This method is restricted to such molecules that exhibit changes/alterations in a dipole moment while vibrating. The changes of amplitude caused by molecular stretching and bending (vibrational motions) are visible with the absorption of IR radiation by the molecule. This takes place when the frequency of the radiation matches the vibrational frequency of the molecule.

For solid materials, FTIR is used not only for the determination of the structure, but it is also adopted for monitoring the interactions between solids and probe molecules. Thus, this technique can be applied for the characterization of active sites on the catalyst. The adsorbed molecules have different bond vibrations than compared with those of free molecules. If the probe molecule is adsorbed, its geometry changes slightly resulting in signal shift in the spectrum. Taking into the consideration the type and strength of the active site, the shift varies. Unlike the TPD technique, FTIR spectroscopy can not only determinate the strength, but also the type of active site. Hence, the Lewis and Brönsted acidic sites can be distinguished.

2 Objectives and Goals of the PhD Thesis

The scope of the PhD thesis will focus on the investigation of the catalytic performance of two remarkably strong solid Lewis acids, aluminium chlorofluoride (ACF) and *high-surface* aluminium fluoride (*HS*-AlF_3). These catalysts are well developed and examined in our research group. They have been the focus of previous research not only because of their outstanding reactivity, but also for their ability to activate otherwise unreactive compounds, which can usually only be activated by homogeneous catalysts. With their unusually high reactivity, they constitute a modern type of catalytically active solids for precious metal-free catalysis performed under mild conditions.

ACF and *HS*-AlF_3 will be tested in various reactions. The activation of sp^3 hybridized C-F and C-Cl bonds will be of interest. Halogenated compounds, which are hard to activate, will be set to tested in the presence of Et_3SiH and more sterically demanding $^{i}Pr_3SiH$, hopefully resulting in a hydrodehalogenation product, or, in the presence of C_6D_6 as a solvent, yielding a Friedel-Crafts addition product. In addition, zirconium chlorofluoride (ZCF) will also be tested for its catalytic ability for selected reactions as another example of strong Lewis acids.

The hydrodehalogenation reaction will be investigated not only in NMR batch reactions, but also in a flow reactor. This offers a novel approach to the activation of C-X (X = Cl, F) bonds under moderate solvent-free, eco-friendly conditions in the gas phase. Here, the influence of various parameters will be tested such as temperature and different gas flows resulting in different contact times. With the help of these gas flow reactions, hopefully the mechanism for hydrodehalogenation reactions in the presence of silane will be elucidated.

Furthermore, the focus will be set to exploring potentially new reactivities of these catalysts by activating unsaturated compounds containing C=O bonds in the presence of Et_3SiH, Et_2SiH_2 and $^{n}BuSiH_3$. The steric and thermodynamic aspects of these reactions will be examined using the two previously mentioned catalysts, ACF and *HS*-AlF_3.

Additionally, the specification of the individual mechanical steps will be supplemented by studies of the local nanoscopic structure adopting different methods, such as *Pulse*TA®, ^{1}H, ^{13}C and ^{19}F MAS NMR spectroscopy, as well as NH_3-TPD, FTIR, EA, and XRD. experiments.

3 Results and Discussion

3.1 Hydrodefluorination

Based on the approach presented by Ahrens *et al.* [48], ACF enables the activation of a strong C-F bond in NMR tube reactions. Fluorinated substrates are activated in the presence of Et_3SiH and C_6D_6 under mild conditions, resulting in hydrodefluorination and Friedel-Crafts products. Thus, a challenge faced in this PhD thesis was to adapt those reactions to the flow reactor, where the contact times are significantly shorter.

Before the results from the flow reactor are presented, it is important to gain a thorough understanding of the differences in the reactivity of both catalytic systems. In consequence, ACF and *HS*-AlF_3 underwent catalytic tests for the activation of various fluorinated methane derivates in NMR tube reactions. These results will be presented in the next section.

3.1.1 Batch reactions

CH_3F, CH_2F_2, CHF_3 were activated in the presence of Et_3SiH with both, ACF and *HS*-AlF_3 as catalysts (Scheme 43).

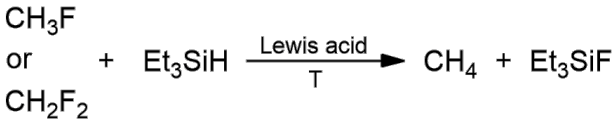

Scheme 43. Hydrodefluorination reaction of C-F compounds in the presence of Et_3SiH.

The reactions were carried at 70 °C for up to 6 days. The conversions were calculated based on signals in the ^1H NMR spectrum, which was recorded every 24 h. The results presented in Table 1 reveal that CH_4 was formed as the only product in all reactions.

Using ACF, CH_3F was completely consumed after 3 days at 70 °C, while only 29% of CH_2F_2 was converted after 3 days. The conversion increased with prolonged reaction time. After 6 days, 45% of CH_2F_2 was activated in hydrodefluorination reaction. Unfortunately, considering the activation of CHF_3 only traces of methane were found after 6 days.

To compare, *HS*-AlF_3 activated CH_3F with a conversion rate of 75% after 3 days at 70 °C, increasing to 88% after 6 days. In contrast, only 2% of CH_2F_2 was consumed in the hydrodefluorination reaction after 6 days. The attempt to activate CHF_3 was not successful (see Table 1).

Table 1. Hydrodefluorination of mono-, di- or trifluorinated methane derivates with excess of Et_3SiH to methane.

entry	subs.	$n_{subs.}$ [mmol]	cat.	t [d]	conv. [%][a]	TON[b]	TOF [h^{-1}][c]
1	CH_3F	1.80	ACF	3	100	72	1
2	CH_3F	1.88	*HS*-AlF_3	3	75	56	0.78
3	CH_3F	1.88	*HS*-AlF_3	6	88	66	0.46
4	CH_2F_2	1.82	ACF	3	29	21	0.30
5	CH_2F_2	1.82	ACF	6	45	33	0.23
6	CH_2F_2	1.90	*HS*-AlF_3	3	2	1.5	0.02
7	CH_2F_2	1.90	*HS*-AlF_3	6	2	1.5	0.01
8	CHF_3	1.85	ACF	3	0	-	-
9	CHF_3	1.85	ACF	6	0	-	-
10	CHF_3	1.86	*HS*-AlF_3	3	0	-	-
11	CHF_3	1.86	*HS*-AlF_3	6	traces	-	-

All reactions were carried out using 25 mg of the catalyst and at 70 °C. [a] The quantification was performed using ^1H NMR spectroscopy, comparing the ratio of the product to the substrate. [b] Calculated based on the amount of the product per number of active acidic sites at the Lewis acids (1 g Lewis acid contains 1 mmol of active sites determined by NH_3-TPD).[44] [c] Calculated based on TON divided by reaction time in h.

The conversions achieved with ACF were higher than those with *HS*-AlF_3 for all reactions. Although both catalysts have comparable Lewis acidity according to pF scale, they differ in their catalytic performance. Thus, the HSAB concept is not a suitable explanation. It is presumably the sterical effects that have a larger impact on the reactivity of both catalysts in this case. The accessibility of the active sites is influenced by their porosity. Based on the previous results, microporous ACF is a more suitable catalyst for the activation of small fluorinated methane derivates rather than mesoporous *HS*-AlF_3. In the micropores of ACF, the substrates are more efficiently retained, resulting in higher conversion rates.

In general, the conversions increase in the order $CHF_3 < CH_2F_2 < CH_3F$. With an increasing number of fluorine atoms in molecules, the C-F bonds will be shorter and stronger at the same time. Additionally, the C-F bond becomes less accessible for the activation due to the steric shielding caused by increasing amount of fluorine substituents.[191]

No partially fluorinated products were detected. Thus, the cleavage of the first C-F bond must be the rate-limiting step, which is consistent with conclusions postulated by Ozerov and co-workers.[49] The authors found that either none or all C-F bonds were broken in the activation of polyfluorinated substrates.

These results are not in accordance with the previously investigated reactions in the author´s diploma thesis[192] and results published by Ahrens *et al.*.[193] Instead these data indicate that *HS*-AlF_3 is more suitable for the activation of fluorinated compounds than ACF.

CH_2F_2 and $PhCF_3$ (Ph= C_6H_5) were activated in the presence of both Et_3SiH and C_6D_6. The results are summarized in Table 2. Ahrens and co-workers demonstrated that ACF can convert 17% of CH_2F_2 after 4 days at room temperature. A total of 95% of the substrate was activated to give the Friedel-Crafts product $Ph^D{}_2CH_2$. Only 5% of CH_2F_2 was consumed in sequential Friedel-Crafts and hydrodefluorination step to Ph^DCH_3. In contrast, 75% of CH_2F_2 was activated with *HS*-AlF_3 after only 2 days at room temperature. Similarly, CH_2F_2 was preferably converted to the Friedel-Crafts product $Ph^D{}_2CH_2$ (97%) and only 3% to Ph^DCH_3.

Table 2. Activation of difluoromethane and trifluorophenylmethane in the presence of both Et_3SiH and C_6D_6.

entry	subs.	subs. [mmol]	cat.	$n_{act.sites}$ [µmol]	t [d]	T [°C]	conv. [%][a]	TON[b]	TOF [h^{-1}][c]
1[1]	CH_2F_2	2.73	ACF	12.5	4	24	17	21	0.22
2[1]	CH_2F_2	3.11	*HS*-AlF_3	12.5	2	24	75	94	1.95
3[2]	$PhCF_3$	0.30	ACF	25.0	7	70	70	25	0.15
4[2]	$PhCF_3$	0.30	*HS*-AlF_3	25.0	3	70	82	30	0.42

All reactions were carried out in C_6D_6 as a solvent. [a] The quantification was performed by ^1H NMR spectroscopy, comparing the ratio of the fluorotriethylsilane to triethylsilane. [b] Calculated based on the amount of the product per number of active acidic sites at the Lewis acids (1 g Lewis acid contains 1 mmol of active sites determined by NH_3-TPD).[44] [c] Calculated based on TON divided by reaction time in h. [1] n_{Et3SiH}= 1.56 [mmol], [2] n_{Et3SiH}= 0.90 [mmol].

Furthermore, the sterically demanding $PhCF_3$ molecule reacted with Et_3SiH and C_6D_6. ACF activated 70% of the substrate at 70 °C after 7 days, whereas for *HS*-AlF_3 a significantly higher conversion of 82% was achieved at 70 °C, after only 3 days. In both cases, 98% of the substrate was converted to $PhPh^DCH_2$ and only 2% to $PhCH_3$. The selectivity of the reactions was comparable for both catalysts regarding the activation of CH_2F_2 and $PhCF_3$.

In the presence of C_6D_6, *HS*-AlF_3 demonstrated a higher catalytic activity. As mentioned above, the interactions between the substrates and the catalyst might play an important role in the reactivity. With the introduction of an additional C_6D_6 substrate into the catalytic system, competition about the active sites between the substrates could have changed, causing different reactivity. However, the steric effects should not be ignored. The mesopores of *HS*-AlF_3 should be more suitable for sterically challenging reactions, where voluminous products are formed, given that the reaction is hampered by the presence of the additional

required substrate. Surprised by these results we decided to investigate the steric effects by *in-situ* FTIR experiments.

3.1.2 Examination of sterical effects

Pyridine-based bases with various steric requirements are suitable molecules to examine the influence of porosity on catalytic potential. They are expected to coordinate at the active sites because of their nitrogen lone pair. With increasing sterical hindrance, the adsorption should decrease.

The *in-situ* FTIR spectra of *HS*-AlF_3 and *HS*-$AlF_3 \circ Et_3SiH$, which were treated with pyridine, 2,6-dimethylpyridine and 2,6-di-tert-butylpyridine, are presented in Figure 10.

Before the results are discussed thoroughly, the technical aspects of the experiment should be explained. When placing a sample into the *in-situ* FTIR spectrometer, short-term contact with air occurs. ACF and *HS*-AlF_3 lose their strong Lewis acidic properties after contact with moisture. ACF will even be irreversibly destroyed in the presence of water. Unlike ACF, water adsorbs reversibly on *HS*-AlF_3.[37] Thus, *in-situ* FTIR experiments were carried out using only *HS*-AlF_3. Previous investigations have shown that catalyst deactivation can be prevented by loading the catalysts with silane.[48] The silane protects the catalyst by adsorbing at the Lewis acidic sites. Therefore, not only unloaded, but also silane-loaded *HS*-AlF_3 was measured. After the introduction of the self-supported disks into the *in-situ* FTIR spectrometer, the samples were heated at 200 °C and simultaneously evacuated at 0.035 mbar for 2 h. This treatment is important for water and silane desorption and to make the Lewis acidic sites accessible again. In the next step, different bases were pulsed (up to 1 mbar) onto the samples. The applied bases successively decreased on the steric demand. After each sequence of base pulses, the sample was re-evacuated at 0.035 mbar for 1 h before the next the measurement was conducted.

The measurement of the background (unloaded *HS*-AlF_3 in vacuum) implies the presence of water molecules on the surface. Even high temperature and vacuum conditions were unseccessful to remove all water from the solid, demonstrating again the strong Lewis acidity of *HS*-AlF_3. Water absorbing at Lewis acidic sites forms weak or moderate Brönsted acidic sites. Thus, the catalyst activity could have altered and should demonstrate both Lewis and Brönsted acidity.

All these forms were detected by investigating the changes $\nu_{8a\text{-}b}$ und $\nu_{19a\text{-}b}$ vibrations of 2,6-di-tert-butylpyridine, 2,6-dimethylpyridine and pyridine.

For 2,6-di-tert-butylpyridine, only signals with low intensity were detected indicating that a negligible number of molecules were able to enter the micropores of the catalyst. The peak at 1620 cm^{-1} is attributed to the molecule bonded to Brönsted sites representing ν_{8a-b} vibrations, whereas the signal at 1453 cm^{-1} can presumably be assigned to ν_{19a-b} vibrations caused by interactions between 2,6-di-tert-butylpyridine and Lewis acidic sites. [194]

Peaks at 1654, 1630 and 1620 cm^{-1} were detected for 2,6-dimethylpyridine. The observation of the bands at 1654 and 1630 cm^{-1} is a unique indication for Brönsted-bonded 2,6-dimethylpyridine. These peaks appear due to ν_{8a} and ν_{8b} vibrations. The peak at 1620 cm^{-1} is caused by the species adsorbed on Lewis sites. Comparing the area under peaks, more Brönsted than Lewis acidic sites exist due to the preparation method. The characteristic bands for the ν_{19a} und ν_{19b} vibrations could not be detected, presumably due to the low intensity of these signals. Contrary to the spectrum of with 2,6-ditertbutylpyridine loaded catalyst, the intensity of the peaks is higher in case of 2,6-dimethylpyridine, supporting the theory that, with a lower steric demand from the probe molecule, the active sites located in the micropores are more accessible. Nonetheless, the peak intensity is very low in the spectrum of *HS*-AlF_3◦Et_3SiH and almost invisible in the spectrum of unloaded *HS*-AlF_3. The slight differences in these signals can be attributed to the protective role of silane for the acidic sites, during the preparation time when the sample is exposed to the air.

For pyridine, the peaks at 1642, 1629, 1620, 1579, 1545, 1493 and 1452 cm^{-1} are clearly detectable, although the sample was previously loaded with 2,6-dimethylpyridine. Active sites, which could not be occupied with more voluminous 2,6-dimethylpyridine, still exist on the surface and could adsorb pyridine. The vibrations at 1629, 1620 and 1579 cm^{-1} are assigned to ν_{8a}, ν_{8b} vibrations, whereas the signals for ν_{19a-b} vibrations are evident at frequencies 1493 and 1452 cm^{-1}. These peaks are caused by pyridine molecules adsorbed on Lewis acidic sites. The signal at 1493 cm^{-1} is also caused by pyridine molecules adsorbed on Lewis bases sites. Regarding the catalytic reactions, the signals at 1620 cm^{-1} and 1629 cm^{-1} are of great importance. These signals can be assigned to ν_{8a}, ν_{8b} vibrations of pyridine adsorbed on weak and strong Lewis acidic sites. Even if the peaks overlap in the spectrum, the amount of weak Lewis acidic sites is probably lower than that of the strong catalytic sites. Pyridine bonded at Brönsted sites gives rise to characteristic peaks at 1642 and 1545 cm^{-1}, which are assigned to ν_{8a} and ν_{19b} vibrations. The signal at 1653 cm^{-1} is attributed to remaining 2,6-dimethylpyridine. Furthermore, the intensity of the bands for unloaded *HS*-AlF_3 is lower than those for the catalyst preloaded with silane.

To conclude, *in-situ* FTIR spectra proved that 2,6-ditertbutylpyrdine, 2,6-dimethyl-pyridine and pyridine are chemisorbed (sample evacuation at 0.035 mbar) at the surface of the catalyst. The adsorption tendency increases with decreasing steric demand of the bases. The steric effects clearly influence the performance of the catalysts. Compared to the spectrum of *HS*-$AlF_3 \circ Et_3SiH$, the lower signals in the spectrum of unloaded catalyst point towards protection of the catalyst by reversible desorption of silane.

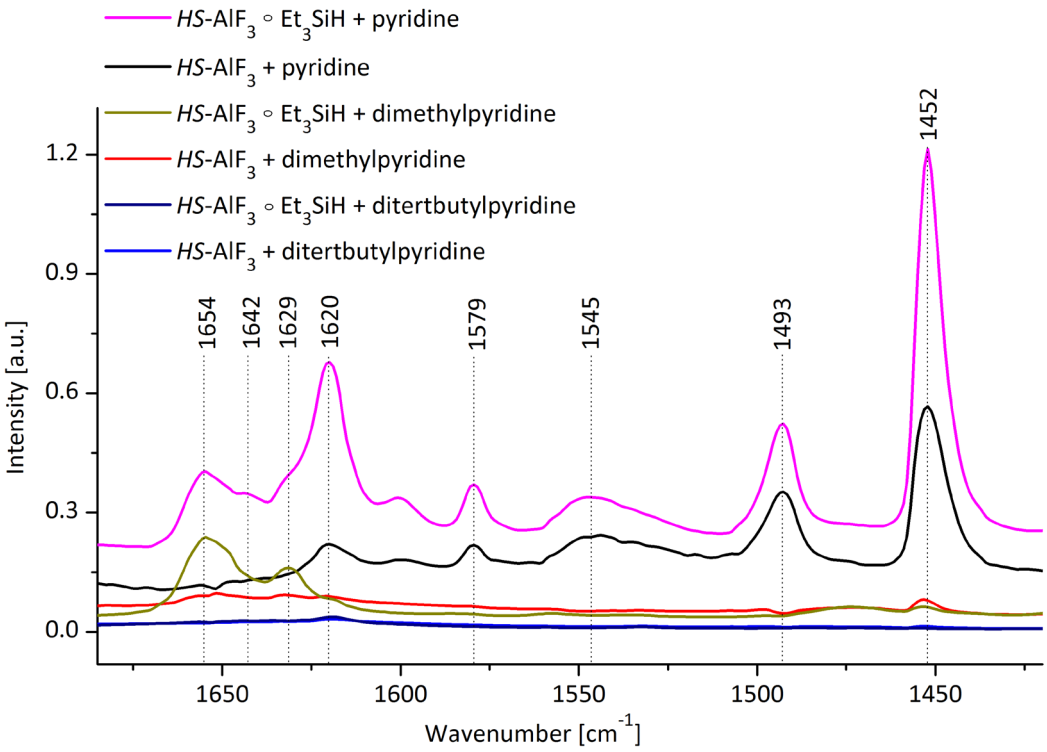

Figure 10. FTIR spectra of *HS*-AlF_3 and *HS*-$AlF_3 \circ Et_3SiH$ loaded with pyridine, 2,6-dimethyl-pyridine and 2,6-di-tert-butylpyridine.

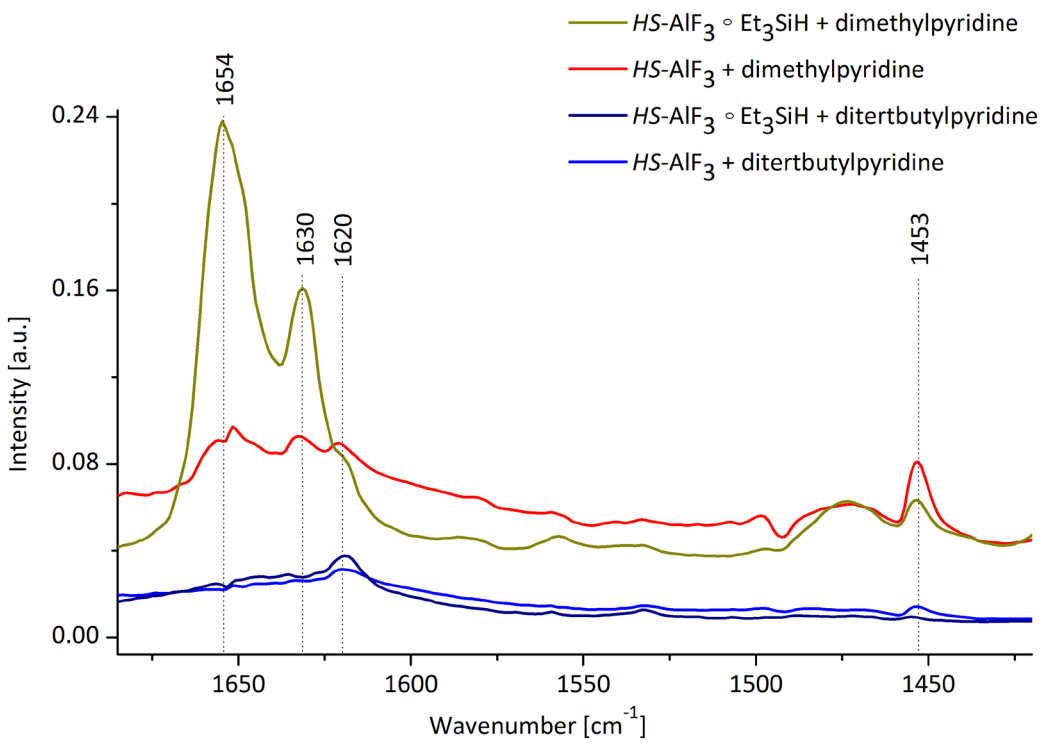

Figure 11. Zoom of Figure 10.

3.1.3 Flow reactor

In order to take full advantage of the heterogeneous nature of both catalysts, the hydrodefluorination reactions should be transferred from a simple batch to a flow reactor. The flow reactor technique offers the possibility to investigate the transport phenomena, which in turn are limited by steric effects. This task is challenging, since demanding conditions prevail in the flow reactor. The reactions will be carried out during very short, but defined contact times. Variable contact times affect the kinetics of the reactions, which can lead to the formation of different products compared to batch reactions or even prevent the reaction at all. The products formed in the flow reactor are kinetically favoured, whereas in the NMR tube they are thermodynamically favoured. Furthermore, industry is always looking for alternatives to avoid the need for solvents and for the possibility to increase the temperature to obtain higher conversions. In the flow reactor, different fluorinated methane derivates, such as CH_3F, CH_2F_2 and CHF_3, were activated in the presence of Et_3SiH on both catalysts ACF and *HS*-AlF_3. In the following sections the results obtained in the flow reactor will be presented, together with a comparative discussion of activation in a batch reactor.

3.1.3.1 Optimization of reaction conditions

Temperature

The activation of CH_2F_2 was carried out at 50, 120, 190 and 250 °C in the presence of Et_3SiH on ACF at 0.6 s contact time, resulting in formation of CH_4. The temperature effects on the catalytic performance are presented in Figure 12 and Table 3. The conversions were calculated by means of GC measurements after its previous calibration.

Table 3. Activation of CH_2F_2 at different temperatures.

entry	$n_{subs.}$ [µmol]	CT [s]	T [°C]	conv. [%][a]	TOF [h][b]
1	1.2	0.6	50	6	2.8
2	0.4	0.6	120	9	1.4
3	1.2	0.6	190	20	10
4	1.0	0.6	250	12	5

All reactions were carried using 180 mg of ACF. [a] The quantification was performed by GC, comparing the ratio of the product to substrate. [b] Calculated based on the amount of the product per number of active acidic sites at the Lewis acids (1 g Lewis acid contains 1 mmol of active sites determined by NH_3-TPD)[44] divided by reaction time in h.

The highest conversion was achieved at 190 °C, which was used as the optimum temperature for all subsequent experiments.

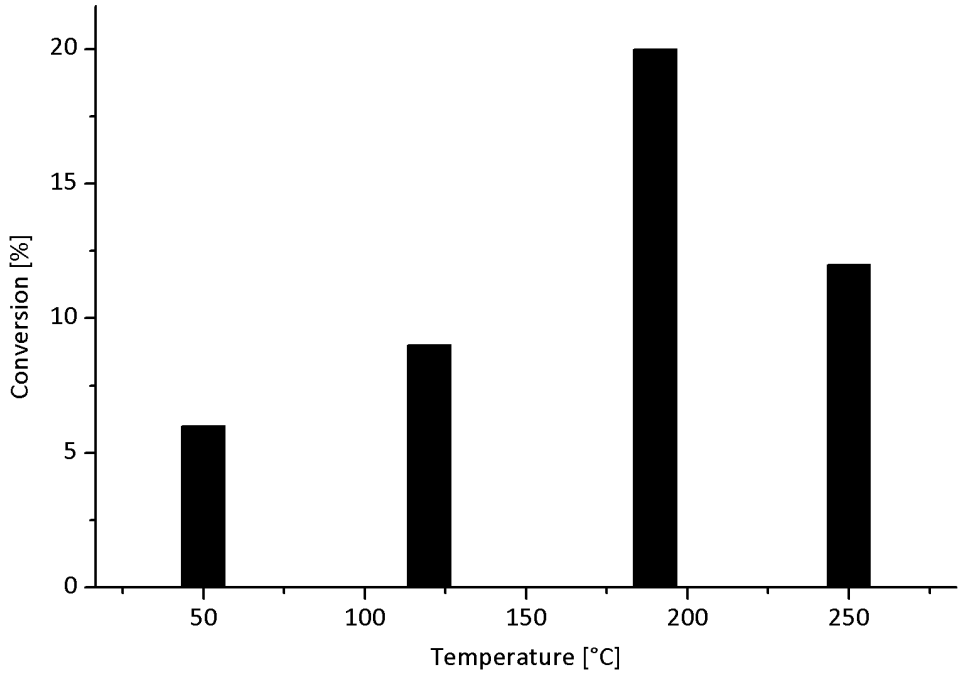

Figure 12. The temperature dependence of the activation of CH_2F_2 in the presence of Et_3SiH in the flow reactor.

Simplified calculations were performed to determine the activation energy. First, the rate constant was evaluated assuming a pseudo-first-order kinetic model. The hydrodehalogenation reaction can be regarded as such, because only the concentration of the substrate CH_2F_2 and the product CH_4 are important. The reaction is carried out in an excess of silane, thus its concentration is considered as constant.

The rate constant k was calculated from the following equation:

$$\frac{d[A]}{-dt} = k[A]$$

After integration;

$$\ln[A]_t - \ln[A]_0 = -k \cdot t$$

and solving of the equation for k, it can be expressed as follows:

$$\frac{\ln([A]_t/[A]_0)}{-t} = k$$

Here, unlike classical calculations, **A** is not the concentration but the amount of CH_2F_2 in µmol, whereas **t** is the contact time. The values used in calculations are summarized in Table 4.

Table 4. Values used in the calculation of activation energy.

entry	n_{CH_4} [µmol][a]	$n_{CH_2F_2\_t}$ [µmol][a]	$n_{CH_2F_2\_0}$ [µmol]	1/T [1/K]	k	lnk
1	0.08	1.24	1.31	0.0031	0.09	-2.39
2	0.04	0.40	0.44	0.0025	0.16	-1.84
3	0.33	1.33	1.66	0.0022	0.37	-1.00
4	0.14	1.00	1.14	0.0019	0.22	-1.52

All reactions were carried out using 180 mg of ACF and 0.6 s contact time. [a] The estimation of the product/substrate amount was performed by GC after previous calibration.

Lastly, the Arrhenius equation was used to determine the value of the activation energy:

$$k = A \cdot e^{\frac{-Ea}{RT}}$$

Taking the natural logarithm this gives:

$$\ln k = \ln A + \left(\frac{-Ea}{R} \cdot \frac{1}{T}\right)$$

The slope of the line is equal to $-E_a/R$, which was used for the calculation of the activation energy. The Arrhenius plot (lnK versus 1/T) is presented in Figure 13.

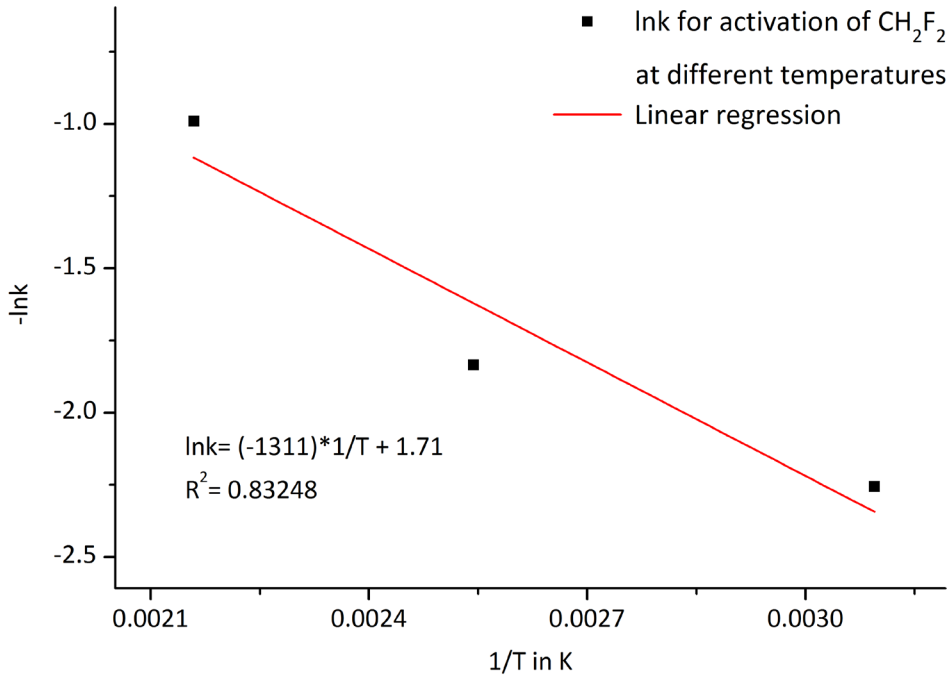

Figure 13. The slope of the Arrhenius plot for activation energy of hydrodefluorination reactions.

Based on these calculations, the minimal required energy to initiate the hydrodefluorination reaction was approximately 11 kJ·mol^{-1}. According to the Van´t Hoff rule, the conversion should be higher at increased temperature. Nonetheless, at 250 °C the experimental conversion decreases. One reason for the lower conversion, apart from the decomposition of silane, could be slowly decomposition of the active sites at high temperatures.

To investigate how the Lewis acidity of the catalyst changes with an increasing pretreatment process temperature, NH_3-TPD experiments were performed. Since ammonia is bound more strongly at highly acidic sites, ammonia at weaker sites will already be desorbed at lower temperatures. This allows to discriminate different strengths of active sites. In general, the higher the amount of the desorbed ammonia is, the more active sites interact with NH_3 indicating a strongly acidic catalyst.

IR spectra were obtained for unloaded ACF preheated at different temperatures, namely 120, 150, 190 and 250 °C. The results are depicted in Figure 14 and summarised in Table 5. Three distinguishable regions of NH_3 desorption were detected. They can be assigned to acidic sites ranging from weak to very strong. The weak acidic sites were detected for ammonia desorbed in the range of 125-275 °C with a local maximum at 250 °C, while ammonia bound to the medium strength sites were desorbed in the range of 275-400 °C. The largest peak of ammonia desorption was detected at about 450 °C. Identical behaviour is observed independently of at which temperature the catalyst was pretreated. At such high temperatures, ACF will be destroyed. The high level of desorption of ammonia only at the decomposition temperature of the catalyst implies the presence of particularly strong acid sites. These are the most interesting sites for the type of catalysis carried out in the following sections.

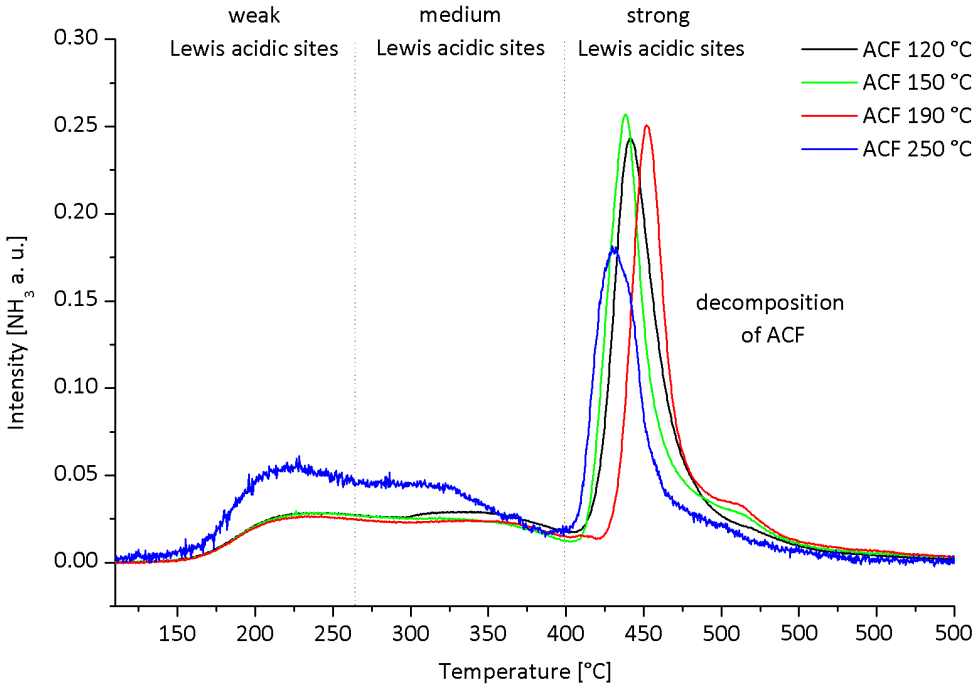

Figure 14. The NH_3-TPD experiments of unloaded ACF pretreated at different temperatures.

Table 5. TPD-NH_3 results of ACF pretreated at different temperatures.

entry	T [°C]	total amount acidic sites [mmol/g]	weak acidic sites [%]	medium acidic sites [%]	strong acidic sites [%]
1	120	1.679	18	18	64
2	150	1.624	18	16	66
3	190	1.545	18	17	65
4	250	0.850	26	28	45

A strong influence of pretreatment temperature on the acidity of ACF is also visible. The amount of adsorbed ammonia decreases with higher pretreatment temperature. ACF is stable up to 190 °C, and it was at 250 °C that the amount of the strong Lewis-acidic sites decreased. Thus, the lower amount of acidic sites with a higher pretreatment temperature is responsible for the lower conversion at 250 °C, and in all likelihood not the decomposition of Et_3SiH. According to the literature[195], SiH_4 decomposes at temperatures ranging from 380 °C to 490 °C. Compared to SiH_4, Et_3SiH shows higher stability.[196] Nevertheless, it is feasible that a Lewis-acidic surface initiates the β-H-elimination process at lower temperatures causing decomposition of Et_3SiH, which in turn might cause carbonisation of the catalyst.[197]

Contact time

To find the optimum contact time for hydrodefluorination reactions, CH_2F_2 was activated at 190 °C and at 0.1, 0.2, 0.3, 0.6 and 1.3 s contact time using both ACF and *HS*-AlF_3 as catalysts. Table 7 summarises the results.

Higher conversions should be achieved with longer contact times. For contact times of up to 0.6 s, similar conversions were achieved, except for reactions at 0.1 s. The conversion decreases if contact time is too short. Also, for contact times longer than 0.6 s, the conversions decreased. This could be explained by the carbonisation of the catalyst during long contact times. The catalyst is deactivated when the molecules remain on the surface too long and begin to decompose there. The highest conversions for both catalysts were achieved at 0.6 s contact time. Thus, further experiments were carried out at 0.6 s contact time and 190 °C.

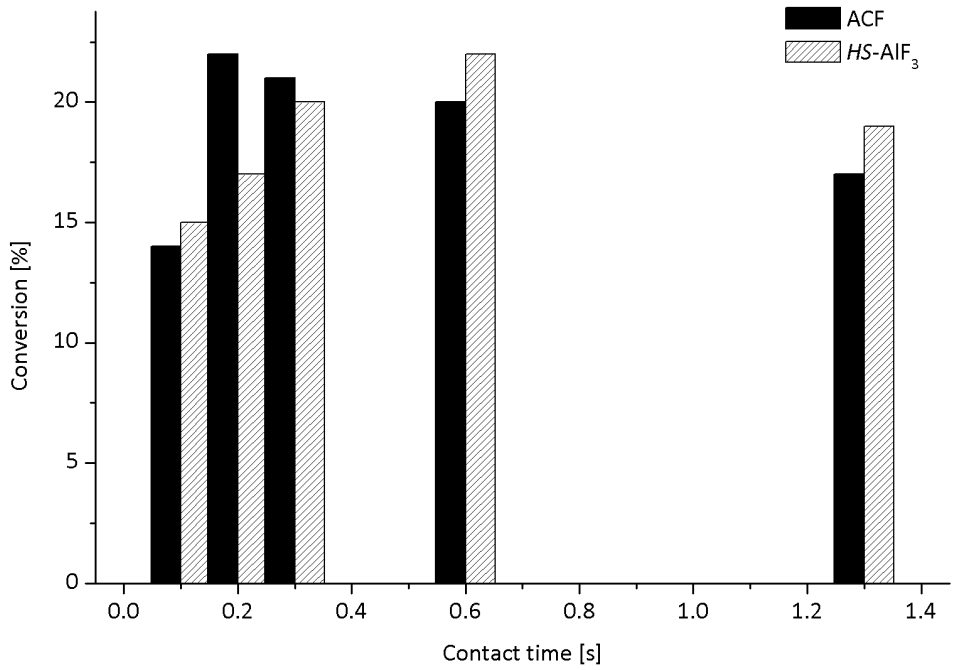

Figure 15. The activation of CH_2F_2 at 190 °C on ACF and *HS*-AlF_3 in the presence of Et_3SiH at different contact time in a flow reactor.

Table 6. Hydrodefluorination of fluorinated methane derivatives in a flow reactor.

entry	subs.	n_{subs} [μmol]	cat.	T [°C]	CT [s]	conv. [%][a]	TOF [h^{-1}][b]
3	CH_2F_2	1.1	ACF	190	0.1	14	38
4	CH_2F_2	1.1	ACF	190	0.2	22	34
5	CH_2F_2	1.2	ACF	190	0.3	21	21
6	CH_2F_2	1.2	ACF	190	0.6	20	10
7	CH_2F_2	1.1	ACF	190	1.3	22	4
9[1]	CH_2F_2	0.8	*HS*-AlF_3	190	0.1	15	29
10[1]	CH_2F_2	0.6	*HS*-AlF_3	190	0.2	17	15
11[1]	CH_2F_2	0.8	*HS*-AlF_3	190	0.3	20	13
12[1]	CH_2F_2	0.9	*HS*-AlF_3	190	0.6	22	8
13[1]	CH_2F_2	1.0	*HS*-AlF_3	190	1.3	19	4

All reactions were carried out using 180 mg of ACF or 190 mg of *HS*-AlF_3. [a] The estimation of the product/substrate amount was performed by GC after previous calibration. [b] Calculated based on the amount of the product per number of active acidic sites at the Lewis acids (1 g Lewis acid contains 1 mmol of active sites determined by NH_3-TPD)[44] divided by reaction time in h [1] single measurement

Stability of the catalysts

The catalytic performance under the selected reaction conditions over a longer period was also investigated. ACF and *HS*-AlF_3 were tested in the activation of CH_2F_2 at 190 °C at 0.6 s contact time over 6 h. (Scheme 44). Similar to previous reactions, the major product was CH_4. As shown in Figure 16, the catalysts were active for the duration of the experiment. No significant changes in the catalyst`s activity were detected. The conclusion is, that the catalysts remain stable delivering constant conversions over a longer period of time. Also at the beginning no attenuation of the reactivity was detected. Thus, for the following experiments, the reactions were carried out for 3 h and at 190 °C.

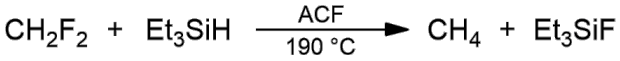

Scheme 44. Hydrodefluorination reaction for the stability tests.

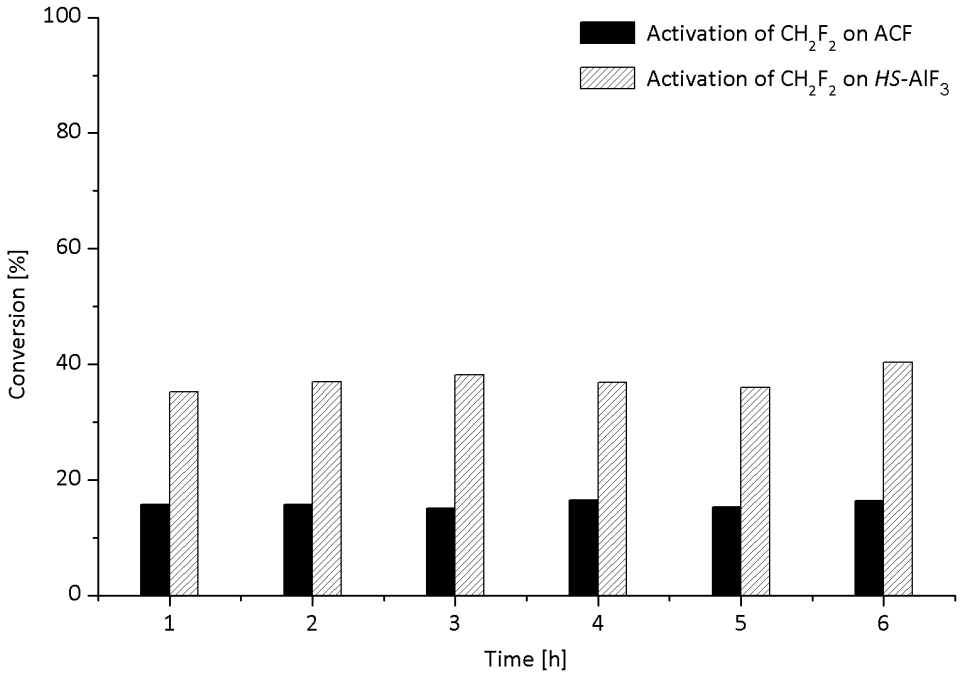

Figure 16. The stability of ACF in the hydrodefluorination reaction of CH_2F_2 in the presence of Et_3SiH in a flow reactor.

Reproducibility

The previous results indicated that as far as one batch is concerned, the catalyst works in a stable way. Next, the differences in catalytic performance between various batches were examined. As shown in Figure 17, the plots indicate a satisfactory reproducibility. Only one of the four plots demonstrates a slightly different conversion. The aluminium-based catalysts are hard to handle. Due to their strong Lewis acidity, they are highly moisture sensitive. Even short contact with air deactivates the catalyst, or as in the case of ACF even destroys it, resulting in a lower catalytic potential.

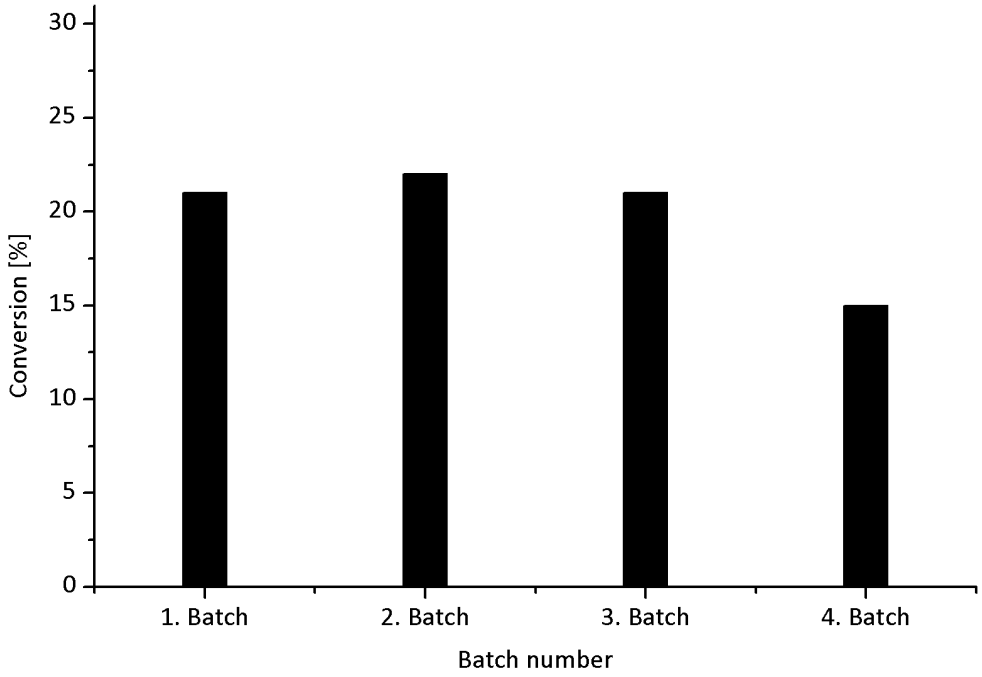

Figure 17. The results of the hydrodefluorination reactions with different batches in a flow reactor using ACF as catalyst.

Catalytic behaviour

The catalyst's behaviour was tested when the equilibrium state existing in the reaction system was disturbed. The reaction was carried out under previously chosen conditions (190 °C and 0.6 s contact time). At first, the catalyst was saturated for 30 min with silane and then the flow of CH_2F_2 was switched on resulting in conversion of 23%. After 3 h the equilibrium was disturbed. The flows of both substrates were switched off. The catalyst was exposed only to carrier gas (N_2) for 1 h. Subsequently, the reaction was restarted yielding a lower conversion of 18% as shown in Figure 18. The catalyst did no longer demonstrate the same reactivity as

before. To conclude, the catalyst cannot be reused if comparable results should be achieved. It is supposed that traces of water in the carrier gas gradually destroy ACF.

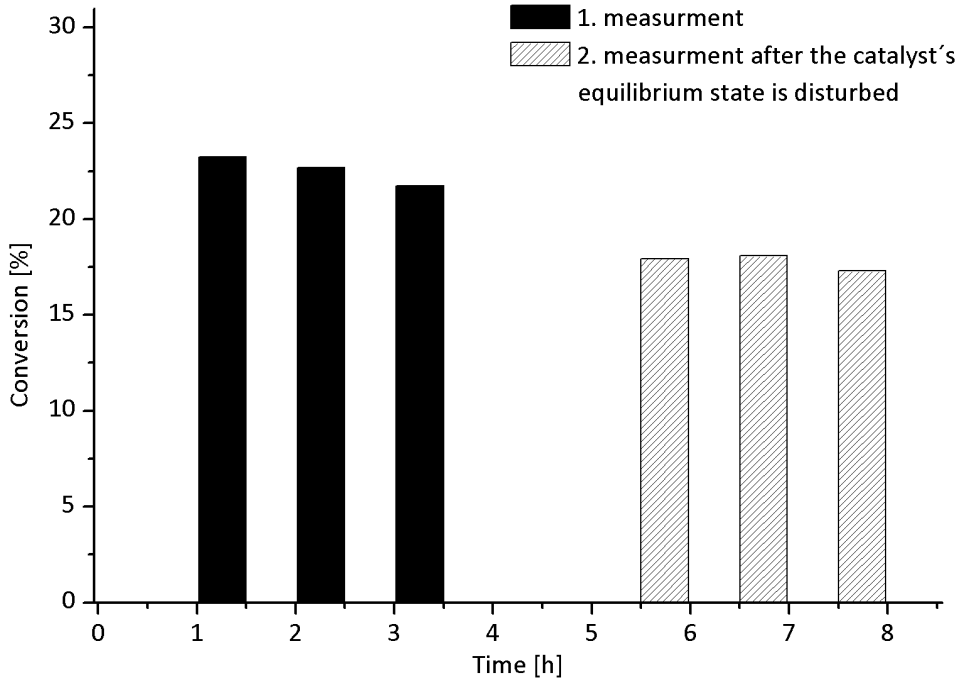

Figure 18. Investigation of the catalytic behaviour of ACF when the equilibrium is disturbed.

3.1.3.2 Results of hydrodefluorination reaction

After the optimum reaction condition and catalyst behaviour were better understood, hydrodefluorination experiments were conducted. Table 7 summarises the results of CH_3F, CH_2F_2 and CHF_3 activation with Et_3SiH in a flow reactor using both ACF and *HS*-AlF_3 as catalysts. All substrates activated at 190 °C and 0.6 s, whereas CH_2F_2 and CHF_3 additionally also at 250 °C.

The activation of fluoromethanes led to the formation of CH_4 as the main product in all examined reactions. At 190 °C and 0.6 s contact time, CH_3F was activated with the conversion of 62% with ACF and 58% with *HS*-AlF_3, whereas only 20% of CH_2F_2 for ACF and 22% by *HS*-AlF_3 was consumed under the same conditions (Figure 19). Unfortunately, CHF_3 yielded only traces of CH_4. Activation at 250 °C brought a slight improvement compared to the reaction at 190 °C. The best activation of CHF_3 was achieved at 250 °C, 0.3 s contact time and with ACF as catalyst resulting in conversion of 5%. No significant improvement was achieved using increased amounts of ACF (entry 11).

We assumed insufficient amount of silane in the reactor to be able to break each individual C-F bond in CHF_3 resulting in lower conversion. We tested raising the temperature of the gas saturator filled with silane to increase the amount of Et_3SiH in the system (entry 12). However, no improvement could be detected. Presumably, the activation energy delivered to this catalytic system is insufficient for cleavage of the first C-F bond in CHF_3. The detection of only CH_4 and no partially defluorinated products implies that the rate determining step is the cleavage of the first C-F bond. This result is in agreement with the outcome obtained in batch reactions (see section 3.1.1).

Table 7. Hydrodefluorination of fluorinated methane derivatives in a flow reactor.

entry	n_{susb}	$n_{susb.}$ [µmol]	cat.	T [°C]	CT [s]	conv. [%][a]	TOF [h^{-1}][b]
1[1]	CH_3F	0.3	ACF	190	0.6	62	14
2[1]	CH_3F	0.1	*HS*-AlF_3	190	0.6	58	6
3	CH_2F_2	1.2	ACF	190	0.6	20	10
4[1]	CH_2F_2	1.0	ACF	250	0.6	12	5
5[1]	CH_2F_2	0.9	*HS*-AlF_3	190	0.6	22	8
6	CH_2F_2	1.0	$AlCl_3$	190	0.6	-	-
7	CHF_3	1.0	ACF	190	0.6	1	0.4
8	CHF_3	1.0	ACF	250	0.1	0	0
9	CHF_3	1.0	ACF	250	0.2	1	0.6
10	CHF_3	1.0	ACF	250	0.3	5	3
11[1,2]	CHF_3	1.0	ACF	250	0.3	6	3
12[1,3]	CHF_3	1.0	ACF	250	0.3	4	3
13	CHF_3	1.1	ACF	250	0.6	2	0.9
14	CHF_3	1.0	ACF	250	1.3	3	0.5

All reactions were carried out using 180 mg of ACF or 190 mg of *HS*-AlF_3. [a] The estimation of the product/substrate amount was performed by GC after previous calibration. [b] Calculated based on the amount of the product per number of active acidic sites at the Lewis acids (1 g Lewis acid contains 1 mmol of active sites determined by NH_3-TPD)[44] divided by conact time in h. [1] single measurements [2] using 360 mg of ACF [3] higher concentration of silane

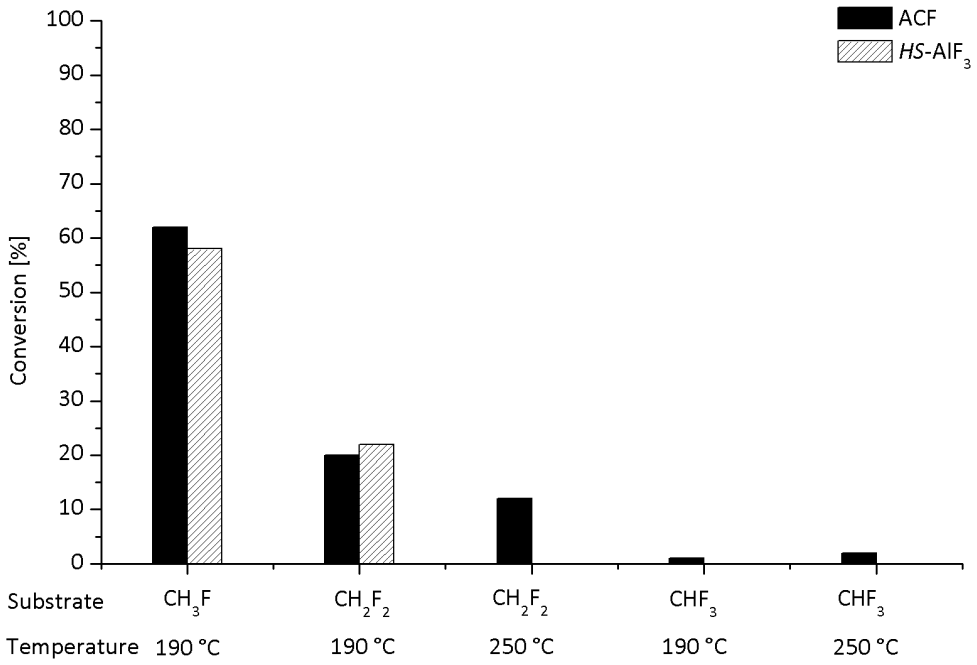

Figure 19. The activation of CH_3F, CH_2F_2 and CHF_3 on ACF and *HS*-AlF_3 in the presence of Et_3SiH at 0.6 s contact time in a flow reactor.

Since the catalytic activity of both catalysts was of similar range, it seems that the short contact times in the flow reactor influence the catalytic potential of ACF and *HS*-AlF_3. Due to the short contact times, longer diffusion pathways into the pores are not possible proving that reactions in the flow reactor are strongly kinetically controlled. Only readily accessible Lewis-acidic sites can take part in the reaction. The porosity has no influence on the activation process in the flow reactor. The similar conversion using either catalyst implies that similar Lewis active sites are responsible for the reactivity of both catalysts in the flow reactor.

Comparing the activation of different fluorinated methane derivatives, both at the same contact time and at a constant temperature, the conversions were higher with lower number of fluorine atoms on the carbon atom, similar to batch reactions. To summarize, the success of hydrodehalogenation reactions depend on the degree of fluorination of methane derivatives. These results are in agreement with simplified theoretical calculations, which are presented below. The enthalpies of reaction for the activation of fluorinated methanes in the presence of Et_3SiH were calculated, utilizing the formation enthalpy for CH_4 and for each substrate except silane. Due to the lack of the data for Et_3SiH and its product Et_3SiF, average binding energies for these substances were used instead.

The reaction enthalpy $\Delta_R H$ was calculated using the following equation:

$$\Delta_R H = \left(\Delta_F H°_{CH_4} + x\, E_{\text{Binding Energy of Si–F}}\right) - \left(\Delta_F H°_{CF_xH_{4-x}} + x\, E_{\text{Binding Energy of Si–H}}\right)$$

The values and results are summarized in Table 8. With increasing number of fluorine atoms in fluoromethanes, they become harder to activate. The reaction enthalpy increases by around 500 $kJ \cdot mol^{-1}$ with each additional fluorine atom in the molecule.

Table 8. Parameters used for the calculations of reaction enthalpy.[198] The calculations assumes that approximated differences in binding enthalpies can be derived from differences in formation enthalpies.

Energy [$kJ \cdot mol^{-1}$]	CH_4	CH_3F	CH_2F_2	CHF_3	'Si-H'	'Si-F'
$\Delta_F H°$	-75	-234	-451	-697	-	-
$E_{\text{Binding energy}}$	-	-	-	-	323	582
$\Delta_R H$	-	418	894	1476	-	-

The formation of ethane as side product in the case of both catalysts and CH_3Cl in the case of ACF is also worth mentioning. Formation of ethane might result from either decomposition of silane, which was added in excess, or the reaction between two CH_3-fragements formed during the reaction on the catalyst surface. To verify this assumption, silane was activated on ACF in the flow reactor under the same conditions as applied for reactions of fluorinated methanes. Ethane was detected as the product of the reaction next to other side products which could not be identified, indicating the decomposition of silane on ACF during the reaction. Furthermore, the formation of CH_3Cl implies that a slow Cl/F exchange reaction takes place in competition to hydrodefluorination and that the catalyst will be further fluorinated.

Aluminium chloride $AlCl_3$, the precursor of ACF is known as a powerful Lewis acid. $AlCl_3$, similar to both, ACF and *HS*-AlF_3, enables the activation of the C-F bond in the presence of silane in NMR reactions. Thus, $AlCl_3$ was tested in the hydrodefluorination of CH_2F_2 in a reactor at 190 °C and 0.6 s contact time (Table 7, entry 6). No formation of CH_4 was detected. $AlCl_3$ in its crystalline form, it is unlikely to be successfully applied as a potential heterogeneous catalyst due to the lack of catalytically-active undercoordinated Al-sites. After dissolving $AlCl_3$, the structure becomes disordered resulting in accessible active sites (Lewis acid-base adduct $AlCl_4^-$), which in turn can react as a homogeneous catalyst achieving high levels of conversion.

3.1.3.3 Mechanism elucidation for hydrodefluorination reactions

The mechanism of the hydrodefluorination reactions was postulated by Ahrens *et al.*. The authors assumed that the reaction proceeds by the silane initially being adsorbed on the Lewis-acidic sites.[48] Such active sites can then activate the Si-H bond of Et_3SiH, which facilitates the cleavage reaction of the C-F bond. This assumption was developed based on a similar mechanism known from homogeneous catalysis and has not been investigated until now.[49] An inverse mechanism is feasible as well, where fluoromethane will be activated first, followed by Si-H bond cleavage (Scheme 45). Thus, we investigated whether the interaction of the silane with the ACF occurs first (a) or if ACF has to interact first with CH_3F (b) for a successful conversion. A wide range of analytical methods and experiments were applied for elucidation of the mechanism. These comprised experiments in flow, batch, NMR-batch reactors as well as *in-situ* FTIR, *Pulse*TA®, NH_3-TPD, MAS NMR, EA and XRD experiments.

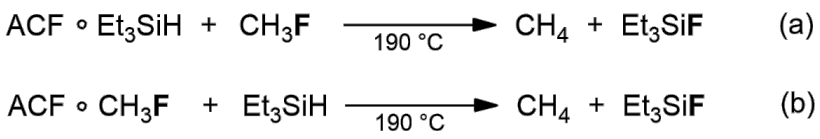

Scheme 45. Two possible mechanisms for hydrodefluorination reactions.

Flow reactor

Under flow conditions, the reactions proceed successfully when ACF is initially saturated with silane. The reversed experiment was also performed, where the catalyst was first treated with CH_3F for 30 min followed by Et_3SiH flow. Surprisingly, the reaction did not proceed in this case. Only the formation of CH_3Cl was detected indicating a further fluorination of ACF. This finding suggests that first formation of the adduct ACF∘Et_3SiH leads to a successful reaction.

Batch reactor

To verify the result of previous reactions in a flow reactor, the experiments were transferred to a batch reactor leading to different reaction kinetics. CH_2F_2 was activated in the presence of ACF previously loaded with Et_3SiH in solid-gas phase reaction in the quasi-static operating conditions (Scheme 46).

Formation of CH_4 as the main product was detected, which is comparable to experiments in the flow reactor. By GC, the conversion was estimated to be only 0.5% after the first 5 min. In Figure 20 a decrease of the methane peak over time is shown. In this catalytic system, the

quantity of silane was limited to the amount already adsorbed on the catalyst. Similar to the reactions in a flow reactor, ethane was also detected. The ethane peak increased over time, which can be explained in various ways. Ethane could either be formed if methyl fragments react with each other due to the decreasing amount of methane or it could be formed by decomposition of silane.

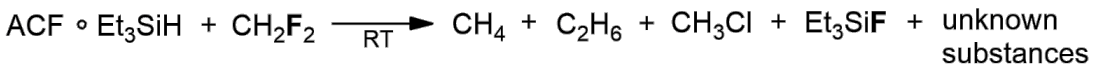

Scheme 46. Hydrodefluorination of CH_2F_2 in the presence of ACF∘Et_3SiH in batch reactor.

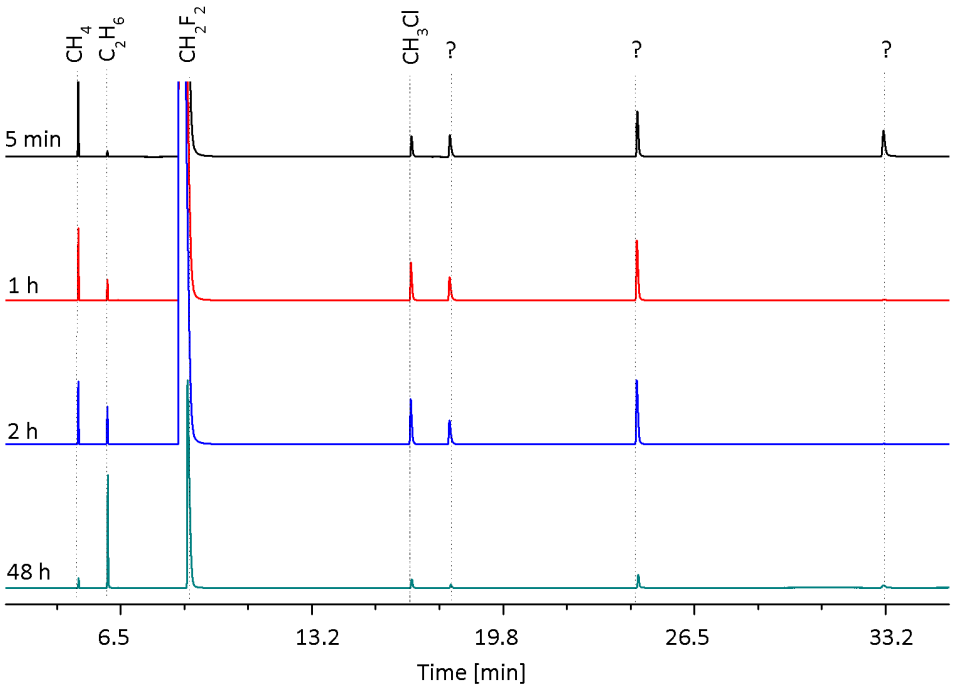

Figure 20. GC chromatogram of the activation of CH_2F_2 on ACF∘Et_3SiH in the batch reactor.

In order to confirm if ethane is formed from decomposed Et_3SiH or from methyl fragments, the reaction was repeated in the presence of ACF loaded with $^{i}Pr_3SiH$ (Scheme 47). Methane was detected again as the main product in a very low conversion of only 0.7% after 5 min. No formation of ethane was observed even after 2 days, providing a final proof that ethane is formed from the ethyl group of Et_3SiH, as shown in Figure 21. Propane was also not detected probably due to higher stability of $^{i}Pr_3SiH$.

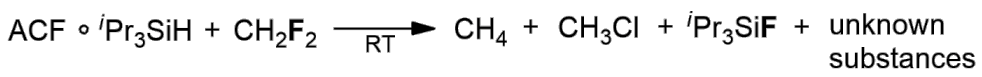

Scheme 47. Hydrodefluorination of CH_2F_2 in the presence of ACF∘^{i}Pr$_3$SiH in the batch reactor.

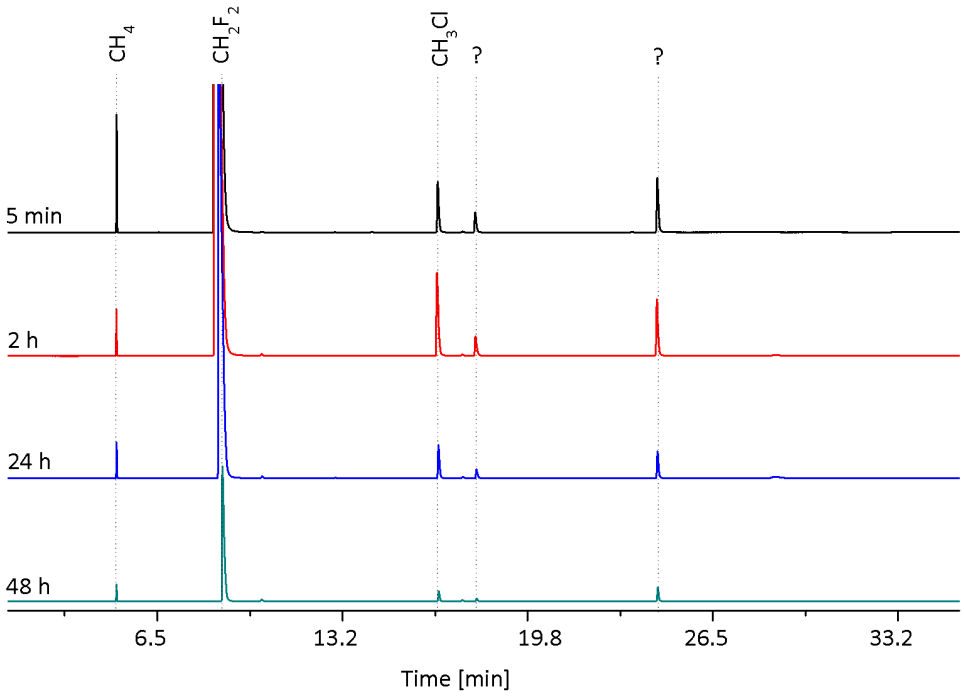

Figure 21. GC chromatogram of the activation of CH_2F_2 on ACF∘^{i}Pr$_3$SiH in batch ractor.

So far, the outcome if only one of the substrates is added to the reaction in the first step has been investigated. The reaction only occurred, if silane was preactivated. It is assumed that the substrates compete for the same active sites. To determine which reaction is thermodynamically favoured, the activation of silane or the interaction with CH_3F, both substrates were added at the same time to ACF. Initially, the catalyst was placed in a flask and remained separated from the other substrates, as shown in Figure 22. Silane was placed in the second flask, while CH_3F filled the part connecting the ACF with Et_3SiH. Before the reaction was started, the flask with silane was evacuated to facilitate evaporation of silane. Then, the valve between silane and fluoromethane was opened to mix both gases before adding them simultaneously to ACF. The reaction was carried out at 70 °C. The formation of methane was observed after only 5 min (Figure 23). After 1 h, the concentration of product reached maximum. Although both substrates were still present in the reaction mixture, the reaction did not proceed any further after that point. Based on the previous experiments, this result suggests that in the first step silane will be activated on the active sites facilitating the hydrodefluorination reaction. However, the interactions with CH_3F are sufficiently strong to suppress silane from the surface and deactivate

the catalyst. Furthermore, the formation of CH_3Cl was also observed. The reason for that could be the Cl/F exchange reaction between chlorine atoms from ACF and CH_3F, which will be closer investigated in the next section.

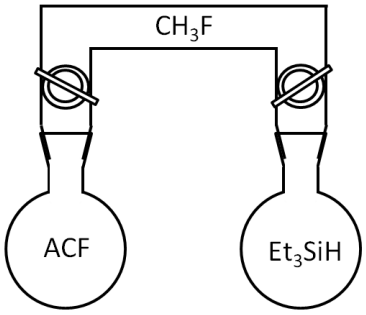

Figure 22. Batch reactor for simultaneous reaction.

$$(Et_3SiH + CH_3\mathbf{F}) \circ ACF \xrightarrow[70\ ^\circ C]{} CH_4 + C_2H_4 + CH_3Cl + Et_3Si\mathbf{F} + \text{unknown substances}$$

Scheme 48. The activation of CH_3F, when CH_3F and Et_3SiH were mixed before adding them simultaneously to the catalyst.

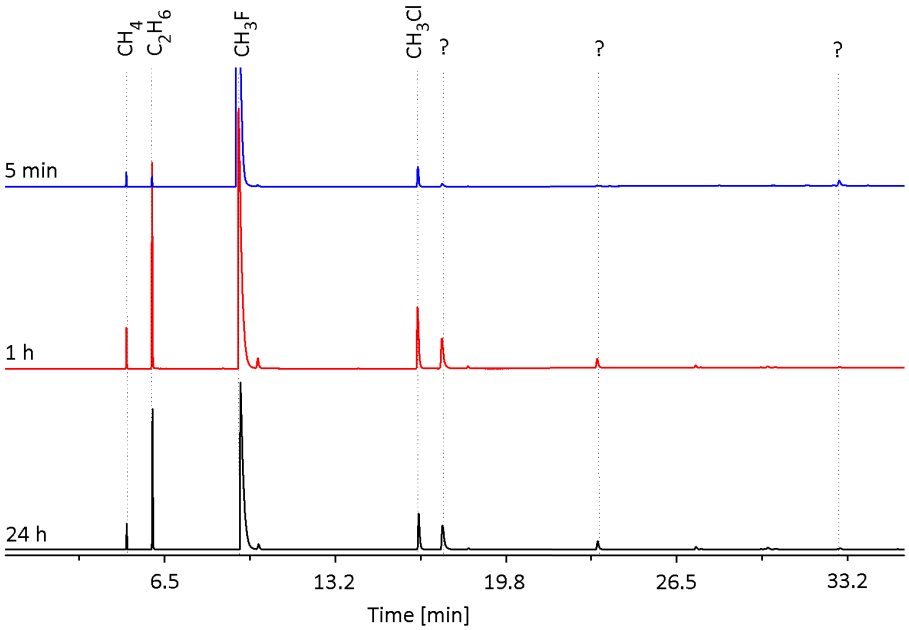

Figure 23. GC chromatogram of the activation of CH_3F, when CH_3F and Et_3SiH were added to ACF simultaneously.

Fluorination of ACF

Elemental analysis (EA)

The experimental data suggests a chemical reaction between ACF and CH_3F, resulting in a further fluorinated, catalytically inactive form of ACF. While loading ACF with CH_3F, the colour of the solid turned from yellow to brown, indicating carbonisation of the catalyst. In experiments in a flow reactor, similar observations were made. The composition of unloaded ACF, the catalyst after reaction in the flow reactor and catalyst loaded with CH_3F were examined by EA. The results presented in Table 9 demonstrate that carbon content was increased by up to 6% after the reactions in both the flow reactor and with CH_3F in the batch reactor. The amount of hydrogen rose to 1.5% for the ACF◦CH_3F adduct and was about 0.7% for the catalyst after a completed experiment in the flow reactor. In the flow reactor, the catalyst will be presumably carbonised due to decomposition of silane causing its gradual deactivation. However, the high content of hydrocarbons in the adduct ACF◦CH_3F implies strong interactions between the catalyst and the substrate revealed in adsorption of monofluromethane. The chlorine content also changed. After the reaction in a flow reactor or the loading of ACF with CH_3F in a batch reactor, the amount of chlorine significantly decreased from 5.5% for ACF to around 1.5%. At the same time, the fluorine content slightly increased, indicating a Cl/F exchange reaction. The amount of fluorination of ACF oscillates around 59% in the flow reactor. According to the literature, complete postfluorination is only possible with strong oxidizing agents such as F_2, resulting in inactive α-AlF_3. However, when using XeF_2 as a fluorination agent, amorphous $AlCl_{0.04}F_{2.96}$ with fluorine content around 66% is formed.[199] Thus, CH_3F seems to act as a mild fluorination agent for ACF.

Table 9. Comparison of the elemental composition of ACF and ACF after a hydrodefluorination reaction in a flow reactor and after loading with CH_3F.

	C (%)	**H (%)**	**Cl (%)**	**F (%)**
ACF	1.197	0.024	5.49	55.45
ACF + CH_3F	6.394	1.553	1.41	57.75
ACF after reaction in flow reactor	5.943	0.692	1.84	58.70

NH$_3$-TPD

NH$_3$-TPD measurements were performed to obtain a better understanding of catalyst deactivation in the presence of CH$_3$F. Figure 24 compares the NH$_3$-TPD profiles of ACF◦CH$_3$F with untreated ACF. For both catalysts, three regions can be distinguished indicating the existence of weak, medium and strong acidic sites. For ACF◦CH$_3$F, the highest amount of desorbed NH$_3$ was determined for temperatures higher than 350 °C, in the typical region for medium-strong Lewis acidic sites. Contrary to result obtained for untreated ACF, the highest amount was not desorbed above temperature, where ACF typically decomposes, but 100°C below. This result suggests that ACF◦CH$_3$F performs by a different reactivity than untreated ACF. The amount of Lewis acidic sites was estimated to be 1.047 mmol·g^{-1} for ACF◦CH$_3$F, which is less compared to untreated ACF (1.545 mmol·g^{-1}), indicating the deactivation of the catalyst as a complex.

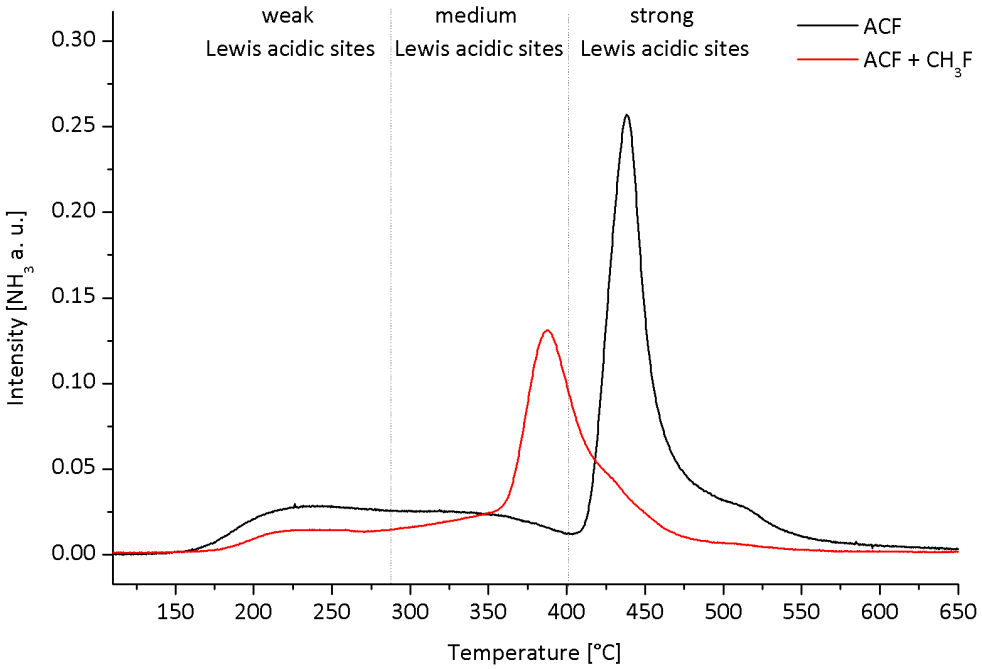

Figure 24. NH$_3$-TPD profiles of ACF and ACF◦CH$_3$F.

NMR experiments to measure the gasphase over ACF◦CH$_3$F

CH$_3$F was added directly to a flask with ACF. The composition of the gas phase over the catalyst was determined using ^{1}H and ^{19}F NMR and GC. Treating the catalyst with gaseous CH$_3$F resulted in an exothermal reaction. The colour of the catalyst turned from yellow to light brown. After one day the glass of the flask became opaque white, which suggests corrosion by formation of HF. The formation of CH$_4$ and CH$_3$Cl was confirmed by GC and ^{1}H NMR

experiments. Additionally, C_2H_6 and CH_2F_2 were measured. The ^{19}F NMR spectrum allows identification of CH_2F_2. No HF could be detected. The results imply that CH_3F was not only adsorbed, but also activated on the ACF surface and underwent further reactions, e.g. further fluorination of ACF.

MAS NMR experiments for ACF◦CH_3F

The adduct ACF◦CH_3F was further characterized by ^{19}F, ^{1}H MAS NMR and related spin echo experiments, as well as ^{1}H-^{13}C CP-MAS NMR. The previous results indicated further fluorination of ACF. As a consequence, the structure of ACF preloaded with CH_3F should change. Figure 25 illustrates the ^{19}F MAS NMR spectra of ACF unloaded and loaded with CH_3F.

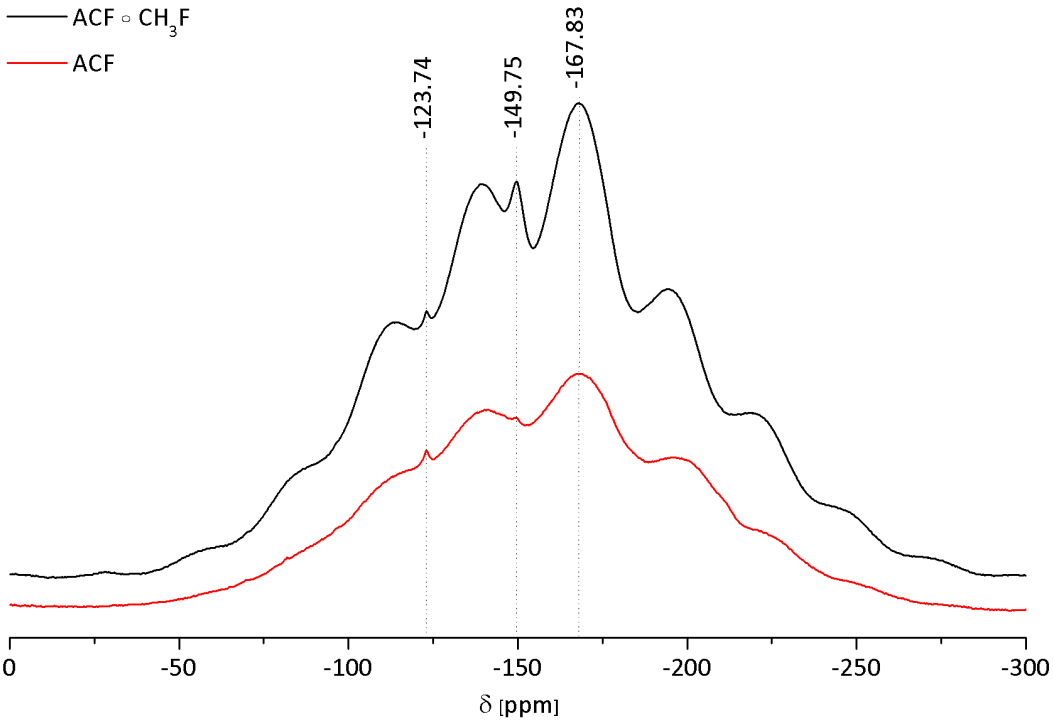

Figure 25. ^{19}F MAS NMR spectra of ACF and ACF◦CH_3F.

The signal at -167.8 ppm is typical for octahedral AlF_6 units in the bulk phase. The peaks at -123.7 ppm and -149.8 ppm are caused by grease. Except a line narrowing, no further changes in the local ACF structure are visible. To confirm this observation, additional rotor-synchronized spin echo ^{19}F MAS NMR experiments were performed, as shown in Figure 26. In the spin echo experiment only less interacting species can be detected on the solid surface. Therefore, this experiment is remarkably useful to assess adsorbed substances on the catalyst

surface. In the spectrum of unloaded ACF, the signal at δ= -177.3 ppm is assigned to the bulk phase fluorine atoms and the peak at δ= -206.1 ppm to the terminal fluorine atoms. The signals at δ= -82.0 ppm, δ= -122.4 ppm and δ= -150.5 ppm originate from grease impurities. Interestingly, the signals assigned to the terminal fluorine atoms at δ= -206.1 ppm disappeared after loading ACF with CH_3F. In the literature, the terminal F atoms are always associated with the high activity of the catalyst. This explains why the catalyst does not show any reactivity after contact with CH_3F. To sum up this experiment, the structure of the catalyst has changed at the surface.

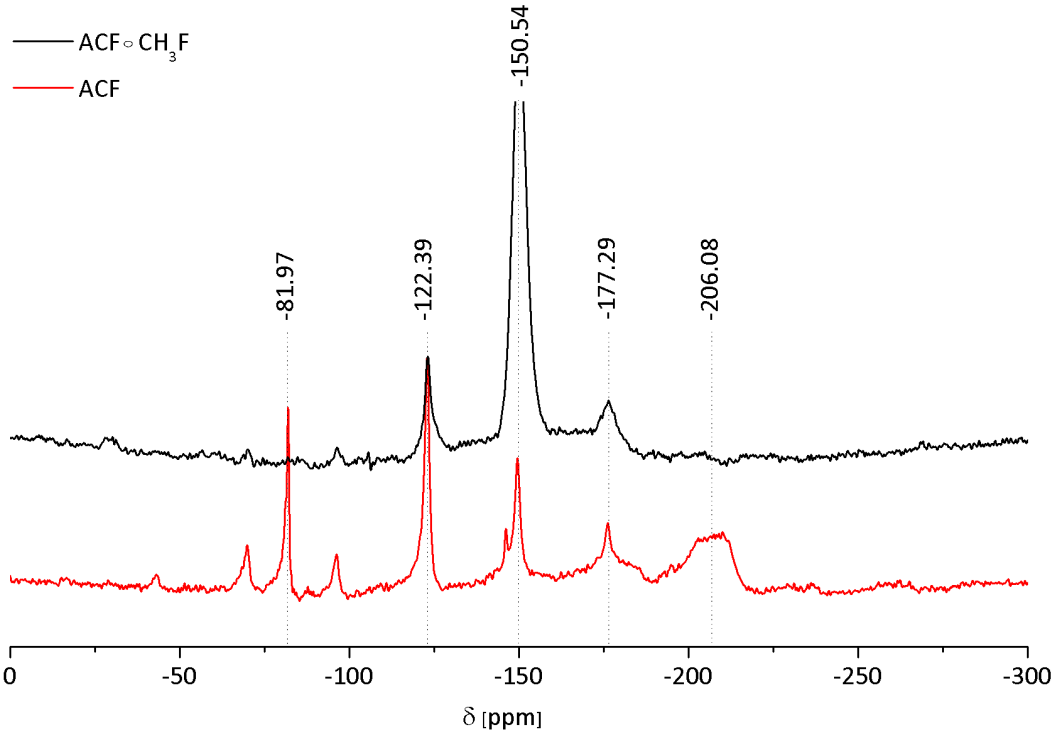

Figure 26. ^{19}F spin echo MAS NMR spectra of ACF before and after the reaction with CH_3F.

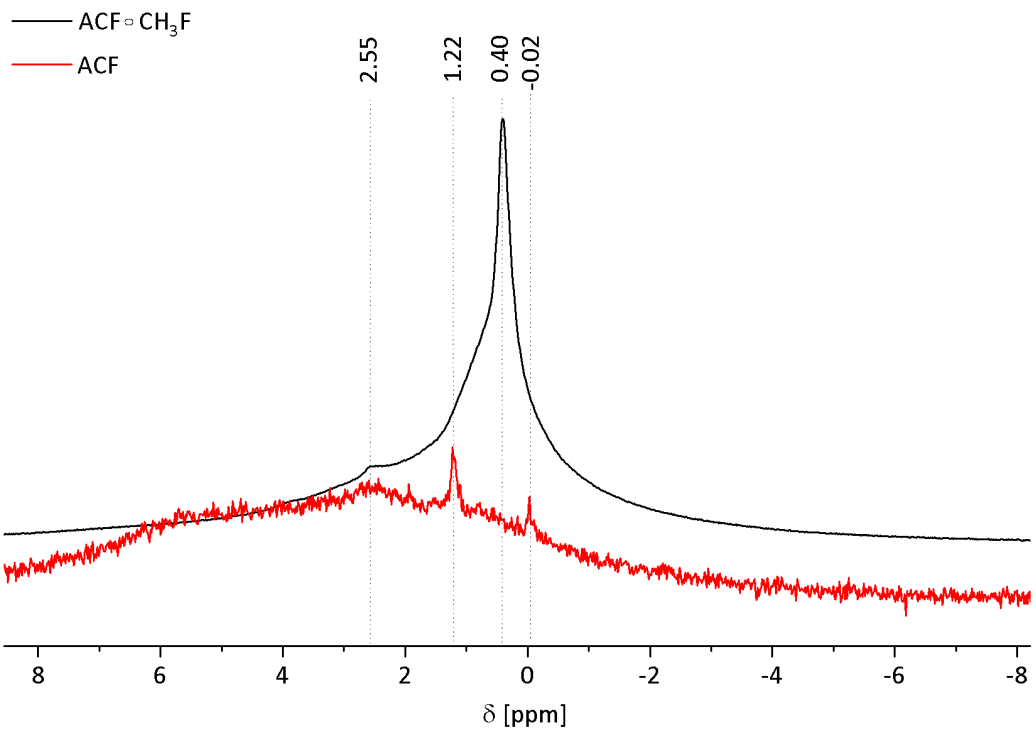

Figure 27. ^{1}H MAS NMR spectra of ACF (increased by factor of 20) and ACF◦CH_3F.

A study of corresponding ^{1}H MAS NMR spectra of ACF unloaded and loaded with CH_3F also reveals some additional information (Figure 27). In the spectrum of unloaded ACF, no peaks with significant intensity were recorded, in contrast to the spectrum of ACF◦CH_3F shows signals at 0.40 and 2.55 ppm.

For a more accurate interpretation, ^{1}H spin echo MAS NMR spectra were recorded (Figure 28). In the spectrum of unloaded ACF, weak but negligible resonances were detected, thus too negligible to require further discussion. In the spectrum of ACF◦CH_3F, the signal at δ= 0.4 ppm indicates the appearance of species containing methyl groups, which are typical for this shift region. The width of this signal (25 Hz) is comparable with the width of signals in liquid NMR indicating unhindered rotation of bound molecules. The signals at δ= 2.6 ppm and δ= 3.9 ppm can presumably be assigned to -CH_3 groups containing downfield shifting electron-withdrawing substitutes, such as Cl^- or F^- substituents.[200]

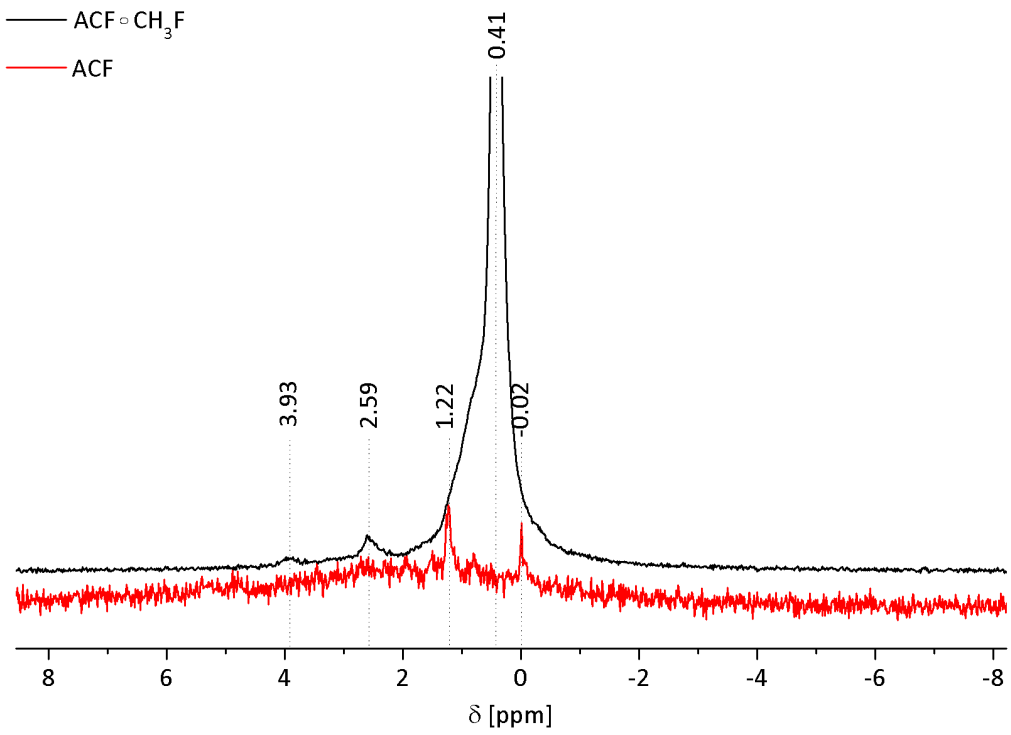

Figure 28. ^{1}H spin echo MAS NMR spectra of unloaded ACF (increased by factor of 5) and ACF previously loaded with CH_3F.

^{1}H-^{13}C CP-MAS NMR spectra for ACF and ACF◦CH_3F are given in Figure 29. Only small signals were detected in the spectrum for unloaded ACF. In ACF◦CH_3F sample, peaks appeared in the region of 0-30 ppm indicating species with methyl groups adsorbed on the surface. As mentioned above, while loading ACF with CH_3F, a strong exothermic reaction and formation of CH_3Cl were observed, proving an F/Cl exchange reaction between the catalyst and CH_3F. In liquid NMR, the signal for CH_3Cl appears at 49.9 ppm and for CH_3F at 71.6 ppm relative to C_6D_6 as reference standard. The 0-70 ppm range is characteristic for sp^3-hybridized species. Thus, the signals detected in the range of 10-30 ppm could be caused by CH_3Cl or CH_3F adsorbed in different binding modes on the surface, which evoked many different signals (a different signal for each binding mode).

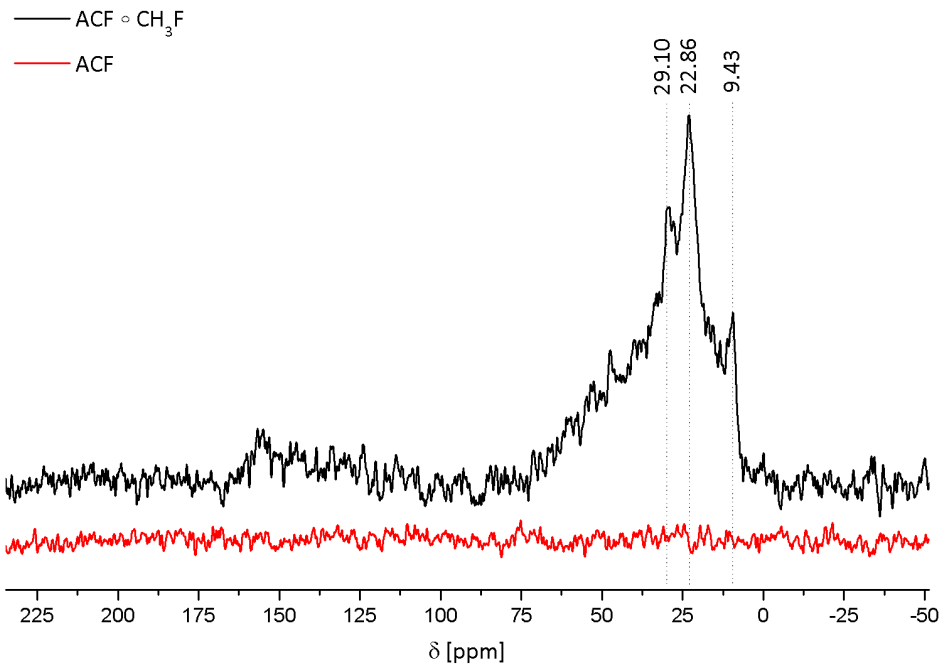

Figure 29. ^{1}H-^{13}C CP-MAS NMR spectra of unloaded ACF and one loaded with CH_3F.

Isomerization reaction

To probe the acidic properties of the catalyst, ACF and ACF◦CH_3F were examined in an isomerisation reaction of CF_3−CBrF−$CBrF_2$ to CF_3−CBr_2−CF_3. The conversions were calculated based on the ratio product to substrate determined by ^{19}F NMR spectroscopy. More than 99% of the substrate was converted by ACF, whereas no conversion was detected for ACF◦CH_3F. This finding is in agreement with the experimental results from flow and batch reactions as well as MAS NMR experiments, suggesting that the terminal fluorine atoms are crucial for catalytic activity. It is worth mentioning, that ACF◦Et_3SiH is also not reactive in this reaction.[48] Presumably, the active sites are occupied by silane preventing the isomerisation but not the hydrodefluorination reaction, which is still possible.

X-ray diffraction results

An analysis of changes in crystallinity was also performed. ACF, ACF◦CH_3F and catalysts removed from the flow reactor after a completed reaction were subjected to X-ray diffraction experiments. Similar to ACF, the modified catalysts were found to be completely amorphous, as shown in Figure 30. The incorporation of additional fluorine atoms and a decreasing amount of chlorine atoms at the same time does not affect the catalyst´s amorphous state.

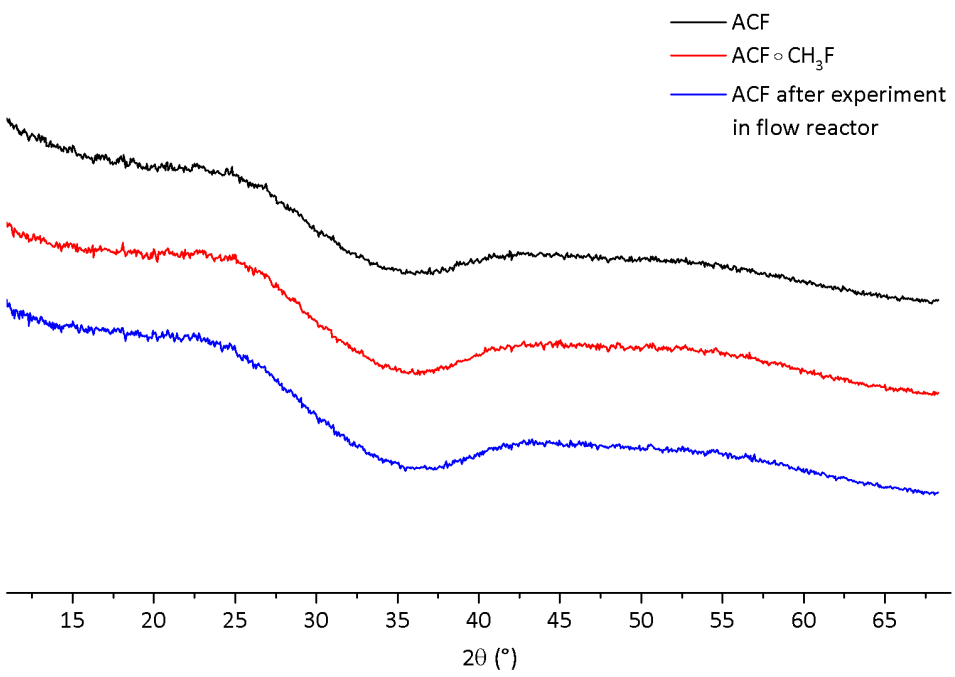

Figure 30. X-ray diffractograms of ACF, ACF◦CH_3F and the catalyst after the hydrodefluorination reaction in a flow reactor.

In-situ FTIR

To obtain further information about the gas-surface interactions between substrates and catalyst, FTIR experiments were conducted. As previously mentioned (Section 3.1.2), the catalyst was initially loaded with silane to protect the active sites before preparing the IR pellets.

Such treated sample was introduced into an IR device and then loaded with Et_3SiH. The excess of silane was removed over 30 min at 0.035 mbar. Even though the sample was evacuated at 0.035 mbar, bands characteristic for silane could still be observed indicating the chemisorption of Et_3SiH.

The peaks at 2095 cm^{-1} overlapping with one at 2054 cm^{-1} are attributed to a Si-H frequency. Compared to the gas phase spectrum of silane, the signals are shifted from 2109 cm^{-1} to lower wavenumbers indicating the adsorption of silane via Si-H bonds. The occurrence of two signals implies that the molecules adsorb on active sites with different strengths. In the spectrum region typical for C-H bonding vibrations, two signals at 1453 and 1415 cm^{-1} were found and attributed to ethyl groups. Compared to the silane peaks appearing at 1467 and 1419 cm^{-1} in the gas phase spectrum, these bands were also shifted indicating interactions with the surface of ACF. No frequency changes were observed for other groups. The band detected at 1243 cm^{-1} was

assigned to deformation vibrations of the Si-CH_3 group, and peaks at 1015 and 973 cm^{-1} could not be clearly associated with any species. The background measurement indicated the presence of water; hence, it is possible that these signals are caused by Si-OH vibrations when Et_3SiH reacts with water to yield silanol. The typical bands for C-H stretching vibrations in the region of 2962-2884 cm^{-1} vanished in the spectrum of bonded silane due to overlapping with signals introduced by water molecules. Also, the peaks detected at 814 cm^{-1} assigned to Si-CH_3 rocking vibrations and at 714 cm^{-1} typical for Si-C stretch vibrations for free silane were no longer detectable in the spectrum of bonded silane.

This outcome indicates that the silane is bonded on Lewis acidic sites via Si-H or ethyl groups, which seems to be implausible. All literature data indicate the polarizsation of Si-H bond in silanes by Lewis acids, and not the interactions with alkyl groups.[48,78,201]

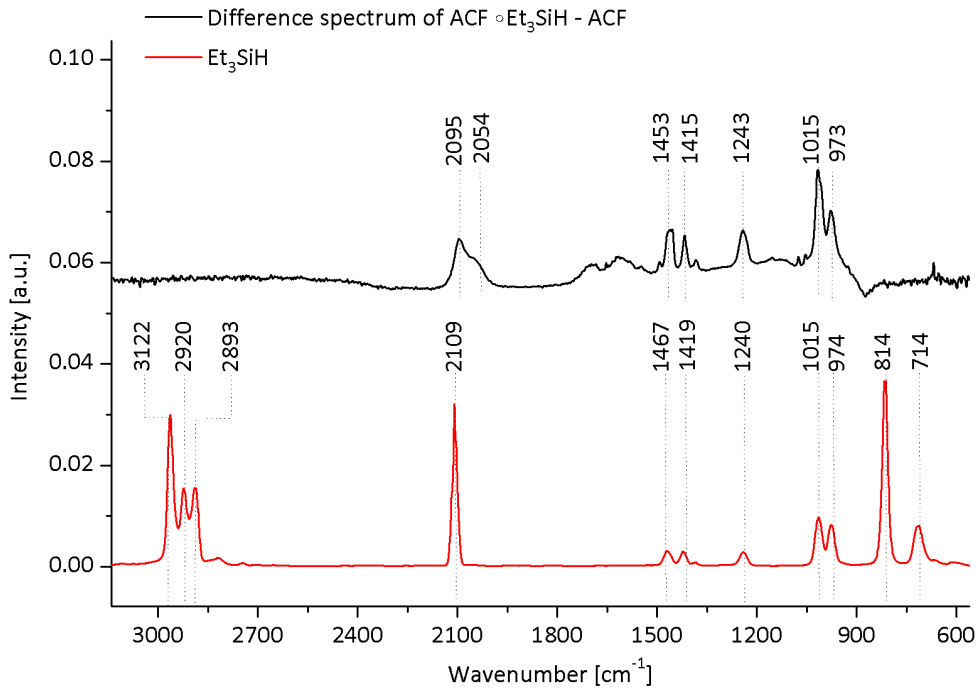

Figure 31. FTIR spectra of free Et_3SiH and Et_3SiH bonded on *HS*-AlF_3.

Furthermore, 2,3,3,3-trifluoro-3-chloropropene ($C_3H_2ClF_3$) was pulsed on the catalyst preloaded with silane (Figure 32 and Scheme 49). The intensity of bands in the region of 2095-2050 cm^{-1} decreased, suggesting a catalytic reaction between ACF◦Et_3SiH and $C_3H_2ClF_3$. Other bands were still present in the spectrum. Thus, *in-situ* FTIR did not give clear evidence for the successful reaction.

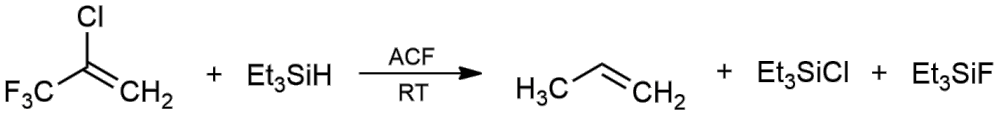

Scheme 49. Pulsing of $C_3H_2ClF_3$ on ACF◦Et_3SiH.

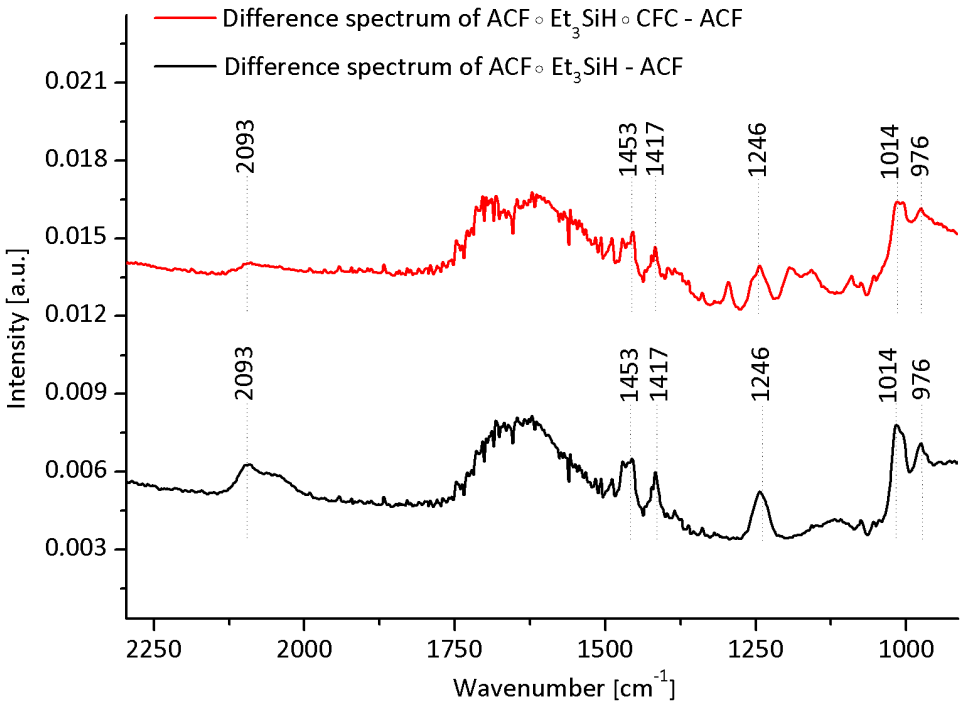

Figure 32. FTIR spectra of ACF◦Et_3SiH and after the pulsing with CFC (1234yf).

*Pulse*TA® experiments

*Pulse*TA® experiments were used for further characterization of interactions between substrates and the catalyst to elucidate the mechanism. According to *Pulse*TA® results given in the literature, ACF certainly interacts with silane.[202] Moreover, the formation of CH_4 was observed by pulsing of CH_3F on ACF∘Et_3SiH. All these experiments support Ahrens *et al.* proposal that Et_3SiH has to be added initially into the reaction mixture[48] and also the previous results.

The previously mentioned experiments published by Feist *et al.* were repeated to prove the reproducibility of the measurements.[202] Figure 33 illustrates loading ACF with silane. With each injection of silane, the exothermal DTA peaks with no endothermal post-effects were observed as well as a continuous mass increase in TG experiment, indicating chemisorption of silane. To follow the mechanism which Ahrens *et al.* proposed[48] (Scheme 50), the subsequent pulses of CH_3F result in large exothermal DTA effects together with a distinct mass gain. The larger first peak in the DTA experiment indicated the formation of methane, which was confirmed by a closer investigation of the peak area ratio A_{CH_3F} to A_{CH_4} (compared to blank experiment), which was in accordance with previous *Pulse*TA® experiments.[202] With each subsequent pulse of CH_3F, no more formation of methane was detected. However, strong exothermal effects were still observed implying that the interactions between ACF and CH_3F predominate over those with silane.

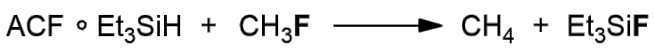

Scheme 50. Loading ACF∘Et_3SiH with CH_3F in the *Pulse*TA® experiment for investigation of the mechanism.

Since the mechanism could proceed inversely, the inverse experiment was performed, as shown below in Scheme 51.

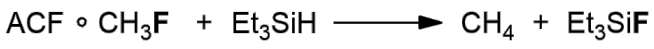

Scheme 51. Inverse loading of ACF∘CH_3F with Et_3SiH in the *Pulse*TA® experiment for investigation of the mechanism.

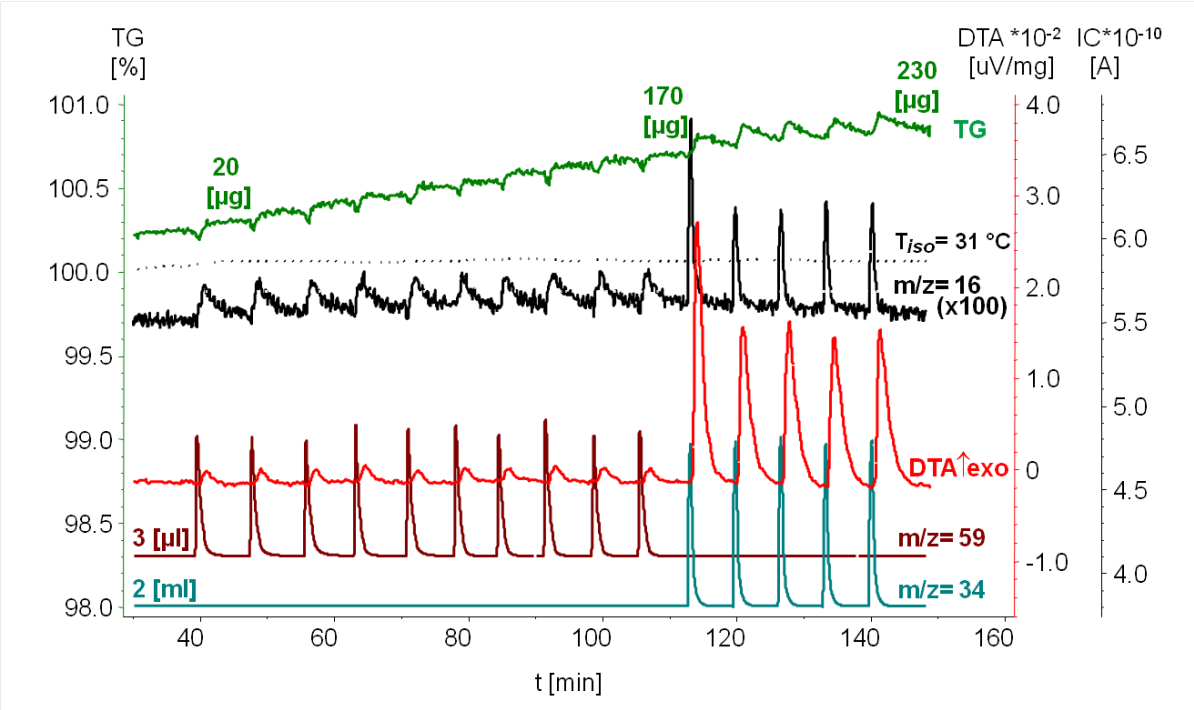

Figure 33. Injection of CH_3F on ACF previously loaded with Et_3SiH in the *Pulse*TA® experiment. The mass curves are assigned to m/z = 16 (CH_4^+), m/z = 34 (CH_3F^+) and m/z = 59 ($C_2H_7Si^+$).

While loading ACF with CH_3F, distinctive exothermal peaks (see DTA curve in Figure 34) and continuous mass gain were detected (see TG curve in Figure 34). An ACF sample treated this way demonstrated no further interactions with Et_3SiH. Neither mass increase nor exothermic effects evidently indicate no chemisorption of Et_3SiH on ACF◦CH_3F takes place. To conclude, CH_3F might block the active sites of the catalyst preventing the reaction with silane, which is consistent with results obtained in flow and batch reactions. The subsequent pulses of CH_3F proceeded as before, resulting in further chemisorption.

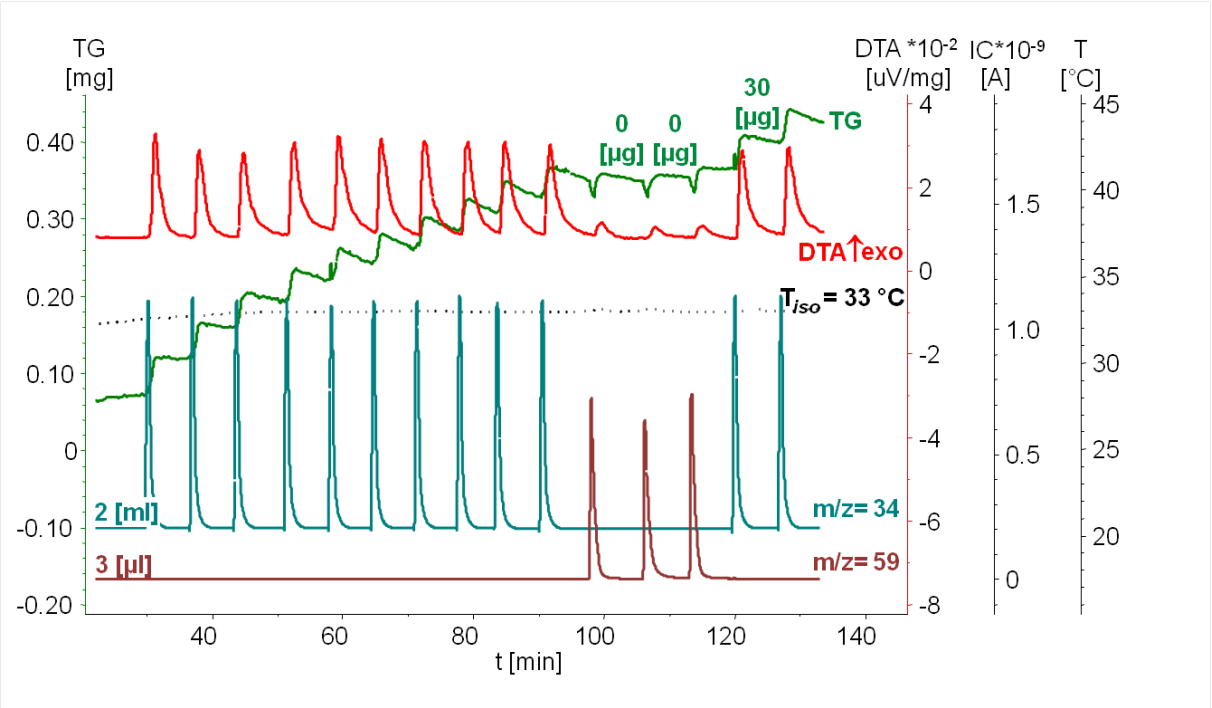

Figure 34. Injection of Et_3SiH on ACF previously loaded with CH_3F in the *Pulse*TA® experiment.

In summury, according to *Pulse*TA® experiments both substrates CH_3F and Et_3SiH interact with the catalyst. *In-situ* FTIR experiments demonstrated that interactions are sufficiently strong to result in silane chemisorption on the active sites of the catalyst. When ACF was exposed to CH_3F, not only an interaction could be demonstrated, but also a chemical reaction, revealing a Cl/F exchange reaction. This is in agreement with elemental analysis results, which demonstrated a lower content of chlorine atoms in the lattice of ACF suggesting its further fluorination. The ^{19}F MAS NMR spectrum of ACF◦CH_3F provided additional information that the terminal fluorine atoms, which are considered to be responsible for the reactivity of the catalyst, are no longer present. In addition, ACF◦CH_3F is not able to catalyse the isomerisation reaction of 1,2- to 2,2-dibromohexafluoropropane. The terminal fluorine atoms dissipate over the course of the reaction, rendering the active site inactive, resulting in loss of its catalytic activity. The results gained in the catalytic reactions in flow as well as batch reactors and with reference to *Pulse*TA® experiments, provided indisputable proof that the formation of ACF◦Et_3SiH is required for a successful reaction. If CH_3F coordinates on the surface of the catalyst in the first step, it deactivates the active sites preventing the interaction with Et_3SiH. All these data let us propose a mechanism for the hydrodefluorination based on the Eley-Rideal model. This is shown schematically in the Figure 35. First, silane coordinates on the ACF surface **(a)**. Next, fluoromethane approaches ACF where silane has already been adsorbed **(b)**. Subsequently, CH_3F reacts with the silane without ever adsorbing on the solid **(c)**. After the

reaction **(d)**, the resulting products are desorbed **(e)**. This mechanism is in agreement with the one proposed by Ozerov *et al.* for the homogeneous catalysis.

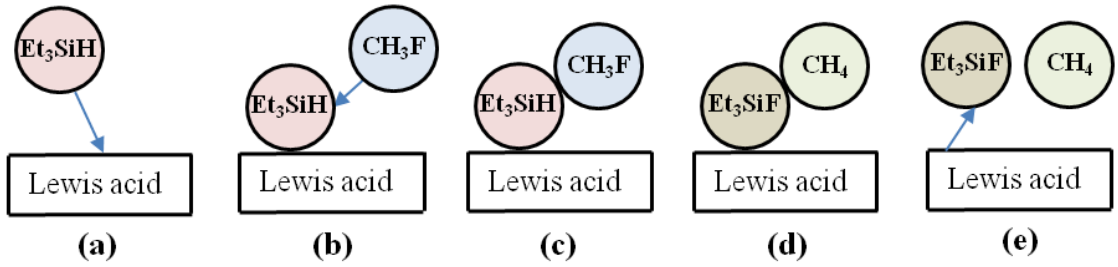

Figure 35. Hydrodefluorination reaction proceeding according to the Eley-Rideal model.

3.1.4 Zirconium chlorofluoride

Zirconium-based catalysts are known for their catalytic ability of C-F bond cleavage reactions. Therefore, zirconium chlorofluoride (ZCF) was synthestised as a heterogeneous alternative to alumnium based catalysts.[40] ZCF is perceived as a potent catalyst for typical Lewis acid catalysed reactions.[203] Following the same synthetic path as for ACF, ZCF was prepared by reacting anhydrous $ZrCl_4$ with CCl_3F at a ratio of 1:6. The fluorinating agent was added to $ZrCl_4$ dispersed in CCl_4. The reaction mixture was stirred at room temperature for 12 h. After the reaction had completed, the solvent had been removed under a vacuum yielding a yellow powder. The final product was characterized by XRD and EA. The diffractograms demonstrate no crystalline peaks, meaning that the new material is amorphous. The elemental content was measured by EA resulting in 26% fluorine content. Based on previous results obtained by our working group, ZCF is considered a mesoporous catalyst. Similar to *HS*-AlF_3, ZCF was tested for catalytic activation of CH_2F_2 by treating it with Et_3SiH or $^{i}Pr_3SiH$ silanes, and C_6D_6, as shown in Figure 36. The results are summarized in Table 10.

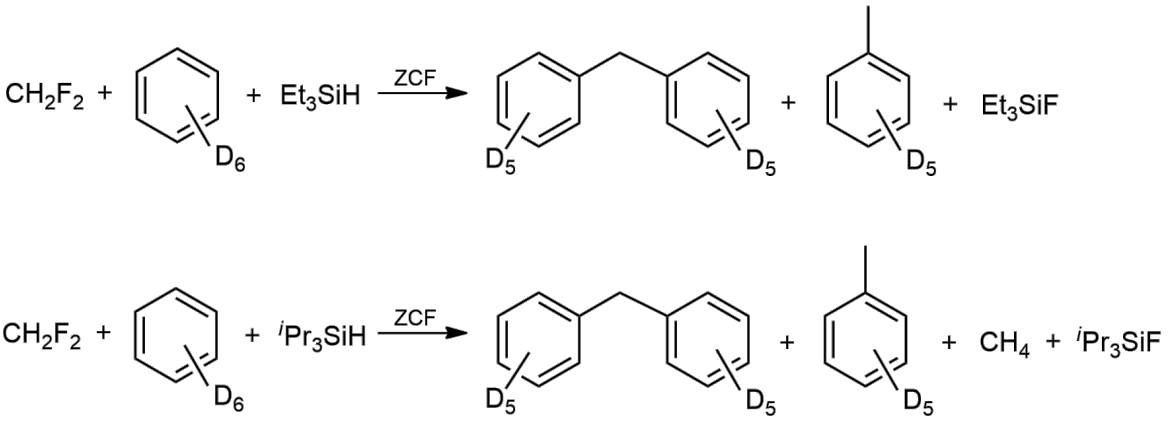

Figure 36. The activation of CH_2F_2 in the presence of silane and C_6D_6.

Table 10. The activation of CH_2F_2 in the presence of different silanes and C_6D_6.

entry	sil.	subs. [mmol]	T [°C]	conv. [%][a]	main product	minor product	TON[b]
1	Et_3SiH	1.21	24	80	$Ph^D_2CH_2$ (97%)	Ph^DCH_3 (3%)	38
2	Et_3SiH	1.15	70	99	$Ph^D_2CH_2$ (96%)	Ph^DCH_3 (4%)	46
3	$^iPrSi_3H$	1.08	24	56	$Ph^D_2CH_2$ (97%)	Ph^DCH_3 (2%) CH_4 (1%)	24
4	$^iPrSi_3H$	1.12	70	98	$Ph^D_2CH_2$ (73%)	Ph^DCH_3 (17%) CH_4(10%)	44

All reactions were carried out in C_6D_6 as a solvent over 5 days. [a] The quantification was performed by ^1H NMR spectroscopy, comparing the ratio of the fluorotriethylsilane to triethylsilane. [b] Calculated based on the amount of the product per number of active acidic sites at the Lewis acids (1 g Lewis acid contains 1 mmol of active sites determined by NH_3-TPD).[44]

Using Et_3SiH, 80% of the substrate was activated at room temperature after 5 days, resulting in a good selectivity to $Ph^D_2CH_2$. Only 3% of substrate was converted to Ph^DCH_3 side product. Conducted at 70°C, the conversion rate increased to about 99%, retaining similar selectivity. To study steric aspects of used silane, $^iPr_3SiH$ was also tested for activation of CH_2F_2. 56% of the substrate was converted after 5 days at room temperature. Similar to Et_3SiH, the reaction proceeded with 97% selectivity, yielding $Ph^D_2CH_2$ as the main product. Ph^DCH_3 and CH_4 (3 mol% total) were formed as side products. In contrast, the distribution of products significantly changed when the substrate was activated at 70 °C. The activation of CH_2F_2 yielded a conversion rate of 98% after 5 days, 73% of which was converted to $Ph^D_2CH_2$, 17% to Ph^DCH_3 and 10% to CH_4.

In summary, ZCF demonstrated good potential towards C-F activation. With $^iPr_3SiH$, lower conversions as well as different product distribution, especially for the reactions at 70°C, were

achieved. Presumably, the steric demand of isopropylgroups influences the catalytic ability of ZCF. However, the conversion rates were lower in comparison with those determined for *HS*-AlF_3.

Since the formation of a silane adduct is crucial for a successful reaction, ^{1}H MAS NMR experiments were performed to identify ZCF◦Et_3SiH. For comparison, the spectrum of *HS*-AlF_3◦Et_3SiH is also depicted, in Figure 37.

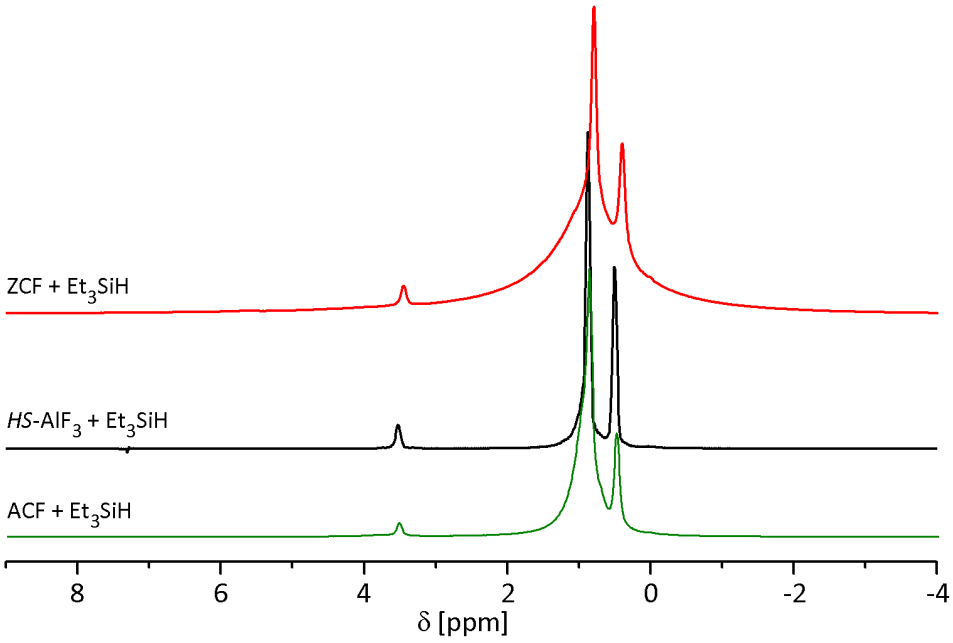

Figure 37. ^{1}H MAS NMR spectrum of ZCF (no suppression of broad spectral components) and ^{1}H MAS NMR echo spectra of *HS*-AlF_3 and ACF loaded with Et_3SiH.

In the ^{1}H MAS NMR spectra all signals typical to silane shifts were observed indicating its adsorption on ZCF. The signal at 3.5 ppm is attributed to the Si-H group, whereas the signals in the region of 0-2 ppm are assigned to the ethyl groups. By closer look at the signal at 3.5 ppm, the ^{29}Si satellites of immobilized Et_3SiH can be clearly identified, which is surprising due to the broad signals typically occurring in MAS NMR (Figure 38). For ZCF◦Et_3SiH, the coupling constant is estimated to be J^{29}Si,H = 176 Hz ,whereas those of free silane (in solution) is J^{29}Si,H = 177 Hz. The slightly lower coupling constant of bonded silane indicates only a weak activation. Smaller coupling constant connote for stronger activation of the Si-H bond. A significant decrease in CC was observed for *HS*-AlF_3, resulting in J^{29}Si,H = 169 Hz, which is consistent with the assumption that it is a stronger Lewis acid than ZCF. The adsorbed silane is

activated not as strongly as in case of ZCF as compared to *HS*-AlF_3, resulting in lower conversion rates.

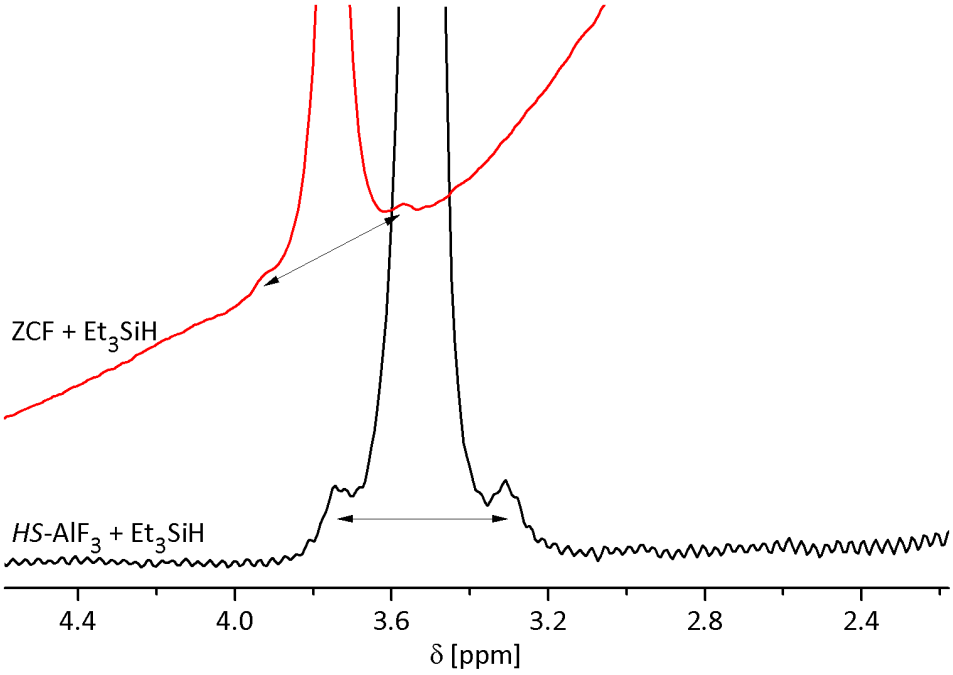

Figure 38. Zoom into Figure 38. The ^{29}Si satellites of immobilized Et_3SiH on the surface of *HS*-AlF_3 and ZCF.

NH_3 TPD experiments were also performed for ZCF to investigate its Lewis acidic properties (Figure 39). The shape of the profile resembles that of ACF. The strongest Lewis acidic sites are also the most abundant found. The absolute amount of active sites could not be determined due to the high content of desorbed acidic species. While heating the sample, the solid presumably suffered from the partial sublimation of $ZrCl_4$.

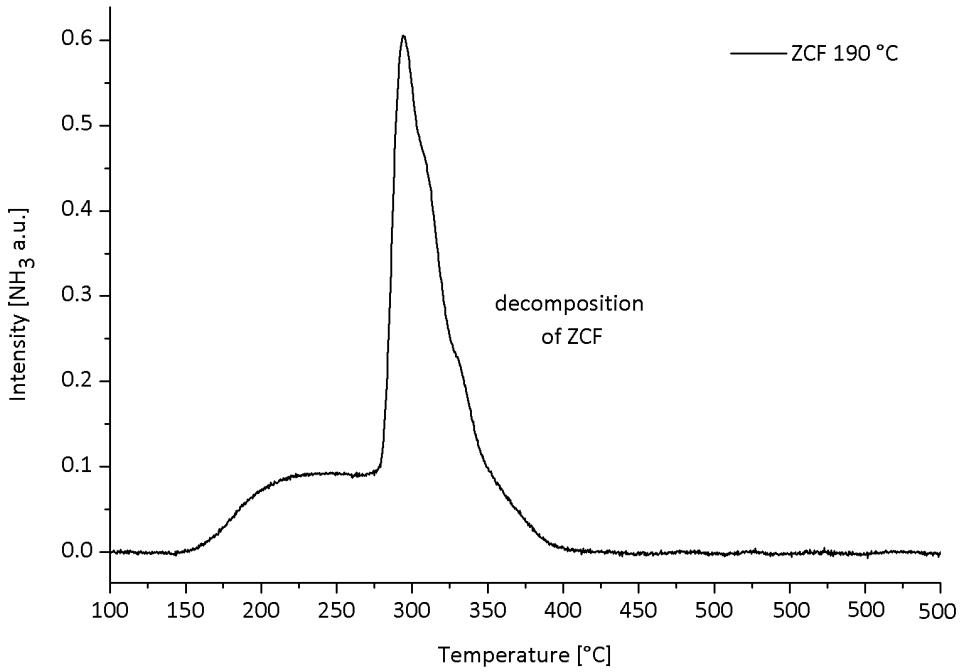

Figure 39. Profile of NH_3-TPD of ZCF preheated at 190 °C.

3.2 Hydrodechlorination

After successful application of aluminium and zirconium chlorofluorides for hydrodefluorination reactions, this approach was tested in the activation of C-Cl bonds. Selected chlorinated substrates were chosen to examine the catalytic activity of ACF and *HS*-AlF_3.

NMR tube reactions

In this section, the catalytic performance of ACF and *HS*-AlF_3 was investigated regarding the activation of monochloromethane CH_3Cl, dichloromethane CH_2Cl_2 and a sterically demanding substrate, 1,2-dichloroethane $C_2H_4Cl_2$. Furthermore, the influence of Et_3SiH and the solvent C_6D_6 on the product distribution was examined. The determination of the product ratio is particularly interesting. Friedel-Crafts-like and hydrodechlorination reactions run simultaneously and appear to be competitive. Depending on the composition of the reaction mixture, the ratio between the hydrodechlorination and Friedel-Crafts-like products can be affected. Therefore, the reactions were carried out with various initial proportions. The substrates were activated in both the presence and the absence of the solvent C_6D_6 or the hydride source Et_3SiH, while the temperature and the reaction time varied. The reactions were conducted at room temperature or at 70 °C, with a reaction time of up to 3 days. The results of the catalytic reactions are discussed below.

3.2.1 Chlorinated methanes

Simultaneous Friedel-Crafts-like and hydrodechlorination reactions

CH_3Cl and CH_2Cl_2 were activated with satisfying results, when using ACF or *HS*-AlF_3 as heterogeneous catalysts, as shown in Table 11. The reactions were performed in the presence of both Et_3SiH and C_6D_6 resulting in both hydrodechlorination and Friedel-Crafts products being observed.

Table 11. Hydrodechlorination of chlorinated methane derivatives in NMR tube reactions.

entry	subs.	subs. [mmol]	cat.	T [°C]	conv. [%][a]	main product	minor product	TON[b]
1	CH_3Cl	1.49	ACF	24	12	Ph^DCH_3 (39%)	CH_4 (61%)	7
2	CH_3Cl	1.48	ACF	70	46	Ph^DCH_3 (54%)	CH_4 (46%)	27
3	CH_3Cl	1.29	*HS*-AlF_3	70	10	CH_4 (82%)	Ph^DCH_3 (18%)	5
4	CH_2Cl_2	0.35	ACF	24	10	$(Ph^D)_2CH_2$ (94%)	Ph^DCH_3 (6%)	1.4
5	CH_2Cl_2	0.35	ACF	70	46	$(Ph^D)_2CH_2$ (95%)	Ph^DCH_3 (5%)	10
7	CH_2Cl_2	0.35	*HS*-AlF_3	70	7	$(Ph^D)_2CH_2$ (92%)	Ph^DCH_3 (8%)	6

All reactions were carried out in C_6D_6 as a solvent over 3 days using 25 mg of catalysts. For the activation of CH_3Cl 1.29 mmol and for CH_2Cl_2 0.70 mmol of silane were used. [a] The quantification was performed by ^1H NMR spectroscopy, comparing the ratio of product to substrate . [b] Calculated based on the amount of the product per number of active acidic sites at the Lewis acids (1 g Lewis acid contains 1 mmol of active sites determined by NH_3-TPD).[44]

The reactions can be compared only based on TONs and not by conversions. It is difficult for gaseous substrates to add them in defined quantities.

The activation of CH_3Cl with ACF yielded a conversion of around 12% (TON= 7) after 3 days at 24 °C and 46% (TON= 27) at 70 °C, whereas only 10% (TON= 5) of the substrate was converted with *HS*-AlF_3 after 3 days at 70 °C. The product distribution differs between ACF and *HS*-AlF_3. With ACF, 54% of converted CH_3Cl reacted via a Friedel-Crafts mechanism to give Ph^DCH_3 as the main product and methane as a side product. Using *HS*-AlF_3, 82% of converted substrate reacted to CH_4 in hydrodechlorination reaction and only 18% to Ph^DCH_3.

Activating CH_2Cl_2 with ACF, 10% (TON= 1.4) of the substrate was converted at 24 °C after 3 days and increased to 46% at 70 °C (TON= 6). Similarly, CH_2Cl_2 was preferably activated in

a Friedel-Crafts type reaction to give 95% of $Ph^{D}_{2}CH_2$ and 5% of the side product $C_6D_5CH_3$ formed in one hydrodechlorination and one Friedel-Crafts step.

Using *HS*-AlF_3 as the catalyst, the main product in the activation of CH_3Cl was in contrast the hydrodechlorination product CH_4. Regarding CH_2Cl_2, it was still preferably consumed to give the Friedel-Crafts product $Ph^{D}_{2}CH_2$. The selectivity for the activation of CH_2Cl_2 was similar to the reaction carried out with ACF.

Compared to fluorinated methanes, the same reactivity trends could be established. The less chlorinated the molecule, the better the observed conversions. The reason for higher conversions with a decreasing number of chlorine atoms at the carbon atom is the decreasing dissociation energy of the C-Cl bond with higher amounts of chlorine atoms in the molecule.

In general, higher conversions were achieved with ACF than with *HS*-AlF_3. Similar to reactions with fluorinated methanes in NMR tube reactions, ACF seems to be a more suitable catalyst for the activation of small molecules such as chlorinated methanes. The difference in catalytic potential of both catalysts can be explained again by their different porosity. The porosity has a significant impact on the accessibility of the active sites for substrates, influencing their reactivity. In the micropores of ACF small substrates are more efficiently retained, which results in a better adsorption. Further, the presence of other substrates such as benzene or silane could also be crucial for the success of hydrodechlorination reaction.

Also note that similar to fluorinated methanes, the partially chlorinated product in the activation of CH_2Cl_2 was not observed suggesting that the activation of the first C-Cl bond is vital for the reaction and the rare limiting step. Moreover, higher conversions were achieved at higher temperatures.

Friedel-Crafts-like reactions

To investigate the influence of silane on the catalyst`s reactivity, CH_3Cl and CH_2Cl_2 were activated in absence of silane expecting only the formation of Friedel-Crafts products. The results are summarised in Table 12.

A total of 27% of CH_3Cl at 24 °C and 46% at 70 °C after 3 days were converted, as expected, exclusively to $Ph^{D}CH_3$ using ACF. In the presence of *HS*-AlF_3, only 19% conversion at 70 °C after 3 days was achieved resulting, again in only one product $Ph^{D}CH_3$.

Activating CH_2Cl_2 with ACF, 95% of the substrate was consumed after 3 days at 24 °C, whereas surprisingly at 70 °C the conversion was only 65%. Similar to previous reactions, the conversion achieved with *HS*-AlF_3 was lower, yielding 52% of $Ph^D{}_2CH_2$ at 70 °C after 3 days. Unexpectedly, in the presence of ACF, besides 99% of the substrate which reacted to $Ph^D{}_2CH_2$, 1% was activated to Ph^DCH_3. Ph^DCH_3 was formed in one Friedel-Crafts, but also in one hydrodechlorination reaction step, which can be explained only by a Cl/H exchange reaction.

The examples of hydride abstraction reactions are scarce in literature, but known to be catalyzed by very strong Lewis acids[204–207], also in a flow reactor.[208] To exclude any other hydride ion source, the reaction was also performed in a PFTE NMR tube. Figure 40 compares the reactions in glass and a PFTE tubes carried out at 24 °C during 5 days. The reactions were monitored via ^1H NMR spectroscopy initially every 2 h and after one day every 24 h. The higher conversions were achieved in glass NMR tubes, resulting in conversion of 95% after 3 days with ACF. $Ph^D{}_2CH_2$ was formed as the main product, whereas 1% of the substrate yielded in Ph^DCH_3. In the PFTE Liner only 71% of the substrate was activated after 3 days. Similar to the reactions carried out in glass NMR tubes, 98% of the substrate reacted to $Ph^D{}_2CH_2$ and 2% to Ph^DCH_3, indicating that hydride ions do not originate from the glass. The purity of the substrates was also investigated, but no significant impurities were found via ^1H NMR and GC/MS experiments.

The course of the reaction is also interesting. 80% of conversion was reacted after only 1 day. The remaining 20% of the reaction was accomplished within the next two days of reaction.

Table 12. Activation of CH_3Cl and CH_2Cl_2 in the presence of C_6D_6 using ACF and *HS*-AlF_3 as catalysts but without silane.

entry	subs.	subs. [mmol]	cat.	T [°C]	t [d]	conv. [%][a]	main product	minor product	TON[b]
1	CH_3Cl	1.50	ACF	24	3	27	Ph^DCH_3 (>99%)	-	16
2	CH_3Cl	1.46	ACF	70	3	79	Ph^DCH_3 (>99%)	-	46
3	CH_3Cl	1.82	*HS*-AlF_3	70	3	19	Ph^DCH_3 (>99%)	-	14
4	CH_2Cl_2	0.35	ACF	24	1h	41	$Ph^D{}_2CH_2$ (99%)	Ph^DCH_3 (1%)	6
5	CH_2Cl_2	0.35	ACF	24	3h	49	$Ph^D{}_2CH_2$ (99%)	Ph^DCH_3 (1%)	7
6	CH_2Cl_2	0.35	ACF	24	5h	58	$Ph^D{}_2CH_2$ (99%)	Ph^DCH_3 (1%)	8
7	CH_2Cl_2	0.35	ACF	24	7h	62	$Ph^D{}_2CH_2$	Ph^DCH_3	9

entry	subs.	subs. [mmol]	cat.	T [°C]	t [d]	conv. [%][a]	main product	minor product	TON[b]
							(99%)	(1%)	
8	CH_2Cl_2	0.35	ACF	24	1	80	$Ph^D_2CH_2$ (99%)	Ph^DCH_3 (1%)	11
9	CH_2Cl_2	0.35	ACF	24	3	95	$Ph^D_2CH_2$ (99%)	Ph^DCH_3 (1%)	13
10	CH_2Cl_2	0.35	ACF	24	4	96	$Ph^D_2CH_2$ (99%)	Ph^DCH_3 (1%)	13
11	CH_2Cl_2	0.35	ACF	24	5	100	$Ph^D_2CH_2$ (99%)	Ph^DCH_3 (1%)	13
12[t]	CH_2Cl_2	0.35	ACF	24	1h	37	$Ph^D_2CH_2$ (98%)	Ph^DCH_3 (2%)	5
13[t]	CH_2Cl_2	0.35	ACF	24	3h	43	$Ph^D_2CH_2$ (98%)	Ph^DCH_3 (2%)	6
14[t]	CH_2Cl_2	0.35	ACF	24	5h	46	$Ph^D_2CH_2$ (98%)	Ph^DCH_3 (2%)	6
15[t]	CH_2Cl_2	0.35	ACF	24	7h	49	$Ph^D_2CH_2$ (98%)	Ph^DCH_3 (2%)	7
16[t]	CH_2Cl_2	0.35	ACF	24	9h	50	$Ph^D_2CH_2$ (98%)	Ph^DCH_3 (2%)	7
17[t]	CH_2Cl_2	0.35	ACF	24	1	55	$Ph^D_2CH_2$ (98%)	Ph^DCH_3 (2%)	8
18[t]	CH_2Cl_2	0.35	ACF	24	2	66	$Ph^D_2CH_2$ (98%)	Ph^DCH_3 (2%)	9
19[t]	CH_2Cl_2	0.35	ACF	24	3	71	$Ph^D_2CH_2$ (98%)	Ph^DCH_3 (2%)	10
20[t]	CH_2Cl_2	0.35	ACF	24	4	71	$Ph^D_2CH_2$ (98%)	Ph^DCH_3 (2%)	10
21[t]	CH_2Cl_2	0.35	ACF	24	5	73	$Ph^D_2CH_2$ (98%)	Ph^DCH_3 (2%)	10
22	CD_2Cl_2	0.35	ACF	24	3	No products detected in 1H spectrum			
23[t]	CD_2Cl_2	0.35	ACF	70	3				
24	CH_2Cl_2	0.35	ACF	70	3	65	$Ph^D_2CH_2$ (99%)	Ph^DCH_3 (1%)	9
25	CH_2Cl_2	0.35	*HS*-AlF_3	70	3	52	$Ph^D_2CH_2$ (>99%)	-	7

All reactions were carried out using 25 mg of the catalysts. [a] The quantification was performed using ^{1}H NMR spectroscopy, comparing the ratio of the product to the substrate. [b] Calculated based on the amount of the product per number of active acidic sites at the Lewis acids (1 g Lewis acid contains 1 mmol of active sites determined by NH_3-TPD).[44] t-reaction in teflon liner, g- reaction in glass NMR tubes

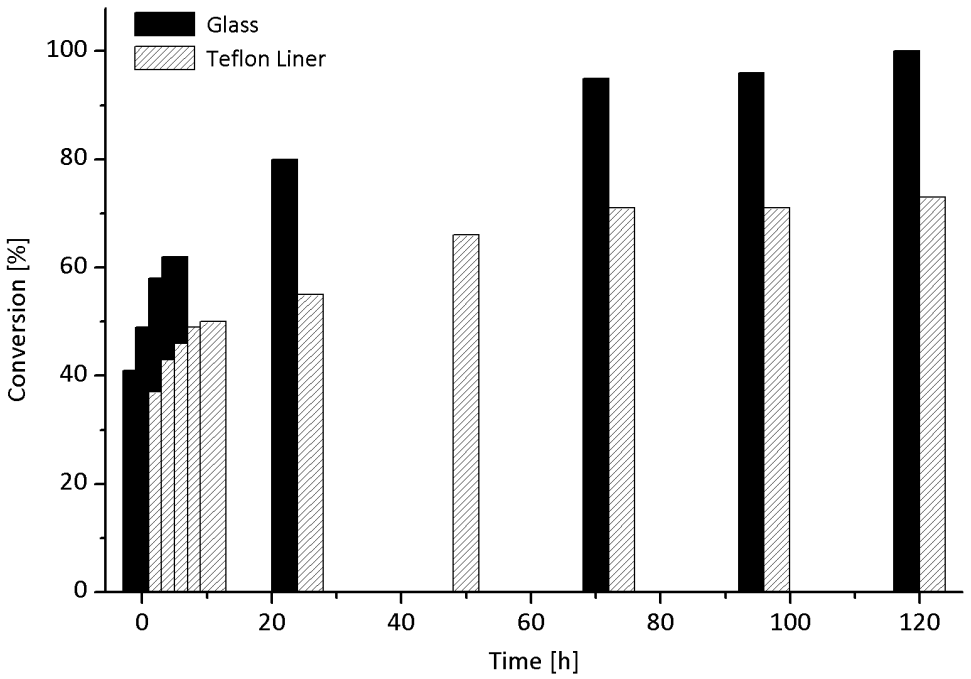

Figure 40. Activation of CH_2Cl_2 in the presence of C_6D_6 using ACF as heterogeneous catalyst.

Another possible hydride source could be ACF itself. Instead of CH_2Cl_2, CD_2Cl_2 was activated in the presence of C_6D_6 in the PTFE tube (Table 12, entries 22, 23). After 3 days at 70 °C no products could be detected which clearly proves that ACF was not the hydride source.

In addition, the conversions achieved in the presence of silane and C_6D_6 are higher, indicating that Friedel-Crafts reactions are preferred over hydrodechlorination reactions. The reason for that will be explained in subsequent parts of the thesis with the help of *Pulse*TA® experiments.

Hydrodechlorination reactions

To prove which reactions are thermodynamically favoured, Friedel-Crafts-like reactions or hydrodechlorination, C_6D_6 was excluded in this set of experiments. Chlorinated methanes were activated exclusively in the presence of Et_3Si, as shown in Table 13. In the presence of ACF, CH_3Cl was activated to methane revealing 13% conversion after 3 days at 70 °C, whereas no reaction was observed for *HS*-AlF_3. Similar results were obtained for CH_2Cl_2. Using ACF, 7% of the substrate was consumed in a hydrodechlorination reaction after 3 days at 70 °C. The conversion increased to 10% after 10 days. No reaction was observed for *HS*-AlF_3. The conversions here were lower than in the case for Friedel-Crafts type reactions in the presence of C_6D_6, again implying that this mechanism is preferred over the hydrodechlorination pathway.

Compared to fluorinated methanes, the conversions of chlorinated substrates were significantly lower. Presumably, the driving force for the Si-H/C-Cl to Si-Cl/C-H metathesis reaction is not as strong as for fluorinated substrates.

Table 13. Hydrodechlorination of CH_3Cl and CH_2Cl_2 in the presence of Et_3SiH

entry	subs.	subs. [mmol]	cat.	T [°C]	t [d]	conv. [%][a]	main product	minor product	TON[b]
1	CH_3Cl	1.82	*HS*-AlF_3	70	3	-	-	-	-
2	CH_3Cl	1.78	ACF	70	3	13	CH_4	-	9
3	CH_2Cl_2	0.35	ACF	70	3	7	CH_4	-	1
4	CH_2Cl_2	0.35	ACF	70	10	12	CH_4	-	2
5	CH_2Cl_2	0.35	HS-AlF_3	70	3	-	-	-	-

All reactions were carried out using 25 mg of the catalysts and in 0.6 ml Et_3SiH. [a] The quantification was performed using ^1H NMR spectroscopy, comparing the ratio of the product to the substrate. [b] Calculated based on the amount of the product per number of active acidic sites at the Lewis acids (1 g Lewis acid contains 1 mmol of active sites determined by NH_3-TPD).[44]

3.2.2 Flow reactor

Hydrodechlorination reactions were also tested in a flow reactor, where different conditions to NMR tubes are applicable (shorter contact times, higher temperatures). We anticipated that the mechanism for the C-Cl bond activation could be elucidated in this set of experiments. Two possible mechanisms were examined.

Choosing the same procedure as for fluorinated substrates, ACF was initially saturated with Et_3SiH and then a flow of CH_3Cl was started. The conversion to methane was 23% with TOF= 10. For the reversed mechanism, where ACF was saturated with CH_3Cl in the first step followed by reaction with Et_3SiH, 10% of the substrate was converted to methane (TOF= 23). Comparing TOFs, the mechanism for the chlorinated compounds appears to proceed differently than for fluorinated methanes indicating that initial polarisation of the C-Cl bond is favoured over the activation of silane. However, the results are not conclusive in terms of which substrate has to be activated first.

Contrary to the results achieved in NMR tubes, where the differences in conversion in the activation of chloro and fluorosubstrates were significant, the results in the flow reactor are comparable, indicating that the reactions are not only thermodynamically but also kinetically controlled.

Table 14. Hydrodechlorination of CH_3Cl

entry	cat.	$n_{subs.}$ [µmol]	T [°C]	CT [s]	conv. [%][a]	TOF [h^{-1}][b]
1	ACF∘$HSiEt_3$	1.0	190	0.6	23	10
2	ACF∘CH_3Cl	3.2	190	0.6	10	23

All reactions were carried out using 180 mg of the catalyst. [a] The quantification was performed using previously calibrated GC comparing the ratio of the product to the substrate. [b] Calculated based on the amount of the product per number of active acidic sites at the Lewis acids (1 g Lewis acid contains 1 mmol of active sites determined by NH_3-TPD).[44] divided by contact time in h.

3.2.3 Thermoanalyses

Since the reactions in the flow reactor did not provide conclusive evidence regarding the mechanism, additional *Pulse*TA® experiments were performed.

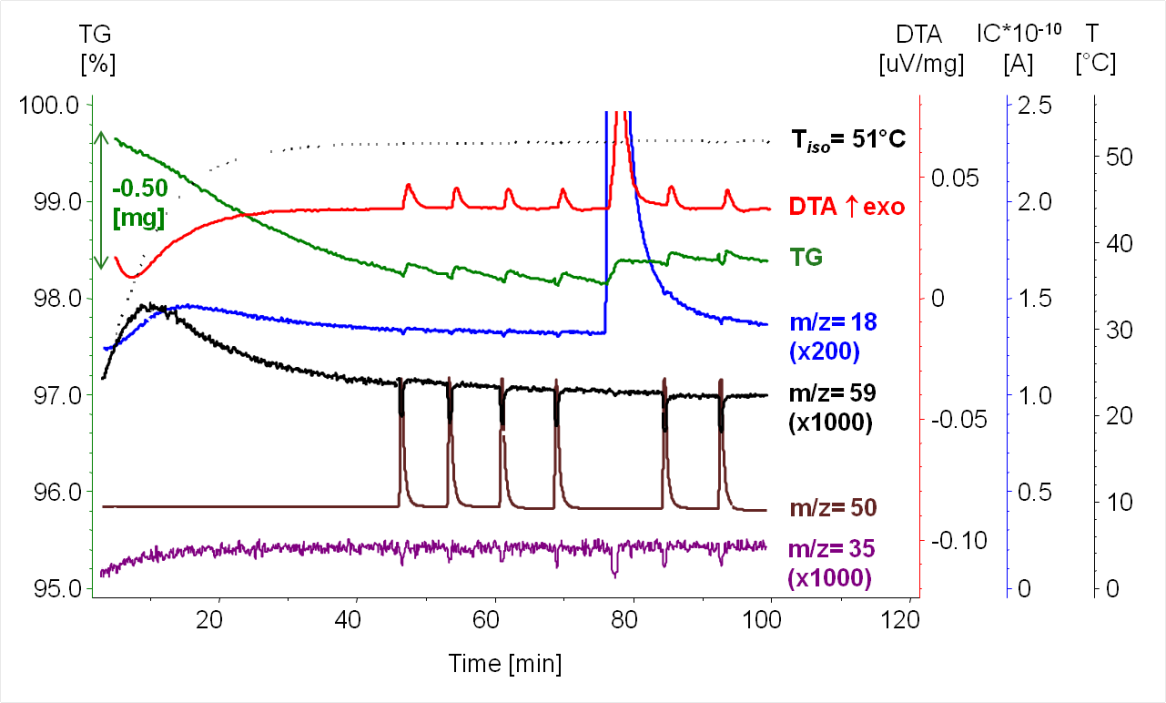

Figure 41. PTA curves of a sequence of injections of gaseous CH_3Cl onto ACF∘Et_3SiH under isothermal condition. The IC curves for the injected water with mass number m/z= 18 (H_2O^+), methyl chloride with mass number m/z= 50 (CH_3Cl^+) and the silane with m/z= 59 ($EtSiH^+$) were recorded. Also the IC curve for the expected product HCl with m/z= 35 (HCl^+) was monitored. The IC curves are shifted for improved clarity.

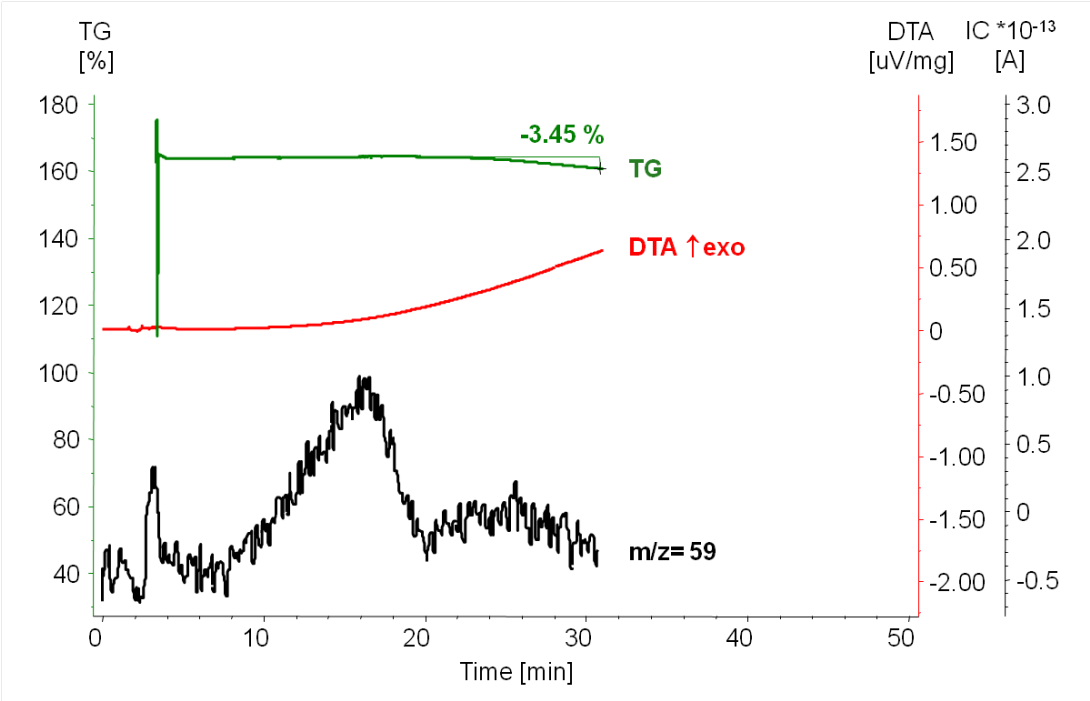

Figure 42. A zoom into the first 20 min of the previous experiment.

Finally, no formation of CH_4 was observed. When analyzing the reason for no methane formation, it is crucial to consider TG and IC curve of m/z= 59 assigned to Et_3SiH recorded during the first 20 min of the experiment before reaching isothermal conditions (see Figure 42 for a closer look at this time frame).

The observed mass decrease at the beginning of the experiment detected by TG indicates the silane desorption from the surface prior the experiment was started. It is possible that no silane was present for the hydrodechlorination reaction. Figure 42 shows that the mass loss detected in TG curve appears slightly later than the peak arising in the IC curve with m/z= 59. The peak in the IC curve does not correspond to desorption of silane.

To confirm the previous result, the sorption behaviour of silane was investigated. Similar to the findings reported by Feist *et al.*[202], the mass gain of 290 µg (0.43 mol-%) observed in Figure 43 represents the amount of chemisorbed silane. The mass increase is accompanied by the appearance of strong exothermal DTA effects with no exothermal post-effects.

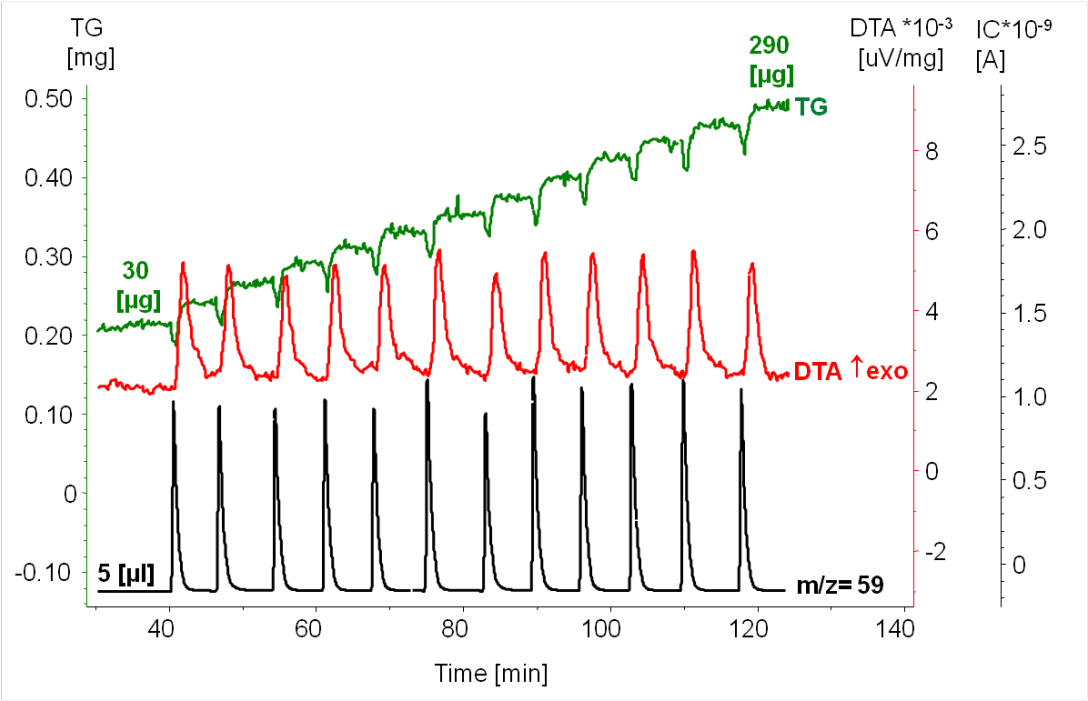

Figure 43. PTA curves of a sequence of injections of 5 µl of Et_3SiH onto ACF. The IC curve for the silane with m/z= 59 ($EtSiH^+$) was recorded. The IC curve is shifted for improved clarity.

To examine the irreversibility of silane adsorption, the sample was thermally treated until the surface was free from Et_3SiH according to IC curve for subsequent silane loading. Figure 44 shows the first loading compared to the amount of adsorbed silane in the reloading process. Performing the same number of injections with similar amounts of silane for second time, only 170 µg (0.31 mol-%) was chemisorbed on ACF, suggesting that the first loading is not fully reversible. This result implies that silane should still be adsorbed on ACF during the first experiment.

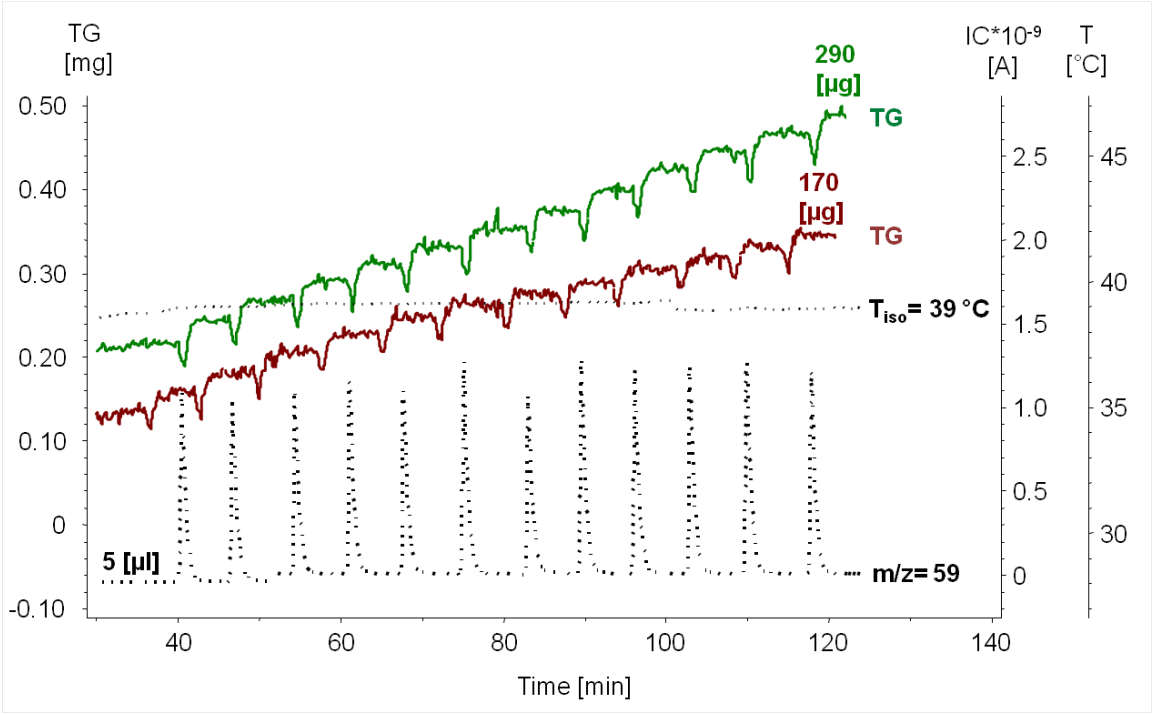

Figure 44. The reloading process of silane (IC curve with mass number m/z= 59) on thermally pre-treated ACF◦Et_3SiH (lower TG curve); for comparison the first loading is also depicted (upper TG curve).

To definitely exclude the possibility that silane could desorb from the catalyst, ACF◦Et_3SiH was repeatedly covered with silane and then treated with CH_3Cl. This is shown in Figure 45. Although with each pulse strong exothermal peaks in DTA were observed, only the first two pulses resulted in a slight mass increase of 30 µg. No formation of CH_4 was observed. The small signals in m/z= 16 occurring with each injection of chlorinated substrate belongs to the defragmentation pattern of CH_3Cl and are not associated with the formation of the potential product CH_4. The experimental data suggest co-adsorption of CH_3Cl at ACF◦Et_3SiH rather than a reaction between ACF◦Et_3SiH and pulsed CH_3Cl, which was consistent with the results of the first experiment.

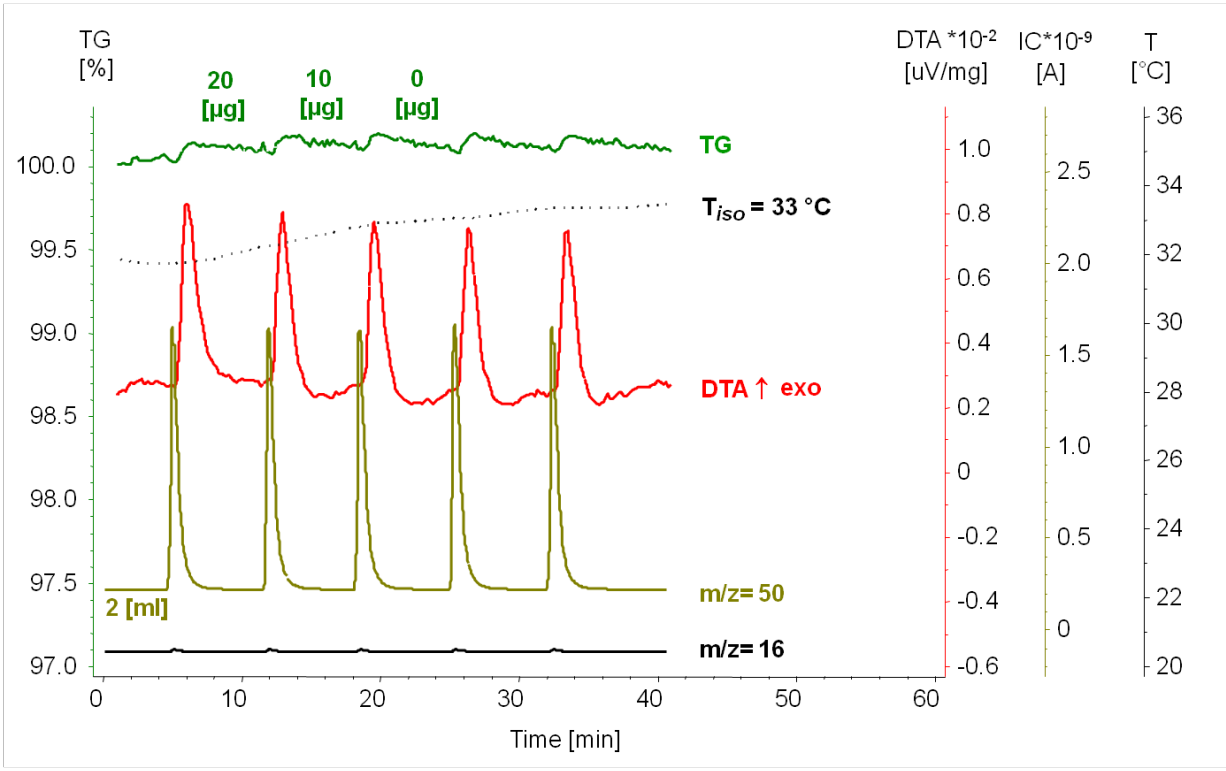

Figure 45. PTA curves for reloaded ACF◦Et_3SiH (39.14 mg) with CH_3Cl (IC curve with m/z= 50) in Ar. Note the DTA peak shape indicating pure chemisorption for the first pulse only, but additional endothermal post-effects for the desorption of physisorbed species for later pulses. No methane was formed (IC curve with m/z= 16).

For a better understanding, whether substrates interact differently with the catalyst, the sample from the previous experiment (where both substrates were adsorbed on the surfaces) was thermally pre-treated. Similar to TPD experiments, the higher the desorption temperature, the stronger the molecules are bonded. Figure 46 shows the simultaneous desorption of Et_3SiH and CH_3Cl, monitored by an IC curve with m/z= 59 for silane and m/z= 50 for monochloromethane. Unfortunately, the desorbed amount is so small that the IC peak has no corresponding signal in the TG curve. It is likely to assume that the substrates are bonded strongly enough that treatment at 200 °C is not sufficient to remove both substrates from the surface.

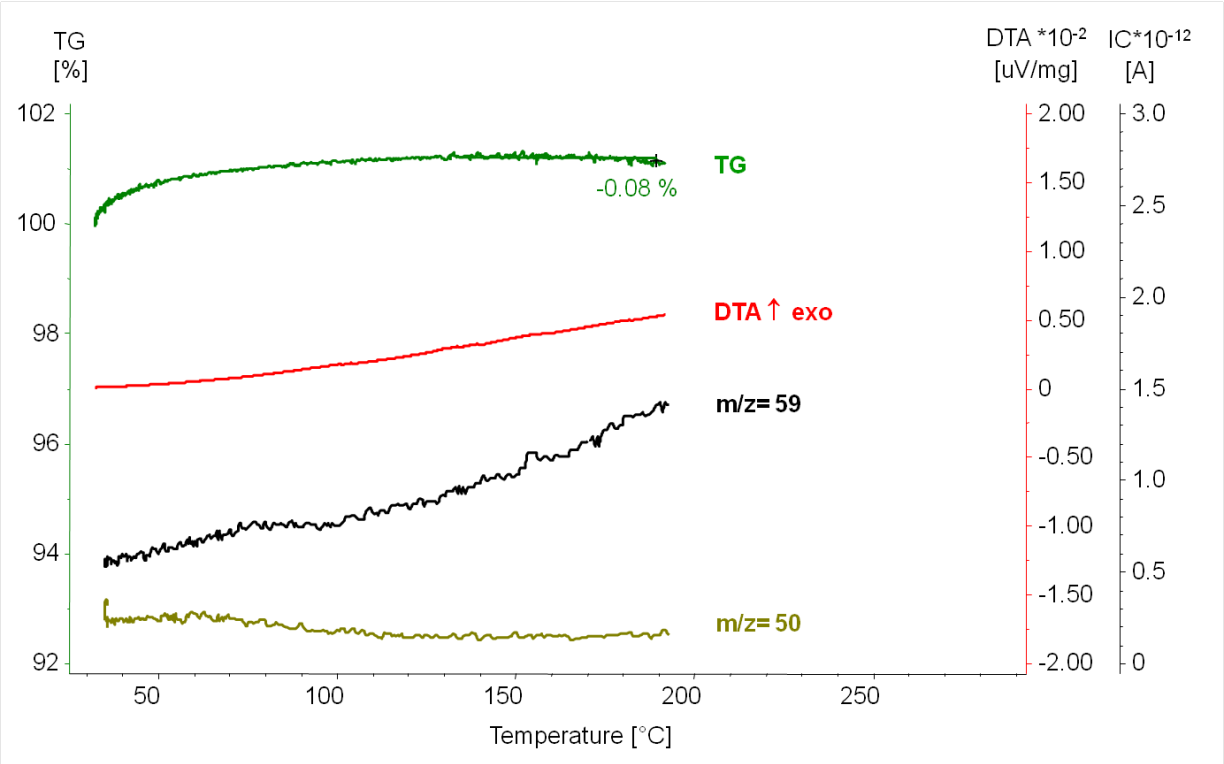

Figure 46. TA-MS curves for ACF◦Et_3SiH (39.16 mg) pulsed with CH_3Cl in Ar showing the desorption of CH_3Cl (IC curve with m/z= 50) and Et_3SiH (IC curve with m/z= 59) after the PTA experiment. Again the adsorbed amount is so small that the IC peak has no correspondence in the TG curve.

Similar to the reactions in previous flow reactor, the sequence of addition was reversed. Figure 47 illustrates the six CH_3Cl injections on ACF. With each pulse, DTA and TG curves feature chemisorption of CH_3Cl (220 µg). A gradual mass increase was observed together with strong exothermal effects. The subsequent three silane pulses of 2·2 µL and 4 µL resulted in no mass change and only small exothermal peaks. Similar to the first experiment, no methane was formed. CH_3Cl adsorbs on the Lewis acidic sites blocks for silane, which then can only interact weakly with the surface.

To sum up, both substrates compete for the same Lewis acidic sites. If the catalyst is saturated with one substrate, the active sites remain blocked for the other one. As shown in Figure 45 only above a certain concentration can one reactant suppress another from the catalyst surface. In contrast to fluorinated methanes, no catalytic reaction was observed. The results are not unequivocal enough to elucidate the mechanism.

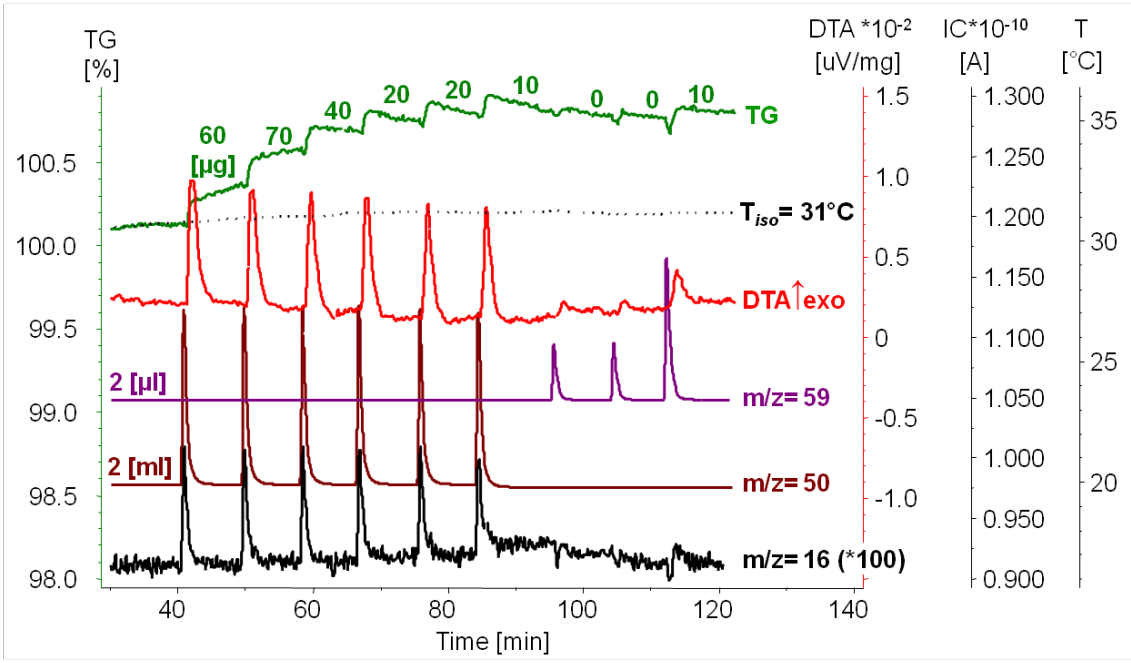

Figure 47. PTA curves of a sequence of injections of 2 ml gaseous CH_3Cl followed by 2 and 5 µl injections of liquid Et_3SiH onto thermally pretreated ACF (34.4 mg) in Ar. The IC curves for the injected methyl chloride with mass number m/z= 50 (CH_3Cl^+) and the silane with m/z= 59 ($EtSiH^+$) were recorded. Also the expected product methane with m/z=16 (CH_4^+) was monitored, however not found. The IC curves are shifted for improved clarity.

In order to understand the interactions between all substrates and the catalyst`s surface, not only hydrodechlorination reactions but also Friedel-Crafts type reactions were simulated. No silane was involved in the subsequent experiments.

Figure 48 shows the injection of six 2 mL pulses of methyl chloride, followed by 2 pulses of benzene. With each methyl chloride pulse, strong DTA peaks together with corresponding TG effects were detected indicating its chemisorbtion. The subsequent two pulses of benzene resulted in weak exothermic effects and no mass gain. Similar to previous results, CH_3Cl interacts with all active sites and prevents interactions with benzene. No formation of toluene was observed (IC curve for m/z= 91).

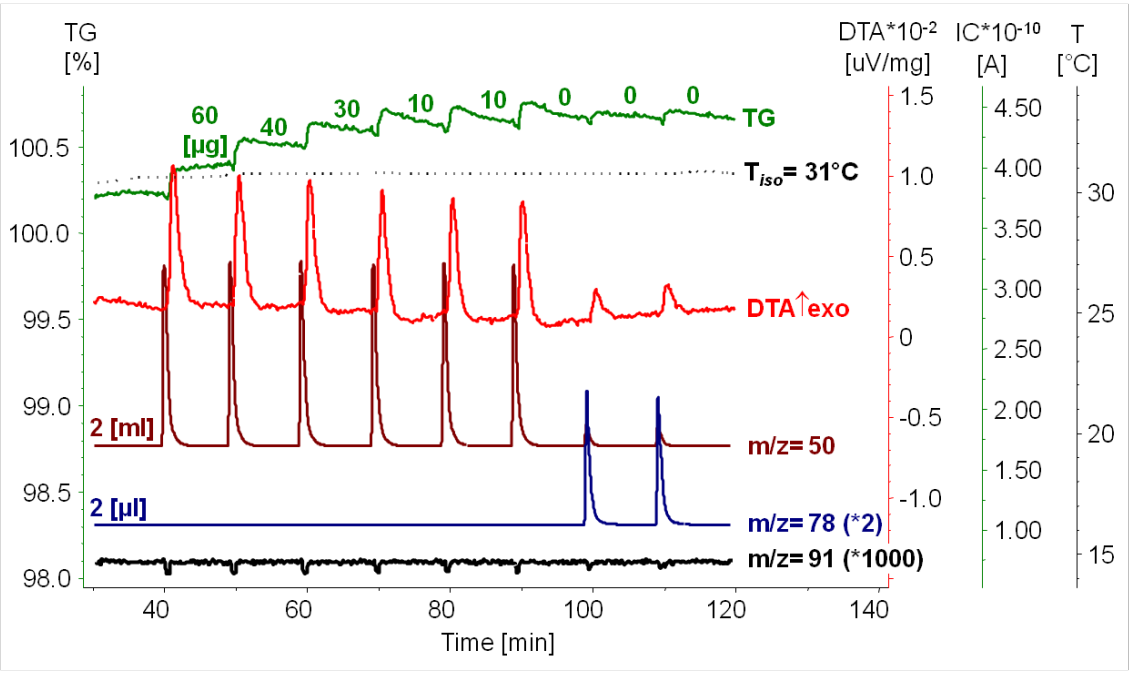

Figure 48. The injections of CH_3Cl onto ACF◦C_6H_6 in Ar under isothermal conditions. The IC curves for the injected methyl chloride with mass number m/z= 50 (CH_3Cl^+) and the benzene with m/z= 78 ($C_6H_6^+$) were recorded. Also the expected product toluene with m/z=91 ($C_7H_8^+$) and was monitored. The IC curves are shifted for improved clarity.

To complete the experiment, the reverse order of substrate addition was tested (Figure 49). The chemisorption of 160 µg C_6H_6 was proven by DTA and TG effects. With each pulse typical moderate thermal effects accompanied by continuous mass increase were recorded indicating chemisorption of C_6H_6. The two subsequent pulses of CH_3Cl resulted in continuously strong adsorption. The DTA effects were stronger than for previously pulsed C_6H_6, i.e. C_6H_6 interacts more weakly with ACF than CH_3Cl and Et_3SiH. Since the surface was still not saturated, C_6H_6 was again injected. Surprisingly, the chemisorption proceeded as before. Again, no formation of toluene was detected (IC curve with mass number m/z= 91).

Obviously, benzene requires a minimum strength of Lewis acidic sites to be adsorbed. When such strong active sites are occupied with other compounds such as CH_3Cl or Et_3SiH, benzene can no longer be adsorbed. Weaker sites are also suitable for the activation of CH_3Cl but not for benzene. The results indicate that the higher conversions will be achieved if all active sites weak and strong ones are involved in the reaction which is the case for CH_3Cl.

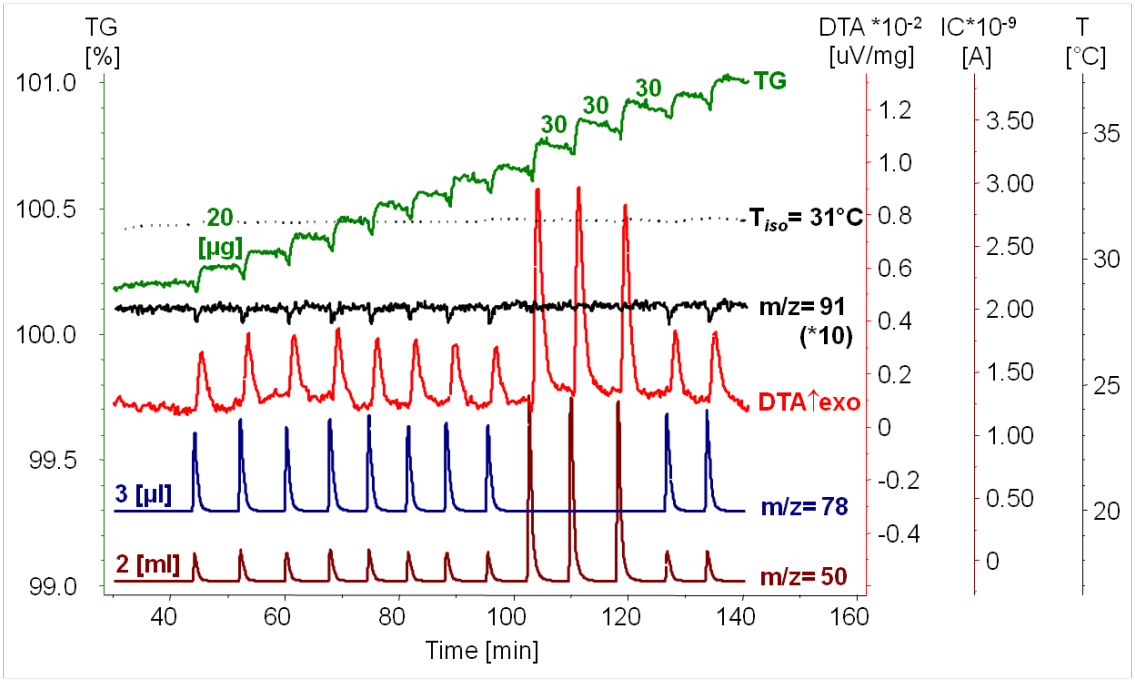

Figure 49. PTA curves of a sequence of injections of 3 µl injections of liquid C_6H_6 onto ACF◦CH_3Cl in Ar. The IC curves for the injected methyl chloride with mass number m/z= 50 (CH_3Cl^+) and the benzene with m/z= 78 ($C_6H_6^+$) were recorded. Also the expected product toluene with m/z= 91 ($C_7H_8^+$) and was monitored. The IC curves are shifted for improved clarity.

3.2.4 Mechanism of the activation of chlorinated molecule

*Pulse*TA® experiments did not offer a clear answer for the elucidation of the mechanism. In contrast to the mechanism for fluorinated substrates, the experiments in flow reactor with chlorinated substrates showed that the mechanism can proceed in both directions. ACF can first be statured with Et_3SiH and then the flow of CH_3Cl can be switch on or vice versa. No chemical reaction was observed between ACF and CH_3Cl. However, a closer look reveals that the higher TOF was achieved for ACF◦CH_3Cl. This suggests that saturation of ACF with chloromethane before addition of Et_3SiH is more effective, as shown in Figure 50.

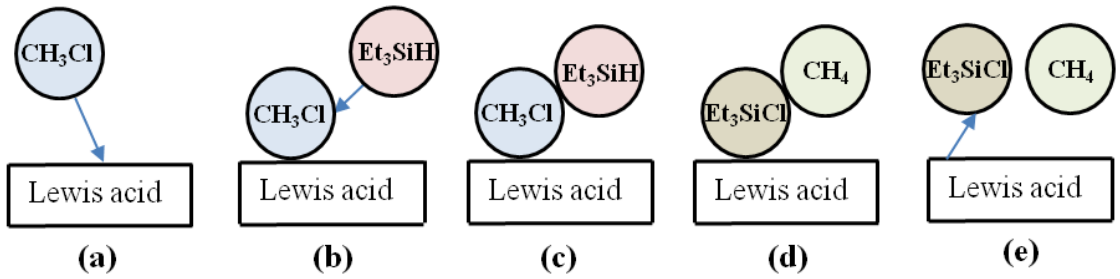

Figure 50. Mechanism for the activation of chlorinated molecules.

3.2.5 1,2-Dichloroethane

The previous results implied that steric effects control the catalytic activities. Therefore, 1,2-dichloroethane was activated as a sterical demanding substrate proceeding as with chlorinated methanes. The results are summarised in Table 15.

Table 15. Activation of $ClCH_2$-CH_2Cl in all contributions of reaction mixtures, in the presence and absence of Et_3SiH and C_6D_6.

entry	sil. [mmol]	cat.	T [°C]	t [d]	conv. [%][a]	main product	minor product	TON[b]
1	0.6	ACF	24	3	3	Ph^DCH_2-CH_2Ph^D (74%)	Ph^DCH_2-CH_3 (18%) $Ph^D{}_2CH$-CH_3 (8%)	0.4
2	0.6	ACF	70	3	63	Ph^DCH_2-CH_2Ph^D (78%)	Ph^DCH_2-CH_3 (13%) $Ph^D{}_2CH$-CH_3 (9%)	16
3[1]	0.6	ACF	70	1	24	Ph^DCH_2-CH_2Ph^D (>99%)	-	3
4	0.6	*HS*-AlF_3	70	3	3	Ph^DCH_2-CH_2Ph^D (79%)	Ph^DCH_2-CH_3 (21%)	0.4
5	-	ACF	24	3	35	Ph^DCH_2-CH_2Ph^D (93%)	Ph^DCH_2-CH_3 (4%) $Ph^D{}_2CH$-CH_3 (2%) $Ph^D{}_2CH$-CH_2Ph^D (1%)	4
6	-	ACF	70	3	60	Ph^DCH_2-CH_2Ph^D (78%)	Ph^DCH_2-CH_3 (9%) $Ph^D{}_2CH$-CH_3 (12%)	7

entry	sil. [mmol]	cat.	T [°C]	t [d]	conv. [%][a]	main product	minor product	TON[b]
							$Ph^D{}_2CH$-CH_2Ph^D (1%)	
7[t]	-	ACF	70	3	61	Ph^DCH_2-CH_2Ph^D (78%)	Ph^DCH_2-CH_3 (16%) $Ph^D{}_2CH$-CH_3 (5%) $Ph^D{}_2CH$-CH_2Ph^D (1%)	7
8[t,2]	-	ACF	70	3	91	$PhCH_2$-CH_2Ph (68%)	$PhCH_2$-CH_3 (10%) Ph_2CH-CH_3 (14%) Ph_2CH-CH_2Ph (8%)	11
9	-	*HS*-AlF_3	70	3	24	Ph^DCH_2-CH_2Ph^D (96%)	Ph^DCH_2-CH_3 (4%)	3
10[3]	5.6	ACF	70	3	19	CH_2=CH-CH=CH_2 (97%)	CH_3-CH_3 (3%)	2
11[3]	5.6	*HS*-AlF_3	70	3	-	-	-	-
12[4]	-	ACF	70	1	1	Cl_2CH-CH_3	-	5
13[4]	-	ACF	70	3	1	Cl_2CH-CH_3	-	5

All reactions were carried out using 25 mg of the catalysts and 0.30 mmol of substrate. [a] The quantification was performed using ^{1}H NMR spectroscopy, comparing the ratio of the product to the substrate. [b] Calculated based on the amount of the product per number of active acidic sites at the Lewis acids (1 g Lewis acid contains 1 mmol of active sites determined by NH_3-TPD).[44] [t] Reaction in Teflon liner, [1] Reaction in the presence of $^iPr_3SiH$, [2] Reaction in the presence of C_6H_6, [3] Reaction in the absence of C_6D_6, [4] Reaction in the absence of silane and C_6D_6, using 0.6 mL of the substrate

To investigate the steric influence $ClCH_2$-CH_2Cl was activated in the presence of $^iPr_3SiH$. To compare the reaction with Et_3SiH, TOF had to be calculated due to different reaction times of these both reactions.

In the presence of Et_3SiH, TOF was calculated to be 0.22 and in the presence of $^iPr_3SiH$ it decreased to 0.13. This means that the reaction in the presence of Et_3SiH is more efficient. Probably due to steric hindrance of substrates and products and due to lower reactivity of $^iPr_3SiH$ the reaction proceeds with less conversion.

Simultaneous Friedel-Crafts-like and hydrodechlorination reactions

1,2-dichloroethane was converted in the presence of both substrates Et_3SiH and C_6D_6. Applying ACF, the conversion reached 3% at 24 °C after 3 days and increased to 63% at 70 °C. 78% of the substrate was converted to Ph^DCH_2-CH_2Ph^D in the Friedel-Crafts like reaction, whereas 13% yielded Ph^DCH_2-CH_3 and 9% $(Ph^D)_2CH$-CH_3. The formation of $(Ph^D)_2CH$-CH_3 can be explained by rearrangement to 1,1-dichloroethane and a subsequent double Friedel-Crafts reaction. The reaction resulted in negligible conversion when *HS*-AlF_3 was applied. It was expected that 1,2-dichloroethane would be activated more efficiently in mesoporous *HS*-AlF_3 due to steric hindrance of voluminous products. Contrary to our assumptions, there must be another influencing factor, which predominates over the impact of steric influences on the reaction, resulting in a higher conversion for ACF.

Friedel-Crafts-like reactions

Similar to chlorinated methanes, the influence of silane was investigated, performing the reactions in its absence.

The activation of the 1,2-dichloroethane with ACF yielded 35% conversion after 3 days at 24 °C and was almost twice that at 70 °C. Applying higher temperatures, the selectivity of the reaction decreased (entries 5 and 6, Table 15). Similar to the reactions in the presence of both substrates, Ph^DCH_2-CH_2Ph^D (78% at 70 °C) is formed as the main product, alongside the formation of the side product $Ph^D{}_2CH$-CH_3 (12%) as a result of a Friedel-Crafts reaction.

Surprisingly, 9% of the substrate was converted to Ph^DCH_2-CH_3 and 1% to $Ph^D{}_2CH$-CH_2Ph^D. Both products can only be formed when a hydride source is present. Similar to the activation of chlorinated methanes, the same reaction was carried out in a PFTE tube to exclude glass as an hydride source. As expected (based on the results of activation of CH_2Cl_2, the reactivity and selectivity did not change. The purity of 1,2-dichloroethane was also assessed by GC/MS and NMR experiments. No impurities were detected. The only explanation for the formation of hydrodechlorination products is the Cl/H exchange reaction initiated by a strong Lewis acid.

The conversion to side products was unequivocally higher than for chlorinated methanes. Ahrens *et al.* proposed that the activation of C-F bonds proceeds over a carbocation intermediate.[48] The stability of this carbocation is influenced by inductive effects of additional groups. With each increasing alkyl chain acting as an electron releasing group, the stability of

the carbocation increases. The electrons from σ-C-H bonds interact with the empty p orbital located on the positively charged carbon, resulting in hyperconjugation, which in turn stabilizes the carbocation. Hence, the abstraction of a hydride ion from 1,2-dichloro-ethane is easier than from dichloromethane, allowing for an easier Cl/H exchange reaction.

In addition, the activation of the substrate in the presence of C_6H_6 demonstrated a higher conversion compared to the reaction in C_6D_6 (entries 6 and 8). Since ACF is known to catalyze the H/D exchange reactions, it can be assumed that in the presence of a deuterated solvent the H-products undergo an H/D exchange reaction and become undetectable in the ^{1}H NMR spectrum of the reaction mixture. Thus, the apparent amount of measured products is lower than when using C_6D_6.

Applying *HS*-AlF_3 as a catalyst, 24% of the substrate was activated demonstrating lower conversion than for ACF, but higher selectivity. 96% of the substrate was converted to $PhCH_2$-CH_2Ph, whereas only 4% yielded $PhCH_2$-CH_3. Similar to chlorinated methanes, the results suggest the predominating type of interaction has a greater impacts on reactivity than sterical effect.

Hydrodechlorination reactions

1,2-dichloerthane was activated in the presence of Et_3SiH. Using only ACF, the reaction proceeded with the conversion of 19%, giving most likely 1,3-butadiene and ethane. As a result of the low product concentration and low spectra resolution the proton couplings could not be identified clearly. As this spectra was evaluated at a later time a repetition of the measurement was no longer possible to reconfirm this assumption

3.3 Summary

In summary, all investigated reactions exhibited increased conversion with decreasing number of halogen atoms in the substrate. This finding is independent whether the substrate is fluorinated or chlorinated or if the reaction is carried out in NMR tubes, batch or flow reactors. An increasing number of halogenides in the substrate leads to shorter and therefore stronger C-X bonds and stronger shielding of reactive sites.

No partially dehalogenated products were detected, suggesting that cleavage of the first C-X (X= Cl, F) bond is the rate-determining step.

In NMR tube reactions, fluorinated and chlorinated methane derivatives as well as more sterically hindered substrates, namely chlorinated ethane derivatives were successfully activated.

For hydrodefluorination and hydrodechlorination reactions in NMR tubes, higher conversions were achieved with ACF catalyst and not *HS*-AlF_3. This finding can most likely be explained by the smaller micro-pores of ACF being more suitable for the reactions to take place as opposed to the more spacious pores of *HS*-AlF_3. The sterical aspects were extensively studied by FTIR experiments.

Different observations were made when an additional substrate was present, for example C_6D_6 to carry out Friedel-Crafts type reactions. In this case *HS*-AlF_3 led to higher conversions of fluorinated substrates, whereas for chlorinated substrates ACF was found to be the better catalyst. Also for the activation of 1,2-dichloroethane ACF seems to be more suitable catalyst than *HS*-AlF_3. These results are difficult to interpret. Due to similar Lewis acidities, it was expected that for the sterically demanding reactions *HS*-AlF_3 would be more suitable catalyst. If in the reaction mixture traces of water are present, Al-Cl bond in ACF can be hydrolyzed. This causes formation of HCl, which binds strongly at the surface. This is not possible using *HS*-AlF_3 due to lack of C-Cl bond. Thus, Brönsted acid sites, which are generated, interact preferentially with C-Cl bond and can remove HCl. If no hydride is available, dehydrochlorination mechanism will occur. Such additional mechanisms modify the catalyst´s surface, which in turn can result in different interactions between catalyst und substrate. [209,210]

Interestingly, the reaction in glass NMR tube gave higher conversion than in Teflon liner.

The experiments in flow reactor showed that catalysts achieved the highest conversions at 190 °C and 0.6 s contact time and that they remain active over a longer period of time. However, any change in the parameters caused disturbance of the equilibrium.

Additionally, the activation of both, fluorinated and chlorinated substrates was possible in flow reactor. The difference in the reactivity of both catalysts was not markedly as for reactions in NMR tubes. Due to short contact times, only short diffusion ways can be exploited by both catalysts, resulting in similar reactivities. Similar to the reactions in NMR tube, the conversion decreased with increasing number of halogenides in the substrate. The same finding is true at

higher temperatures, which can be explained by decreasing numbers of active sites due to substrate decomposition. It is also conceivable, that silane deteriorated due to beta elimination.

In flow reactor, ACF was further fluorinated while activating fluoro methane derivatives. Additional experiments like reactions in batch, dismutation reactions, MAS NMR and NH_3-TPD experiments strongly suggest a chemical reaction between ACF and fluorinated substrate which is irreversible and leads to loss of catalyst activity.

In consequence, this means that ACF should to be saturated first with silane, which has a protective role for the catalysts and suppresses fluorination of the catalyst, in order to allow the reaction to proceed as intended, as shown in Figure 51.

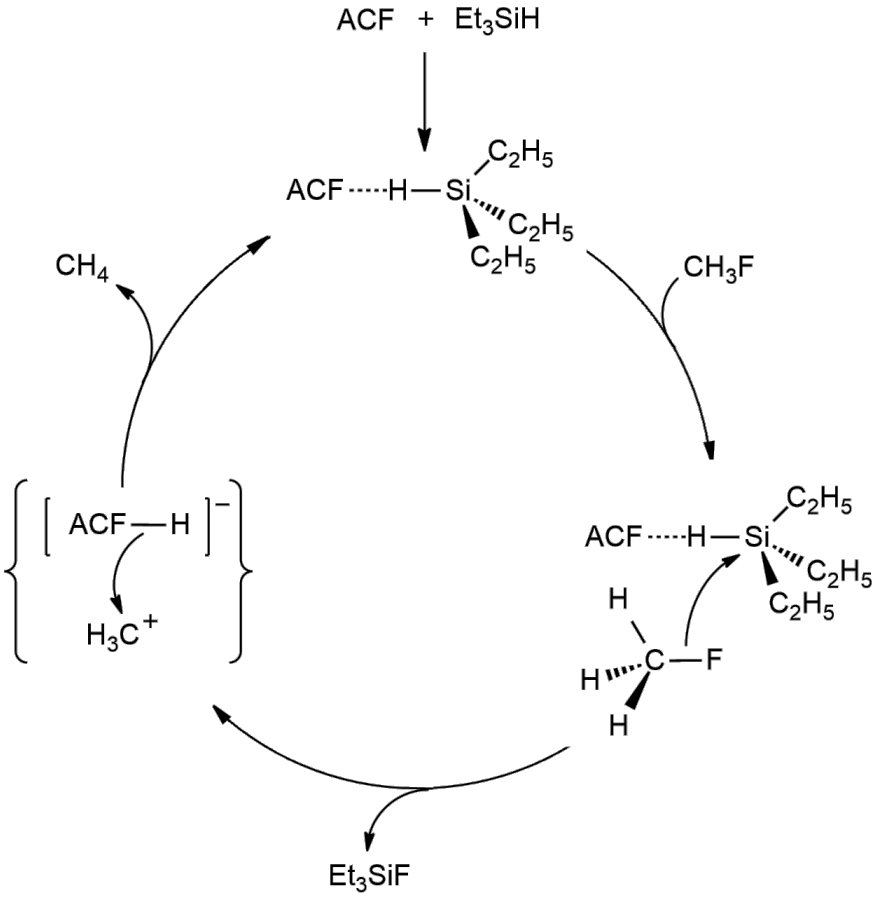

Figure 51. Mechanism of hydrodelfluorination

Interestingly, for chlorinated substrates the reaction proceeds in both directions. However, additional experiments in flow reactor strongly implicate that it is better if chloromethane is activated first, as shown in Figure 52. *Pulse*TA® experiments were not clearly conclusive in this regard.

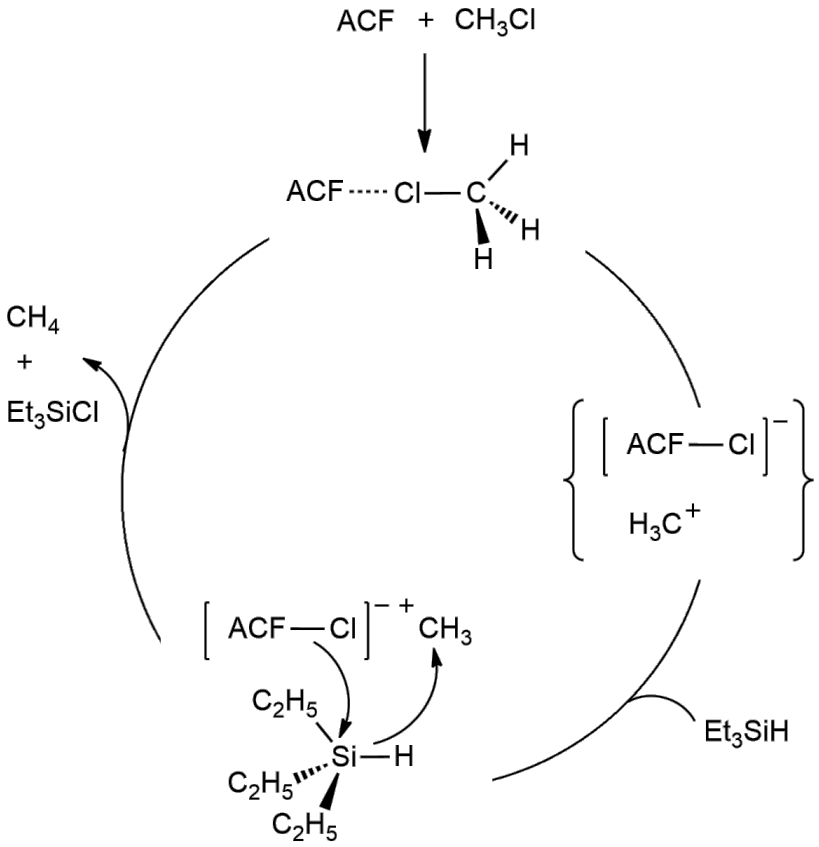

Figure 52. Mechanism of hydrodechlorination

3.4 Hydrosilylation

A further goal of this research was to investigate the hydrosilylation reaction of ketones. The activation of starting molecules which contain heteroatoms is particularly interesting, as it is well accepted in Lewis acid chemistry that free electron pairs of heteroatoms can block strong Lewis acidic sites of a catalyst and suppress further reaction.

In this thesis the reactions of various ketones (3-pentanone, chloroacetone, 1,1-dichloro-acetone, isobutyrophenone, 1-phenyl-1-butanone, 1-phenylethanone and 1-(4-fluoro-phenyl)-ethanone) with silanes (Et_3SiH, Et_2SiH_2, $^nBuSiH_3$) were examined activated by the Lewis acid

catalysts ACF and *HS*-AlF_3. Reactions were carried out with or without the solvent C_6D_6. Sterical and electronical aspects of these reactions will be discussed in the following chapter.

3.4.1 Hydrosilylation of 3-Pentanone

First the reaction of the symmetrical ketone 3-Pentanone **5** was investigated with Et_3SiH, Et_2SiH_2, $^nBuSiH_3$ in the presence or absence of C_6D_6 using ACF and *HS*-AlF_3 as catalysts. Results are summarized in Table 16. The reactions proceeded to the products of monohydrosilalytion **6**, E/Z-alkenes **8** and in rare cases to the dihydrosilylation product **7** (see Scheme 52).

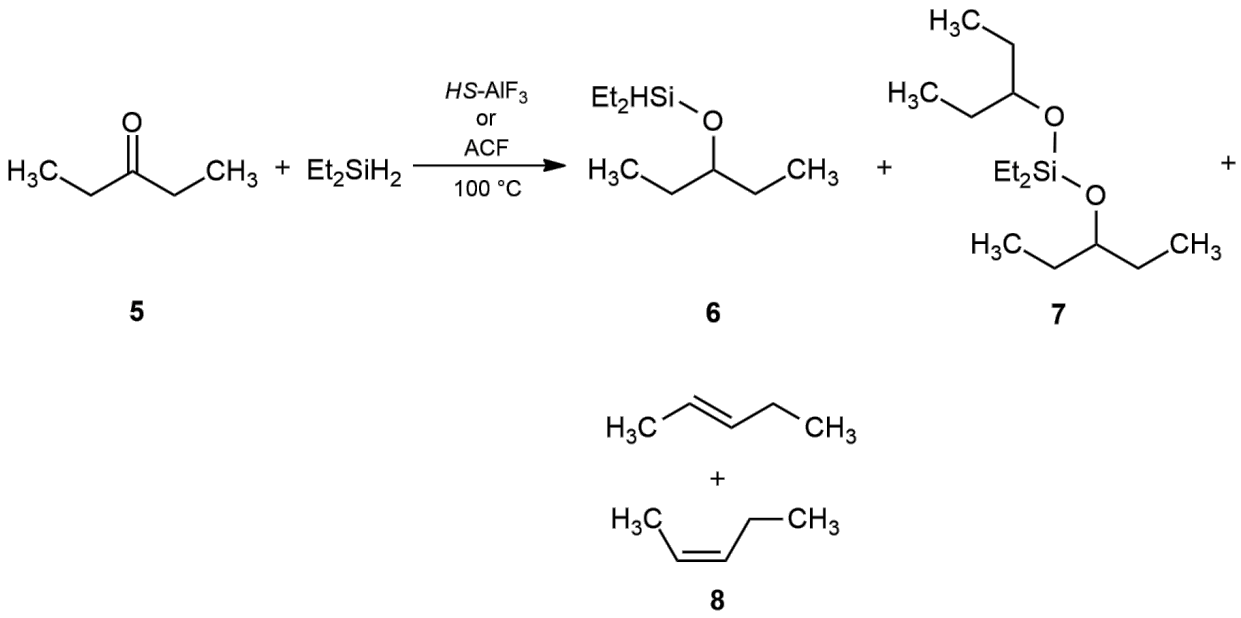

Scheme 52. Hydrosilylation of 3-pentanone in the presence of Et_2SiH_2.

In the reaction of 3-pentanone **5** with Et_3SiH activated by ACF in the absence of C_6D_6 49% of **5** was consumed after 3 days. Conversion increased to 66% after 6 days, giving a final product distribution of 27% of monohydrosilalytion product **6** and 11% of pentene **8**. Approximately 28% of converted substrate could not be found in the nmr spectrum. It is assumed that this substrate is immobilized at the surface of the catalyst. Due to other substrates in the reaction mixture, which adsorb on the surface of the catalyst, no CHN analyses were possible. Therefore, this assumption remains unproved at the moment. In a second reaction double amount of substrate was used. In this reaction only 24% of **5** was consumed in the reaction after 6 days, yielding 12% of alkene as the only product. With the more reactive Et_2SiH_2, 100% of the substrate was converted after 3 days giving 29% of **6** and 31% of **8**. Interestingly after 6 days the yield of **6** decreased to 11%, and **8** increased to 45%. A comparable result and trend was

detected for ^{n}BuSiH$_3$. After 3 days 30% of the substrate was consumed to **6** and 16% to **8**, whereas after 6 days conversion of **6** decreased to 14% and **8** increased to 27%.

With ACF in the presence of C_6D_6, no reaction with Et$_3$SiH was observed. Applying Et$_2$SiH$_2$, 53% of **5** was consumed after 3 days to 10% of **6**, 4% to dihydrosilylation product **7** and 1% to **8**. Additional 3 days gave only minor conversion improvement. Using ^{n}BuSiH$_3$, 87% of **5** was converted after 3 days to 12% of **6**, 9% of **7** and 4% of **8**. The full conversion was achieved after 6 days giving 12% of **7** and 29% of **8**.

Table 16. Hydrosilylation of 3-pentanone in the absence and presence of C_6D_6 and different silanes.

entry	sil.	cat.	C_6D_6	t [d]	**5** conv. [%][a]	**6** yield [%][a]	**7** yield [%][a]	**8** yield [%][a]	TON[b]
1	Et$_3$SiH	ACF	-	3	49	22	n.d.	5	2
2	Et$_3$SiH	ACF	-	6	66	27	n.d.	11	2
3[1]	Et$_3$SiH	ACF	-	3	19	n.d	n.d	10	0.6
4[1]	Et$_3$SiH	ACF	-	6	24	n.d	n.d	12	0.7
5	Et$_2$SiH$_2$	ACF	-	4	100	29	n.d	31	4
6	Et$_2$SiH$_2$	ACF	-	6	100	11	n.d.	45	3
7	^{n}BuSiH$_3$	ACF	-	3	100	30	n.d.	16	3
8	^{n}BuSiH$_3$	ACF	-	6	100	14	n.d.	27	2
9	Et$_3$SiH	ACF	+	3	-	-	-	-	-
10	Et$_3$SiH	ACF	+	6	-	-	-	-	-
11	Et$_2$SiH$_2$	ACF	+	3	53	10	4	1	0.9
12	Et$_2$SiH$_2$	ACF	+	6	74	8	8	3	1
13	^{n}BuSiH$_3$	ACF	+	3	87	12	9	4	2
14	^{n}BuSiH$_3$	ACF	+	6	100	n.d.	12	29	3
15	Et$_3$SiH	*HS*-AlF$_3$	+	6	-	-	-	-	-
16	Et$_2$SiH$_2$	*HS*-AlF$_3$	+	3	40	5	n.d	n.d	0.3
17	Et$_2$SiH$_2$	*HS*-AlF$_3$	+	6	49	4	n.d.	2	0.4
18	^{n}BuSiH$_3$	*HS*-AlF$_3$	+	3	100	9	n.d.	13	1
19	^{n}BuSiH$_3$	*HS*-AlF$_3$	+	6	100	4	n.d.	36	2

All reactions were carried out by activating 0.3 mmol of substrate with 50 mg catalyst at 100 C and with or without C_6D_6 as a solvent. [a] The quantification was performed by ^{1}H NMR spectroscopy, with pyridine as internal standard. [b] Calculated TON based on the product molecules per number of acidic Lewis sites (Number of sites was 1 mmol per 1 g Lewis acid catalyst - Acid sites were determined by NH$_3$-TPD).[44] [1] activation of 0.6 mml of substrate

The same reactions were carried out in the presence of *HS*-AlF$_3$ and C_6D_6. Similar to ACF, no conversion was detected using Et$_3$SiH. In the presence of Et$_2$SiH$_2$, 40% of substrate **5** was converted after 3 days to 5% of **6**. After 6 days the conversion increased to 49%, giving 4% of **6** and 2% of **8**. Higher conversion was achieved with ^{n}BuSiH$_3$. After 3 days the substrate was

fully consumed and 9% of **6** and 13% of **8** were formed. The yield increased after additional 3 days to 4% of **6** and 36% of **8**.

Generally, higher conversions were obtained in the absence of solvent than with C_6D_6 especially for Et_2SiH_2.

In the absence of C_6D_6, the reactivity decreased in the following row Et_2SiH_2 > ^{n}BuSiH$_3$ > Et_3SiH. For Et_2SiH_2 and ^{n}BuSiH$_3$ the formation of alkene was preferred. Using Et_3SiH, the reaction delivered mainly monohydrosilylation products.

In the presence of C_6D_6, no differences in the reactivity between ACF and *HS*-AlF_3 were observed. However, the distribution of the products depends on which catalyst was used. Applying *HS*-AlF_3, the reactions proceed to monohydrosilylation product and alkenes. In the presence of ACF, dihydrosilylation product is formed additionally. Interestingly, without solvent, only monohydrosilylation and alkene were detected. For both catalysts, no Friedel-Crafts like products were detected. Comparing to reactions in the absence of the solvent, the reactions carried out with Et_3SiH did not work. Higher conversions were achieved for ^{n}BuSiH$_3$ than for Et_2SiH_2. The finding for both catalysts was that when using Et_2SiH_2 the hydrosilylation product was favored over the alkene, whereas applying ^{n}BuSiH$_3$ the reversed trend was observed.

Kinetics of the reaction

To investigate the kinetics of hydrosilylation reaction, conversion of **5** in the presence of ^{n}BuSiH$_3$ as reagent activated by ACF in the absence of solvent was followed by NMR experiments from 1 to 14 days (see Figure 53).

The substrate was fully consumed after one day already. During the first day the amount of monosilylether increased significantly to almost 50%, followed by constant consumption over the course of the reaction. Almost no more silylether was detected at the termination of the experiment. The yield of (E/Z)-pentenes increased continuously from the first day on.

Interestingly, within the first 24 h all of substrate was consumed, however, only about 55% of it could be observed as reaction products. Based on earlier observations of hydrodehalogenation reactions, it can be assumed that the missing amount of substrate interacts with the catalyst and is probably absorbed on its surface. It is possible that the ketone occupies the active sites,

deactivates the catalyst and no more monosilylether can be formed. In the subsequent reaction monosilylether is consumed to give alkene, which concentration continuously increase.

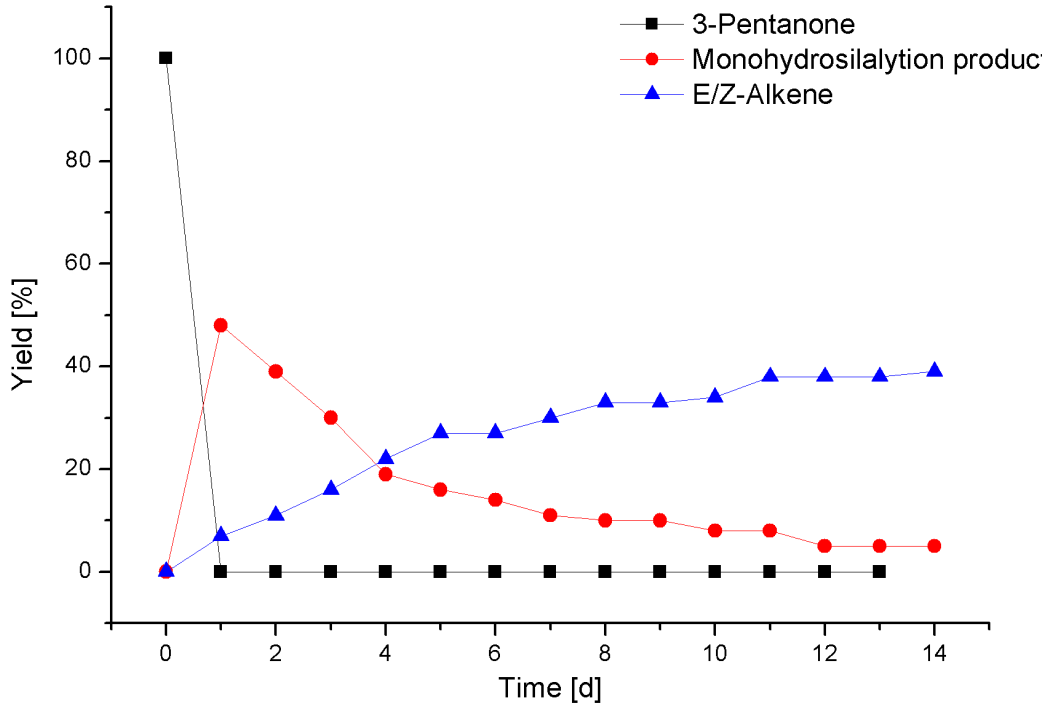

Figure 53. The course of the activation reaction of 3-pentanone by ACF monitored for 14 days.

Similar trends were observed for *HS*-AlF_3, also if the reaction was carried out in the presence of C_6D_6 (see Figure 54). Monohydrosilylation product was formed first, which subsequently reacted to alkenes. The strong increase in the yield of pentene on the sixth day is within the range of the measurement inaccuracy. However, the decrease in pentene starting from the day 12 on indicates that also this product is further converted in subsequent reactions, for example in cationic polymerization.

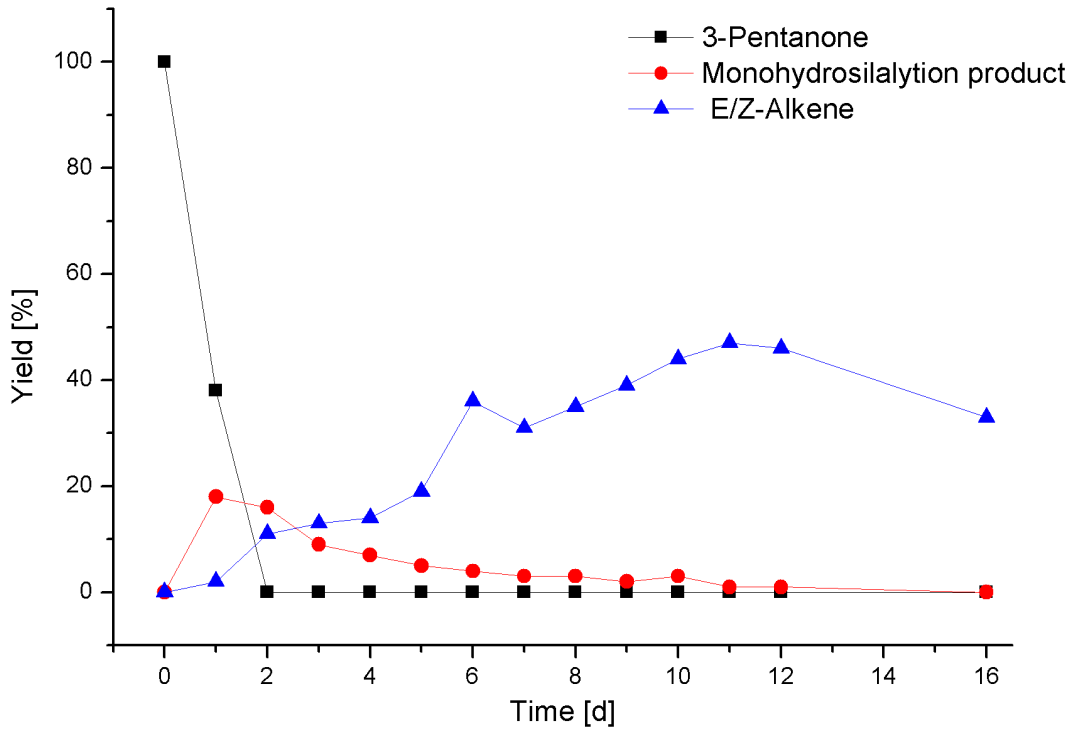

Figure 54. The course of the activation reaction of 3-pentanone by HS-AlF_3 monitored for 16 days.

3.4.2 Activation of Chlorinated Molecules

In the presence of the solvent C_6D_6 3-pentanone did not react with Et_3SiH. Thus, it was investigated if different substituents on the alkyl chain of the starting molecule can influence the reactivity. Chloroacetone **9** (see Table 17) and 1,1-dichloroacetone (see Table 18) were activated in the presence of Et_3SiH and the solvent.

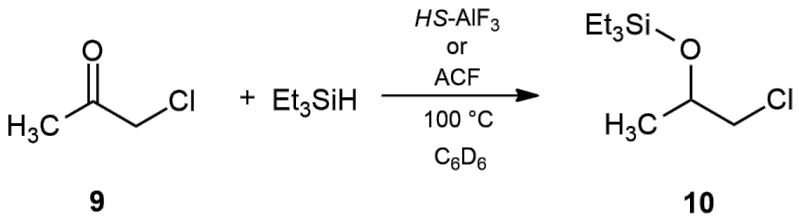

9 **10**

Scheme 53. Activation of chloroacetone with Et_3SiH in the presence of C_6D_6.

Interestingly chloroacetone and 1,1-dichloroacetone delivered reasonable conversions in the reaction with Et_3SiH and in presence of the solvent, reacting to chlorinated silylether as main product. In the presence of ACF, 66% of chloroacetone was reacted after 3 days giving 22%

of **10**. After 6 days the conversion increased to 77% and resulted in 27% of the product. Comparable results were achieved for *HS*-AlF_3.

Similar results were obtained for 1,1-dichloroacetone. Although the conversions with ACF are smaller than for chloroacetone, more product was overall formed. After 3 days 29% of the ketone was converted to monosilylether, which increased to 36% after 3 additional days. *HS*-AlF_3 delivered higher conversions. Up to 84% of the substrate was activated, giving a maximum of 44% of silylether after 6 days. In addition, Et_3SiCl was formed as a side-product.

Table 17. Hydrosilylation of chloroacetone using Et_3SiH in the presence of C_6D_6.

entry	sil.	cat.	C_6D_6	t [d]	conv. [%][a]	yield [%][a]	TON[b]
1	Et_3SiH	ACF	+	3	66	22	1.3
2	Et_3SiH	ACF	+	6	77	27	1.6
3	Et_3SiH	*HS*-AlF_3	+	3	66	23	1.4
4	Et_3SiH	*HS*-AlF_3	+	6	74	27	1.6

All reactions were carried out by activating 0.3 mmol of substrate with 50 mg catalyst at 100 °C and in presence of C_6D_6 as a solvent. [a] The quantification was performed by ^1H NMR spectroscopy, with pyridine as internal standard. [b] Calculated based on the amount of the product per number of active acidic sites at the Lewis acids (1 g Lewis acid contains 1 mmol of active sites determined by NH_3-TPD).[44]

Table 18. Hydrosilylation of 1,1-dichloroacetone using Et_3SiH in presence of C_6D_6.

entry	sil.	cat.	C_6D_6	t [d]	conv. [%][a]	yield [%][a]	TON[b]
1	Et_3SiH	ACF	+	3	45	29	1.7
2	Et_3SiH	ACF	+	6	56	36	2.2
3	Et_3SiH	*HS*-AlF_3	+	3	73	35	2.1
4	Et_3SiH	*HS*-AlF_3	+	6	84	44	2.6

All reactions were carried out by activating 0.3 mmol of substrate with 50 mg catalyst at 100 °C and in presence of C_6D_6 as a solvent. [a] The quantification was performed by ^1H NMR spectroscopy, with pyridine as internal standard. [b] Calculated based on the amount of the product per number of active acidic sites at the Lewis acids (1 g Lewis acid contains 1 mmol of active sites determined by NH_3-TPD).[44]

3.4.3 Hydrosilylation of isobutyrophenone

Besides chlorinated substrates, also phenyl substituted starting molecules were investigated (see Table 19). As a first example, isobutyrophenone **11** was activated (see Scheme 54). This molecule has a high steric demand. Reaction led exclusively to deoxygenated products like isobutenylbenzene **12** and isobutylbenzene **13**.

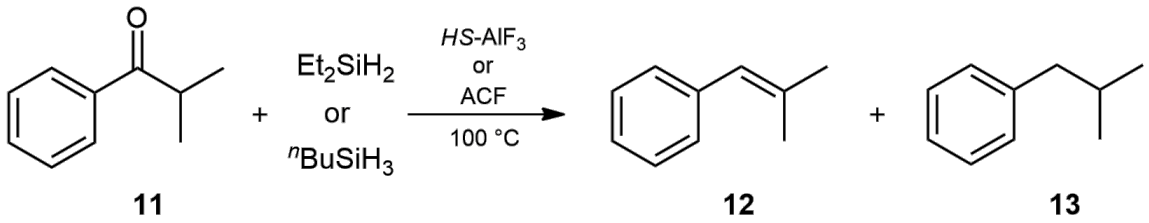

Scheme 54. The hydrosilylation reaction of isobutyrophenone catalysed by Lewis acids.

Table 19. Hydrosilylation of isobutyrophenone in the presence and absence of C_6D_6 and different silanes.

entry	sil.	cat.	C_6D_6	t [d]	**11** conv. [%][a]	**12** yield [%][a]	**13** yield [%][a]	TON[b]
1	Et_2SiH_2	ACF	-	3	16	0	4	0.2
2	Et_2SiH_2	ACF	-	6	25	0	5	0.3
3	^{n}BuSiH$_3$	ACF	-	3	18	0	6	0.4
4	^{n}BuSiH$_3$	ACF	-	6	22	0	6	0.4
5	Et_2SiH_2	*HS*-AlF_3	-	3	100	51	30	5
6	Et_2SiH_2	*HS*-AlF_3	-	6	100	51	30	5
7	^{n}BuSiH$_3$	*HS*-AlF_3	-	3	100	38	35	4
8	^{n}BuSiH$_3$	*HS*-AlF_3	-	6	100	38	38	5
9	Et_2SiH_2	ACF	+	3	17	11	5	0.9
10	Et_2SiH_2	ACF	+	6	34	20	6	1.6
11	^{n}BuSiH$_3$	ACF	+	3	22	5	7	0.7
13	^{n}BuSiH$_3$	ACF	+	6	27	7	7	0.9
14	Et_2SiH_2	*HS*-AlF_3	+	3	83	57	5	4
15	Et_2SiH_2	*HS*-AlF_3	+	6	100	74	6	5
16	^{n}BuSiH$_3$	*HS*-AlF_3	+	3	82	49	8	3
17	^{n}BuSiH$_3$	*HS*-AlF_3	+	6	90	56	8	4

All reactions were carried out by activating 0.3 mmol of substrate with 50 mg catalyst at 100 °C and in presence or absence of C_6D_6 as a solvent. [a] The quantification was performed by ^{1}H NMR spectroscopy, with pyridine as internal standard. [b] Calculated based on the amount of the product per number of active acidic sites at the Lewis acids (1 g Lewis acid contains 1 mmol of active sites determined by NH_3-TPD).[44]

In the absence of the solvent C_6D_6, activation of isobutyrophenone by ACF showed no significant conversion. With *HS*-AlF_3 conversions achieved were significantly higher. After 3 days the substrate was fully converted. When using Et_2SiH_2 about 50% of **12** and 30% of **13**

were formed after 3 days. Product distribution and yields change when using more reactive silanes. In contrast to Et_2SiH_2, in the presence of $^nBu_3SiH$ **12** and **13** were formed in comparable amounts and in about 35% yield for both. The conversion did not increase with longer reaction time.

Likewise, in the presence of C_6D_6, ACF did not deliver good conversions. The best results were achieved when applying Et_2SiH_2. The substrate was converted to **12** with 20% and to **13** with 6% yield after 6 days. With $^nBuSiH_3$ no conversion could be detected. Using *HS*-AlF_3, significantly higher conversions were achieved. However, the product distribution varied and gave mostly alkenes. After 3 days and in the presence of Et_2SiH_2, **12** was formed with 57% and **13** only with 5% yield. The conversion increased to 74% for **12**, whereas the alkane remained about the same. When applying $^nBuSiH_3$, **12** was also preferably formed. After 3 days, **12** was detected with 49% yield and raised to 56% after 6 days. 8% of **13** was formed after 3 days and did not increase further.

When comparing the catalysts, higher conversions were achieved with *HS*-AlF_3 than with ACF, independently if the reactions were carried out in presence or absence of the solvent. For ACF slightly better results were achieved in the presence of C_6D_6 than without solvent. When using *HS*-AlF_3 the conversions were comparable for reactions with or without C_6D_6 present.

Only alkene and alkane products were detected for isobutyrophenone. In almost all reactions, alkene product was favored over alkane. No hydrosilylation products could be detected. In the presence of C_6D_6, the reaction did not proceed to Friedel-Crafts products.

Based on previous experiments, the activation was not carried out in the presence of Et_3SiH. In contrast to activation of 3-pentanone, better results were achieved here for Et_2SiH_2 than for $^nBuSiH_3$.

3.4.4 Hydrosilylation of 1-phenyl-1-butanone

Furthermore, less-branched phenyl substituted molecules were activated. Based on previous results, it can be stated that they are activated with higher conversions then no-phenyl substituted molecules. The reactions were carried out only in the presence of Et_2SiH_2 and in the absence of C_6D_6 investigating both catalysts.

Activation of 1-phenyl-1-butanone **14** led to only two products, namely alkene **15** and alkane **16** (see Scheme 55**)**.

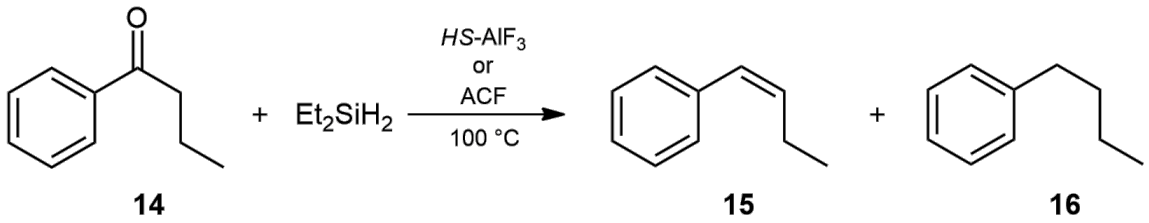

Scheme 55. The hydrosilylation reaction of isobutyrophenone catalysed by Lewis acids.

Table 20. Hydrosilylation of 1-phenyl-1-butanone in the absence of C_6D_6 and applying both catalysts.

entry	sil.	cat.	C_6D_6	t [d]	**14** conv. [%][a]	**15** yield [%][a]	**16** yield [%][a]	TON[b]
1	Et_2SiH_2	ACF	-	3	28	10	7	1
2	Et_2SiH_2	ACF	-	6	37	11	8	1
5	Et_2SiH_2	*HS*-AlF_3	-	3	100	68	22	5
6	Et_2SiH_2	*HS*-AlF_3	-	6	100	68	20	5

All reactions were carried out by activating 0.3 mmol of substrate with 50 mg catalyst at 100 °C and in presence and absence of C_6D_6 as a solvent. [a] The quantification was performed by ^{1}H NMR spectroscopy, with pyridine as internal standard. [b] Calculated based on the amount of the product per number of active acidic sites at the Lewis acids (1 g Lewis acid contains 1 mmol of active sites determined by NH_3-TPD).[44]

Using ACF, a total of 28% of the substrate was converted after 3 days, increasing to 37% after additional 3 days. Only 10% was transformed to **15** and 7% to **16** after 3 days. In the presence of *HS*-AlF_3, the substrate was fully converted. After 3 days, 68% of **14** was transformed to **15** and 22% to **16**. In both cases, prolonging the reaction time did not cause any improvement in yields.

Similarly to isobutyrophenone, higher conversions were achieved with *HS*-AlF_3 than with ACF. Only alkene and alkane products were detected. No hydrosilylation products were formed.

3.4.5 1-phenylethanone and 1-(4-fluorophenyl)ethanone

1-phenylethanone **17**, a phenyl substituted molecule but with shorter alkyl chain, and its fluorinated counterpart 1-(4-fluorophenyl)ethanone **20** were activated (see Scheme 56 and Scheme 57). The advantage of the fluorinated substrate was the possibility to follow the reaction by ^{19}F NMR experiments which, in contrast to ^{1}H NMR data, resulted in higher signal resolution and allowed for significantly better assignment of formed products.

The substrates were reacted with Et_2SiH_2 and ^{n}BuSiH_3 in the presence of *HS*-AlF_3 and absence of the solvent C_6D_6.

Applying Et_2SiH_2, substrate **17** (see Table 21**)** was converted to 24% alkene **18** and to 19% alkane **19** after 3 days. After additional 3 days the product ratio was nearly reversed. The yields increased when using ^{n}BuSiH$_3$. After 3 days, 35% of **18** and 23% of **19** were formed, but here the ratio changed only slightly after additional 3 days.

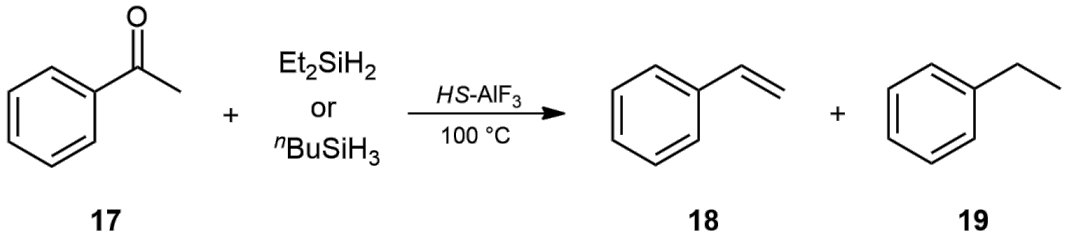

17 **18** **19**

Scheme 56. The hydrosilylation reaction of 1-phenylethanone catalysed by *HS*-AlF_3.

Table 21. Hydrosilylation of 1-phenylethanone in the absence of C_6D_6 and different silanes.

entry	Sil.	cat.	C_6D_6	t [d]	**17** conv. [%][a]	**18** yield [%][a]	**19** yield [%][a]	TON[b]
1	Et_2SiH_2	*HS*-AlF_3	-	3	100	24	19	3
2	Et_2SiH_2	*HS*-AlF_3	-	6	100	17	24	3
3	^{n}BuSiH$_3$	*HS*-AlF_3	-	3	100	35	23	3
4	^{n}BuSiH$_3$	*HS*-AlF_3	-	6	100	32	25	3

All reactions were carried out by activating 0.3 mmol of substrate with 50 mg catalyst at 100 °C and in presence and absence of C_6D_6 as a solvent. [a] The quantification was performed by ^{1}H NMR spectroscopy, with pyridine as internal standard. [b] Calculated based on the amount of the product per number of active acidic sites at the Lewis acids (1 g Lewis acid contains 1 mmol of active sites determined by NH_3-TPD).[44]

The activation of **20** (see Table 22) proceeded to 36% of alkene **21** and 20% of alkane **22** in the presence of Et_2SiH_2 after 3 days. After 6 days, the yield of **21** slightly decreased, while **22** increased slightly to 22%. When applying ^{n}BuSiH$_3$, only 28% of **21** and 20% to **22** were detected.

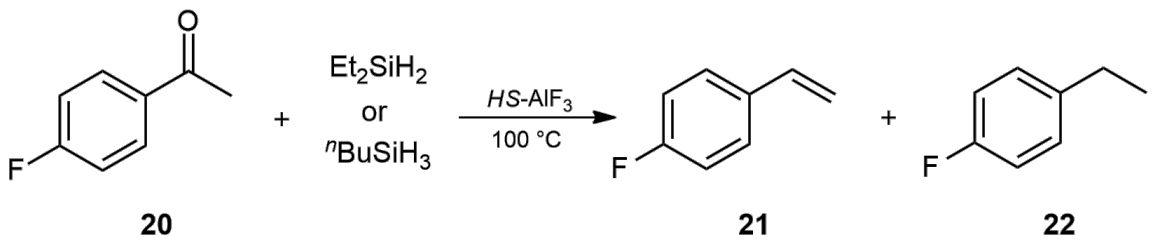

20 **21** **22**

Scheme 57. The hydrosilylation reaction of 1-(4-fluorophenyl)ethanone catalysed by *HS*-AlF_3.

Table 22. Hydrosilylation of 1-(4-fluorophenyl)ethanone in the absence of C_6D_6 and different silanes.

entry	sil.	cat.	C_6D_6	t [d]	**20** conv. [%][a]	**21** yield [%][a]	**22** yield [%][a]	TON[b]
1	Et_2SiH_2	*HS*-AlF_3	-	3	100	36	20	3
2	Et_2SiH_2	*HS*-AlF_3	-	6	100	32	22	3
3	^{n}BuSiH$_3$	*HS*-AlF_3	-	3	100	28	20	3
4	^{n}BuSiH$_3$	*HS*-AlF_3	-	6	100	28	23	3

All reactions were carried out by activating 0.3 mmol of substrate with 50 mg catalyst at 100 °C and in presence and absence of C_6D_6 as a solvent. [a] The quantification was performed by ^{1}H NMR spectroscopy, with pyridine as internal standard. [b] Calculated based on the amount of the product per number of active acidic sites at the Lewis acids (1 g Lewis acid contains 1 mmol of active sites determined by NH_3-TPD).[44]

In all reactions the substrate was fully converted. Only alkene and alkane products were detected, no hydrosilylation products.

When comparing these two substrates, the higher conversion of **17** was achieved with ^{n}BuSiH$_3$ and for **20** with Et_2SiH_2. For all reaction, with exception of entry 2, alkene product was the preferred one.

3.4.6 Conclusions

Unlike the common assumption that heteroatoms in the substrate block active sites of a Lewis acid catalyst and therefore prevent the hydrosilylation reaction, this work shows that the reaction proceeded successfully. It is assumed that the catalyst is protected by silane, similar to the results found for hydrodefluorination reactions (see 3.1.3.3). The driving force for this reaction is presumably the formation of a strong "Si-O" bond and is energetically favored due to formation of two sigma bonds from one sigma and one pi bond.

Although conversions of up to 90% could be achieved, the calculated TONs are low. Some reaction did not even proceed catalytically. The main product depends on reaction and reaction time as products are further converted in subsequent reactions. Most likely, not all side products could be identified. Due to overlapping signals in the NMR spectra, results were sometimes inconclusive. However, the reactions of fluorinated molecule **20** followed by higher resolution ^{19}F NMR delivered the expected primary products. Extrapolation of these results to unfluorinated substrates should therefore be possible and allowed.

Reactions are influenced by different factors like substrate substituents, reactivity and sterical effects of the catalyst, reactivity of silane and the presence or absence of solvent. Trends and

effects caused by these factors will be discussed in the following section as well as a proposed mechanism of the activation.

3.4.7 Influence of Substituents and Mechanism

The influence of the substituents was clearly observed. The activation of 3-pentanone with Et_3SiH in the presence of solvent C_6D_6 was not successful. Chloroacetone and 1,1-dichloroacetone, on the other hand, deliver reasonable yields. Although the alkyl chain of acetone is shorter, it was assumed that the alkyl substituents do not have a major influence on the reactivity of the carbonyl group as long as they are not sterically demanding. In general, inductive +I effects of alkyl chains are weak and thus the differences between various alkyl chains are mostly negligible. Hence, it is assumed that the –I effect of chlorine is responsible for the higher conversion. This is supported by possible mechanisms. In homogeneous catalysis mechanisms for the hydrosilylation reaction are well investigated and require the addition of silane to the carbonyl group resulting in the formation of silylether. As already mentioned, this reaction is thermodynamically favored. However, substrates have to be activated by a catalyst in order to enable reaction.

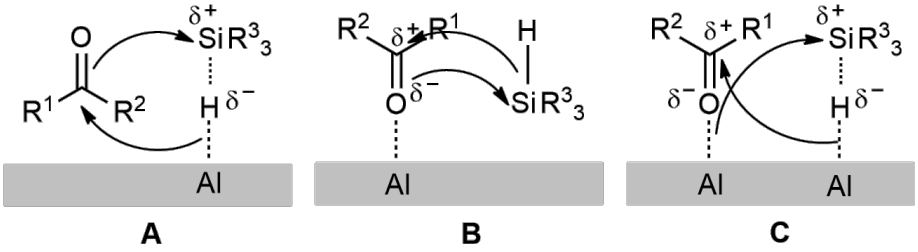

Figure 55. Possible mechanisms of the hydrosilylation reaction.

Similarly to hydrodehalogenation reactions, two different mechanisms can be considered for this, as shown in Figure 55. Based on the Eley-Rideal mechanism, either silane by activation of Si-H bond **A** or carbonyl group of ketone **B** interacts with the active sites located on the catalyst's surface. According to the Langmuir-Hinshelwood mechanism **C** both substrates must be activated simultaneously. The mechanism A is highly unlikely due to high affinity of aluminium to oxygen. It is unlikely that only silane interacts with the active sites. In mechanism B only the interaction of ketone with the catalyst is required. Based on the result obtained by the activation of 3-pentanone in the absence of solvent, increasing the amount of substrate led to a decreased reactivity as observed by less amount of products formed (see Table 16, entry 3,4). These findings suggest that a higher concentration of free electron pairs from the carbonyl group deactivates the catalyst most likely by blocking the active sites, which in turn means that

this mechanism is also unlikely. Mechanism **C** is the most likely one. Following this mechanism the catalyst will be blocked and partly deactivated by adsorption of the ketone. However, the strong interactions between the catalyst and ketone could be weakened by preceding silane adsorption. The silane adsorption could cause a local decrease of the Lewis acidity of the catalyst by transferring electron densitiy from silane to the catalyst. Thus, it is probable that the strong interactions between ketone and active sites, which first led to deactivation of the catalyst, now by means of lowering the acidity, allow for the activation of the ketone. However, it should be noted that if the ratio of ketone to silane is too high, the amount of silane is probably too low to allow for enough weakening of the ketone-catalyst interaction.

Based on previous investigation the characteristic course of the reaction was observed (see 0), which can also be explained best with mechanism C. Over the course of the reaction, substrate was consumed after max 2 days. First, the silylether was formed, which successively declined, by simultaneous increase in the amount of alkene. During the activation with *HS*-AlF_3, also the subsequent decrease of alkene was observed, which can probably be explained by the subsequent reaction to pentene oligomers as a result of cationic polymerization. At the beginning of the reaction, silane will be added to the catalyst and thus being activated. Thereby, catalyst is protected by this adsorbed silane. Next, ketone is added to the reaction mixture, which will also be activated and at the same time reacts with the activated silane to silyl ether. Thus, the amount of the ketone decreased, and at the same time the product silyl ether increases, reacting further to alkene. After the reaction ended the silylether desorbes. The active site, on which the reaction happened, will be again free. It can be occupied either by silane or ketone for the next cycle.

However, the amount of substrate consumed doesn't correspond to an equimolar experimental formation of product. This finding indicates that the ketone is adsorbed at the catalyst with higher affinity than silane, leading to catalyst poisoning and decreased activity. Since the catalytic activity is reduced, the formation of silyl ether is slower. The strong interactions between ketone and the surface were also proven by the rise of the amount of the substrate, which caused reduction of catalytic activity. Also, the diffusion probability plays an important role. Both silane and ketone have to diffuse to the active sites (which are still unoccupied and not poisoned), where they will be activated. If these diffusion processes are very slow, it causes decreased reaction speed.

When determining the mechanism, it is noticeable that all mechanisms involve a nucleophilic attack at the carbonyl group of ketone. The more electrophilic the carbon of a carbonyl group is, the higher is the reactivity, facilitating the nucleophilic attack by the silane. This assumption plays an important role for the explanation, why the activation of chloro-substituted substrates delivered higher conversions (see Figure 56).

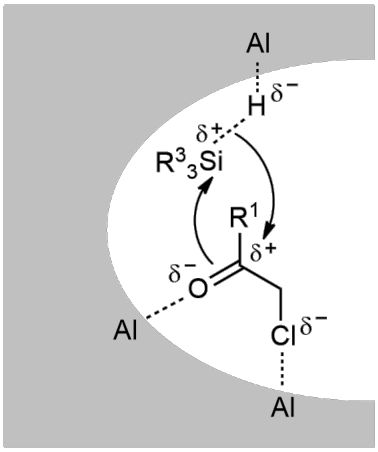

Figure 56. Depiction of the hydrosilylation of chlorinated substrate in the pore of the catalyst for better understanding of the influence of –I electron-withdrawing inductive effect on the reactivity.

The chloro-substituents exert –I electron-withdrawing inductive effect resulting in higher electrophilicity of the carbonyl carbon. Furthermore, the ketone interacts with the catalyst via electron lone pairs at the oxygen as well as at the chlorine substituent, an effect similar to chelation known from homogeneous complexes. This leads to even more increased electrophilic properties at the carbonyl carbon atom. With the introduction of a second chlorine substituent, both effects are further enhanced, leading to even higher yields. These effects are presumably responsible for higher conversion when using chloro-substituted substrates

Activation of phenyl substituted substrates

Similar effects were initially expected for the phenyl group. This group also exerts a small –I effect, which should lead to enhanced electrophilic properties at the carbonyl carbon. Since this effect is rather small, the reduction of electron density at the carbonyl is reduced much less compared to chlorine substituted substrates. Furthermore, phenyl groups have an electron donating mesomeric +M effect which surpasses the small -I effect by several magnitudes. This should lead to enhanced electron density at the carbonyl carbon and thus reduce electrophilic properties. This concept is true for the activation of isobutyrophenone by ACF with or without C_6D_6 and with any of the applied silanes, resulting in lower yields than for 3-pentanone in all

cases. The only exception in this series of experiments was the activation of isobutyrophenone with ACF in the presence of C_6D_6 and Et_2SiH_2, which delivered higher conversion than the activation of 3-pentanone.

Interestingly, the reversed trend was observed for *HS*-AlF_3. In presence of solvent, isobutyrophenone was activated with higher yields than 3-pentanone. It is assumed that in case of *HS*-AlF_3 steric effects (of substrate, solvent, silane and product) become noticeable and bulkier substrates like isobutyrophenone are more likely to fit into the mesopores of the catalyst *HS*-AlF_3, whereas with smaller substrates the diffusion effects are less prominent, leading to lower binding probability in the larger space of the mesopores and the substrates are less efficiently activated. Additionally, due to the larger space in mesopores of *HS*-AlF_3 the phenyl group could make stronger interactions with active sites of the metal catalyst in terms of better alignment of interacting orbitals between the aromatic system and metal centers (see Figure 57). This leads to higher binding affinities between substrate and catalyst which then allows for better activation.

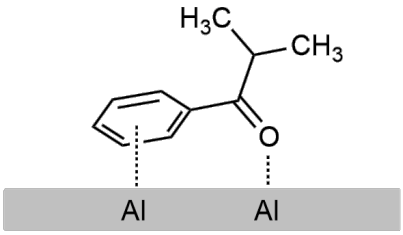

Figure 57. Interaction of phenyl group in the substrate with the surface of the catalyst.

Applying *HS*-AlF_3 did not only lead to better activation of phenyl substituted substrates than compared to 3-pentanone and chlorinated substrates, but also much higher conversions were achieved as compared to ACF. As already suggested, mesopores of *HS*-AlF_3 are more suitable for the activation of sterically demanding substrates. In the case of non-halogenated substrates, alkene was formed (in almost every reaction) as the main product. For the activation of 3-pentanone some exceptions were detected. However, the conversions are low, so it could be caused by the measurement accuracy. Summarizing, ACF is better for the activation of smaller molecules and *HS*-AlF_3 for the sterically demanding substrates.

Influence of silane

In addition to porosity of the catalysts and different substituents at the substrate molecule, the influence of silanes Et_3SiH, Et_2SiH_2 and $^nBuSiH_3$ was investigated. The higher electronegativity of carbon (EN = 2.55) compared to silicon (EN = 1.90) is responsible for the lower electron density at the "Si-H" group with each additional alkyl group. Thus, with increasing number of alkyl substituents, the nucleophilic character of the hydride decreases. Also, the concentration (or number) of hydrides is higher with a lower number of alkyl groups, which increases the probability of the reaction. Additionally, steric effects play an important role. When a more sterically demanding silane is used, theoretically the reaction should be become more difficult. Hence, it was expected that the highest conversion will occur with the most reactive silane $^nBuSiH_3$. However, in most reactions the best conversion was achieved using Et_2SiH_2. A reason could be that the high reactivity of $^nBuSiH_3$ leads to the formation of various side products, which cannot be identified due to overlapping signals in ^1H NMR.

In almost all reactions, alkene was formed as the main product. Only with Et_3SiH and 3-pentanone, the silyl ether was the main product (Table 16, entry 2) indicating that the reactivity and the concentration of silane was too low the push the reaction to alkene as main product.

Interestingly, as already mentioned the hydrosilylation products were detected only for the activation of 3-pentanone and chlorinated alkyl substituted ketones. In the conversion of phenyl substituted substrates the reaction proceeds exclusively to alkenes and further to alkanes. Alkenes are probably formed by cleavage of a silyl ether, as shown in Scheme 58.

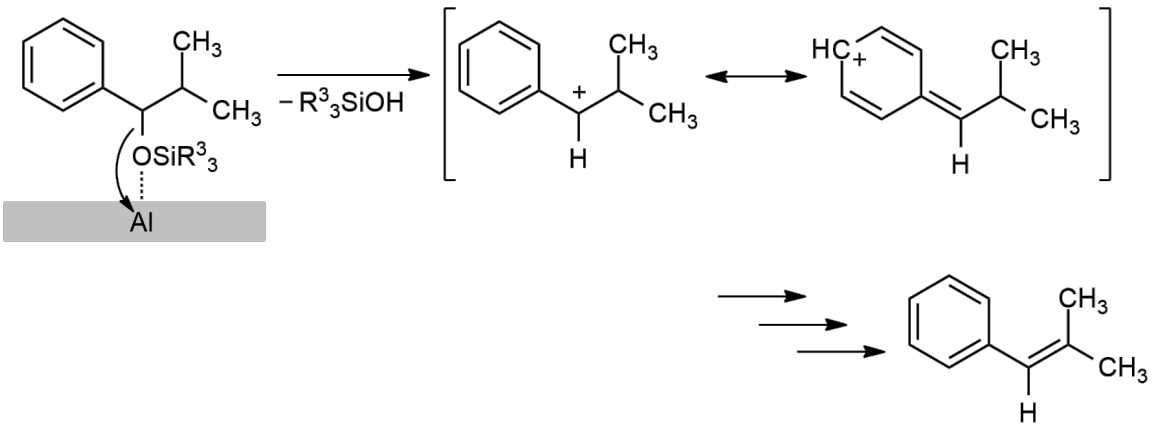

Scheme 58. Formation of alkene from silyl ether.

Formation of alkanes

Alkanes are subsequent products of the hydrogenation of alkenes. Formally, H_2 will be added to the double bond. Silane can be considered as H^- source and H^+ can originate from silanol formed by cleavage of the silyl ether, which adsorbs on the catalyst surface, as shown in Scheme 59.

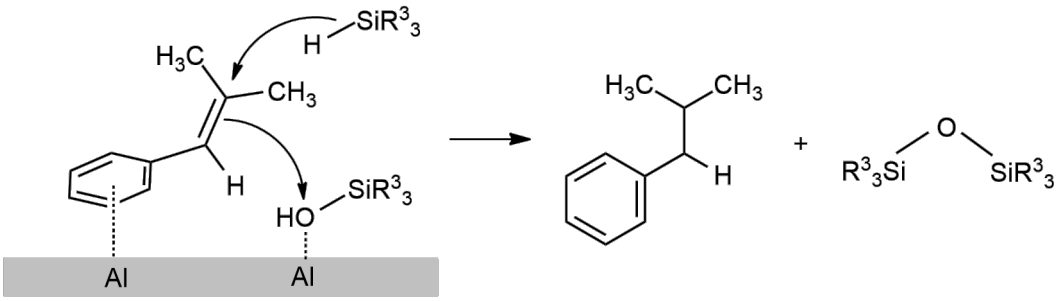

Scheme 59. Formation of alkane from alkene.

As side product disiloxane is formed, which is presumably the driving force of this reaction.

Activation to alkenes (and subsequent hydride reduction to alkanes) seems to be favored in cases of phenyl substituted substrates. The reason is most likely the stabilizing +M effect of the adjacent phenyl group on the intermediate carbocation, leading to a more energetically favored cleavage of the preceding silylether. For phenyl substituted substrates the sum of alkene and alkane products was found to be higher than for 3-pentanone. For chlorinated substrates only silylether, but no alkenes or alkanes could be detected. This is most likely due to the -I effect of chloro-substituents leading to an energetically disfavored reaction pathway via carbocations.

Influence of solvent

The last factor influencing the reaction is the solvent. Comparing the reactions with and without solvent no systematic trends could be observed. For 3-pentanone, ACF-activation led to higher conversions in absence of the solvent, whereas for isobutyrophenone ACF-activation led to better results in the presence of the solvent. For *HS*-AlF_3 the conversions were similar in the presence and absence of C_6D_6. However, the distribution of the products changed. What surprising is, in the presence of C_6D_6, no Friedel-Crafts products were detected. This is an unexpected finding when compared to the activation of chlorinated substrates, where in the presence of C_6D_6 Friedel-Crafts like products were detected. This implies that the Friedel-Crafts reaction pathway is suppressed as far as ketones are used as substrates.

3.4.8 Elucidation of the mechanism

For the elucidation of the corresponding mechanism and the identification of the individual surface-species ^{1}H spin echo experiments of *HS*-AlF_3 loaded with different silanes and 3-pentanone were performed.

Et_2SiH_2

In ^{1}H spin echo MAS NMR spectrum of *HS*-AlF_3 loaded with Et_2SiH_2 the signals between 0 - 1.5 ppm (alkyl chain protons) and 3 - 5 ppm (SiH-group) were identified (see Figure 58).

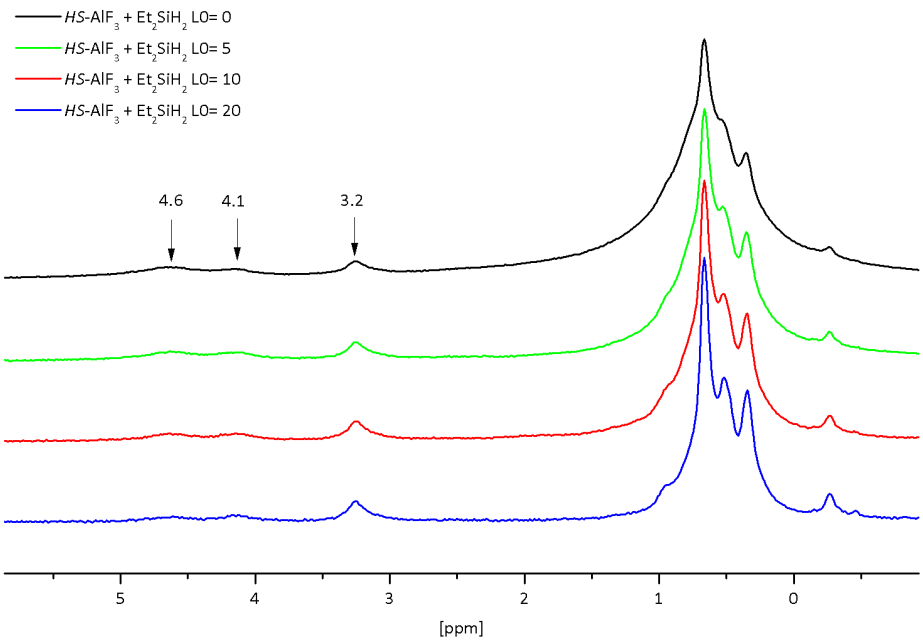

Figure 58. ^{1}H spin echo MAS NMR spectra of *HS*-AlF_3 loaded with Et_2SiH_2.

It is conspicuous that in the range of 3 - 5 ppm three signals could be identified, and not only one as expected and known from liquid phase NMR. The broad signals around 4 ppm were noticed also in spectrum of unloaded *HS*-AlF_3. However, they differ in intensity and shape from those detected in *HS*-AlF_3 loaded with Et_2SiH_2. Thus, it can be supposed that these three signals originate from silane. The signals at 4.13 ppm and 4.63 ppm are lowfield shifted, which can be attributed to enhanced interactions of a "Si-H" group with the catalyst. These interactions lead to the translocation of electron density from the hydride to the catalyst which causes deshielding of the nuclei and shifting to lowfield. By applying longer echo times, the intensity of these signals decreased significantly faster than those of the signal at 3.21 ppm, which also points to high mobility of these species on the surface.

Thus, the silane undergoes different interactions with the catalyst surface resulting in different forms of binding modes as shown in Figure 59. Silane can bind either via one hydride or via two hydrides to the surface. This leads to variable strong activation of the silane. Due to these differences in the reactivity, it is possible that only part of the silane is able to react with the ketone, which in turn leads to lower conversions.

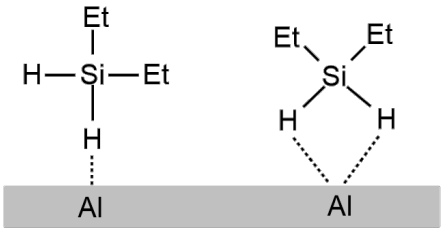

Figure 59. Possible binding modes of Et_2SiH_2 on the catalyst´s surface.

^{n}BuSiH$_3$

The same experiment was carried out for *HS*-AlF_3 loaded with ^{n}BuSiH$_3$ (see Figure 60). Again, the signals in the range of 0 - 1.5 ppm can be assigned to the butyl group and in the range of 3 - 5 ppm to the "Si-H" group. The signal at 4.6 ppm is broad and disappears in spin echo experiment. In contrast, the signal at 3.1 ppm is relatively narrow and hardly loses the intensity in the spin echo experiment. Compared with Et_2SiH_2, these signals are presumably generated by different binding modes of the silane to the catalyst.

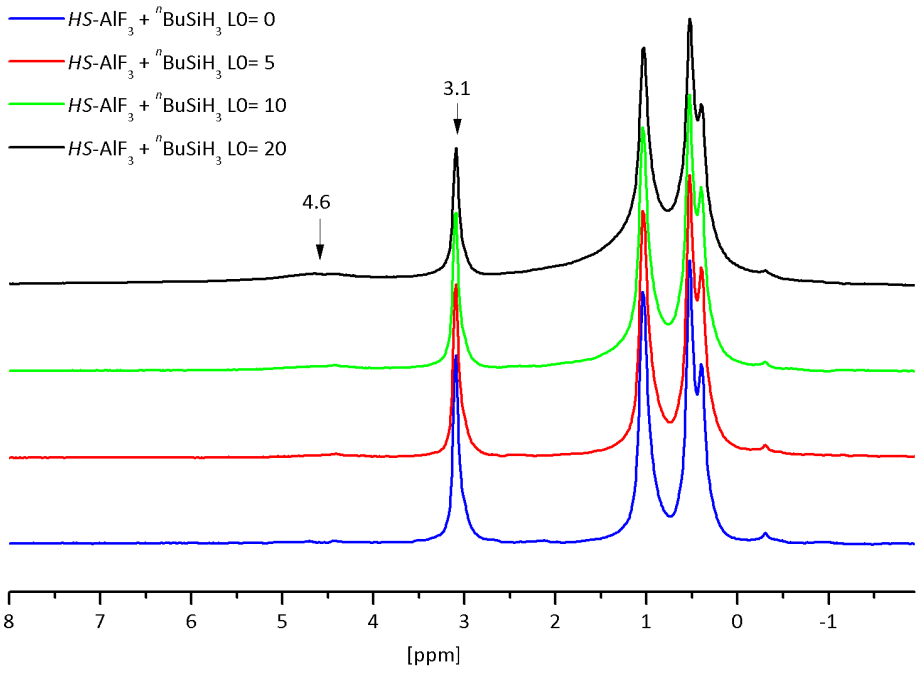

Figure 60. ^{1}H spin echo MAS NMR spectra of *HS*-AlF_3 loaded with ^{n}BuSiH$_3$.

3-pentanone

To complete the series of measurements, *HS*-AlF_3 loaded with 3-pentanone was investigated. In this ^1H spectrum 4 groups of signals are visible, as shown in Figure 61. However, from liquid phase NMR experiments only two signals were expected. The signals in the range of 0 – 1 ppm originate from the protons of CH_3 group. The signal at 0.47 ppm is narrow and loses almost no intensity during the spin echo experiment. It could come from a strong interacting methyl group with the surface of the catalyst. In contrast, the signal at 0.92 ppm is broad and loses the intensity during the spin echo experiment. Furthermore, the signal at 2.45 ppm is broad and can be assigned to protons of CH_2 group. The intensity of this signal decreases in spin echo experiments, which indicates mobility of this species on the surface and weak interactions of these protons with the catalyst. The signals below 0 ppm are probably caused by impurities.

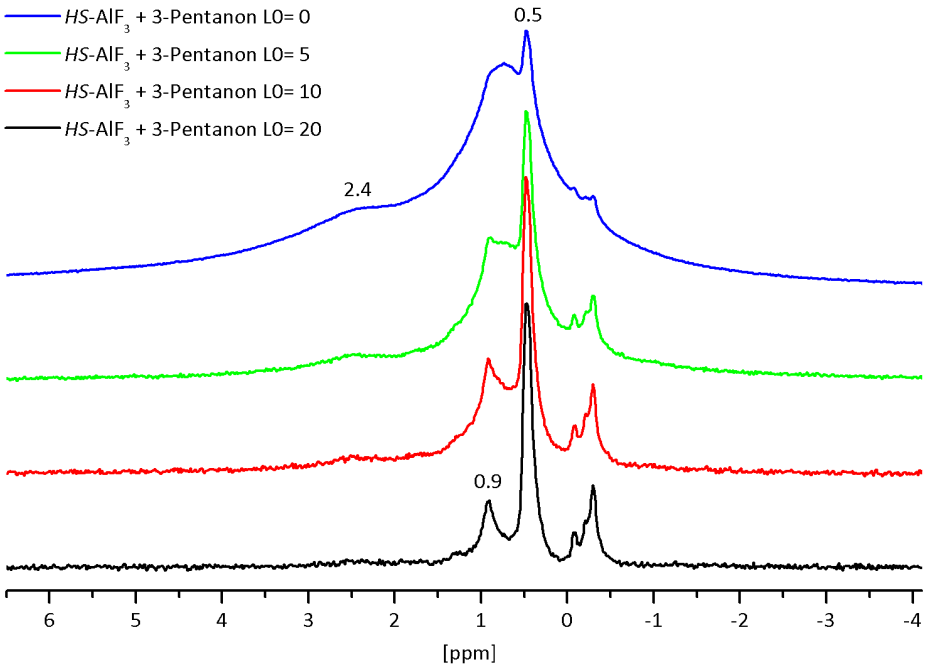

Figure 61. ^1H spin echo MAS NMR spectra of *HS*-AlF_3 loaded with 3-pentanone.

To get more insights into the catalytic system of *HS*-AlF_3 loaded with 3-pentanone, ^1H-^{13}C CP MAS NMR experiments were performed (see Figure 62). Theoretically, due to free electron pairs of oxygen and its electron withdrawing effects, the strongest interactions should take place via the carbonyl group.

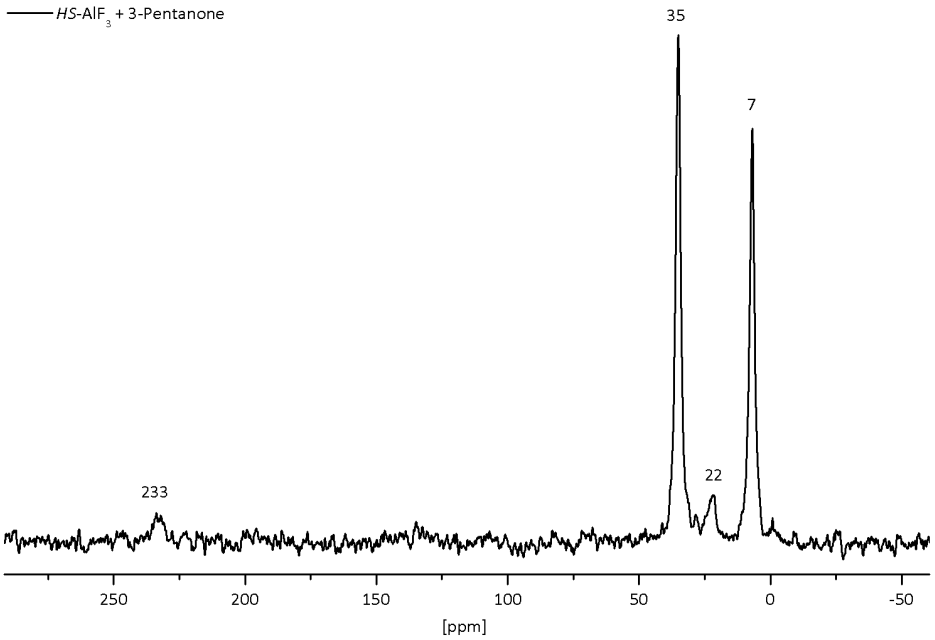

Figure 62. ^{1}H-^{13}C CP MAS NMR spectrum of *HS*-AlF_3 loaded with 3-pentanone.

The signals at 7 ppm and 35 ppm, come from CH_3 and CH_2, respectively. The signal at 233.2 ppm is assigned to the carbon atom of the carbonyl group. Compared to solution phase NMR (209.0 ppm) it is lowfield shifted, indicating strongly reduced electron density at that carbon by the metal catalyst.

Summarizing, by applying spin echo MAS NMR experiments it was proven that all substrates interact with the catalyst. Interestingly, silane remains probably on the surface in different binding modi, which could also be an explanation for the low yields.

4 Experimental Section

4.1 Materials

Aluminium chloride	99.99%	Sigma Aldrich
Aluminium triisopropoxide	≥98%	Sigma Aldrich
Argon	-	Air Liquide
Benzene	≥99.0%	Sigma Aldrich
n-Butylsilane	> 97%	Sigma Aldrich
Chloracetone	95%	Sigma Aldrich
Chlorodifluoromethane	-	Solvay Fluor GmbH
Chloromethane	≥99.5%	Sigma Aldrich
1,2-Dibromohexafluoropropane	95%	Alfa Aesar
1,2-Dichloroethane	≥99%	Sigma Aldrich
Dichloromethane	≥99.5%	Sigma Aldrich
Dichloromethane-d_2	≥99.5%	Sigma Aldrich
1,1-Dichloro-2-propanone	>96%	Sigma Aldrich
Diethylsilane	99%	Sigma Aldrich
Difluoromethane	-	Solvay Fluor GmbH
Fluoromethane	-	ABCR
1-(4-Fluorophenyl)ethanone	99%	Merck
Isopropanol	99.5%	Carl Roth
Isopropylphenylketone	95%	Merck

3-Pentanone	98%	ACROS ORGANICS
1-Phenyl-1-butanone	≥99%	Sigma Aldrich
1-Phenylethanone	≥98%	Sigma Aldrich
Tetrachloromethane	≥99.5%	Sigma Aldrich
Trichlorofluoromethane	≥99.5%	Sigma Aldrich
Triethylsilane	97%	Sigma Aldrich
2,3,3,3-Trifluoro-3-chloropropene	-	Solvay Fluor GmbH
Trifluoromethane	-	Solvay Fluor GmbH
α,α,α-Trifluorotoluene	≥99%	Sigma Aldrich
Triisopropylsilane	98%	Sigma Aldrich

4.2 Analytical methods

FTIR experiments

For the FTIR experiments the samples *HS*-AlF_3 and *HS*-$AlF_3{\circ}Et_3SiH$ were pressed in self-supporting disc in air. The disc was placed in a quarz cell equipped with KBr windows. Before starting adsorption, samples were heated at 473 K and simultaneously evacuated at 0.035 mbar for 2 h. After cooling of the sample to room temperature, 2,6-di-tert-butylpyridine, 2,6-dimethylpyridine and pyridine were consecutively pulsed (up to 1 mbar) onto the samples. Each cycle of base addition was followed by evacuation to 0.035 mbar for 1 h before the next the measurement was conducted. For investigation of further substrate-surface interactions also Et_3SiH was pulsed onto catalyst in additional experiments. FTIR spectra were recorded at room temperature on a Nicolet iS10 FTIR spectrometer of Thermo Fisher Scientific Inc. Data analysis was performed with the software Omnic 8.1. The Spectra are presented as difference spectra, which mean spectrum of non-loaded catalyst was subtracted from spectrum of bases loaded sample.

Elemental analysis (EA)

Carbon and hydrogen content were determined by means of EURO EA equipment (HEKAtech GmbH). The fluorine content was determined with a fluoride sensitive electrode after conversion of the solids with Na_2CO_3/K_2CO_3 into a soluble form.

***Pulse*TA®**

Thermal analysis experiments were performed by using the thermoanalyzer Netzsch STA 409 C *Skimmer*® equipped with Balzers QMG 421 mass spectrometer. For the monitoring of gas-solid processes, the thermoanalytical curves (T, DTA, TG, and DTG) were recorded together with the ionic current (IC) curves in the multiple ion detection (MID) mode. A DTA–TG sample carrier system with platinum crucibles (Beaker, 0.8 mL) and Pt/PtRh10 thermocouples was used. Around 30 mg of the catalyst was measured versus empty reference crucibles. The samples were kept in a constant gas flow of 70 mL min^{-1} argon 5.0 (AirLiquide) and a constant heating rate of 10 K min^{-1} or an isothermal regime with T_{iso} ~50 °C was applied.

Data analysis was performed with the software Proteus® (v. 4.3) and Quadstar® 422 (v. 6.02) with no further data treatment. The substrate was injected by using the commercial PTA box or manually with the help of millilitre syringe. The liquid substrates were introduced by using self-made injection unit (heated at 120°C) and mico litre glass syringe.

NH_3-TPD

For TPD experiments, about 30 mg of the samples filled with around 100 mg of quartz glass beads (to avoid clocking of the reactor) were added in a quartz flow reactor and heated at 523 K under nitrogen flow for 1 hour, unless otherwise indicated. Afterwards, ammonia was adsorbed onto the surface of the samples at 393 K. After flushing the excess NH_3 with N_2 for 1 h and cooling to 353 K the TPD program was started (10K/min up to 773 K, then holding until no more NH_3 is desorbed). Desorbed ammonia was continuously monitored by IR spectroscopy (FT-IR System 2000, Perkin-Elmer) following the band at 930 cm^{-1}. For quantification, the total amount of desorbed ammonia was reacted with diluted solution of sulfuric acid and then titrated with sodium hydroxide solution.

MAS NMR

The solid-state MAS NMR spectra were collected with a Bruker AVANCE 400 Spectrometer at room temperature. The samples were prepared in the glove box. The isotropicchemical shift values are given with respect to TMS (0 ppm) using adamantan as secondary standard for ^{1}H and ^{13}C measurements. ^{19}F chemical shifts are referred to $\delta = 0$ ppm of $CFCl_3$ and α-AlF_3 was used as a secondary standard for calibration.

Table 23. Measurement Parameters

figure	exp.	Larmor freq. [MHz]	π/2 pulse [µs]	rotor size [mm]	accum. nr.	dipolar ev.time [ms]	spinning rate [kHz]
26	^{19}F depth[1)]	376.4	2.4	4	32	---	10
27	^{19}F spin echo	376.4	2.4	4	64	1	10
28	^{1}H depth[1)]	400.1	2.7	4	32	---	10
29	^{1}H spin echo	400.1	2.7	4	32	1	10
30	^{1}H-^{13}C CP	100.6	---[2)]	4	20000 1760	---	10
38	^{1}H spin echo	400.1	3.7	2.5	128	1.6	25
58	^{1}H spin echo	400.1	2.7	4	32	0; 0.5; 1; 2	10
60	^{1}H spin echo	400.1	2.7	4	32	0; 0.5; 1; 2	10
61	^{1}H spin echo	400.1	2.7	4	32	0; 0.5; 1; 2	10
62	^{1}H-^{13}C CP	100.6	---[2)]	4	4928	---	10

Recycle delay = 5 [s]
[1)] Existent background signals were suppressed with the application of a phase-cycled depth pulse sequence according to Cory and Ritchey[211]
[2)] Contact time = 1 [ms]

NMR

The liquid state NMR spectra (^{1}H, ^{13}C, ^{13}C DEPT, ^{1}H-^{13}C HMBC, ^{1}H-^{13}C HSQC, ^{19}F, ^{29}Si) were recorded at a Bruker DPX 300, a Bruker AVANCE II 300 or a Bruker AVANCE II 500 spectrometer at room temperature. ^{1}H and ^{13}C NMR chemical shifts were referenced to benzene C_6D_6 at $\delta = 7.16$ ppm and $\delta = 128.06$ ppm, respectively.

XRD

For X-ray powder diffraction measurments, a XRD3003-TT diffractometer (Seiffert & Co., Freiberg), with Cu-Kα as radiation source (l = 1.542 Å) was applied. To protect the samples from the moisture, they were prepared in the glovebox and covered with Kapton® film during the measurement.

4.3 Synthesis procedures

All samples were prepared under an argon atmosphere using conventional Schlenk or glove box techniques.

4.3.1 Synthesis of catalysts

Aluminum chlorofluoride (ACF; $AlCl_xF_{3-x}$, x = 0.05 - 0.15) was synthesized according to the literature [40] using anhydrous aluminum chloride $AlCl_3$ (Sigma Aldrich, 99.99%, anhydrous powder). The fluorination agent CCl_3F (Sigma Aldrich, ≥99.5%) was slowly added to the $AlCl_3$ immersed in the inert solvent CCl_4. After the completed reaction all volatile compounds were removed.

High-surface aluminumfluoride (*HS*-AlF_3) was synthesized according to the literature [31] using anhydrous aluminum triisopropoxide $Al(OiPr)_3$ (Sigma Aldrich, ≥98%). In the first step, $Al(OiPr)_3$ was dissolved in dry isopropanol under heating, and after cooling down treated with hydrogen fluoride dissolved in isopropanol. After the completed reaction all volatile compounds were removed. The compound was then post-fluorinated with gaseous Chlorodifluoromethane (Solvay, R22) at 240 °C.

From NH_3-TPD measurements the concentration of Lewis-acid sites was deduced for ACF and *HS*-AlF_3 to be about 1 mmol g^{-1}.[44]

4.3.2 Isomerization of 1,2-dibromohexafluoropropane to 2,2-dibromohexa-fluoropropane

25 mg of the catalyst were suspended in 250 µL 1,2-dibromohexafluoropropane (100 µl per 10 mg of catalyst). The reaction mixture was stirred at room temperature. After 2 h water was added to stop the reaction. to dissolve the product. The organic phase was separated and investigated by ^{19}F NMR. Conversion was calculated by integration of the signals of substrate and product in the spectra.

4.3.3 Dismutation of $CHClF_2$

For studying catalyst activity, dismutation of $CHClF_2$ was performed in a flow reactor. Only very strong Lewis acids are able to perform this reaction with full conversion at room temperature. The reaction was investigated by chromatographic analyses (GC) using Shimadzu GC-2010 instrument equipped with a flame-ionisation detector and a HP-1 column (100m x 0.250mm x 0.5µm). Nitrogen was used as a carrier gas. Conversions were calculated relatively by ratio of $CHClF_2$ to the following products CHF_3, $CHCl_3$, $CHCl_2F$.

4.3.4 Fluorination of ACF

ACF (500 mg) was placed in inert Schlenk flask and evacuated. Then, CH_3F was added directly to a flask with the catalyst under atmospheric pressure. The reaction mixture was kept for 24 h at room temperature. The gas phase was injected by syringe to the GC. Additionally, the gaseous phase over the catalyst was condensed in a JYoung NMR tube with C_6D_6 as the solvent and investigated by ^{1}H and ^{19}F NMR spectroscopy.

4.3.5 Preparation of catalyst◦Et_3SiH or catalyst◦$^{i}Pr_3SiH$

ACF or *HS*-AlF_3 (200 mg) was suspended in excess of Et_3SiH (0.5 mL) or $^{i}Pr_3SiH$ (0.5 mL) in Schlenk flask. The reaction mixture was stirred for 20 min at room temperature. The excess of silane was removed under reduced pressure.

4.3.6 General procedure for the activation of fluorinated methanes in Et_3SiH

In a JYoung NMR tube 25 mg or 12.5 mg of the catalyst were suspended in Et_3SiH (0.5 mL). Then CH_3F, CH_2F_2 or CHF_3 was condensed into the reaction mixture from a 25 mL bulb filled with 1 atm of the gaseous substrate. The weight of the substrate was calculated on the basis of the weight difference of the bulb after the condensation and the fully filled bulb. Note that the dissolved amount of gaseous substrate is limited by their solubility in Et_3SiH. The reaction mixture was kept at 70 °C up to 6 days. The reaction progress was monitored each day by ^{1}H NMR spectroscopy. The spectra were calibrated externally to C_6D_6, which was also used as standard for quantification. The conversions were evaluated based on the ratio of consumed substrate or product to substrate. The TONs are calculated based on the amount of product per amount of active sites of the catalyst. It was assumed that 1 g of ACF or *HS*-AlF_3 contains roughly 1 mmol of catalytically active sites.[44] TOFs are calculated based on TON divided by reaction time in h.

Table 24. Hydrodefluorination of fluorinated methanes in excess of Et_3SiH.

Entry	subs.	subs. [mmol]	catalyst	t [d]	conv. [%]	TON	TOF [h^{-1}]
1	CH_3F	1.80	ACF	1	74	53	2.2
2	CH_3F	1.80	ACF	2	88	63	1.3
3	CH_3F	1.80	ACF	3	100	72	1.0
4	CH_3F	1.80	ACF	4	100	72	-
5	CH_3F	1.80	ACF	5	100	72	-
6	CH_3F	1.80	ACF	6	100	72	-
7	CH_3F	1.88	HS-AlF_3	1	49	37	1.5
8	CH_3F	1.88	HS-AlF_3	2	68	51	1.1
9	CH_3F	1.88	HS-AlF_3	3	75	56	0.8
10	CH_3F	1.88	HS-AlF_3	4	82	62	0.6
11	CH_3F	1.88	HS-AlF_3	5	83	62	0.5
12	CH_3F	1.88	HS-AlF_3	6	88	66	0.5
13	CH_2F_2	1.82	ACF	1	10	7	0.3
14	CH_2F_2	1.82	ACF	2	20	15	0.3
15	CH_2F_2	1.82	ACF	3	29	21	0.3
16	CH_2F_2	1.82	ACF	4	26	19	0.2
17	CH_2F_2	1.82	ACF	5	36	26	0.2
18	CH_2F_2	1.82	ACF	6	45	32	0.2
19	CH_2F_2	1.90	HS-AlF_3	1	2	2	-
20	CH_2F_2	1.90	HS-AlF_3	2	2	2	-
21	CH_2F_2	1.90	HS-AlF_3	3	2	2	-
22	CH_2F_2	1.90	HS-AlF_3	4	2	2	-
23	CH_2F_2	1.90	HS-AlF_3	5	2	2	-
24	CH_2F_2	1.90	HS-AlF_3	6	2	2	-
25	CHF_3	1.85	ACF	1	0	-	-
26	CHF_3	1.85	ACF	2	0	-	-
27	CHF_3	1.85	ACF	3	0	-	-
28	CHF_3	1.85	ACF	4	0	-	-
29	CHF_3	1.85	ACF	5	0	-	-
30	CHF_3	1.85	ACF	6	0	-	-
31	CHF_3	1.86	HS-AlF_3	1	0	-	-
32	CHF_3	1.86	HS-AlF_3	2	0	-	-
33	CHF_3	1.86	HS-AlF_3	3	0	-	-
34	CHF_3	1.86	HS-AlF_3	4	0	-	-
35	CHF_3	1.86	HS-AlF_3	5	0	-	-
36	CHF_3	1.86	HS-AlF_3	6	traces	-	-

4.3.7 General procedure for the activation of chlorinated methanes and ethanes in Et_3SiH as solvent

In a JYoung NMR tube 25 mg of the catalyst were suspended in Et_3SiH (0.6 mL). Then CH_3Cl was condensed into the reaction mixture from a 25 mL bulb filled with 1 atm of the gaseous substrate. The weight of the substrate was calculated on the basis of the weight difference of the bulb after the condensation and the fully filled bulb. Note that the dissolved amount of gaseous substrate is limited by their solubility in Et_3SiH. If liquid substrate was used, 0.35 mmol of CH_2Cl_2 or 0.30 mmol of $ClCH_2$-CH_2Cl were added to the reaction mixture. The reaction mixture was kept at 70 °C up to 6 days. The reaction progress was monitored each day by ^1H NMR spectroscopy. The spectra were calibrated externally to C_6D_6. Pyridine was used as external standard for quantification. The conversions were evaluated based on the ratio of consumed substrate or product to substrate. The TONs are calculated based on the amount of product per amount of active sites of the catalyst. It was assumed that 1 g of ACF or *HS*-AlF_3 contains roughly 1 mmol of catalytically active sites.[44]

4.3.8 General procedure for the activation of chlorinated methanes and ethanes in Et_3SiH and C_6D_6

In a JYoung NMR tube 25 mg of the catalyst were suspended in C_6D_6 (0.6 mL). Then silane was added. Subsequently, CH_3Cl was condensed into the reaction mixture from a 25 mL bulb filled with 1 atm of the gaseous substrate. The weight of the substrate was calculated on the basis of the weight difference of the bulb after the condensation and the fully filled bulb. Note that the dissolved amount of gaseous substrate is limited by their solubility in Et_3SiH. If liquid substrate was used, 0.35 mmol of CH_2Cl_2 (or CD_2Cl_2) or 0.30 mmol of $ClCH_2$-CH_2Cl were added to the reaction mixture. The reaction mixture was kept at 70 °C up to 6 days. The reaction progress was monitored each day by ^1H NMR spectroscopy. The spectra were calibrated externally to C_6D_6. Pyridine was used as external standard for quantification. The conversions were evaluated based on the ratio of consumed substrate or product to substrate. The TONs are calculated based on the amount of product per amount of active sites of the catalyst. It was assumed that 1 g of ACF or *HS*-AlF_3 contains roughly 1 mmol of catalytically active sites.[44]

4.3.9 General procedure for the activation of chlorinated methanes and ethanes in C_6D_6

In a JYoung NMR tube 25 mg of the catalyst were suspended in C_6D_6 (0.6 mL). Then CH_3Cl was condensed into the reaction mixture from a 25 mL bulb filled with 1 atm of the gaseous substrate. The weight of the substrate was calculated on the basis of the weight difference of the bulb after the condensation and the fully filled bulb. Note that the dissolved amount of gaseous substrate is limited by their solubility in Et_3SiH. If liquid substrate was used, 0.35 mmol of CH_2Cl_2 or 0.30 mmol of $ClCH_2$-CH_2Cl were added to the reaction mixture. The reaction mixture was kept at 70 °C up to 6 days. The reaction progress was monitored each day by ^1H NMR spectroscopy. The spectra were calibrated externally to C_6D_6. Pyridine was used as external standard for quantification. The conversions were evaluated based on the ratio of consumed substrate or product to substrate. The TONs are calculated based on the amount of product per amount of active sites of the catalyst. It was assumed that 1 g of ACF or *HS*-AlF_3 contains roughly 1 mmol of catalytically active sites.[44] TOFs are calculated based on TON divided by reaction time in h.

4.3.10 General procedure for the activation of ketones

In a JYoung NMR tube 50 mg of the catalyst were suspended in Et_3SiH (0.4 mL). If C_6D_6 was used as a solvent, 0.4 mL were added. Subsequently, 0.3 mmol of ketone were added to the reaction mixture. The reaction was kept at 100 °C for up to 16 days. The reaction progress was monitored each day by ^1H NMR spectroscopy. The spectra were calibrated externally to C_6D_6. To identify as many products as possible the solution was also analysed by means of ^{13}C, ^{13}C-DEPT, ^1H-^1H COSY, ^1H-^{13}C HMBC, ^1H-^{13}C HSQC and ^1H-^{29}Si HMBC NMR spectroscopy. The conversions were evaluated based on the ratio of product to substrate using pyridine as external standard. The TONs are calculated based on the amount of product per amount of active sites of the catalyst. It was assumed that 1 g of ACF or *HS*-AlF_3 contains roughly 1 mmol of catalytically active sites.[44]

4.4 Different kind of reactors

Chemical reactions can be carried out in different types of reactors, which are categorized by their contact times as batch, continuous and pulse reactors (Figure 63).

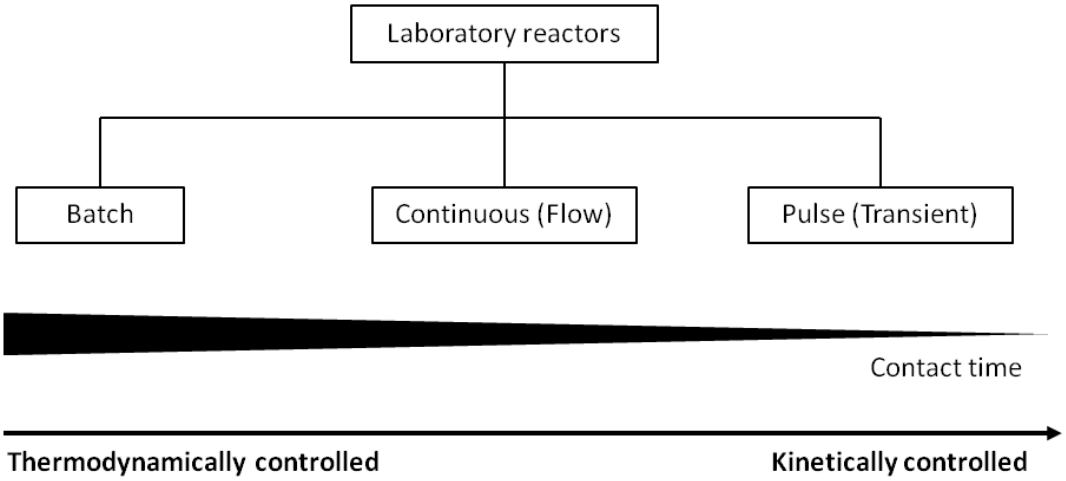

Figure 63. Different types of reactors.

The reactor with the longest contact time is the batch reactor, in which the catalyst works until a state of thermodynamical equilibrium is reached. Such batch reactors are remarkably suitable for slow reactions allowing the substrates to diffuse deep into pores to approach the active sites of catalyst. The second reactor is the flow reactor. The contact times are shorter than in batch reactors. Due to the shorter contact times, the reactions are subjected to both kinetic and thermodynamic control. The reactions are limited to easily accessible active sites. The longer diffusion pathways cannot be used, meaning that such reactions are hard to perform. However, the activation in flow reactors is of interest, since the activation occurs under eco-friendly and solvent-free conditions. The pulse reactor is the most intense form of flow reactor with very short contact times. Kinetic products are favoured at those contact times. Thus, the product distribution might differ when compared to batch reactors.

*Pulse*TA® experiments can be classified as a special type of pulse reactor. The substrates are pulsed on the catalyst, in a similar manner to the transient reactor. In *Pulse*TA® experiments, the substrates are mixed across in contrast to the pulse reactor, where lateral mixing is avoided. Thus, the kinetics has changed.

The selection of an appropriate laboratory reactor is crucial for evaluating the kinetics of the catalytic processes, especially in heterogeneous catalysis, where reactions are highly diffusion-controlled. The conversion and selectivity of these reactions depend not only on the type of

interaction with the substrates, but also on the spatial limitations occurring during diffusion processes. The size of the substrates as well as the pore architecture of the heterogeneous catalyst can influence selectivity and efficiency of reactions. Therefore, the steric aspects and the dependency on the interactions in these reactions were examined using two catalysts differing in both porosity and chemical composition, ACF and *HS*-AlF_3, in batch (solid-gas and liquid-gas reactions) and flow reactor as well as in *Pulse*TA® experiments.

4.4.1 Flow reactor

For the chromatographic analyses (GC) Shimadzu GC-17A instrument equipped with a flame-ionisation detector and a column (GS-GASPRO, 60 m x 0.320 mm) was used.

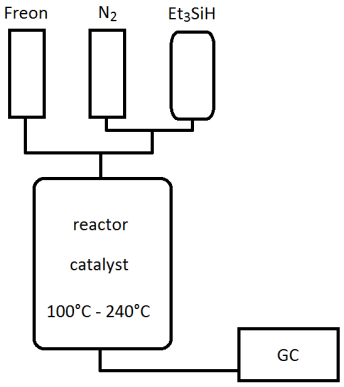

Figure 64. Flow reactor.

The flow reactor is built as shown in Figure 64. A flow reactor contains a stainless tube (reactor) placed in a vertical oven. The flow of the gases is controlled by the mass flow controllers from MKS instruments. The calibration of these mass flow controllers has been carried out at room temperature with each particular working gas for the quantification. The flow controllers are connected with the reactor through Teflon pipes, which are heated at 120°C. The valves and connectors have been obtained from *Swagelok* and *Bohlender.* The 0.25 ml catalyst (180 mg of ACF or 190 mg of *HS*-AlF_3) combined with 0.25 ml glass beads is placed on silver wool in the middle of the tube. The oven is operated at different temperatures and different flows resulting in different contact times. Firstly, the catalyst is saturated with silane for 30 min (gas saturator at 40 °C). Then, the reaction is initiated by switching on the flow of substrate. The reactor is operated at steady state.

Table 25. Correlation between contact time and adjusted flow.

contact time [s]	Flow N_2 [mL*min-1]	Flow substrate [mL*min-1]
0.1	100	10
0.2	60	6
0.3	40	4
0.6	20	2
1.3	10	1
0.5	10	20

4.4.2 Batch reactions

250 mg of the ACF◦Et_3SiH or ACF◦$^iPr_3SiH$ were placed in the 50 mL flask filled with the gaseous substrates (CH_2F_2, CH_3F) under atmospheric pressure in order to activate them. The reactions were carried out at room temperature up to 24 h. The conversions were determined by GC analyses. Additionally, ^1H, ^{13}C and ^{19}F NMR spectroscopy was performed to identify all the products. For that experiment, the gaseous phase over the catalyst was condensed in a JYoung NMR tube with C_6D_6 as the solvent.

4.5 NMR Data

CF_3−CBrF−$CBrF_2$

^{19}F-NMR (282.4 MHz , $CDCl_3$) δ= -133.3 (m, 1F, C**F**Br), -74.3 (m, 3F, -C**F_3**), -59.2 (dm, 1F, -C**F**FBr, ^2J(F,F)= 176 Hz), −57.2 (dm, 1F, -CF**F**Br, ^2J(F,F)= 176 Hz) in ppm

CF_3−CBr_2−CF_3

^{19}F-NMR (282.4 MHz , $CDCl_3$) δ= −72.1 (s, 6F, -C**F_3**) in ppm

CH_3F, solvent Et_3SiH

^{1}H-NMR (300.1 MHz , C_6D_6) δ= 3.10 (d, 3H, ^2J(H,F)= 48.0 Hz) in ppm

^{19}F-NMR (282.4 MHz , C_6D_6) δ= -267.5 (q, 1F, ^2J(F,H)= 47.9 Hz) in ppm

CH_2F_2, solvent Et_3SiH

^{1}H-NMR (300.1 MHz , C_6D_6) δ= 4.52 (t, 2H, ^2J(H,F)= 51.0 Hz) in ppm

^{19}F-NMR (282.4 MHz , C_6D_6) δ= -141.5 (t, 2F, ^2J(F,H)= 50.0 Hz) in ppm

CHF_3, solvent Et_3SiH

^{1}H-NMR (300.1 MHz , C_6D_6) δ= 5.33 (q, 1H, ^2J(H,F)= 78.0 Hz) in ppm

^{19}F-NMR (282.4 MHz , C_6D_6) δ= -78.5 (t, 3F, ^2J(F,H)= 78.1 Hz) in ppm

CH_4, solvent Et_3SiH

^{1}H-NMR (300.1 MHz , C_6D_6) δ= 0.17 (s, 4H) in ppm

Toluene

^{1}H-NMR (400.1 MHz , C_6D_6) δ= 2.14 (s, 3H, C**H_3**) in ppm

^{13}C-NMR (100.6 MHz , C_6D_6) δ= 137.3 (s, 6C, arom. **C**H), 21.3 ppm (s, 1C, -**C**H_3) in ppm

PhCF_3

^{19}F-NMR (282.4 MHz , C_6D_6) δ= -62.7 (s, 3F, -CF_3) in ppm

Et_3SiH

^{1}H-NMR (400.1 MHz , C_6D_6) δ= 3.89 (h, 1H, -Si**H**, ^3J(H,H)= 6.2Hz),
0.98 (t, 9H, -CH_2C**H_3**, ^3J(H,H)= 7.9 Hz),
0.55 (qd, 6H, -C**H_2**CH_3, ^3J(H,H)= 7.9 Hz) in ppm

^{13}C-NMR (100.6 MHz , C_6D_6) δ= 8.5 (s, 3C, -CH_2**C**H_3),
2.8 (s, 3C, -**C**H_2CH_3) in ppm

^{29}Si-NMR (79.5 MHz , C_6D_6) δ= 0.14 (s, 1Si, -**Si**H) in ppm

Et_3SiF

^{1}H-NMR (400.1 MHz , C_6D_6) δ= 0.92 (t, 9H, -$CH_2C\mathbf{H_3}$, ^3J(H,H)= 8.0 Hz),
0.72 (q, 6H, -$C\mathbf{H_2}CH_3$, ^3J(H,H)= 7.9 Hz) in ppm

^{13}C-NMR (100.6 MHz , C_6D_6) δ= 6.3 (d, 3C, -$CH_2\mathbf{C}H_3$, ^3J(C,F)= 1.8 Hz),
5.2 (d, 3C, -$\mathbf{C}H_2CH_3$, ^2J(C,F)= 14.2 Hz) in ppm

^{19}F-NMR (282.4 MHz , C_6D_6) δ= -175.5 (m, 1F) in ppm

^{29}Si-NMR (79.5 MHz , C_6D_6) δ= 32.1 (d, 1Si, -**Si**F, ^1J(Si,F)= 289.1 Hz) in ppm

Et_3SiCl

^{1}H-NMR (400.1 MHz , C_6D_6) δ= 0.92 (t, 9H, -$CH_2C\mathbf{H_3}$, ^3J(H,H)= 7.9 Hz),
0.61 (q, 6H, -$C\mathbf{H_2}CH_3$, ^3J(H,H)= 7.8 Hz) in ppm

^{13}C-NMR (100.6 MHz , C_6D_6) δ= 8.2 (s, 3C, -$CH_2\mathbf{C}H_3$),
7.2 (s, 3C, -$\mathbf{C}H_2CH_3$) in ppm

^{29}Si-NMR (79.5 MHz , C_6D_6) δ= 36.8 (s, 1Si, -**Si**Cl) in ppm

$^i Pr_3SiH$

^{1}H-NMR (400.1 MHz , C_6D_6) δ= 3.53 (q, 1H, -Si**H**, ^3J(H,H)= 1.8 Hz,
1.09-1.06 (m, 21H, $C\mathbf{H_3}C\mathbf{H}C\mathbf{H_3}$) in ppm

^{13}C-NMR (100.6 MHz , C_6D_6) δ= 8.5 (s, 6C, $\mathbf{C}H_3CH\mathbf{C}H_3$),
2.8 (s, 3C, $CH_3\mathbf{C}HCH_3$) in ppm

^{29}Si-NMR (79.5 MHz , C_6D_6) δ= 0.13 (s, 1Si, -**Si**H) in ppm

$^i Pr_3SiF$

^{13}C-NMR (100.6 MHz , C_6D_6) δ= 17.9 (s, 6C, $\mathbf{C}H_3CH\mathbf{C}H_3$),
14.0 (s, 3C, $CH_3\mathbf{C}HCH_3$) in ppm

CH_3Cl

^{1}H-NMR (400.1 MHz , C_6D_6) δ= 2.41 (s, 3H) in ppm

^{13}C-NMR (100.6 MHz , C_6D_6) δ= 48.3 (s, 1C) in ppm

CH_2Cl_2

^{1}H-NMR (400.1 MHz , C_6D_6) δ= 5.06 (s, 2H) in ppm

^{13}C-NMR (100.6 MHz , C_6D_6) δ= 53.6 (s, 1C) in ppm

Cl-CH_2-CH_2-Cl

^{1}H-NMR (400.1 MHz , C_6D_6) δ= 3.75 (s, 4H) in ppm

^{13}C-NMR (100.6 MHz , C_6D_6) δ= 43.6 (s, 2C) in ppm

$PhCH_3$

^{1}H-NMR (400.1 MHz , C_6D_6) δ= 2.14 (s, 3H, -$C\mathbf{H_3}$) in ppm

^{13}C-NMR (100.6 MHz , C_6D_6) δ= 21.3 (s, 1C, -$\mathbf{C}H_3$) in ppm

$PhPh^{D}CH_2$

^{1}H-NMR (400.1 MHz , C_6D_6) δ= 3.75 (s, 2H, -C**H_2**-) in ppm

^{13}C-NMR (100.6 MHz , C_6D_6) δ= 41.9 (s, 1C, -**C**H_2-) in ppm

$Ph^{D}CH_2$-CH_2Ph^{D}

^{1}H-NMR (400.1 MHz , C_6D_6) δ= 2.75 (s, 4H, -C**H_2**-) in ppm

^{13}C-NMR (100.6 MHz , C_6D_6) δ= 38.1 (s, 2C, -**C**H_2-) in ppm

$Ph^{D}CH_2$-CH_3

^{1}H-NMR (400.1 MHz , C_6D_6) δ= 2.44 (q, 2H, -C**H_2**CH_3, ^{3}J(H,H)= 7.7 Hz), 1.09 (t, 3H, -CH_2C**H_3**, ^{3}J(H,H)= 7.7 Hz) in ppm

^{13}C-NMR (100.6 MHz , C_6D_6) δ= 28.7 (s, 1C, -**C**H_2CH_3), 15.3 (s, 1C, -CH_2**C**H_3) in ppm

Ph^{D}_2CH-CH_3

^{1}H-NMR (400.1 MHz , C_6D_6) δ= 3.94 (q, 1H, -C**H**-CH_3, ^{3}J(H,H)= 7.2 Hz), 1.44 (d, 3H, -CH-C**H_3**, ^{3}J(H,H)= 7.2 Hz) in ppm

^{13}C-NMR (100.6 MHz , C_6D_6) δ= 44.6 (s, 1C, -**C**H-CH_3), 21.5 (s, 1C, -CH-**C**H_3) in ppm

Ph^{D}_2CH-CH_2- Ph^{D}

^{1}H-NMR (400.1 MHz , C_6D_6) δ= 4.15 (t, 1H, -C**H**-CH_2-), 3.21 (d, 2H, -CH-C**H_2**-) in ppm

^{13}C-NMR (100.6 MHz , C_6D_6) δ= 53.0 (s, 1C, -**C**H-CH_2-) , 41.9 (s, 1C, -CH-**C**H_2-) in ppm

CH_2=CH-CH=CH_2

^{1}H-NMR (300.1 MHz , C_6D_6) δ= 6.40 (m, 2H, CHH'-C**H**-), 6.21 (dd, 2H, C**H**H'-CH-, ^{3}J(H,H')= 9.0 Hz), 5.34 (dd, 2H, CH**H'**-CH-, ^{3}J(H,H)= 15.0 Hz) in ppm

Cl_2CH-CH_3

^{1}H-NMR (300.1 MHz , C_6D_6) δ= 5.95 (q, 1H, Cl_2C**H**-, ^{3}J(H,H)= 6.0 Hz), 2.03 (d, 3H, -C**H_3**, ^{3}J(H,H)= 6.0 Hz) in ppm

CH_3-CH_3

^{1}H-NMR (300.1 MHz , C_6D_6) δ= 1.42 (s, 3H, -C**H_3**) in ppm

Et_2SiH_2

^{1}H-NMR (400.1 MHz , C_6D_6) δ= 3.83 (p, 2H, -Si**H_2**, ^{3}J(H,H)= 6.2Hz), 0.96 (t, 6H, -CH_2C**H_3**, ^{3}J(H,H)= 7.9 Hz), 0.55 (qd, 6H, -C**H_2**CH_3, ^{3}J(H,H)= 7.9 Hz) in ppm

^{13}C-NMR (100.6 MHz , C_6D_6) δ= 9.2 (s, 2C, -CH_2**C**H_3), 1.3 (s, 2C, -**C**H_2CH_3) in ppm

^{29}Si-NMR (79.5 MHz , C_6D_6) δ= -22.8 (s, 1Si, -**Si**H_2) in ppm

^{n}BuSiH_3

^{1}H-NMR (300.1 MHz , C_6D_6) δ= 3.59 (t, 3H, -Si**H$_3$**, ^{3}J(H,H)= 3.9 Hz), 1.22 (m, 4H, -C**H$_2$**-C**H$_2$**-CH_3), 0.80 (t, 3H, -CH_2-CH_2-C**H$_3$**, ^{3}J(H,H)= 7.9 Hz), 0.51 (m, 2H, H_3Si-C**H$_2$**-) in ppm

^{29}Si-NMR (99.4 MHz , C_6D_6) δ= -59.7 (s, 1Si, -**Si**H_3) in ppm

3-Pentanone $C_5H_{10}O$

^{1}H-NMR (300.1 MHz , C_6D_6) δ= 1.86 (q, 4H, COC**H$_2$**-CH_3, ^{3}J(H,H)= 7.3 Hz), 0.89 (t, 6H, COC**H$_2$**-CH_3, ^{3}J(H,H)= 7.3 H) in ppm

^{13}C-NMR (75.5 MHz , C_6D_6) δ= 209.0 (s, 1C, **C**OCH_2-CH_3), 35.1 (s, 2C, CO**C**H_2-CH_3), 7.9 (s, 2C, $COCH_2$-**C**H_3) in ppm

E-pent-2-ene (8)

^{1}H-NMR (400.1 MHz, C_6D_6) δ= 5.41 (m, 2H, -**H**C=C**H**-), 1.94 (m, 2H, -C**H$_2$**CH_3), 1.59 (m, 3H, C**H$_3$**-C=C), 0.93 (t, ^{3}J(H,H) = 7.5 Hz, 3H, CH_2C**H$_3$**) in ppm

^{13}C-NMR (100.6 MHz , C_6D_6) δ= 133.4 (s, 1C, CH_3CH=**C**H-); 123.9 (s, 1C, CH_3**C**H=CH-); 26.1 (s, 1C, -CH=CH-**C**H_2-); 18.1 (s, 1C, **C**H_3-CH=CH-); 14.2 (s, 1C, -CH=CH-CH_2-**C**H_3) in ppm

Z-pent-2-ene (8)

^{1}H-NMR (400.1 MHz, C_6D_6) δ = 5.42 (m, 2H, C**H**=C**H**), 1.99 (m, 2H, C=C-C**H$_2$**), 1.52 (m, 3H, C**H$_3$**-C=C), 0.91 (t, ^{3}J(H,H) = 7.5 Hz, 3H, CH2-C**H$_3$**) in ppm

^{13}C-NMR (100.6 MHz , C_6D_6) δ= 132.4 (s, 1C, CH_3CH=**C**H-); 123.3 (s, 1C, CH_3**C**H=CH-); 20.5 (s, 1C, CH_3CH=CH**C**H_2-); 14.2 (s, 1C, -CH=CH-CH_2-**C**H_3); 12.7 (s, 1C, **C**H_3-CH=CH-) in ppm

Butyl-(1-ethylpropoxy)-silane (6)

^{1}H-NMR (500.1 MHz, C_6D_6) δ= 4.83 (t, 2H, -Si**H$_2$**, ^{3}J(H,H)= 2.7 Hz), 3.42 (p, ^{3}J(H,H)= 5.5 Hz, -OC**H**) 1.43 (4H, -OCH**C H$_2$**CH_3, overlapped) in ppm

Butyl-bis(1-ethylpropoxy)-silane (7)

^{1}H-NMR (500.1 MHz, C_6D_6) δ= 4.99 (t, 1H, -Si**H**, ^{3}J(H, H)= 2.6 Hz), 3.88 (p, 2H, -OC**H**, ^{3}J(H, H)= 5.8 Hz), 1.54 (8H, -OCHC**H$_2$**CH$_3$) in ppm

^{13}C-NMR (125.8 MHz , C_6D_6) δ= 75.3 (s, 2C, -O**C**H), 18.0 (s, 4C, -OCH**C**H$_2$CH$_3$) in ppm

Chloroacetone 9

^{1}H-NMR (300.1 MHz, C_6D_6) δ= 3.19 (s, 2H, -C**H$_2$**Cl), 1.56 (s, 3H, -C**H$_3$**) in ppm

^{13}C-NMR (125.8 MHz , C_6D_6) δ= 198.4 (s, 1C, -**C**O); 48.2 (s, 1C, -**C**H$_2$Cl); 26.1 (s, 1C, -**C**H$_3$) in ppm

1,1-Dichloroacetone

^{1}H-NMR (400.1 MHz, C_6D_6) δ= 5.12 (s, 1H, -C**H**Cl$_2$), 1.75 (s, 3H, -C**H$_3$**) in ppm

^{13}C-NMR (100.6 MHz , C_6D_6) δ= 193.2 (s, 1C, CH$_3$**C**OCHCl$_2$), 70.2 (s, 1C, **-C**HCl$_2$), 21.6 (s, 1C, -**C**H$_3$) in ppm

Monosilylether formed from 1,1-Dichloroacetone

^{1}H-NMR (500.1 MHz, C_6D_6) δ= 5.25 (d, 1H, C**H**Cl$_2$, ^{3}J (H,H)= 4.3 Hz,), 4.85 (1H, Si**H**), 4.08 (m, 1H, **H**COSiHEt$_2$, overlapped), 1.16 (d, 3H, -C**H$_3$**, overlapped), 0.91 (t, 6H, CH$_2$C**H$_3$**, overlapped), 0.61 (m, 4H, C**H$_2$**CH$_3$, overlapped) in ppm

^{13}C-NMR (125.8 MHz , C_6D_6) δ= 76.4 (s, 1C, **C**HCl$_2$); 73.9 (s, 1C, H**C**OSiHEt$_2$); 18.7 (s, 1 C, **C**H$_3$) in ppm

^{29}Si-NMR (99.4 MHz , C_6D_6) δ= 15.5 (s, 1Si, HCO**Si**HEt$_2$) in ppm

isobutyrophenone 11

^{1}H-NMR (500.1 MHz, C_6D_6) δ= 7.86-7.81 (m, 2H, **ortho-H**), 7.25-7.02 (m, 3H, **meta-H**, **para-H**), 3.11 (h, 1H, ^{3}J(H,H)= 6.9 Hz, PhCOC**H**(CH$_3$)$_2$), 1.06 (d, 6H, ^{3}J(H,H) = 6.9 Hz, PhCOCH(C**H$_3$**)$_2$) in ppm

isobutenylbenzene 12

^{1}H-NMR (500.1 MHz, C_6D_6) δ= 7.25-7.01 (m, 5H, Ar−**H**); 6.28 (m, 1H, PhC**H**-C(CH$_3$)$_2$), 1.71 (d, ^{3}J(H,H)= 12.9 Hz, 6H, PhCH-C(C**H$_3$**)$_2$) in ppm

isobutylbenzene 13

^{1}H-NMR (500.1 MHz, C_6D_6) δ= 2.34 (d, 2H, ^{3}J(H,H) = 7.2 Hz, ArC**H$_2$**CH(CH$_3$)$_2$), 1.73 (m, 1H, ArCH$_2$C**H**(CH$_3$)$_2$, overlapped), 0.83 (d, 6H, ^{3}J(H,H)= 6.6 Hz, ArCH$_2$CH(C**H$_3$**)$_2$) in ppm

1-phenyl-1-butanone 14

^{1}H-NMR (300.1 MHz, C_6D_6) δ= 8.04 (d, 2H,ortho-H, ^{3}J(H,H) = 9.0 Hz), 7.56 (m, 1H, para-H), 7.51 (m, 2H, metha-H), 2.99 (t, 2H, -CO-C**H$_2$**-, ^{3}J(H,H) = 6.0 Hz), 1.90 (m,2H, -COCH$_2$C**H$_2$**-), -CH$_3$ signal overlapped, in ppm

^{13}C-NMR (75.5 MHz , C_6D_6) δ= 197.6 (s, 1C, -**C**O), 136.2 (s, 1C, -**C**-CO), 133.8 (s, 1C, -**C**H-CH-CH-C-CO), 129.0 (s, 2C, -CH-**C**H-CH-C-CO), 128.6 (s, 2C, -CH-CH-**C**H-C-CO), 40.9 (s, 1C, CO-**C**H$_2$-), 18.3 (s, 1C, -**C**H$_2$-CH$_3$), 14.3 (s, 1C, -CH$_2$-**C**H$_3$) in ppm

Alkene 15

^{1}H-NMR (300.1 MHz, C_6D_6) δ= 7.19 (m, 4H, arom-H), 6.49 (d, 1H, C-C**H**-, ^{3}J(H,H) = 15.0 Hz), 6.30 (dt, 1H, CCH-C**H**-, ^{3}J(H,H) = 6.0 Hz), 2.33 (m, 2H, C**H$_2$**-CH$_3$), 1.24 (t, 3H, CH$_2$-C**H$_3$**) in ppm

Alkane 16

^{1}H-NMR (300.1 MHz, C_6D_6) δ= 7.37 (m, 4H, arom-H), 2.71 (t, 2H, -C-C**H$_2$**-, ^{3}J(H,H) = 6.0 Hz), 1.73 (m, 2H, CCH$_2$-C**H$_2$**-CH$_2$-), 1.47 (m, 2H, CCH$_2$-CH$_2$-C**H$_2$**-), 1.38 (t, 3H, -C**H$_3$**, ^{3}J(H,H) = 6.0 Hz) in ppm

1-phenylethanone 17

^{1}H-NMR (300.1 MHz, C_6D_6) δ= 7.96 (d, 2H,ortho-H, ^{3}J(H,H) = 9.0 Hz), 7.48 (m, 1H, para-H), 7.44 (m, 2H, metha-H), 2.52 (s, 3H, -CO-C**H$_3$**) in ppm

Alkene 18

^{1}H-NMR (300.1 MHz, C_6D_6) δ= 7.46, (m, 4H, armo-H), 6.79 (m, 1H, CC**H**=CHH'), 5.82 (dd, 1H, CCH=CH**H'**,^{3}J(H',H) = 18.0 Hz), 5.28 (dd, 1H, CCH=C**H**H',^{3}J(H,H) = 12.0 Hz) in ppm

Alkane 19

^{1}H-NMR (300.1 MHz, C_6D_6) δ= 7.21 (m, 4H, arom-H), 2.76 (q, 2H, -C**H$_2$**-CH$_3$,^{3}J(H,H) = 6.0 Hz), 1.38 (t, 3H, -CH$_2$-C**H$_3$**,^{3}J(H,H) = 6.0 Hz) in ppm

1-(4-fluorophenyl)ethanone 20

^{1}H-NMR (300.1 MHz, C_6D_6) δ= 7.81 (m, 2H, C**H**CHCCO), 6.92 (t, 2H, CHC**H**CCO, ^{3}J(H,H) = 9.0 Hz), 2.35 (s, 3H, -CO-C**H$_3$**) in ppm

Alkene 21

^{1}H-NMR (300.1 MHz, C_6D_6) δ= 7.41, (m, 4H, armo-H), 6.76 (m, 1H, CC**H**=CHH'), 5.72 (dd, 1H, CCH=CH**H'**,^3J(H',H) = 18.0 Hz), 5.26 (dd, 1H, CCH=C**H**H',^3J(H,H) = 12.0 Hz) in ppm

Alkane 22

^{1}H-NMR (300.1 MHz, C_6D_6) δ= 7.17 (m, 4H, arom-H), 2.75 (q, 2H, -C**H$_2$**-CH_3,^3J(H,H) = 9.0 Hz), 1.40 (t, 3H, -CH_2-C**H$_3$**,^3J(H,H) = 9.0 Hz) in ppm

5 References

[1] J. J. Berzelius, *Årsberättelsen om Fram. i Fys. och kemi [Annual Rep. Prog. Phys. Chem.* **1835**.

[2] E. Mitscherlich, *Ann. der Phys. und Chemie* **1834**, *31*, 273–282.

[3] a J. B. Robertson, *Platin. Met. Rev.* **1975**, *19*, 64–69.

[4] J. Wisniak, *Educ. quim.* **2010**, *21*, 60–69.

[5] M. Beller, A. Renken, R. Van Santen, *Catalysis: From Principles to Applications*, Wiley-VCH Verlag GmbH & Co. KGaA, Weinheim, **2012**.

[6] B. Lindström, L. J. Pettersson, *CATTECH* **2003**, *7*, 130–138.

[7] G. Ertl, H. Knözinger, J. Weitkamp, *Handbook of Heterogenous Catalysis*, VCH Verlagsgesellschaft MbH, Weinheim, **1997**.

[8] J. Weitkamp, R. Gläser, *Winnacker-Küchler: Chemiesche Technik - Prozesse Und Produkte Katalyse*, Wiley-VCH Verlag GmbH & Co. KGaA, Weinheim, **2004**.

[9] J. R. Anderson, M. Boudart, *The History of the Catalytic Synthesis of Ammonia in Catalysis (Science and Technology)*, Springer-Verlag, Berlin, Heidelberg, **1985**.

[10] A. P. Kieboom, J. A. Moulijn, P. W. N. M. Van Leeuwen, R. A. Van Santen, *Catalysis: An Integrated Approach*, Elsevier, Amsterdam, **1999**.

[11] V. Polshettiwar, R. S. Varma, *Green Chem.* **2010**, *12*, 743–754.

[12] S. B. Singh, P. K. Tandon, *J. Energy Chem. Eng.* **2014**, *2*, 106–115.

[13] D. Astruc, F. Lu, J. R. Aranzaes, *Angew. Chem. Int. Ed.* **2005**, *44*, 7852–7872.

[14] S. Chaturvedi, P. N. Dave, N. K. Shah, *J. Saudi Chem. Soc.* **2012**, *16*, 307–325.

[15] G. Ertl, *Reactions at Solid Surfaces*, John Wiley & Sons, Inc., Hoboken, NJ, USA, **2009**.

[16] Y.-C. Lin, G. W. Huber, *Energy Environ. Sci.* **2009**, *2*, 68–80.

[17] W. H. Weinberg, *Acc. Chem. Res.* **1996**, *29*, 479–487.

[18] C. Wang, X. Gu, H. Yan, Y. Lin, J. Li, D. Liu, W. Li, J. Lu, *ACS Catal.* **2017**, *7*, 887–891.

[19] C. Doornkamp, V. Ponec, *J. Mol. Catal. A Chem.* **2000**, *162*, 19–32.

[20] G. N. Lewis, *Valence and The Structure of Atoms and Molecules*, The Chemical Catalog Company, Inc., New York, U.S.A., **1923**.

[21] R. G. Pearson, *J. Chem. Educ.* **1968**, *45*, 581–587.

[22] K. O. Christe, D. A. Dixon, D. McLemore, W. W. Wilson, J. A. Sheehy, J. A. Boatz, *J. Fluor. Chem.* **2000**, *101*, 151–153.

[23] V. Parvulescu, E. Kemnitz, *New Materials for Catalytic Applications*, Elsevier, **2016**.

[24] L. O. Müller, D. Himmel, J. Stauffer, G. Steinfeld, J. Slattery, G. Santiso-Quinones, V. Brecht, I. Krossing, *Angew Chem* **2008**, *120*, 7772–7776.

[25] J. F. Kögel, D. A. Sorokin, A. Khvorost, M. Scott, K. Harms, D. Himmel, I. Krossing, J. Sundermeyer, *Chem. Sci.* **2018**, *9*, 245–253.

[26] I.-C. Hwang, K. Seppelt, *Angew. Chem. Int. Ed.* **2001**, *40*, 3690–3693.

[27] L. Greb, *Chem. Eur.J.* **2018**, *24*, 17881–17896.

[28] A. Corma, H. García, *Chem. Rev.* **2003**, *103*, 4307–4365.

[29] T. Krahl, A. Vimont, G. Eltanany, M. Daturi, E. Kemnitz, *J. Phys. Chem. C* **2007**, *111*, 18317–18325.

[30] S. K. Ruediger, U. Groß, M. Feist, H. A. Prescott, S. C. Shekar, S. I. Troyanov, E. Kemnitz, *J. Mater. Chem.* **2005**, *15*, 588–597.

[31] E. Kemnitz, U. Groß, S. Rüdiger, C. S. Shekar, *Angew. Chemie - Int. Ed.* **2003**, *42*, 4251–4254.

[32] R. F. Krause, T. B. Douglas, *J. Phys. Chem.* **1986**, *72*, 3444–3451.

[33] A. C. Sievert, C. G. Krespan, F. J. Weigert, (DuPont Co.) U.S. Patent Number: 5, 157, 171, **1992**.

[34] C. G. Krespan, (DuPont Co.) US Patent Number: 5, 162, 594, **1992**.

[35] D.-C. T. Krahl, Amorphes Aluminiumchlorofluorid Und -Bromofluorid — Die Stärksten Bekannten Festen Lewis-Säuren, Humboldt-Universität zu Berlin, **2005**.

[36] E. Kemnitz, U. Groß, S. Rüdiger, C. S. Shekar, *Angew. Chemie* **2003**, *115*, 4383–4386.

[37] S. Rüdiger, G. Eltanany, U. Groß, E. Kemnitz, *J. Sol-Gel Sci. Technol.* **2007**, *41*, 299–311.

[38] A. Makarowicz, Surface Characterisation of Functionalised Fluoride Materials, Dissertation, University of Manchester, **2008**.

[39] G. Eltanany, Sol-Gel Synthesis and Properties of Nanoscopic Aluminum Fluoride, Dissertation, Mathematisch-Naturwissenschaftlichen Fakultät I H, **2007**.

[40] T. Krahl, E. Kemnitz, *J. Fluor. Chem.* **2006**, *127*, 663–678.

[41] T. Krahl, R. Stösser, E. Kemnitz, G. Scholz, M. Feist, G. Silly, J. Y. Buzaré, *Inorg. Chem.* **2003**, *42*, 6474–6483.

[42] J. K. Murthy, U. Gross, S. Ru, V. V. Rao, V. V. Kumar, A. Wander, C. L. Bailey, N. M. Harrison, E. Kemnitz, *J. Phys. Chem. B* **2006**, *110*, 8314–8319.

[43] E. Kemnitz, G. Eltanany, S. Ru, *J. Mater. Chem.* **2008**, *18*, 2268–2275.

[44] M. H. G. Prechtl, M. Teltewskoi, A. Dimitrov, E. Kemnitz, T. Braun, *Chem. Eur. J.* **2011**, *17*, 14385–14388.

[45] V. A. Petrov, C. G. Krespan, B. E. Smart, *J. Fluor. Chem.* **1998**, *89*, 125–130.

[46] C. G. Krespan, D. A. Dixon, *J. Fluor. Chem.* **1996**, *77*, 117–126.

[47] C. G. Krespan, V. a. Petrov, *Chem. Rev.* **1996**, *96*, 3269–3302.

[48] M. Ahrens, G. Scholz, T. Braun, E. Kemnitz, *Angew. Chemie* **2013**, *125*, 5436–5440.

[49] V. J. Scott, C. Remle, O. V Ozerov, *J. Am. Chem. Soc.* **2005**, *127*, 2852–2853.

[50] B. Calvo, J. Wuttke, T. Braun, E. Kemnitz, *ChemCatChem* **2016**, *8*, 1945–1950.

[51] G. Meißner, M. Feist, T. Braun, E. Kemnitz, *J. Organomet. Chem.* **2017**, *847*, 234–241.

[52] S. Ruediger, E. Kemnitz, *Dalt. Trans.* **2008**, 1117–1127.

[53] K. Teinz, S. Wuttke, F. Börno, J. Eicher, E. Kemnitz, *J. Catal.* **2011**, *282*, 175–182.

[54] M. Nickkho-amiry, G. Eltanany, S. Wuttke, S. Ru, E. Kemnitz, J. M. Winfield, *J. Fluor. Chem.* **2008**, *129*, 366–375.

[55] D. Dambournet, G. Eltanamy, A. Vimont, J.-C. Lavalley, J.-M. Goupil, A. Demourgues, E. Durand, J. Majimel, S. Rüdiger, E. Kemnitz, et al., *Chem. - A Eur. J.* **2008**, *14*, 6205–6212.

[56] I. K. Murwani, K. Scheurell, E. Kemnitz, *Catal. Commun.* **2008**, *10*, 227–231.

[57] S. M. Coman, P. Patil, E. Kemnitz, *Chem. Commun.* **2009**, 460–462.

[58] S. M. Coman, S. Wuttke, A. Vimont, M. Daturi, E. Kemnitz, *Adv. Synth. Catal.* **2008**, *350*, 2517–2524.

[59] P. T. Patil, A. Dimitrov, H. Kirmse, W. Neumann, E. Kemnitz, *Appl. Catal. B Environ.* **2008**, *78*, 80–91.

[60] M. Bonarowska, O. Machynskyy, D. Łomot, E. Kemnitz, Z. Karpiński, *Catal. Today* **2014**, *235*, 144–151.

[61] K. Scheurell, E. Kemnitz, *J. Mater. Chem.* **2005**, *15*, 4845.

[62] A. Corma, J. M. Lopez-Nieto, N. Paredes, M. Perez, Y. Shen, H. Cao, S. L. Suib, *Stud. Surf. Sci. Arid Catal.* **1992**, *72*, 213–220.

[63] K. Kim, Z. Shon, H. Thi, E. Jeon, *Atmos. Environ.* **2011**, *45*, 1369–1382.

[64] W. Tsai, *Chemosphere* **2005**, *61*, 1539–1547.

[65] M. Molteni, C. Pesenti, M. Sani, A. Volonterio, M. Zanda, *J. Fluor. Chem.* **2004**, *125*, 1735–1743.

[66] W. R. J. Dolbier, *J. Fluor. Chem.* **2005**, *126*, 157–163.

[67] T. Ahrens, J. Kohlmann, M. Ahrens, T. Braun, *Chem. Rev.* **2015**, *115*, 931–972.

[68] J. L. Kiplinger, T. G. Richmond, C. E. Osterbergt, *Chem. Rev.* **1994**, *94*, 373–431.

[69] M. K. Whittlesey, E. Peris, *ACS Catal.* **2014**, *4*, 3152–3159.

[70] H. Amii, K. Uneyama, *Chem. Rev.* **2009**, *109*, 2119–2183.

[71] T. A. Unzner, T. Magauer, *Tetrahedron Lett.* **2015**, *56*, 877–883.

[72] Q. Shen, Y. Huang, C. Liu, J. Xiao, Q. Chen, Y. Guo, *J. Fluor. Chem.* **2015**, *179*, 14–22.

[73] C. Bonds, J. Choi, D. Y. Wang, S. Kundu, Y. Choliy, T. J. Emge, K. Krogh-jespersen, A. S. Goldman, *Science* **2011**, *332*, 1545–1548.

[74] J. Terao, H. Todo, S. Ara Begum, H. Kuniyasu, N. Kambe, *Angew. Chem. Int. Ed.* **2007**, *46*, 2086–2089.

[75] J. Terao, H. Watabe, N. Kambe, *J. Am. Chem. Soc.* **2005**, *127*, 3656–3657.

[76] J. Terao, A. Ikumi, H. Kuniyasu, N. Kambe, *J. Am. Chem. Soc.* **2003**, *125*, 5646–5647.

[77] G. A. Olah, S. J. Kuhn, *J. Org. Chem.* **1964**, *29*, 2317–2320.

[78] C. Douvris, O. V Ozerov, *Science* **2008**, *321*, 1188–1190.

[79] D. G. Gusev, O. V Ozerov, *Chem. Eur. J.* **2011**, *17*, 634–640.

[80] C. Douvris, C. M. Nagaraja, C. Chen, B. M. Foxman, O. V. Ozerov, *J. Am. Chem. Soc.* **2010**, *132*, 4946–4953.

[81] R. Panisch, M. Bolte, T. Müller, *J. Am. Chem. Soc.* **2006**, *128*, 9676–9682.

[82] O. Allemann, K. K. Baldridge, J. S. Siegel, *Org. Chem. Front.* **2015**, *2*, 1018–1021.

[83] S. Duttwyler, C. Douvris, N. L. P. Fackler, F. S. Tham, C. A. Reed, K. K. Baldridge, J. S. Siegel, *Angew. Chemie* **2010**, *122*, 7681–7684.

[84] O. Allemann, S. Duttwyler, P. Romanato, K. K. Baldridge, J. S. Siegel, *Science* **2011**, *332*, 574–577.

[85] A. Jana, P. P. Samuel, G. Tavcar, H. W. Roesky, C. Schulzke, *J. Am. Chem. Soc.* **2010**, *132*, 10164–10170.

[86] V. S. V. S. N. Swamy, N. Parvin, K. V. Raj, K. Vanka, S. S. Sen, *Chem. Commun.* **2017**, *53*, 9850–9853.

[87] W. Gu, M. R. Haneline, C. Douvris, O. V. Ozerov, *J. Am. Chem. Soc.* **2009**, *131*, 11203–11212.

[88] M. Klahn, C. Fischer, A. Spannenberg, U. Rosenthal, I. Krossing, *Tetrahedron Lett.* **2007**, *48*, 8900–8903.

[89] C. B. Caputo, D. W. Stephan, *Organometallics* **2012**, *31*, 27–30.

[90] T. Stahl, H. F. T. Klare, M. Oestreich, *ACS Catal.* **2013**, *3*, 1578–1587.

[91] G. B. Deacon, P. C. Junk, D. Werner, *Eur. J. Inorg. Chem.* **2015**, *2015*, 1484–1489.

[92] M. Janjetovic, A. M. Träff, G. Hilmersson, *Chem. Eur. J.* **2015**, *21*, 3772–3777.

[93] W. Fei, H. Jinbo, *Chin. J. Chem.* **2009**, *27*, 93–98.

[94] M. Dryzhakov, J. Moran, *ACS Catal.* **2016**, *6*, 3670–3673.

[95] M. R. Crimmin, M. J. Butler, A. J. P. White, *Chem. Commun.* **2015**, *51*, 15994–15996.

[96] T. Chu, Y. Boyko, I. Korobkov, G. I. Nikonov, *Organometallics* **2015**, *34*, 5363–5365.

[97] C. E. Pitsch, X. Wang, *Chem. Commun.* **2017**, *53*, 8196–8198.

[98] A. Comas-Vives, M. Schwarzwaelder, C. Coperet, P. Sautet, *J. Phys. Chem. C* **2015**, *119*, 7156–7163.

[99] A. Hess, E. Kemnitz, A. Lippitz, W. E. S. Unger, D. H. Menz, *J. Catal.* **1994**, *148*, 270–280.

[100] S. Imamura, T. Shiomi, S. Ishida, K. Utani, *Ind. Eng. Chem. Res.* **1990**, *29*, 1758–1761.

[101] J. Fan, J. T. Yates, *J. Phys. Chem.* **1994**, *98*, 10621–10627.

[102] T. Furusawa, T. Ogawa, T. Numao, M. Sato, N. Suzuki, *J. Chem. Eng. Japan* **2012**, *45*, 459–465.

[103] M. M. Farris, A. A. Klinghoffer, J. A. Rossin, D. E. Tevault, *Catal. Today* **1992**, *11*, 501–516.

[104] S. Karmakar, H. L. Greene, *J. Catal.* **1994**, *151*, 394–406.

[105] H. Onoda, T. Ohta, J. Tamaki, K. Kojima, *Appl. Catal. A Gen.* **2005**, *288*, 98–103.

[106] A. Hess, E. Ã. Kemnitz, *Catal. Letters* **1997**, *49*, 199–205.

[107] W. B. Feaver, J. A. Rossin, *Catal. Today* **1999**, *54*, 13–22.

[108] W. Han, Y. Chen, B. Jin, H. Liu, *Greenh. Gas Sci Technol.* **2014**, *4*, 121–130.

[109] O. Papaianina, K. Y. Amsharov, *Chem. Commun.* **2016**, *52*, 1505–1508.

[110] J. W. Edwards, P. A. Small, *Ind. Eng. Chem. Fundamen.* **1965**, *4*, 396–400.

[111] A. H. Fainberg, S. D. Fetterman, H. Murray, U. S. Patent Number: 3,262,981, **1964**.

[112] W. L. Luyben, *Ind. Eng. Chem. Res.* **1988**, *27*, 208–211.

[113] N. J. Buttler, *J. Am. Chem. Soc.* **1962**, *84*, 1393–1398.

[114] D. J. Moon, M. J. Chung, H. Kim, Y. S. Kwon, B. S. Ahn, *Ind. Eng. Chem. Res.* **2002**, *41*, 2895–2902.

[115] P. Zhang, L. Cao, R. Pan, Z. Jiang, K. Qin, Q. Li, *Procedia Eng.* **2013**, *62*, 337–341.

[116] W. Han, E. M. Kennedy, H. Liu, Y. Li, A. A. Adesina, J. C. Mackie, B. Z. Dlugogorski, *J. Fluor. Chem.* **2010**, *131*, 698–703.

[117] A. Vakulka, G. Tavcar, T. Skapin, *J. Fluor. Chem.* **2012**, *142*, 52–59.

[118] W. Han, H. Yu, E. M. Kennedy, J. C. Mackie, B. Z. Dlugogorski, *Environ. Sci. Technol.* **2008**, *42*, 5795–5799.

[119] R. Baumgartner, G. K. Stieger, K. McNeill, *Environ. Sci. Technol.* **2013**, *47*, 6545–6553.

[120] S. Sabater, J. A. Mata, E. Peris, *Organometallics* **2014**, *34*, 1186–1190.

[121] X. Ma, S. Liu, Y. Liu, G. Gu, C. Xia, *Sci. Rep.* **2016**, *6*, 1–11.

[122] R. Baumgartner, K. McNeill, *Environ. Sci. Technol.* **2012**, *46*, 10199–10205.

[123] B. Coq, J. M. Cognion, F. Figueras, D. Tournigant, *J. Catal.* **1993**, *141*, 21–33.

[124] V. Y. Borovkov, V. I. Kovalchuk, F. Lonyi, J. L. D'Itri, *J. Phys. Chem.* **2000**, *104*, 5603–5609.

[125] D. Huang, L. Yin, J. Niu, *Environ. Sci. Technol.* **2016**, *50*, 5857−5863.

[126] Z.-J. Shi, *Catalysis In C–Cl Activation, in Homogeneous Catalysis for Unreactive Bond Activation*, John Wiley & Sons, Inc., Hoboken, NJ, USA, **2014**.

[127] C. C. C. J. Seechurn, M. O. Kitching, T. J. Colacot, V. Snieckus, *Angew. Chemie* **2012**, *124*, 5150–5175.

[128] N. Panda, A. K. Jena, *Org. Chem. Curr. Res.* **2015**, *4*, 1–21.

[129] A. Rudolph, M. Lautens, *Angew. Chem. Int. Ed.* **2009**, *48*, 2656–2670.

[130] J. K. Kochi, M. Tamura, *J. Am. Chem. Soc.* **1971**, *93*, 1483–1485.

[131] N. Kambe, T. Iwasakia, J. Terao, *Chem. Soc. Rev.* **2011**, *40*, 4937–4947.

[132] A. C. Frisch, M. Beller, *Angew. Chem. Int. Ed.* **2005**, *44*, 674–688.

[133] L. Yin, J. Liebscher, *Chem.Rev.* **2007**, *107*, 133–173.

[134] M. Sharma, M. Sharma, A. Hazarika, L. Satyanarayana, G. V. Karunakard, K. K. Bania, *Mol. Catal.* **2017**, *432*, 210–219.

[135] M. Mora, C. Jiménez-sanchidrián, J. R. Ruiz, *Curr. Org. Chem.* **2012**, *16*, 1128–1150.

[136] A. Fihri, M. Bouhrara, B. Nekoueishahraki, J.-M. Basset, V. Polshettiwar, *Chem. Soc. Rev.* **2011**, *40*, 5181–5203.

[137] M. Julia, M. Duteil, C. Grard, E. Kuntz, *Bull. Soc. Chim. Fr.* **1973**, 2791–2794.

[138] R. B. Bedford, M. Betham, D. W. Bruce, S. A. Davis, M. Frost, M. Hird, *Chem. Commun.* **2006**, 1398–1400.

[139] A. Berrichi, R. Bachir, M. Benabdallah, N. Choukchou-Braham, *Tetrahedron Lett.* **2015**, *56*, 1302–1306.

[140] M. Rahman, A. K. Bagdi, A. Majee, A. Hajra, *Tetrahedron Lett.* **2011**, *52*, 4437–4439.

[141] J. H. Kim, Y. K. Chung, *Chem. Commun.* **2013**, *94*, 11101–11103.

[142] R. M. Rioux, C. D. Thompson, N. Chen, F. H. Ribeiro, *Catal. Today* **2000**, *62*, 269–278.

[143] N. Chen, R. M. Rioux, F. H. Ribeiro, *J. Catal.* **2002**, *211*, 192–197.

[144] M. A. Álvarez-montero, L. M. Gómez-sainero, A. Mayoral, I. Diaz, R. T. Baker, J. J. Rodriguez, *J. Catal.* **2011**, *279*, 389–396.

[145] M. Makkee, A. Wiersma, E. J. A. . X. Van de Sandt, H. Van Bekkum, J. A. Moulijn, *Catal. Today* **2000**, *55*, 125–137.

[146] M. Martin-Martinez, L. M. Gomez-Sainero, M. A. Alvarez-Montero, J. Bedia, J. J. Rodriguez, *Appl. Catal. B, Environ.* **2013**, *132–133*, 256–265.

[147] H. P. Aytam, V. Akula, K. Janmanchi, S. R. R. Kamaraju, K. R. Panja, K. Gurram, J. W. Niemantsverdriet, *J. Phys. Chem. B* **2002**, *106*, 1024–1031.

[148] S. Y. Kim, H. C. Choi, O. B. Yanga, K. H. Lee, J. S. Lee, Y. G. Kim, *J. Chem. Soc. Chem. Commun.* **1995**, 2169–2170.

[149] K. Early, V. I. Kovalchuk, F. Lonyi, S. Deshmukh, J. L. D'Itri, *J. Catal.* **1999**, *182*, 219–227.

[150] S. Deshmukh, J. L. d'Itri, *Catal. Today* **1998**, *40*, 377–385.

[151] H. Berndt, H. Bozorg Zadeh, E. Kemnitz, M. Nickkho-Amiry, M. Pohl, T. Skapin, J. M. Winfield, *J. Mater. Chem.* **2002**, *12*, 3499–3507.

[152] F. D. Kopinke, K. Mackenzie, R. Koehler, A. Georgi, *Appl. Catal. A Gen.* **2004**, *271*, 119–128.

[153] M. Lu, X. Li, B. Chen, M. Li, H. Xin, L. Song, *J. Nanosci. Nanotechnol.* **2014**, *14*, 7315–7318.

[154] R. J. Hofmann, M. Vlatkovic, F. Wiesbrock, *Polymers (Basel).* **2017**, *9*, 534–571.

[155] L. H. Sommer, E. W. Pietrusza, F. C. Whitmore, *J. Am. Chem. Soc.* **1947**, *69*, 188–188.

[156] H. Gilman, D. Wittenberg, *J. Org. Chem.* **1958**, *23*, 501–502.

[157] R. Calas, N. Duffaut, *C. R. Acad. Sci.* **1957**, *245*, 906–907.

[158] V. I. Boiadjiev, G. M. Brown, L. A. Pinnaduwage, G. Goretzki, P. V. Bonnesen, T. Thundat, *Langumir* **2005**, *21*, 1139–1142.

[159] K. Riener, M. P. Högerl, P. Gigler, F. E. Kühn, *ACS Catal.* **2012**, *2*, 613–621.

[160] I. Ojima, M. Nihonyanagi, Y. Nagai, *Bull. Chem. Soc. Jpn.* **1972**, *45*, 3722.

[161] I. Ojima, T. Kogure, M. Kumagai, S. Horiuchi, T. Sato, *J. Organomet. Chem.* **1976**, *122*, 83–97.

[162] B. Bantu, K. Wurst, M. R. Buchmeiser, *J. Organomet. Chem.* **2007**, *692*, 5272–5278.

[163] N. Schneider, M. Finger, C. Haferkemper, S. Bellemin-laponnaz, P. Hofmann, L. H. Gade, *Angew. Chem. Int. Ed.* **2009**, *48*, 1609–1613.

[164] S. Park, M. Brookhart, *Organometallics* **2010**, *29*, 6057–6064.

[165] T. T. Metsänen, P. Hrobarik, H. F. T. Klare, M. Kaupp, M. Oestreich, *J. Am. Chem. Soc.* **2014**, *136*, 6912–6915.

[166] C. Song, C. Ma, Y. Ma, W. Feng, S. Ma, Q. Chai, M. B. Andrus, *Tetrahedron Lett.* **2005**, *46*, 3241–3244.

[167] X. Feng, H. Du, *Tetrahedron Lett.* **2014**, *55*, 6959–6964.

[168] D. Addis, N. Shaikh, S. Zhou, S. Das, K. Junge, M. Beller, *Chem. Asian J.* **2010**, *5*, 1687–1691.

[169] N. S. Shaikh, S. Enthaler, K. Junge, M. Beller, *Angew. Chemie - Int. Ed.* **2008**, *47*, 2497–2501.

[170] M. Flückiger, A. Togni, *European J. Org. Chem.* **2011**, *2011*, 4353–4360.

[171] H. Brunner, K. Fisch, *J. Organomet. Chem.* **1991**, *412*, C11–C13.

[172] J. Yun, S. L. Buchwald, *J. Am. Chem. Soc.* **1999**, *121*, 5640–5644.

[173] T. Bleith, L. H. Gade, *J. Am. Chem. Soc.* **2016**, *138*, 4972–4983.

[174] R. Calas, *Pure Appl. Chem.* **1966**, *13*, 61–79.

[175] D. J. Parks, W. E. Piers, *J. Am. Chem. Soc.* **1996**, 9440–9441.

[176] T. Mahdi, D. W. Stephan, *Angew.Chem.* **2015**, *127*, 8631–8634.

[177] Y.-S. Song, B. R. Yoo, G.-H. Lee, I. N. Jung, *Organometallics* **1999**, *18*, 3109–3115.

[178] J. Choi, Y. Kang, *Bull. Korean Chem. Soc.* **2005**, *26*, 343–344.

[179] A. Corma, C. González-Arellano, M. Iglesias, F. Sánchez, *Angew. Chem. Int. Ed.* **2007**, *46*, 7820–7822.

[180] Y. Kawanami, H. Yuasa, F. Toriyama, S. Yoshida, T. Baba, *Catal. Commun.* **2003**, *4*, 455–459.

[181] A. Volkov, K. P. J. Gustafson, C.-W. Tai, O. Verho, J.-E. Bäckvall, H. Adolfsson, *Angew. Chem. Int. Ed.* **2015**, *54*, 5122–5126.

[182] D. Addis, S. Zhou, S. Das, K. Junge, H. Kosslick, J. Harloff, H. Lund, A. Schulz, M. Beller, *Chem. Asian J.* **2010**, *5*, 2341–2345.

[183] M. Tan, Y. Zhang, J. Y. Ying, *Adv. Synth. Catal.* **2009**, *351*, 1390–1394.

[184] G. Hamasaka, A. Ochida, K. Hara, M. Sawamura, *Angew. Chem. Int. Ed.* **2007**, *46*, 5381–5383.

[185] B. H. Lipshutz, B. A. Frieman, A. E. Tomaso, *Angew. Chem. Int. Ed.* **2006**, *45*, 1259–1264.

[186] H. Friebolin, *Ein- Und Zweidimensionale NMR-Spektroskopie*, Wiley-VCH Verlag GmbH & Co. KGaA, Weinheim, **2013**.

[187] M. Feist, *ChemTexts* **2015**, *1:8*, 12.

[188] A. Auroux, *Calorimetry and Thermal Methods in Catalysis*, Springer-Verlag Berlin Heidelberg, **2013**.

[189] R. Kellner, M. Otto, M. Widmer, J. M. Mermet, *Analytical Chemistry*, Wiley-VCH Verlag GmbH & Co. KGaA, Weinheim, **1998**.

[190] Y. Leng, *Materials Charakterization. Introduction to Microscopic and Spectroscopic Methods*, Wiley-VCH Verlag GmbH & Co. KGaA, **2013**.

[191] J. Burdeniuc, B. Jedlicka, R. H. Crabtree, *Chem. Ber.* **1997**, *130*, 145–154.

[192] A. K. Siwek, Aktivierung von Halogenmethanen an Lewis-Sauren Aluminium-fluoridoberflächen, Humboldt- Universität zu Berlin, **2013**.

[193] M. Ahrens, G. Scholz, T. Braun, E. Kemnitz, *Angew. Chemie Int. Ed.* **2013**, *125*, 5436–5440.

[194] K. Tarach, M. Choi, *J. Org. Chem.* **2014**, *118*, 12266–12274.

[195] T. R. Hogness, T. L. Wilson, W. C. Johnson, *J. Am. Chem. Soc.* **1880**, *58*, 108–112.

[196] J. Lozano, A. Brickman, S. Yeninas, D. Early, J. H. Craig, *Appl. Surf. Sci.* **2007**, *253*, 3066–3071.

[197] B. Darlington, M. Foster, A. Campion, *Surf. Sci. Lett.* **1994**, *304*, 407–412.

[198] M. W. Chase, Jr., *NIST-JANAF Thermochemical Tables*, The American Chemical Society And The American Institute Of Physics For National Institute Of Standars And Technology, **1998**.

[199] T. Krahl, Amorphes Aluminiumchlorofluorid Und -Bromofluorid - Die Stärksten Bekannten Festen Lewis-Säuren, Humboldt-Universität zu Berlin, **2005**.

[200] A. T. Trueba, M. C. Kroon, C. J. Peters, I. L. Moudrakovski, C. I. Ratcliffe, S. Alavi, J. A. Ripmeester, *J. Chem. Phys.* **2014**, *140*, 214703–214714.

[201] D. W. Stephan, G. Erker, *Angew. Chem. Int. Ed.* **2015**, *54*, 6400–6441.

[202] M. Feist, M. Ahrens, A. Siwek, T. Braun, E. Kemnitz, *J. Therm. Anal. Calorim.* **2015**, *121*, 929–935.

[203] H. Aoyama, S. Kohno, S. Koyama, (Daikin Industries Ltd.) U.S. Patent Number: 5, 557, 019, **1996**.

[204] C. D. Nenitzescu, I. P. Cantuniari, *Ber.* **1933**, *66*, 1097–1100.

[205] J. Holmes, R. Pettit, *J. Org. Chem.* **1963**, *28*, 1695–1696.

[206] G. A. Olah, J. Lukas, *J. Am. Chem. Soc.* **1967**, *89*, 4739–4744.

[207] C. J. A. Mota, D. L. Bhering, A. Ramirez-Solis, *J. Quantum Chem.* **2005**, *105*, 174–185.

[208] T. Xu, D. H. Barich, P. W. Goguen, W. Song, Z. Wang, J. B. Nicholas, J. F. Haw, *J. Am. Chem. Soc.* **1998**, *120*, 4025–4026.

[209] G. Tavoularis, M. A. Keane, *J. Mol. Catal. A Chem.* **1999**, *142*, 187–199.

[210] J. Lu, W. Mao, Y. Bai, W. Wang, B. Wang, Q. Xu, L. Shi, C. Li, *ChemCatChem* **2017**, *9*, 824–832.

[211] D. G. Cory, W. M. Ritchey, *J. Magn. Reson.* **1988**, *80*, 128–132.

6 List of Figures

7 List of Schemes

8 List of Tables

9 Acknowledgement

First, I would like to thank Prof. Kemnitz and Prof. Braun for allowing me to pursue the interesting topic, for the freedom granted during my research and the support provided.

Next, I would like to thank the two research groups for the good cooperation and the pleasant working atmosphere.

Many thanks to everyone who contributed to the analytical evaluation of my work. PD Dr. Gudrun Scholz , Kerstin Scheurell and Dr. Detlef Heidemann for the execution of the MAS NMR measurements, the support during the evaluation, their great interest in this thesis and the commitment with which they supported me. Dr. Feist for carrying out the thermal analysis and for the countless discussions, which helped me to understand the results. Mrs. Bäßler for conducting the TPD experiments. The NMR service of the Humboldt University of Berlin for many NMR spectroscopic experiments. Dr. A. Zehl for performing the elementary analyses.

My special thanks go to Martin M., who not only helped me a lot with settling in Switzerland, but also for numerous proofreading and his patience in doing so.

Furthermore, I would like to thank Kathi T., Felix H. and Larisa Sch. for their proofreading and technical discussions.

I would like to express my sincere gratitude to the School of Analytical Sciences Adlershof team for their continuous support. Funding by DFG GSD1013 SALSA is gratefully acknowledged.

Finally, I would like to thank my family, Beat R. and his family and all my friends, especially Daniel B. and Valentina S., who have supported me and have always believed in me.

10 Declaration of Originality

Ich erkläre, dass ich die Dissertation selbständig und nur unter Verwendung der von mir gemäß § 7 Abs. 3 der Promotionsordnung der Mathematisch-Naturwissenschaftlichen Fakultät, veröffentlicht im Amtlichen Mitteilungsblatt der Humboldt-Universität zu Berlin Nr. 17/2012 am 27.06.2012 angegebenen Hilfsmittel angefertigt habe.

Agnieszka Kinga Siwek Schlieren, den 01.03.2020